

Computational Modeling of Tow-Placed Composite Laminates with Fabrication Features

C. Fagiano

Computational Modeling of Tow-Placed Composite Laminates with Fabrication Features

Proefschrift

ter verkrijging van de graad van doctor
aan de Technische Universiteit Delft,
op gezag van de Rector Magnificus Prof.ir. K.C.A.M. Luyben,
voorzitter van het College van Promoties,
in het openbaar te verdedigen op donderdag 09 december 2010 om 10:00 uur
door Christian FAGIANO,
ingenieur Luchtvaart- en Ruimtevaart,
geboren te Turijn, Italië.

Dit proefschrift is goedgekeurd door de promotor:
Prof. dr. Z. Gürdal

Samenstelling promotiecommissie:

Rector Magnificus	voorzitter
Prof. dr. Z. Gürdal	Technische Universiteit Delft, promotor
Prof. dr. E. Carrera	Polytechnic of Turin, Italy
Prof. dr. A. Metrikine	Technische Universiteit Delft
Prof. dr. J. N. Reddy	University of Texas, U.S.A
Prof. dr. C. Soutis	University of Sheffield, UK
Dr. A. Obst	European Space Agency ESTEC, The Netherlands
Dr. M. M. Abdalla	Technische Universiteit Delft
Prof. dr. ir. A. Rothwell	Technische Universiteit Delft, reservelid

The research described in this thesis was supported by Delft University of Technology.

ISBN 978-94-91109-01-0

Keywords: Composites, Variable Stiffness Laminates, Finite Element Numerical Modeling, Interlaminar Stress Recovery.

Copyright © 2010 by C. Fagiano

All rights reserved. No part of the material protected by this copyright notice may be reproduced or utilized in any form or by any means, electronic or mechanical, including photocopying, recording or by any information storage and retrieval system, without written permission of the author.

Printed in The Netherlands

Summary

The full potential of advanced composites can only be achieved by tailoring a laminate to a specific structural application. In this manner, it is possible to respond more adequately to planar stress variations and it is possible to divert loads from the most sensitive regions of a composite structure such as holes and notches. One method for tailoring a composite laminate is to use non-conventional laminates. The designation non-conventional laminates refers to two types of configurations: (i), laminates that explore the whole range of possible ply orientations, and (ii), composite panels with lay-ups that vary orientation angles continuously from point to point. A continuously varying lay-up is achieved using non-traditional curvilinear fibre paths within the plane of a ply, and, compared to the first option (i), it offers more freedom in the design of laminates subjected to a non-uniform stress state within each ply. In such cases, the laminate stiffness also varies with the in-plane coordinates of the laminate, hence these configurations are termed Variable-Stiffness Panels (VSP).

Fibre-steered laminate designs require an accurate fibre placement system. Hand laying methods will not provide the required precision for laying the fibres at the correct angles and keeping these angles during curing. Moreover, variability in the quality of a laminate resulting from the manual process has to be addressed. Automated fabrication processes are able to provide repeatable and improved quality component production with a reduced production cycle time. The Tow-Placement (TP) technology is of particular interest among the automated fabrication methods available in the aerospace industry. This technology combines the differential tow payout capability of filament winding and the compaction and cut-restart capabilities of automated tape laying. A TP machine is a high-precision robot, capable of wide freedom of movement, that is computer controlled to produce a composite component without human intervention: TP technology allows the design and production of components that would be extremely difficult or even impossible to produce using other automated methods.

The potential of fibre-steered laminates led to the birth of a new branch of research in laminated composite materials aimed at properly modelling and predicting the responses of such laminates. A VSP has, by definition, a nonuniform in-plane stiffness distribution that might result in large in-plane stress gradients. Such gradients contribute to the amplification of the interlaminar stresses, and possibly render delamination the dominant failure mode in these configurations. Furthermore, the manufacturing of VSP imposes either the overlapping of some fibre tows within a ply or their cutting (dropping). While the tow-overlapping method results in local increases of the panel thickness, the tow-dropping method generates fibre-free, resin-rich regions in the laminates. Both methods have negative effects on the failure response of the structures when compared with idealised designs. This is because

manufacturing characteristics such as course edges, tow-drops and overlaps may act as discontinuities and stress concentration zones that locally excite the interlaminar stresses further, similarly to mechanisms triggered close to material discontinuities such as free edges, e.g. in holes, notches and ply drop-offs. Although many researchers have paid their attention to the analysis of VSP, the knowledge about the variable-stiffness configurations that lead to the highest ultimate loads is still rather limited. Furthermore, the full details of the mechanisms that lead to failure of VSP are not yet fully understood, particularly the influence of local effects such as tow-drops or tow overlaps. This is because these local effects require an accurate finite element modeling that is not of easy conception using customary procedures.

Interlaminar stresses are continuous both across and along layer interfaces in multilayer composite laminates. Nonetheless, the continuity of interlaminar stresses is difficult to enforce in C^0 interpolated elements. Nodal values of the stresses are usually retrieved using extrapolation techniques from Barlow or super-convergent points, if known, inside the element, i.e. Gauss points for Lagrangian class of elements. Stress fields within an element can be deduced using either constitutive relations or variationally consistent procedures. In either case, spurious oscillations in stress fields may be encountered leading to a reduced accuracy of the recovered stresses at nodes. Moreover, inaccuracy in the recovered interlaminar stress distributions may be obtained at the interfaces between the layers in the case of high transverse stress gradients.

The main goal of the research reported in this thesis was to develop a three-dimensional finite element computational strategy for reliable future stress analyses of variable stiffness panels. The procedure had also to be able to overcome the aforementioned problems that would be encountered in the modeling and analysis of such laminates using customary procedures. In particular, the procedure had to be conceived in such a way that areas where the failure initiation is primarily due to delamination, such as tow-drop resin-rich and overlapping-tows areas, can be easily modeled and analysed without the need to employ finite element models requiring demanding computational resources.

A sound technique for a proper modeling of such laminates might be to mesh the complete variable stiffness laminate by simulating the procedure followed during the manufacturing process by the tow-placement machine's head. This means that a proper mesh can be inherently adopted in each course based on the assumed construction method. A finite element pre-processing procedure was then developed based on this idea. The starting point of the procedure is to partition a tow-steered laminate in such a way that every ply can be considered to be an independent subdomain. In this manner, the user is enabled to decide the most adequate method to generate the mesh in every single ply. Compatibility between the subdomains was reestablished using Lagrange multipliers. Then, the final system of governing equations was solved using a procedure for distributed computing generally employed in domain decomposition methods, i.e. the finite element tearing and interconnecting (FETI) method. The simultaneous use of multiple compute resources to solve a computational problem, i.e. parallel computing, definitely broaden the range of applications of the proposed procedure. In particular, the choice to implement the FETI method was due to its parallel scalability and its ability to outperform several popular direct and iterative algorithms on both sequential and parallel computers.

The FETI method was also particularly suitable to be combined with a post-processing stress recovery procedure developed to retrieve accurate nodal values of the interlaminar

stresses. The proposed interlaminar stress recovery procedure does not rely on extrapolation techniques from super-convergent or integration points, commonly adopted in customary procedures instead. Interlaminar stress values are retrieved directly at nodes and stress continuity at the inter-element boundary is automatically satisfied. The complete stress states were obtained by employing a variational consistent recovery procedure for the recovery of the in-plane stress distributions. The complete procedure was developed within the MATLAB framework, and validated by analysing moderately-thick/thin conventional straight fibers composite plates of various geometries. The results were compared with available exact and finite element solutions. Conforming meshes between the plies were considered. Excellent agreement was obtained with available exact solutions, and convergence was reached using considerably fewer degrees of freedom compared to other finite elements procedures. The proposed procedure was able to generate a minimum percentage reduction of 72% in the total number of degrees of freedom required to achieve accurate interlaminar stress distributions compared to other finite element formulations. It was also shown that smooth distributions were easily generated without the need to employ smoothing techniques, as usually required when using customary stress recovery procedures. Moreover, the procedure was shown to be as accurate as assumed stress methods without the need to include stress degrees of freedoms in the solution process. The procedure was also combined with a failure stress criterion available in the open literature to determine onset of delamination in areas where singular stress states are generated. Special emphasis was placed on the problem of a loaded plate with an open circular hole. Despite the presence of oscillations in the interlaminar stress distributions encountered close to the hole edge, the present procedure could be used to produce convergent averaged interlaminar stresses over a distance from the hole edge. Then, the procedure could be effectively combined with an average failure stress criterion to predict delamination initiation in presence of curved free edges and stress concentrations. In this case, the minimum percentage reduction in the total number of degrees of freedom required to achieve accurate interlaminar stress distributions was reduced to around 23% compared to other finite element formulations.

The developed post-processing procedure was also combined with the commercial finite element software ABAQUS 6.8TM with the aim of broadening the applicability of the method to general 3-D shell type structures. Moderately-thick/thin conventional straight fibers composite plate and shell laminates of various geometries were analysed. The finite element model was generated within the ABAQUS framework, and compatibility between the layers was reestablished using a contact formulation available in ABAQUS instead of the FETI method. Conforming meshes between the laminates were initially considered. The finite element model was obtained using ABAQUS's built-in solid *C3D8I* element. The excellent results obtained for plate laminates were also confirmed for shell laminates. In particular, the proposed procedure was able to improve considerably the accuracy of the stress distributions obtained using ABAQUS's built-in *C3D8I* element. Smooth and accurate interlaminar stress distributions were obtained using a considerable reduced number of degrees of freedom, especially in the analyses of multilayered shell structures, even compared to ABAQUS's built-in quadratic formulations. The proposed procedure was able to generate a minimum percentage reduction of 77% in the total number of degrees of freedom required to achieve accurate interlaminar stress distributions compared to ABAQUS's formulations that still failed to converge.

The idea of meshing a complete variable stiffness laminate by simulating the procedure

followed by the tow-placement machine's head during the manufacturing process inevitably leads to the generation of non-conforming meshes between the plies. Then, analyses employing non conforming meshes between the plies were also considered. These analyses were performed within ABAQUS's framework. Plies with a regular mesh composed of *C3D8I* elements were alternated at plies meshed using a combination of linear brick *C3D8I* elements and linear triangular prism *C3D6* elements. The triangular prism *C3D6* element was employed because it might be particularly suitable for modeling both the areas close to the sides of a variable stiffness panel and the resin-rich areas generated during the manufacturing procedure of such laminates. Then, the *C3D6* element needed to be tested in combined use with ABAQUS's *C3D8I* element, which was shown to be a sound element for the modeling of composite laminates elsewhere. Oscillatory behaviours were encountered in the retrieved transverse stress distributions. Thus, inaccurate nodal values of the interlaminar transverse stresses were obtained. However, these oscillations showed the same trends of the distributions obtained using conforming meshes, that were taken as reference solutions. An averaging technique was developed to smooth out these distributions. The developed technique consists of averaging the stress values obtained in each node with the stress values obtained in the nodes of the surrounding elements sharing the node under consideration. In general, smooth and accurate distributions were obtained by using the proposed averaging technique within three-four iterations for both plates and shell laminates. However, much more refined meshes had to be adopted compared to the case employing conforming meshes between the plies. Moreover, inaccuracies in the retrieved transverse stress distributions were generated close to the boundaries of the laminates.

Future research should first focus on improving the proposed method for analyses employing non-conforming meshes between the plies of conventional composite laminates. It is extremely necessary to pay attention to this aspect before moving to the analysis of VSP. In fact, the demanding computational resources required, and the inaccuracies generated close to the boundaries of conventional laminates make the proposed procedure not enough accurate for reliable interlaminar stress analyses of VSP. Moreover, interlaminar stress analyses of VSP would not bring in at this stage of the work any additional understanding concerning the accuracy of the procedure in the analysis of such laminates. This is also because no comparison with available interlaminar stress data can be made. Attention should be also paid to non-linear analyses of conventional composite laminates.

Analyses of tow-steered laminate configurations can then be performed once the required improvements are introduced in the proposed procedure. Variable stiffness laminates with tow-drops should first be taken into account. The procedure might also be easily extendible to the analysis of variable stiffness panels with overlaps. This is because the resin-rich areas generated by the overlap between two courses can be modeled using the same triangular prism elements adopted for the analysis of the tow-drop areas. However, additional validation of the proposed method is required in this direction. The proposed procedure combined with integrating geometric design tools such as CATIA and fiber placement simulation software might be the right tool for an accurate design of a variable stiffness laminate.

Samenvatting

Het volledige potentieel van geavanceerde composieten kan alleen worden bereikt door een laminaat op maat te maken voor een specifieke toepassing. Op deze manier is het mogelijk om adequater in te spelen op spanningsvariaties in het vlak en is het mogelijk om krachten om de meest gevoelige gebieden van een composieten constructie heen te leiden, waarbij te denken valt aan gaten en inkepingen. Een methode voor het op maat maken van een composiet laminaat is het gebruik van niet-conventionele laminaten. De aanduiding niet-conventionele laminaten verwijst naar twee soorten configuraties: (i), laminaten die uitgaan van het hele scala aan mogelijke vezelorientaties, en (ii), composiet panelen met een lay-up waarvan de vezelhoekorientatie continu verandert van punt naar punt. Een continu wisselende lay-up wordt gerealiseerd met behulp van niet-traditionele gebogen vezel paden binnen het vlak van een laag en biedt meer ontwerpvrijheid dan de eerste optie (i), voor het geval dat de spanningstoestand in elke laag van het laminaat varieert. In dergelijke gevallen varieert de stijfheid van het laminaat ook met de coördinaten in het vlak van het laminaat. Daarom zullen in deze tekst dergelijke laminaten aangeduid worden als variabele stijfheid panelen (VSP).

Vezelgestuurde laminaatontwerpen stellen hoge eisen aan de nauwkeurigheid van het vezelplaatsingssysteem. Handmatige productiemethoden zullen niet kunnen voldoen aan de vereiste nauwkeurigheid bij het leggen van vezels onder de juiste hoeken en het behouden van deze hoeken bij het uitharden van het laminaat. Bovendien moet rekening gehouden worden met de variatie van de kwaliteit van het laminaat, die ten gevolge van het handmatige productieproces optreedt. Geautomatiseerde productieprocessen zijn in staat om onderdelen van consistente en betere productiekwaliteit te fabriceren tegen een lagere productietijd. Tow-Placement (TP) technologie neemt een speciale plaats in onder de geautomatiseerde productiemethoden die beschikbaar zijn in de lucht-en ruimtevaartindustrie. Deze technologie combineert vrijheid in vezelhoevervariatie van filamentwikkelen en de compressie en stop-herstart mogelijkheden van geautomatiseerd tape-leggen. Een TP-machine is een hoge-precisie robot, met een grote bewegingsvrijheid, die in staat is computergestuurd composieten componenten te produceren zonder menselijke tussenkomst: TP-technologie stelt ons in staat om componenten te ontwerpen en te produceren die zeer moeilijk of zelfs onmogelijk te produceren zijn door middel van andere geautomatiseerde productiemethoden.

Het potentieel van vezelgestuurde laminaten leidde tot de opkomst van een nieuwe tak in het onderzoek naar gelaagde composietmaterialen gericht op het goed modelleren en voorspellen van de respons van dergelijke laminaten. Een VSP heeft, per definitie, een niet-uniforme stijfheidsverdeling in het vlak die zou kunnen resulteren in grote spanningsvari-

aties in het vlak. Dergelijke gradienten dragen bij aan de versterking van de interlaminaire spanningen en zorgen er mogelijk voor dat delaminatie het dominante bezwijkmechanisme wordt voor dergelijke configuraties. Bovendien is bij de productie van VSP het overlappen van een aantal plies of het beëindigen van tows binnen een laag (afvallen) haast onontkomelijk. Overlappende tows resulteren in een toename van de laminaatdikte, terwijl het laten afvallen van een tow leidt tot vezelvrije, harsrijke regio's in het laminaat. Beide methoden hebben een negatief effect op het bezwijkmechanisme van een constructie in vergelijking met het ideale geval. Dit komt omdat de productietekenen zoals de randen van tow-paden, het afvallen van tows en overlappings kunnen resulteren in discontinuïteiten en spanningsconcentraties die lokaal de interlaminaire spanningen doen toenemen, en voorts op dezelfde manier het bezwijkmechanisme op gang brengen, op een vergelijkbare wijze als voor vrije randen, zoals bijvoorbeeld bij gaten, inkepingen en het laten afvallen van tows. Hoewel veel onderzoek geweid is aan de analyse van VSP, is de kennis over variabele stijfheid configuraties die leiden tot de hoogste bezwijkwaarden is nog tamelijk beperkt. Bovendien zijn de volledige details van de mechanismen die leiden tot het falen van VSP nog niet volledig begrepen, met name de invloed van lokale effecten, zoals het laten afvallen van tows of het overlappen daarvan. Dit komt omdat een passend eindig elementen model van dergelijke panelen dat de genoemde lokale fenomenen in kan vangen niet gemakkelijk te verkrijgen is met behulp van gebruikelijke methodes, zelfs niet wanneer een beroep wordt gedaan op rekentechnisch veeleisende eindige elementen modellen.

Interlaminaire spanningen zijn continu zowel in als langs laaginterfaces in meerlagige composiet laminaten. Niettemin, is de continuïteit van interlaminaire spanningen moeilijk af te dwingen in C^0 geantepoleerd elementen. Nodale waarden van de spanningen worden doorgaans verkregen met behulp van de extrapolatietechnieken van Barlow of superconvergente punten, indien bekend, in het element, dat wil zeggen Gauss punten voor elementen uit de Lagrange klasse. Spanningsvelden binnen een element kunnen worden afgeleid met behulp van constitutieve relaties of variationeel consistente procedures. In beide gevallen kunnen valse variaties in de spanningsvelden optreden, hetgeen leidt tot een verminderde nauwkeurigheid van de verkregen spanningen voor nodes. Als bovendien een door-de-dikte mesh van het laminaat wordt gebruikt dat niet voldoende verfijnd is in combinatie met hoge transversale spanningsgradienten, kunnen er onnauwkeurigheden in de verkregen spanningsverdeling op de interface tussen de lagen optreden.

Het belangrijkste doel van het onderzoek beschreven in dit proefschrift was het ontwikkelen van een drie-dimensionale eindige elementen rekenstrategie die geschikt is om betrouwbare toekomstige spanningsanalyses van variabele stijfheid panelen uit te voeren, en die in staat is om de bovengenoemde problemen die zich zouden kunnen voordoen in het modelleren en analyseren van dergelijke laminaten met behulp van de gebruikelijke procedures te overwinnen. De procedure moest vooral zodanig worden opgezet dat gebieden waar het bezwijkmechanisme ingang wordt gebracht door delaminatie te kunnen modeleren en analyseren, zoals gebieden waar tows afvallen, die harsrijk zijn of waar tows overlappen, zonder daarbij rekentechnisch veeleisende eindige elementen modellen te gebruiken. Aandacht werd besteed aan de ontwikkeling van de procedure voor de analyse van VSP met afgevallen tows, maar de procedure is ontworpen op een dusdanige wijze dat het concept eenvoudig is uit te breiden naar de analyse van VSP met overlappings.

Een gedegen techniek voor een goede modellering van dergelijke laminaten zou kunnen zijn om het volledige variabele stijfheids laminaat te meshen op een manier die de afgelegde

paden van de tow-placementmachine tijdens het productieproces simuleert. Dit betekent dat een inherent goede mesh gebruikt kan worden voor elk towpad gebaseerd op de veronderstelde bouwmethode. Een eindige elementen pre-processing procedure is vervolgens ontwikkeld op basis van dit idee. Het uitgangspunt van de procedure is de partitie van een tow-gestuurd laminaat op een dusdanige wijze dat elke laag kan worden beschouwd als een onafhankelijke subdomein. Op deze wijze, de gebruiker voor iedere ply beslissen wat de beste methode is om het mesh te genereren. Compatibiliteit tussen de subdomeinen werd hersteld met behulp van Lagrange multipliers. Vervolgens werd de definitieve stelsel geldende vergelijkingen opgelost met behulp van een procedure voor distributed computing, normaal gesproken toegepast voor domein decompositie methoden, d.w.z. de eindige elementen scheur- en verbindmethode (FETI). Het gelijktijdig gebruiken van meerdere rekenmethoden om een rekenprobleem op te lossen, d.w.z. parallel computing, verbreden hoe dan ook het scala van toepassingen van de voorgestelde procedure. De keuze om de FETI methode toe te passen was vooral gebaseerd op de parallele schaalbaarheid die deze methode biedt en het feit dat deze methode beter presteert dan populaire iteratieve algoritmes zowel sequentiale en parallele computers.

De FETI methode is ook bijzonder geschikt om te worden gecombineerd met een post-processing procedure die ontwikkeld is om nauwkeurige nodale waarden van de interlaminaire spanningen te kunnen verkrijgen. De voorgestelde interlaminaire het herstelprocedure voor de spanningen doet geen beroep op extrapolatietechnieken van super-convergente of integratie punten, zoals meestal het geval is voor gebruikelijke procedures. Interlaminaire spanningswaarden worden direct van de nodes verkregen en aan de spanningscontinuïteit op de inter-elementgrens wordt automatisch voldaan. De volledige spanningsstaat werd verkregen door het ophalen van de spanningsverdeling in het vlak met behulp van variationele consistente herstelprocedures. De volledige procedure werd ontwikkeld in MATLAB, en gevalideerd door het analyseren van matig dikke/dunne conventionele composieten platen met rechte vezels van verschillende geometrien. De resultaten werden vergeleken met de beschikbare exacte en eindige elementen oplossingen. Conforme meshes tussen lagen verkregen met behulp van een lineaire solid-shell element werden beschouwd. Goede overeenkomst met exacte oplossingen werd bereikt, en convergentie werd bereikt met aanzienlijk minder vrijheidsgraden in vergelijking met andere eindige elementen procedures, waardoor de procedure meer geschikt is voor ontwerpdoeleinden. Er werd ook aangetoond dat een geleidelijke verdeling eenvoudig werd gegenereerd, zonder de noodzaak om smoothing technieken te gebruiken, zoals gewoonlijk vereist is bij gebruik van de gebruikelijke spanningsherstelprocedures. Bovendien werd aangetoond dat de procedure net zo nauwkeurig is als de veronderstelde spanningsmethoden met behulp van grovere meshes, en zonder de noodzaak spanningsvrijheidsgraden mee te nemen in de oplossing. De procedure werd ook gecombineerd met een spanningsbezwijkcriterium, beschikbaar in de open literatuur, om het begin van delaminatie te bepalen in gebieden waar een enkelvoudige spanningstoestand heerst. Bijzondere nadruk werd gelegd op het probleem van een belaste plaat met een open rond gat. Ondanks de aanwezigheid van oscillaties in de interlaminaire spanningsverdeling dicht bij de rand van het gat, kon de huidige procedure worden gebruikt om convergerende gemiddelde interlaminaire spanningen te verkregen op een afstand van het gat. Vervolgens kon de procedure effectief gecombineerd worden met gemiddelde spanningsbezwijkcriteria om het begin van delaminatie in de nabijheid van een vrije gekromde rand te voorspellen.

De ontwikkelde post-processing procedure werd ook gecombineerd met het commerciële eindige elementen softwarepakket ABAQUS 6.8TM met als doel de toepasbaarheid van de methode te verruimen naar generieke 3-D schaalstructuren. Matig dikke/dunne composieten platen en schalen met rechte vezels van verschillende geometrieën werden geanalyseerd. In dit geval werd het eindig elementen model gegenereerd in ABAQUS, en de compatibiliteit tussen de lagen werd verkregen met behulp van een contactformulering beschikbaar in ABAQUS. Conforme meshes werden aanvankelijk beschouwd tussen de laminaten. Het eindig elementen model werd verkregen met behulp van het ingebouwde vaste ABAQUS *C3D8I* element. De voordelen van de voorgestelde procedure voor de eerder genoemde plaatlaminaten werden ook bevestigd voor schaalaminaten. De voorgestelde procedure was in het bijzonder in staat om een aanzienlijke verbetering van de nauwkeurigheid van de respons te bewerkstelligen voor het ABAQUS *C3D8I* element in vergelijking tot de in ABAQUS ingebouwde spanningsherstelprocedure. Gladde en nauwkeurige interlaminaire spanningsverdelingen werden verkregen met een aanzienlijke kleiner aantal vrijheidsgraden, met name voor meerlaagse schaalconstructies, zelfs in vergelijking met de in ABAQUS ingebouwde kwadratische formuleringen.

Het meshen van een volledig variabele stijfheidslaminaat door het simuleren van het proces dat door de kop van een tow-placement machine doorlopen wordt tijdens productie leidt onvermijdelijk tot niet-conforme meshes tussen de lagen in het laminaat. Niet-conforme meshes tussen de lagen werden ook onderzocht in de procedure met het gecombineerde gebruik van de eindige elementen commerciële software ABAQUS 6.8TM gebruikt als pre-processor, en de voorgestelde post-processing procedure ontwikkeld in MATLAB. Lagen met een regelmatig mesh bestaand uit *C3D8I* elementen werden afgewisseld met lagen met een mesh gecombineerd uit lineaire baksteen *C3D8I* elementen en lineaire driehoekige prisma *C3D6* elementen. Het driehoekige prisma *C3D6* element werd geïntroduceerd, omdat het bijzonder geschikt is voor het modelleren van gebieden dicht bij de zijanten van een variabele stijfheids panel en hars-rijke gebieden die tijdens het fabricageproces van een variabele stijfheids paneel ontstaan. Vervolgens, werd het gebruik van *C3D6* elementen getest in combinatie met ABAQUS' *C3D8I* elementen, en het werd aangetoond dat het toelaatbaar is deze elementen ook elders in de constructie toe te passen. Variaties in de verkregen dwarsspanningsverdeling werden waargenomen. Hierdoor werden onnauwkeurige waarden voor de interlaminaire dwarsspanning verkregen. Deze variaties vertoonden echter dezelfde trends als de verdelingen die worden verkregen door middel van conforme meshes, die als referentie oplossingen genomen werden. Een middelingstechniek werd ontwikkeld deze verdelingen geleidelijker te maken. De ontwikkelde techniek middelt de in elke node verkregen spanningswaarden met die van de spanningswaarden van de nodes van omringende elementen die dezelfde node delen. Over het algemeen werden met behulp van de voorgestelde middelingstechniek gladde en nauwkeurige verdelingen verkregen binnen drie tot vier iteraties voor zowel plaat- als schaalaminaten. De meshes moesten echter veel fijner zijn dan het geval was voor conforme meshes, en voor sommige van de dwarse spanningscomponenten traden er onnauwkeurigheden op in de gegenereerde spanningsverdelingen dicht bij de randen van het laminaat. De componenten waarvoor deze onnauwkeurigheid optreedt verschillen per probleem, dat wil zeggen randvoorwaarden, belastingen, etc.

Toekomstig onderzoek zal zich moeten richten op de verbetering van de methode voor de niet-conforme meshes, op het uitvoeren van niet-lineaire analyses van conventionele

rechte vezel composiet laminaten, en op het uitvoeren van analyses van de vezel-gestuurde laminaatconfiguraties. De ontwikkelde methode in dit proefschrift is rechtstreeks van toepassing voor het analyseren van VSP met afvallende tows, maar de methode kan worden uitgebreid om variabele-stijfheids panelen met overlappingen te analyseren. Dit komt omdat de hars-rijke gebieden in het laminaat, vanwege de overlap tussen twee paden, kunnen worden gemodelleerd met behulp van dezelfde driehoekige prisma elementen als gebruikt voor laminaten met afvallende tows, maar wel anders georiënteerd in de globale mesh. Aanvullende analyses zijn echter nodig om de methode voor de analyse van de VSP te valideren.

Acknowledgements

It was a great opportunity for me to join the group of aerospace structures at TU Delft in June 2006. In this regard, the financial support for this Ph.D. effort by TU Delft is gratefully acknowledged. I am thankful to my promoter, Prof. Dr. Zafer Gürdal, who offered to me this opportunity, believed in me, advised me and supported me even in the difficult moments. I am also very thankful to my daily supervisor, Dr. M.M. Abdalla. During this incredible experience I was always been very proud to be able to daily work with him, and to have the great opportunity to improve my knowledges and technical skills thanks to his unlimited knowledges and availability. Moreover, with his natural behaviour and humour he was kind enough to nurture a relation beyond strict professional lines. I also acknowledge my colleagues and friends for the wonderful working environment. In particular, I want to thank my office mates whom were supportive of me even when I was stressed out and not in a good mood.

I address special thanks to Jan Hol, who was involved in the resolution of issues related to the computational resources required for the numerical simulations, and others. I am very thankful to Miranda Aldam-Breary for helping me to write this thesis in a proper English, in particular for her patience and availability. I am also grateful to Eddy Van Den Bos for the help with Catia's drawings, and to Julien Van Campen for the Dutch translation of the summary of this thesis, i.e. Samenvatting. I shall also not forget the help of Annemarie Van Lienden, Angela De Gier and Laura Chant with all the paperwork required for different subjects during these years. In particular, I am very thankful to Laura Chant because she helped me even beyond her duties. Laura's help had great consequences during the last year of my experience at TU Delft.

The elaboration of this thesis was helped by the contribution of Prof. Dr. D.J. Rixen from the Department of Precision and Microsystems Engineering of TU Delft on the development and coding of the Finite Element Tearing and Interconnecting Method for parallel computing. I am also very grateful for the advise and help of Christos Kassapoglou, Agnes Blom, Attila Nagy, Sam Ijsselmuiden and Claudio Lopes in various subjects covered by this thesis.

I am also very grateful to SIMULIA B.V. for covering part of the printing cost of this thesis and their interest in my work.

Finally, I am grateful to my family which has always believed in me. Without their support and help since the beginning of my academical path I would not have had the opportunity to realize my dream to become an aerospace engineer and, almost, a doctor in aerospace engineering. My last thanks are for Myriam, who has shared with me the last nine month of this experience. She has been supportive and patient in the final stages of my work, and she has motivated me to do better and better. She is the woman that makes me a

better man. Thank you! I dream of a great future with you.

Christian
Delft, October 2010

Contents

Summary	i
Samenvatting	v
Acknowledgements	xi
Table of Contents	xiii
1 Introduction and Objectives	1
1.1 Lightweight Structures	1
1.2 Non-Conventional Laminates	2
1.3 Tow-Placement Technology	3
1.4 Tow-Steered Laminates	5
1.5 Structural Response	8
1.5.1 Stiffness and Buckling Performance	9
1.5.2 Failure Performance	10
1.5.3 Computational Modeling of Manufacturing Characteristics	11
1.6 Thesis Objectives and Outline	12
2 Theories for Multilayered Anisotropic Composite Structures	17
2.1 Introduction	17
2.2 Anisotropy's Effects on Layered Structures	18
2.3 Strategies for the Development of Plate/Shell Theories	20
2.3.1 Available 2D Approaches	20
2.3.2 Displacement and Mixed Formulations: Variational Statements	22
2.3.3 Multilayered Form Description: Classical Equivalent Single Layer Theories and their Refinements	23
2.3.4 Layer-Wise Theories	29
2.3.5 Zig-Zag Theories	31
2.4 Conclusions	34
3 Stress Recovery Techniques	37
3.1 Introduction	37
3.2 Stress Recovery Techniques for Displacement Based Finite Elements	38
3.3 Mixed Formulations as Stress Recovery Techniques	46

3.3.1	Hellinger-Reissner Functional	46
3.3.2	Hu-Washizu Functional	48
3.3.3	Enhanced Assumed Strain Method	50
3.4	Conclusions	53
4	A Finite Element Procedure for Interlaminar Stress Analyses	55
4.1	Introduction	55
4.2	Finite Element Model	56
4.3	Parallel Computing	64
4.3.1	FETI Method	66
4.4	Variationally Consistent Stress Recovery Procedure	68
4.5	Interlaminar Stress Recovery Procedure	71
4.6	Numerical Results	73
4.6.1	Simply Supported Plate Subjected to Bisinusoidal Pressure Load . .	73
4.6.2	Stress Analyses of Laminated Composite Plates with Open Hole Subjected to Uniaxial Tension	87
4.7	Conclusions	100
5	Interlaminar Stress Analyses of Multilayered Laminates having Non-Conforming Meshes between the Plies	101
5.1	Introduction	101
5.2	Interlaminar Stress Recovery Procedure	102
5.3	Numerical Results	105
5.3.1	Simply Supported Plates Subjected to Bisinusoidal Pressure Load .	105
5.3.2	Varadan and Bhaskar's Cylindrical Shells	113
5.3.3	Spherical Curved Surfaces	124
5.4	Conclusions	131
6	Recommendations and Future Developments	133
6.1	Pre-Processing Procedures	133
6.2	Post-Processing Procedure	136
6.3	Future Challenges	137
	Bibliography	139
	Curriculum Vitae	153

Chapter 1

Introduction and Objectives

1.1 Lightweight Structures

The unrelenting passion of the aerospace industry and manufacturers to enhance the performance of aircraft is constantly driving the development of improved, high performance structural materials. In particular, with the increasing costs of energy, there is pressure to produce lighter structures and, in response to this, composite materials have come to play a significant role in current and future aerospace components. Composite materials are particularly attractive for aviation and aerospace applications because of their exceptional strength and stiffness-to-density ratios. Another advantage of composite materials is that they can be formed into more complex shapes than their metallic counterparts. This reduces the number of parts needed to make a given component, and reduces the need for fasteners and joints. There are two main advantages to this: (i), fasteners and joints can be the weak points of a component due to stress concentration and reducing the need for fasteners and joints reduces the number of potential crack-initiation sites on a structure, and (ii), fewer fasteners and joints leads to shorter assembly times and thus cost savings.

A composite material typically consist of relatively strong, stiff fibres in a tough resin matrix. Wood and bone are natural composite materials. Some well known man-made composite materials are Fibre Reinforced Plastics (FRP): FRP offer the best values of specific stiffness (stiffness/density) and specific strength (strength/density) amongst engineering materials. All FRP are advanced composites where long fibres, e.g. glass - GFRP, carbon - CFRP, are embedded in a polymer matrix. Characterised by high stiffness and strength, the role of the fibers is to reinforce the relatively low-strength matrix. Therefore, it is possible to combine the properties of a lightweight matrix with those of the strong fibres. Overall, this technique results in a lighter material than its monolithic counterparts, e.g. metal, while still maintaining high-stiffness and high-strength properties along a predetermined direction, the direction of the fibers. Fibrous composites are anisotropic, i.e. their properties vary depending on the direction of the load with respect to the orientation of the fibres. This anisotropy is overcome by stacking layers, each one often only fractions of a millimeter thick, with the fibres oriented at different angles to form a laminate. Specific stiffness properties of a laminate can be achieved by stacking the differently oriented layers in a specific sequence to tailor the properties of the laminate to withstand the loads optimally, therefore achieving

the best structural performance.

Practical considerations have dictated that the design variables of conventional laminates are reduced to the number of plies, the fibre angle within each ply and the stacking sequence in the design of composite laminates. Moreover, the fibre angles are often chosen from a small number of discrete values: 0° , 90° , $\pm 45^\circ$. Within this conventional design practice the design space results rather limited because it only allows for configurations with constant properties along the laminate planar dimensions. Consequently, it is not possible to tailor a panel to respond in the most efficient manner to non-uniformly distributed in-plane stresses, for example those caused by holes and notches.

The full potential of advanced composites can only be achieved by tailoring a laminate to each specific structural application. In this way, it is possible to respond more adequately to planar stress variations and it is possible to divert loads from the most sensitive regions of a composite structure such as holes and notches: e.g. Biggers and Srinivasan (1993) and Biggers and Pageau (1994) tailored laminates by positioning unidirectional lamina through the thickness and over the planform of rectangular plates to create beneficial stiffness patterns against compression and shear buckling. This solution can lead to stress concentrations and delaminations. DiNardo and Lagace (1989) achieved in-plane laminate tailoring by dropping off plies. In their work, experimental and analytical investigations have shown that ply dropoffs have a marked effect on plate buckling and postbuckling behaviour. Another method of tailoring a composite laminate is to use *non-conventional laminates*.

1.2 Non-Conventional Laminates

The designation *non-conventional laminates* refers to two types of configurations: (i), laminates that explore the whole range of possible ply orientations, and (ii), composite panels with lay-ups that vary continuously from point to point. A continuously varying lay-up is achieved using non-traditional curvilinear fiber paths within the plane of a ply. In such cases, the laminate stiffness also varies with the in-plane coordinates of the laminate, hence these configurations are termed Variable-Stiffness Panels (VSP). The illustration in Figure 1.1 shows that at each point in the platform of a VSP there is a distinct, non-conventional, lay-up of type (i). One of the first theoretical investigations on the effects of tailoring elastic properties of laminates by varying the fibre orientations was carried out by Muser and Hoff (1982). These authors provide a closed-form solution for the stress concentration around a hole of an orthotropic plate subjected to uniaxial tension and containing a radial variation in elastic properties. Their analysis shows that the introduction of a $\pm 45^\circ$ fiber arrangement in the vicinity of the hole, that gradually varies to a quasi-isotropic lay-up at the outer edges of the plate, is very effective for reducing stress concentrations. Yau and Chou (1988) inserted metal pins into woven-fabric composite laminates prior to curing, effectively pushing the fiber tows apart to create a molded hole. This was designed to reduce the sensitivity to open holes compared to similar laminates used with drilled holes. The resulting laminates possessed curvilinear fibers around the hole and exhibited improved open-hole strength.

Hyer and Charette (1991) applied the concept of curvilinear fibers to a plate with a central hole. According to them, a gain in structural efficiency can be achieved by aligning the fibers in some, or all of the layers, in a laminate with the principal stress directions in those layers. The stress-based Tsai-Wu failure criterion (Tsai and Wu, 1971) applied on a Finite

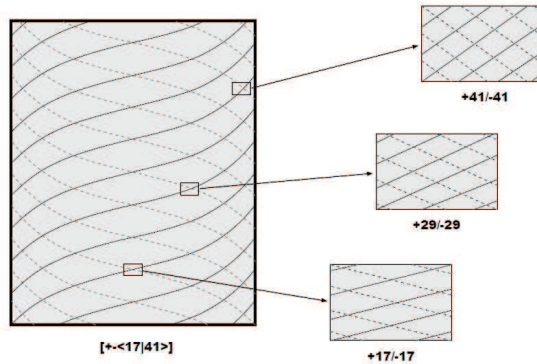


Figure 1.1: Example of a 2-ply VSP.

Element (FE) solution predicted marked improvement of the failure behaviour of these panels over their traditional, straight-fibre counterparts. Although the tension behaviour was improved with the variable fibre-orientation format, the same tendency was not observed with respect to the buckling response. In a follow-up work by Hyer and Lee (1991), both a sensitivity analysis and a gradient search technique were employed, leading to increased buckling loads compared to the traditional straight-fiber design. It was shown that it is possible to place the fibers in such orientations that the loads are transferred away from the unsupported hole region of the plate to the supported edges, thus increasing the buckling capacity. It was also shown that combining both straight and curvilinear fibre plies within a laminate, resulting in *hybrid laminates*, produced the best buckling and failure results.

Other examples of fiber orientation angle tailoring include theoretical and numerical studies have been done by Banichuk (1995), Pedersen (1991), Duvaut et al. (2000), Crothers et al. (1997). The motivation of these studies was the optimisation of the spatial variation of fibre orientation within the domain of a composite panel to improve its stiffness, buckling or strength characteristics.

1.3 Tow-Placement Technology

The fibre-steered laminate designs discussed in the previous section require an accurate fibre placement system. Hand laying methods would not provide the required precision for laying the fibres at the correct angles and keeping these angles during curing. Moreover, variability in quality resulting from the manual process has to be addressed. Automated fabrication processes are able to provide repeatable and improved quality component production with a reduced production cycle time.

Filament winding is a traditional automated method where a pressure vessel can be fabricated by winding strands or tows of fibers around a mandrel formed in the shape of the vessel (Mondo et al., 1997; Pasanen et al., 1997). Filament winding has also been successfully extended to stiffened structural components such as grid-stiffened panels and geodetically stiffened shells. Filament winding, however, has limitations in terms of the shapes that can be produced, which are basically restricted to convex geometries since a

concave surface would be bridged over because of the high tension necessary to hold the fibres in place.

Tow-Placement (TP) is a technology that combines the differential tow payout capability of filament winding and the compaction and cut-restart capabilities of automated tape laying (Gürdal et al., 2005). A TP machine is a high-precision robot, capable of wide freedom of movement, and computer controlled to produce a composite component without human intervention (Bullock et al., April 1990; Enders and Hopkins, 1991): TP technology allows the design and production of components that would be extremely difficult or even impossible with other automated methods. In the TP process, individual prepreg tows are fed through a fibre delivery system (Figure 1.2(a)) into a fibre placement head (Figure 1.2(b)) and grouped together to form a band of parallel fibers. A tow-placement head can

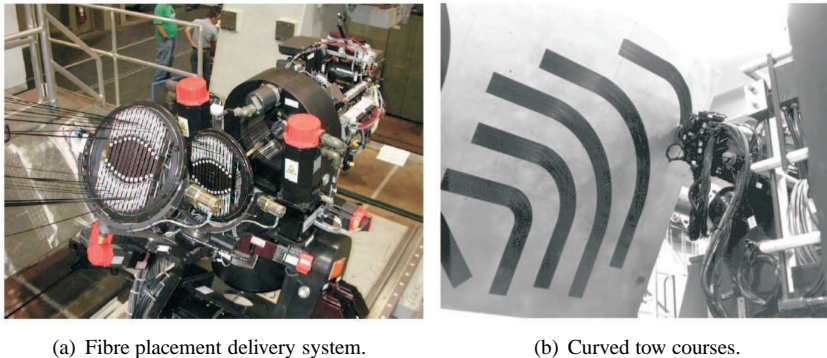


Figure 1.2: Fiber Placement (FP) technology: system characteristics (courtesy of Ingersoll Machine Tools (Ing)).

accommodate up to 32 tows. A typical tow placement head is shown in figure 1.3. When

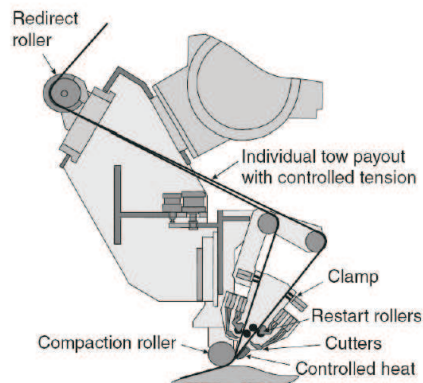


Figure 1.3: Typical tow-placement head (courtesy of Evans (2001)).

starting a course, the individual tows are fed through the head and compacted onto a surface. As the course is laid down, the processing head can cut or restart any of the individual tows.

Hence, the width of the fibre band can be increased or decreased allowing for the elimination of excessive gaps or overlaps between adjacent courses. At the end of the designed course, the remaining tows are cut to match the shape of the ply boundary. The range of motion described by the tow-placement head allows the tows to be aligned in any direction, therefore enabling the production of double-curved parts. Each tow is dispensed at its own speed during the placement of a course, allowing it independently to conform to the surface of the part. This different payout system enables the fibers to be steered in such a way that specified designs can be met, as shown in Figure 1.2(b), whereas filament winding and automated tape laying are confined to near geodesic path since they rely on the friction and the tension of the material to hold individual fibre paths in place. More technical information on TP technology and fabrication issues encountered during manufacture can be found in the work done by Gürdal et al. (2005) and Lopes (2009).

1.4 Tow-Steered Laminates

The potential of fibre-steered laminates led to the birth of a new branch of research in laminated composite materials aimed at properly modelling and predicting the responses of such laminates. A simple method of modelling complete tow paths was developed in the research initiated by Gürdal and Olmedo (Gürdal and Olmedo, 1993; Olmedo and Gürdal, 1992, 1993). The work led by Gürdal resulted in the formulation of a tow steered ply definition with a minimum number of parameters. A simple formulation is necessary for the attractiveness of the concept, and to allow for fast optimization algorithms to produce the best manufacturable structural design. Being manufacturable implies that the curvilinear ply paths can be fabricated using existing fibre placement technology, thus the range of possible designs is bounded by the constraints of the machine used.

In the formulation proposed by Gürdal and Olmedo (Gürdal and Olmedo, 1993; Olmedo and Gürdal, 1992, 1993), it is assumed that the fibre angle of a reference fibre path varied linearly from the value T_0 at a fixed position in the panel, typically its geometrical center, to T_1 at a specific distance d , as illustrated in Figure 1.4. This distance is often taken as a characteristic dimension of the composite panel being designed. Using this formulation the orientation of a single curvilinear fibre path can be denoted by $\langle T_0|T_1 \rangle$. This curve is the *reference path* for the course followed by the TP machine head when laying a band of tows. A more general fibre path definition can be achieved by rotating the axis of variation of the fibre orientation by an angle, ϕ , from the geometric axis of the panel. This rotation defines a new fibre orientation variation axis denoted by x' . According to the formulation, the fibre path defined by $\phi \langle T_0|T_1 \rangle$ varies linearly along the x' direction, rotated from the x -axis by an angle ϕ . In order to construct the remainder of the ply, Gürdal and Olmedo (Gürdal and Olmedo, 1993; Olmedo and Gürdal, 1992, 1993) suggested shifting the reference path in a direction perpendicular to its axis of fibre variation. This method gives increases of up to 50% in the axial stiffness and up to 80% in the critical buckling load of TP panels when compared to traditional straight-fibre laminates.

These theoretical benefits, e.g. those suggested by Gürdal et al. (2008), may be bounded by the real manufacturing conditions and limitations imposed by the TP machine (Gürdal et al., 2005). For instance, as a consequence of the discrete tow course shifting, the boundaries of constant-width neighbouring courses do not match for all locations along the x' -axis

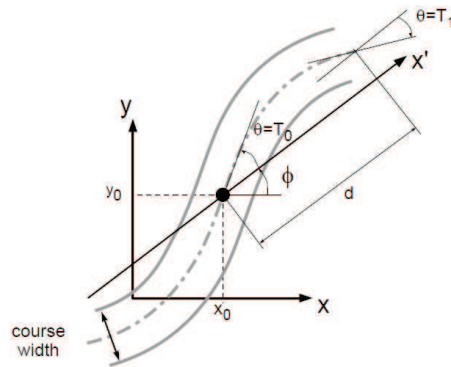


Figure 1.4: Linear fibre angle variation reference path.

and, consequently, areas having fibre gaps and/or tows overlapping each other are created. Allowing tows to overlap generates local thickness buildup, and this process is referred to as the *tow-overlap method*. This effect may not be desirable, for example, in parts that act as control surfaces, yet it can also be advantageous for other parts since these thicker regions can act as “*integral stiffeners*”.

Overlapping regions can be eliminated by using the tow-cutting and restarting capability of the TP machine. The tows are cut individually perpendicular to the fibre direction, resulting in a jagged edge. It is possible to determine the degree to which a smooth boundary is covered by the discrete tows of the course using a user-defined parameter furnished by the tow-placement software, referred to as the “*coverage parameter*” (Gürdal et al., 2005; Tattling and Gürdal, 2003). This process is referred to as the *tow-drop method*. Three examples are given in figure 1.5. For 0% coverage, each tow is cut so that its leading edge does not

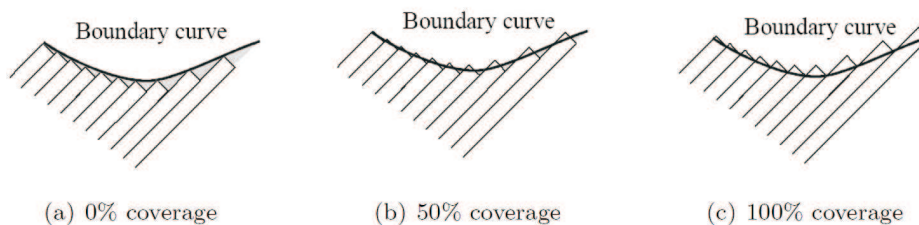


Figure 1.5: Tow-dropping with different coverage parameters (courtesy of Gürdal et al. (2005)).

extend past the limiting curve. This results in a small fibre-free triangular area that is likely to be filled with resin during curing, therefore creating a “*resin rich*” region which may be termed a *tow-drop area*. A constant thickness fibre-steered laminate can be produced by applying this technique. This scenario is displayed in Figure 1.6 where a close-up of an overlap region and the tow-dropping that occurs is highlighted. At 100% coverage, the tow is cut only when both tow-edges cross the boundary, creating a small triangular overlap area.

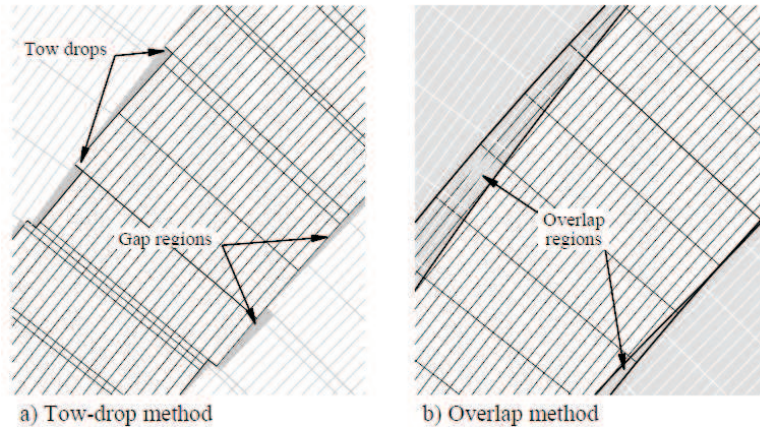


Figure 1.6: Close-ups of overlap regions using both shifted methods (courtesy of Gürdal et al. (2005)).

Intermediate values contain both gaps and small thickness variations. Examples of panels manufactured by the tow-drop and tow-overlap methods are shown in figure 1.7.

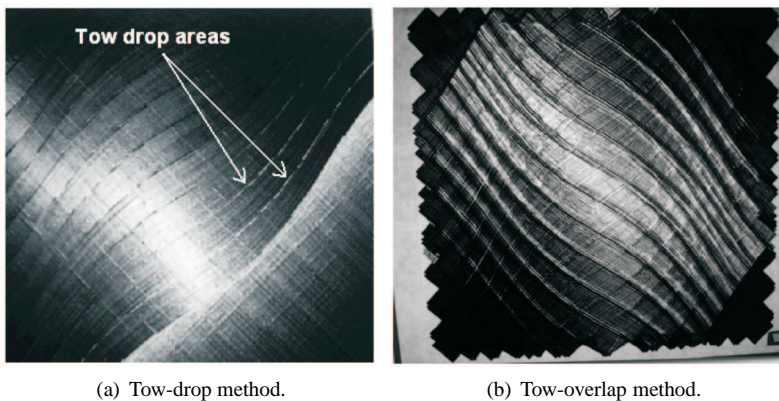


Figure 1.7: Examples of tow-steered composite panels manufactured according to two fabrication methods.

The effects of manufacturing issues on the laminate response, such as tow-drops and tow overlaps, constraints of fabrication, addressed in detail in the work of Gürdal et al. (2005), and the residual thermal stresses due to panel curing, are important aspects that need to be properly addressed in both the design and analysis stages of a tow-steered laminate. For instance, the *ply staggering* technique (Gürdal et al., 2005) can be adopted in the design stage of a tow-steered laminate to avoid the collocation of course edges, tow drops or tow overlaps, that would occur at the same places through-the-thickness of a laminate in clustered plies, i.e. adjacent plies with the same fiber angle distribution. Collocation of course edges has two different effects depending on the manufacturing method. If the tow-drop method

is used, local resin-rich regions can occur throughout the panel thickness, and this can degrade the laminate strength. If the tow-overlaps method is used, coincident course edges generate the highest thickness buildups which can be smoothed by ply staggering, allowing the production of smooth thickness laminates with no appreciable decrease in performance (Jegley et al., 2003). This technique is illustrated in figure 1.8 in which a panel that contains

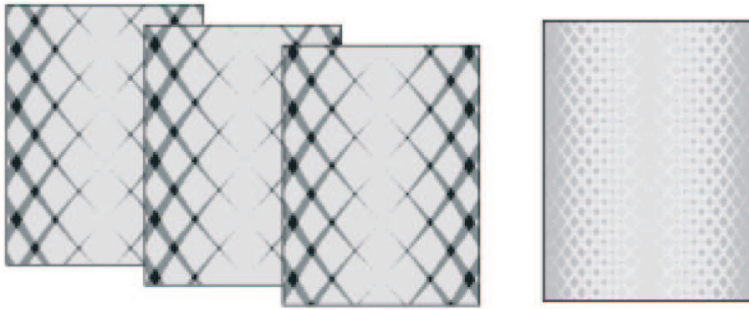


Figure 1.8: Ply staggering of tow-steered plies using the tow-overlap method construction (courtesy of Gürdal et al. (2005)).

three ply groups using the tow-overlap construction method is represented. The first ply group on the left is a $0 \pm < 45/60 >$ ply group, where the dark regions denote the thickness build-up, and the next two ply groups contain the same angle definition, though each is displaced by one-third of the shift distance in the vertical direction. The combination of the three ply groups leads to a smoother thickness distribution compared to the one that would have been obtained if the three ply groups of $0 \pm < 45/60 >$ were not staggered. When the tow-drop construction method is used instead, this technique provides an added bonus of distributing the gaps more evenly within the structure. Nevertheless, the designer of VSP should be aware that ply staggering causes the actual lay-up to be locally asymmetric and unbalanced. Gürdal et al. (2005) have presented several options to achieve the same benefit of ply staggering with a reduced impact on panel performance. A detailed overview providing additional considerations on manufacturing and design of VSP is presented by Lopes (2009).

1.5 Structural Response

The primary objective of varying the orientation of fibres within the plane of laminates is to increase the structural performance of fibre-reinforced composites in terms of stiffness, buckling and failure characteristics, when compared to traditional straight-fibre laminates. Since the creation of the concept, the structural response of variable-stiffness laminates has been analysed by several authors, whose investigations have been overviewed by Lopes (2009) and briefly described in the following paragraphs.

1.5.1 Stiffness and Buckling Performance

Gürdal and Olmedo (Gürdal and Olmedo, 1993; Olmedo and Gürdal, 1992) used a numerical iterative technique to solve the system of coupled elliptic partial differential equations governing the in-plane response of VSP. The results showed increases in the axial stiffness of VSP of up to 50% compared to straight-fibre laminates. Further work of the same authors (Olmedo and Gürdal, 1993) employed the Rayleigh-Ritz Method to find the buckling loads and modes for two different cases of fibre angles variation. In the first case the fiber orientation varied in the direction of the applied load and improvements in the buckling load were obtained compared to the straight-fiber configurations. Higher performance improvements in the buckling load, up to 80% over straight-fiber configurations, were found in the second case in which the fiber orientation varied perpendicularly to the loading direction.

In the follow-up work carried out by Waldhart et al. (1996) and Waldhart (1996) the buckling loads of compression and shear loaded tow-steered panels were analysed by solving the elliptical partial differential equations governing the panel behaviour. Increased buckling performance, compared to the straight-fibre counterparts, was reported.

Wu et al. (2002) and Wu (2006) conducted experimental and FE studies to characterise the structural response of two different compression-loaded variable-stiffness composite panels. The panels were designed and manufactured according to the tow-drop method and the tow overlap method, respectively. A baseline cross-ply laminate was also analysed and tested for comparative purposes: VSP, especially the ones with overlapping tows, showed significantly better structural efficiency than the baseline laminate. Experimental data showed transition loads up to 5 times that of the baseline laminate. Differences in structural response between the two variable-stiffness panels were attributed to the regions of overlapping tows which act as local stiffeners, hence increasing the load-carrying capability of the panel manufactured according to the tow-overlap method. The FE predictions far exceeded the experimental buckling loads. It was determined that the difference between predicted and actual performance was the result of the residual stresses induced by the curing process, which, in general, are also responsible for the superior performance demonstrated by tow-steered laminates compared with straight-fibre composites. Non-linear FE analyses with thermal prestresses were performed to correlate better the predictions with the test results. This analysis resulted in a more consistent correlation with test results.

Tatting and Gürdal (2001) optimised a panel with central hole for compressive buckling load. First, a panel without a hole was considered for the optimisation study. Then, a hole was added to the best lay-up and the panel analysed in the FE code STAGS (Structural Analysis of General Shells) (Rankin et al., June 2000). Compared to the baseline panel, the best curvilinear-fibre panel achieved an improvement in load-carrying capability of over 60% with no appreciable increase in weight. Then, the chosen configurations, and baseline panel, and a curvilinear-fibre panel without central hole, were manufactured and tested by Jegley et al. (2003, 2005). Reasonable agreement was observed for the straight-fibre specimens but buckling and post-buckling behaviour was not as accurately predicted for the tow-steered specimens.

An overview of the effects of fibre-steering on the in-plane stiffness and buckling responses of tow-steered panels is presented in Gürdal et al. (2008). These analyses have been further refined by Abdalla et al. (2009) with the inclusion of residual thermal stresses. The variable stiffness concept has been extended to structures other than plates. Tatting

(1998) investigated the application of the variable stiffness concept to thin cylindrical shells of various length. Conical shells have been studied by Blom et al. (2008a,b).

1.5.2 Failure Performance

First-ply failure analysis and failure test have been the subject of a few works on variable-stiffness laminates. Waldhart et al. (1996) and Waldhart (1996) considered failure as a constraint on the production of tow-steered panels. The Tsai-Hill first ply failure criterion (Rowlands, 1985) was applied to rule out configurations with first-ply failure loads lower than buckling loads. The reason for this is that the potential applications of tow-steered composite panels are compression-loaded structural parts for which the buckling loads are generally the limiting factor. The use of the Tsai-Hill criterion was chosen over other failure prediction methods, such as the maximum stress and maximum strain theories, because it offers a more continuous strength variation that accompanies changes in orientation angle and it incorporates interactions between the failure strengths that some other theories completely neglect. Although the Tsai-Hill criterion takes into account quadratic interaction between stress components, its formulation is based on curve-fitting techniques that do not account for the effect of the ply thickness on the strength. Furthermore, it does not reveal the mechanism of failure.

Wu *et al.* (Wu, 2006; Wu et al., 2002) analysed and tested tow steered panels and a baseline cross-ply plate under compression loads up to failure. The tests performed on the variable stiffness panels showed a linear pre-buckling load-deflection response, followed by a non-linear response until failure which occurred at load levels about three times greater than the buckling loads. The weight-normalised failure loads were found to be approximately 28% and 8% greater than the baseline panel, respectively for the tow-steered laminates with and without overlapping tows. Attempts to simulate numerically the nonlinear postbuckling response, relying solely on geometrically nonlinear analysis, resulted in inaccurate results. The introduction of nonlinear shear behaviour allowed the correct simulation of the postbuckling path.

Jegley et al. (2003, 2005) tested compression and shear loaded VSP up to global structural failure, and compared the results with straight-fibre configurations. The geometries included central holes of various sizes. The Tsai-Hill first-ply failure criterion was initially applied on candidate designs to guarantee that the panels produced would fail at loads much higher than the buckling loads. The panels manufactured by the tow-overlap method carried loads more than three times their buckling loads while shear loaded specimens reached at least twice their buckling load levels before failure. Overall, VSP had a failure performance up to 60% higher than the constant-stiffness configurations.

More recently, Lopes et al. (2007, 2008) have demonstrated the advantages of variable stiffness over straight-fibre laminates in terms of compressive buckling and first-ply failure. A user-developed continuum damage model was employed in the finite element code ABAQUS for the identification of damage initiation and material stiffness degradation in the post-buckling regime. Moreover, a physically based set of failure criteria, able to predict the various modes of failure of composites laminate structure, was also implemented. The improvements gained using tow-steered laminates over traditional straight-fibre laminates concerning first-ply failure were remarkable. The improvements achieved by the tow-drop method (24.8%) were even surpassed by the overlap method (33.9%).

Alhajahmad *et al.* (Alhajahmad, 2008; Alhajahmad *et al.*, 2008a,b) designed tow-placed pressurised fuselage panels with and without cutouts for maximum strength performance. The Tsai-Wu first ply failure criterion (Tsai and Wu, 1971) was used in the optimization algorithm. Improvements in panel load carrying capacity of 50% and above were achieved compared to constant-stiffness configurations.

Strength-based criteria are the usual methodology for predicting the onset of failure events in composite structures due to their ease of use with the finite element method. However, the mechanism that leads to failure can not be fully understood when using these approaches Lopes (2009). Physically-based failure criteria have been also developed and proposed. These represents a step further in the quest to identify the phenomena at the origin of the failure process. Phenomenological-based criteria are widely applicable, as opposed to curve-fitting based criteria whose applicability is restricted to the particular load cases from which they are derived. In this regard, a detailed literature overview can be found in Lopes (2009).

1.5.3 Computational Modeling of Manufacturing Characteristics

In the analyses of the tow-placed structures with constant thickness by Tatting and Gürdal (2001, 2002, 2003), Blom *et al.* (2008a,b), Lopes *et al.* (2007, 2008), the course boundaries have been assumed to be smooth. In reality, tows are cut perpendicular to the fibre directions, resulting in small triangular resin-rich areas, as shown in figure 1.6. Only Blom *et al.* (2009) have done a theoretical, numerical investigation of the influence of these tow-drop areas on the strength and stiffness of constant thickness variable stiffness laminates. In particular, the influence of tow-width, laminate thickness and ply staggering, in combination with tow-drop areas, on the in-plane failure performance of variable stiffness laminates was analysed using parametric studies.

The commercially available FE package ABAQUS (ABAQUS, 2005) was used together with the user-developed continuum damage model (Maimì *et al.*, 2007a,b) to perform progressive failure analysis. The finite element model consisted of fully integrated S4 shell elements, and a refined mesh was adopted since the elements have to be small enough to capture the tow-drop areas. Good agreement with the experimental failure results were obtained, and the authors concluded that the failure of VSP are inevitably affected by the presence of tow-drops. It was shown that damage can be triggered by the resin-rich areas, preferentially in regions where the angle between the loading vector and fiber orientations is the largest. It could be also stated that ply staggering can mitigate the stress concentrations in the neighbourhood of course edges and fibre-free areas. However, the occurrence of delaminations, traditionally caused by interlaminar stresses that arise due to differences in ply compliance and out-of-plane loadings, was neglected altogether in the model.

In other loading situations, such as cyclic loading, the failure initiation around tow-drop regions may primarily be delamination (Lagace and Bonello, 1993; Shim and Lagace, 2004). Hence, the work of Blom *et al.* (2009) was a preliminary assessment of tow-steered configurations, based only on their in-plane behaviour. In this way the analyses were substantially simplified, the modelling difficulties were kept low, but a sound basis for the comparison of VSP with straight-fiber laminats was still achieved. However, care should be taken in drawing definite conclusions about an obtained failure performance.

1.6 Thesis Objectives and Outline

Delamination, caused or potentiated by interlaminar stresses (Pagano and Schoeppner, 2000), is a key failure mode in laminated materials. A VSP has, by definition, a nonuniform in-plane stiffness distribution that might result in large in-plane stress gradients (Lopes, 2009). Such gradients contribute to the amplification of the interlaminar stresses, as demonstrated in Saeger et al. (2002), and possibly to render delamination the dominant failure mode in these configurations. Furthermore, VSP have manufacturing characteristics, such as course edges, tow-drops and overlaps, as described in section 1.4, which may act as discontinuities and stress concentration zones that locally excite the interlaminar stresses further. Similar mechanisms develop in material discontinuities (Bath and Lagace, 1994) such as free edges, e.g. in holes, notches and ply drop-offs (Shim and Lagace, 2006). Although many researchers have paid their attention to the analysis of VSP, the knowledge about the variable-stiffness configurations that lead to the highest ultimate loads is still rather limited. Furthermore, the full details of the mechanisms that lead to failure of VSP are not yet known, particularly the influence of local effects such as tow-drops or tow overlaps. This is because these local effects require an accurate finite element modeling that is not of easy conception using customary procedures.

An interesting analysis on the mechanisms and structural parameters affecting the interlaminar stress field in laminates with ply drop-offs is provided in Mukherjee and Varughese (2001) and in Shim and Lagace (2004). The overall insights gained from these works are useful in understanding damage/failure characteristics, and are helpful in preliminary design stages when it has to be chosen the laminate configurations that alleviate the interlaminar stress concentrations, and thus, increase the delamination load. This is because a sense of the propensity for delamination of a particular laminate configuration can be obtained. However, a detailed analysis on onset of delamination of such laminates requires more accurate procedures, such as three-dimensional finite element analyses combined with three-dimensional failure criteria.

Tows have to be cut at the course boundary to manufacture a variable stiffness laminate with constant thickness, which results in small triangular resin-rich areas without any fiber, as shown schematically in figure 1.9. Tow-drops are likely to be in different locations across the planform of the laminate from ply to ply depending on the stacking sequence. Then, it becomes extremely difficult to capture the local stress states generated in the final laminate using conventional two-dimensional finite element procedures, even by resorting to computationally expensive meshes. For instance, a computationally expensive in-plane meshes is required to model the tow-drop locations of every ply by adopting a two-dimensional model, as the one used in Blom et al. (2009) generated using fully integrated *S4* shell elements. This is because the elements have to be small enough to capture the tow-drop areas present in the complete laminate. Moreover, even though two-dimensional models can be adopted for a preliminary assessment, these models are not able to analyse properly the local three-dimensional stress states generated at the tow-drop locations, hence the onset of delamination, due to their intrinsic theoretical assumptions. Then, three-dimensional displacement-based models represents a sound basis for proper analyses of tow-steered laminates. However, difficulties arise using conventional three-dimensional procedures in the development of a finite element model that is able to capture properly all the locations of interest within the complete laminate.

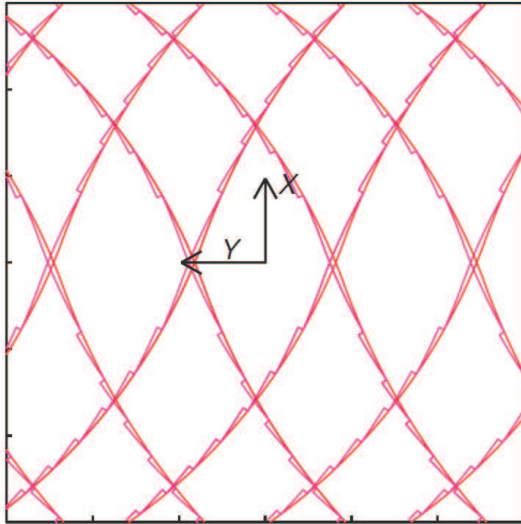


Figure 1.9: Schematic representation of a variable stiffness laminate, designed according to the tow-drop method. (Blom et al., 2009).

Although interlaminar stresses have to be continuous both across and along layer interfaces, the continuity of interlaminar stresses is difficult to enforce in C^0 interpolated elements. Accurate stresses are generally retrievable at Gauss points using constitutive relations or variationally consistent procedures in conventional Lagrangian formulations. However, interlaminar stress failure is likely to initiate at the interface between layers in tow-steered laminates, in particular at the tow-drop and overlaps locations, making necessary to have accurate stresses on the interface, as opposed to Gauss points. Accurate extrapolation techniques from Gauss points are usually required in conventional finite element procedures to achieve an appropriate level of accuracy of the interlaminar stress fields at the element nodes. However, stress distributions evaluated using constitutive relations or variationally consistent procedures may generate severe oscillations in the transverse stress distributions when thin laminates are analysed. Moreover, inaccuracy in the recovered interlaminar stress distributions may be obtained at the interfaces between the layers in the case of high transverse stress gradients.

Based on what is stated above, the main goal of the research reported in this thesis was to develop a three-dimensional finite element computational strategy for reliable future stress analyses of variable stiffness panels. Moreover, the procedure had to overcome the aforementioned problems that would be encountered in the modeling and analysis of such laminates using customary procedures. In particular, the procedure had to be conceived in such a way that areas where the failure initiation is primarily due to delamination, such as tow-drop and overlapping-tows areas, can be easily modeled and analysed without requiring demanding computational resources. The procedure had also to be conceived such that the stress states generated can be combined with three-dimensional failure criteria commonly used for delamination initiation in multilayered composite laminates. Attention was paid to the development of a procedure for the analysis of VSP with tow-drops, but the procedure

itself was conceived in such a way that the concept is easily extendible to the analysis of VSP with overlaps.

The starting point of the present procedure is to partition a tow-steered laminate in such a way that every ply can be considered to be an independent subdomain. This means that the compatibility between the subdomains has to be reestablished subsequently by imposing adequate interfacial conditions. Then, a mesh based on the combined use of both linear brick and linear triangular prism elements is adopted for every ply. Thus, the triangular shape of the tow-drop locations, known from the procedure developed in Blom et al. (2009), can be modeled properly using triangular elements. Moreover, the user is enabled to decide the most adequate method to generate the mesh in every single ply. For instance, the user could decide to mesh every course independently. Thus, the final mesh of the complete laminate could be obtained by simulating the procedure followed by the tow-placement machine's head during the manufacturing process. This means that a proper mesh can be inherently adopted in each course based on the assumed construction method. Another possible option is to directly mesh the complete ply using a reliable mesh generator tool. For instance, using the commercial finite element software ABAQUS 6.8TM it is possible to import the geometry of each ply using the partition method (ABAQUS, 2005). Then, it is possible to control the mesh using the mesh generator of ABAQUS in such a way that brick element are adopted within the courses, and triangular prism elements are adopted in the triangular resin-rich areas, i.e. hex-dominated element shape and structured mesh control (ABAQUS, 2005). However, both the methods would lead to non conforming meshes between the subdomains. Thus, the procedure needed to be conceived in such a way that non-conforming meshes can also be taken properly into consideration.

In order to broaden the range of numerical applications of the proposed approach, a procedure for distributed computing generally employed in domain decomposition methods, i.e. *the finite element tearing and interconnecting method* Kruis (2007), was employed to solve the system of algebraic equations. An efficient interlaminar stress recovery procedure for three-dimensional finite element formulations was also developed as a post-processing procedure. This interlaminar stress recovery procedure was conceived to overcome the aforementioned problems usually encountered using customary procedures, and is based on retrieving the interlaminar stress values directly at nodes. Thus transverse stress continuity at the inter-element boundary is automatically satisfied, making the procedure neither dependent on the knowledge of superconvergent point nor sensitive to the stress recover method employed to obtain element stress distributions, i.e. constitutive relations or variationally consistent procedures. The post-processing procedure was completed by employing a variationally consistent procedure for the recovery of the in-plane stresses.

An adequate modeling strategy for non conventional composite laminates could be developed only if a proper understanding of the behaviour of conventional laminates was achieved. The thesis is set out as follows: in chapter 2 attention is paid to providing a proper understanding of the complicate effects arising in conventional composite layered constructions due to the typical anisotropic behaviour of these laminates. In this context, high transverse deformability, zig-zag effects and interlaminar continuity, summarized as C_z^0 requirements of multilayered composite structures, are addressed in detail. Variational principles that have been established in the open literature to derive governing equations of a structural problem are also discussed. Then, an overview of available two-dimensional ax-

isotropic theories for analysing multilayer, anisotropic, composite plates and shell structures is presented to help understand limits and advantages of these theories compared to three-dimensional approaches. Common finite element procedures used to recover stress field measurements in displacement based formulations are overviewed in detail in chapter 3. Then, stress recovery expressions obtained using these procedures are compared with stress recovery expressions obtained using hybrid formulations. The proposed finite element procedure is presented in detail in chapter 4. The reliability of the approach is tested analysing several benchmark problems concerning multilayered plate structures. Comparisons with finite element software and available solutions in the literature are also reported. Finally, the proposed procedure is combined with the commercial Finite Element software ABAQUS in chapter 5, and benchmark problems concerning multilayer plate and shell structures are analysed. Comparisons with ABAQUS' built-in stress recovery and available solutions in the literature are used to confirm the accuracy of the procedure. This thesis is concluded in chapter 6 with an exposition of the lessons learned from the work reported in the previous chapters, and a perspective on the research to be carried in the future based on the drawn conclusions.

Chapter 2

Theories for Multilayered Anisotropic Composite Structures

2.1 Introduction

Tow steered composite laminates require a comprehensive treatment of regions such as tow-drop and/or overlapping-tows areas since three-dimensional stress states are common in these areas. This is similar to what happens near geometric and material discontinuities, i.e. free edges, cut-outs, which also give rise to stress concentration phenomena and to failure initiation that is primarily due to delamination. An appropriate analysis of the onset of delamination requires an efficient modeling strategy able to detect the local three-dimensional stress states, and this can only be developed if it is fully understood how conventional composite laminates function. Compared to isotropic structures, the anisotropic behaviour of multilayered composite laminates introduces complicated effects, such as high transverse deformability, zig-zag effects, i.e. rapid change in the slope of displacement fields in the thickness direction in correspondence with each layer interface, and interlaminar continuity of transverse stresses. These effects have to be carefully taken into account especially when dealing with stress analyses of such laminates. The chapter begins with a discussion concerning these complicating effects. Three-dimensional (3D) approaches are the obvious tool of choice when attempting to reach an appropriate level of accuracy in the recovered stress fields, especially in presence of local phenomena such as those mentioned above, but the computational costs of these analyses can be prohibitive for practical problems. A two-dimensional model can be used to obtain a valuable alternative, and an overview of the available modeling theories will be given in this chapter so that the limits and advantages of these approaches compared to three-dimensional models can be understood. In particular, due to the impact that the axiomatic approach has had, and continues to have on the modeling of composite structures, attention will be paid to the axiomatic type theories and related finite element implementations. Classical lamination theories and their refinements are considered first, where an equivalent single layer description is adopted, meaning that the number of the unknown variables is considered to be independent of the number of constitutive layers. Then, layer-wise variables descriptions, in which each layer is seen as an

independent plate and compatibility of displacements components is imposed as a constraint at each interface, are considered. These theories will be addressed in both the framework of displacement formulations, in which only the displacements are assumed as unknown variables of the structural problem, and in mixed formulations, in which additional fields are introduced as unknown variables of the structural problem, i.e. strains, stresses. The chapter ends with a set of conclusions drawn from the forgoing discussion of multilayered composite laminates analyses.

2.2 Anisotropy's Effects on Layered Structures

Unlike their homogeneous isotropic counterparts, the heterogeneous anisotropic constitution of laminated composite structures often results in the appearance of many unique phenomena that can occur on different geometric scales, i.e. at the global or laminate level, the ply level, or the fiber/matrix level. For example, global deformation of laminated composite structures is often characterized by complex coupling between the extension, bending, and shearing modes, leading to relevant complications in the procedure used to find a solution to the governing equations of the problem (Jones, 1999; Reddy, 2004).

Advanced composite materials commonly used in aerospace applications may exhibit in-plane anisotropy (IA), that is, the structure has different mechanical-physical properties in different in-plane directions: IA is generated by high values of Young's moduli orthotropic ratio ($E_L/E_T = 40 \div 5$ where L denotes the fiber direction and T denotes the orthogonal directions to L), coupled with low values for the transverse shear moduli ratio ($G_{LT}/E_T \approx G_{TT}/E_T = 1/10 \div 1/200$). The effect of IA is that higher transverse shear and normal stress deformability with respect to in-plane deformability is reached compared to isotropic structures. Moreover, IA introduces an additional relevant consequence: a coupling between in-plane and out-of-plane strains may be introduced as it is the case for unsymmetrically laminated plates, causing large displacements in the structure even if low levels of the applied loadings are considered (Carrera, 2002; Jones, 1999; Reddy, 2004).

Further complications arise in laminated composite structures due to the transverse discontinuous mechanical properties, i.e. transverse anisotropy (TA) of multilayered constructions leading to displacement fields in the thickness direction that present a rapid change of their slopes in correspondence with each layer interface. This is known as the Zig-Zag (ZZ) form of displacement fields in the thickness direction of the laminate (Carrera, 2002). A comparison of the possible scenario between a one-layer composite structure and a three-layer composite structure of both displacement and stress components distributions along the thickness direction of the laminate is shown in figure 2.1, as it would appear from an exact 3D analysis or from experimental data (Carrera, 1997). For the sake of simplicity, reference is made to plate geometries. The stress components are referred to the global laminate Cartesian coordinates system (x, y, z) shown in figure 2.2, in which the local lamina coordinate system (x_1, x_2, x_3) is also reported. In contrast to the in-plane stress components $\sigma_p = (\sigma_{11}, \sigma_{22}, \sigma_{12})$ that can be, in general, discontinuous at each layer interface, the transverse stress components $\sigma_p = (\sigma_{13}, \sigma_{23}, \sigma_{33})$, for equilibrium reasons, i.e. the Cauchy theorem, must be continuous at each layer interface. It is evident from figure 2.1 that both the displacement and transverse stress distributions, for reasons of compatibility and equilibrium, respectively, are C^0 -continuous functions in the thickness z direction. It

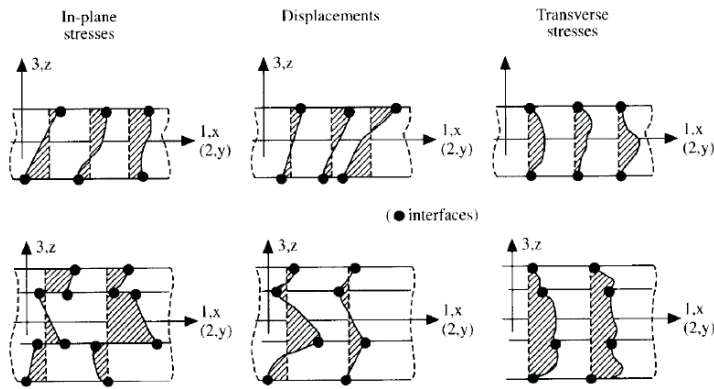


Figure 2.1: C_z^0 Requirements. Comparison concerning possible scenarios of both displacement and stress thickness distributions between a one-layer composite laminate and a three-layered composite laminate (courtesy of Carrera (1997)).

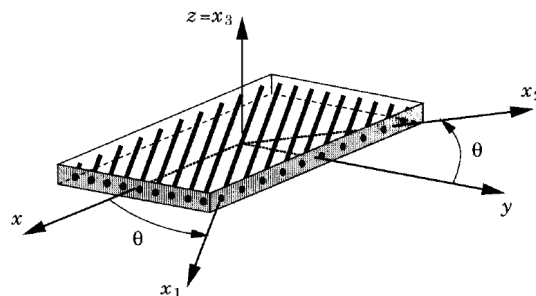


Figure 2.2: A lamina with local and global coordinate systems.

should also be noted that both the distributions have discontinuous first derivatives corresponding to each interface. The ZZ and the interlaminar continuity, (IC), of the transverse stresses are referred to as C_z^0 -Requirements in Carrera (1996a, 1997). The fulfillment of C_z^0 -Requirements are crucial to the development of any theory suitable for the analysis of multilayered structures. It should also be taken into account that laminated composites often exhibit transverse stress concentrations near material and geometric discontinuities at the ply level, the free edge effect, that can lead to damage in the form of delamination and matrix cracking. At the fiber/matrix level, stress concentrations can cause fiber/matrix separation, radial matrix cracking, and other forms of cumulative damage that degrade the stiffness of the individual ply, thus causing a complex load redistribution.

2.3 Strategies for the Development of Plate/Shell Theories

The obvious approach to use to analyse multilayered composite plates and shells is to solve directly, in a strong or in a weak sense, the fundamental differential equations of three-dimensional 3D elasticity, that are the equilibrium equations, the compatibility equations, and the physical 'constitutive' relations or Hooke's law (Reddy, 2004). Whenever a plate/shell problem is approached using the direct solution of the fundamental differential equations of three-dimensional 3D elasticity, a 3D analysis is obtained. In general, these solutions cannot be given in strong form for most cases of geometry, laminate layout, boundary and loading conditions (Carrera, 1997). A considerable body of literature exists concerning the development of computational techniques implemented for layered plates and shell analyses, and among which the Finite Element Method (FEM) plays a predominant role (Kant and Swaminathan, 2000). The finite element implementation of the 3D approach requires the use of 3D brick elements. Highly accurate, models based on 3D brick elements are, in general, computationally expensive, which can be prohibitively costly for practical problems (Reddy and Robbins, 1994). A two-dimensional, 2D, model can be used to obtain a valuable alternative, and two-dimensional plate/shell theories for composite, multilayered structures can be developed by making an appropriate choice for each of the following points:

- elimination of the thickness coordinate z : available 2D approaches.
- choice of the unknown variables: displacement and mixed formulations.
- choice of the variables, multilayered form description: Equivalent Single Layer or Layer-Wise models.

These points are addressed in detail in the following subsections.

2.3.1 Available 2D Approaches

Composite laminates have planar dimensions that are one to two orders of magnitude larger than their thickness due to how they are constructed, and, by making suitable assumptions concerning the kinematics of deformation or the stress state through the thickness of the laminate, it is possible to reduce the 3D problem to a 2-D problem. This reduction transforms a problem which is defined in each point P_{Σ} of the 3D continuum body with domain Σ and x, y, z defining a system of thriorthogonal coordinates into a problem which is defined in each point $P_{\Omega}(\alpha, \beta)$ of a reference shell/plate surface Ω , usually the middle surface, see figure 2.3, with α, β and z defining a thriorthogonal curvilinear system. This reduction can in practice be made according to several approaches and techniques that have been proposed over the last century, i.e. continuum based models, asymptotic and axiomatic type approaches. A detailed overview of these approaches and developed finite elements is given in Carrera (2002).

In continuum based models, a 3D continuum is seen as a surface on which correspondence stress resultants are defined making use of the Cosserat surface concept (Cosserat and Cosserat, 1999). The most remarkable advantage of this approach is that, being based on a 3D continuum, it does not present any difficulties in the formulation of nonlinear theories in both the case of geometric nonlinear behaviour, large displacements and large rotations,

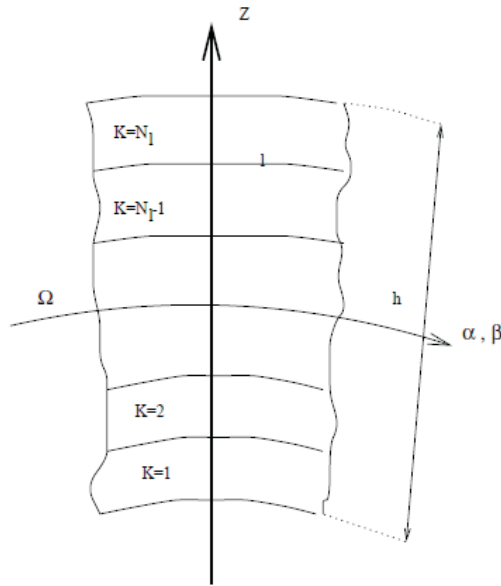


Figure 2.3: Geometry and notations used for a multilayered shell (courtesy of Carrera (2002)).

and physical nonlinear behaviour, plasticity, viscoelasticity. In the framework of asymptotic approaches for monocoque structures, the 3D governing equations are expanded in terms of a perturbation parameter δ , usually the shell thickness to length ratio, and theories related to the same order in δ are derived. For instance, the expanded equilibrium equations could appear in the following form:

$$\mathbf{E}_{\Sigma} \approx \mathbf{E}_{\Sigma}^1 \delta^{p_1} + \mathbf{E}_{\Sigma}^2 \delta^{p_2} + \dots + \mathbf{E}_{\Sigma}^N \delta^{p_N} \quad (2.1)$$

where $p_i, i = 1, N$ are the exponents of the perturbation parameter δ (Carrera, 2002). The expansion is usually derived using a certain variational statements (see next section). The asymptotic approach furnishes 'consistent' approximations in the sense that all the terms which have the same order of magnitude as the introduced perturbation parameter δ are retained in a given asymptotic theory, however, the convergence rate is poor in the case of moderately thick-thick laminates. Moreover, further difficulties arise in multilayered structures since, in addition to δ , a mechanical layer parameter which takes into account the anisotropy of composite layers needs to be introduced (Carrera, 2002).

Axiomatic type approaches are the most commonly used approaches in composite structure modeling. Then, the discussion in the rest of this chapter attention will be restricted to these kind of theories. Using an axiomatic type approach, an 'intuitive' approximation of the plate/shell behaviour is introduced but nothing can be established as far as the convergence of the model to 3D solutions is concerned. This approximation postulates, usually, a certain displacement and/or stress field in the thickness direction of the laminate that in

Cartesian rectangular coordinates assumes the following form:

$$f(x, y, z) = f_1(x, y)F_1(z) + \dots + f_N(x, y)F_N(z) \quad (2.2)$$

where f is the generic component of the unknown field variable, f_i are introduced unknowns defined on the reference plate/shell surface, and F_i are the polynomials introduced as base functions for the expansion along the thickness, and N is the number of introduced unknowns.

2.3.2 Displacement and Mixed Formulations: Variational Statements

The fundamental differential equations of three-dimensional 3D elasticity, equilibrium equations, compatibility equations and physical constitutive relations, are given in terms of displacements, strains and stresses. Approximated 3D or 2D solutions of these equations are usually derived by choosing the unknown variables. Many variational tools, theorems, equations or principles, have been established in the open literature to derive governing equations of a structural problem consistent to the selected unknown variables (Carrera, 2002; Reddy, 2002, 2004). The governing equations of a structural problem are usually obtained by using the classical, and well known, *Principle of Virtual Displacements* (PVD) (Reddy, 2004). The PVD approach is a displacement based approach since it involves only a compatible displacement field as a variable and it can be stated as: *if a continuous body is in equilibrium, the virtual work of all actual forces moving through a virtual displacement is zero*, that is

$$\delta U + \delta V \equiv \delta W = 0 \quad (2.3)$$

where δU and δV are, respectively, the internal and external virtual works. For a solid body, the principle can be expressed as:

$$\underbrace{\int_{\Omega} \boldsymbol{\sigma} : \delta \boldsymbol{\epsilon} d\Omega}_{\delta U} - \underbrace{\int_{\Omega} \mathbf{b}^* \cdot \delta \mathbf{u} d\Omega - \int_{\partial_t \Omega} \mathbf{t}^* \cdot \mathbf{u} d\Gamma}_{\delta V} = 0 \quad (2.4)$$

where \mathbf{u} is the displacement, $d\Omega$ is a differential element of volume, \mathbf{b}^* is the body force per unit volume, $\partial_t \Omega$ is the part of $\partial\Omega$ on which the boundary traction \mathbf{t}^* is specified, $\boldsymbol{\epsilon} := \text{symm}(\nabla \mathbf{u}) \equiv \mathcal{G} : \nabla \mathbf{u}$ is the strain tensor, with $\nabla(\cdot) := [\partial(\cdot)/\partial \mathbf{x}]^T$, in which $\mathbf{x} := (x^1, x^2, x^3) \in \mathbb{R}^3$ is a material point, and $D\boldsymbol{\epsilon} \cdot \delta \mathbf{u} := \mathcal{G} : \nabla \mathbf{u}$, and in which \mathcal{G} is a fourth-order tensor such that $\mathcal{G} : \mathbf{A} = \frac{1}{2}(\mathbf{A} + \mathbf{A}^T) \equiv \text{symm}(\mathbf{A})$ for any second order tensor \mathbf{A} , and $\boldsymbol{\sigma}$ is the stress tensor. It is clear that the virtual work statement (2.4) is precisely the weak form of the equilibrium equations and is valid for linear and non-linear stress-strain relations.

The same functional (2.4) can also be obtained using the *principle of minimum total potential energy*. It states that 'of all the admissible displacements, those which satisfy the equilibrium equations make the total potential energy a minimum' (Reddy, 2002). Then, the governing equations are obtained by seeking the minimum of the Potential Energy (PE) functional of a solid body

$$\Pi_{PE}(\mathbf{u}) := \int_{\Omega} w(\boldsymbol{\epsilon}) d\Omega - \int_{\Omega} \mathbf{b}^* \cdot \mathbf{u} d\Omega - \int_{\partial_t \Omega} \mathbf{t}^* \cdot \mathbf{u} d\Gamma \quad (2.5)$$

where $w(\epsilon)$ is the stored energy function.

If kinematic compatibility is introduced in the functional (2.5) as a condition of constraint through a Lagrange multiplier, which turns out to be the stress field, the Hu-Washizu (HW) Variational Principle (Felippa, 1994; Mota and Abel, 2000; Washizu, 1982) is obtained from the PVD variational statement as follows:

$$\Pi_{HW}(\mathbf{u}, \bar{\epsilon}, \bar{\sigma}) := \int_{\Omega} w(\bar{\epsilon}) d\Omega + \int_{\Omega} \bar{\sigma} : (\epsilon - \bar{\epsilon}) d\Omega - \int_{\Omega} \mathbf{b}^* \cdot \mathbf{u} d\Omega - \int_{\partial_r \Omega} \mathbf{t}^* \cdot \mathbf{u} d\Gamma \quad (2.6)$$

where $\bar{\epsilon}$ and $\bar{\sigma}$ are the independent strain and stress fields. Hence, one obtains a three-field functional with displacements, strains and stresses as variables. On the other hand, if the functional (2.5) is modified by the Legendre transform:

$$\int_{\Omega} w(\epsilon) d\Omega = \int_{\Omega} \bar{\sigma} : \epsilon d\Omega - \int_{\Omega} w_c(\bar{\sigma}) d\Omega \quad (2.7)$$

which introduces the stress $\bar{\sigma}$ as an additional variable, and in which $w_c(\bar{\sigma})$ is the complementary stored energy function, the well known two-field Hellinger-Reissner (HR) principle (Brezzi and Fortin, 1991; Mota and Abel, 2000; Washizu, 1982) is obtained:

$$\Pi_{HR}(\mathbf{u}, \bar{\sigma}) := \int_{\Omega} \bar{\sigma} : \epsilon d\Omega - \int_{\Omega} w_c(\bar{\sigma}) d\Omega - \int_{\Omega} \mathbf{b}^* \cdot \mathbf{u} d\Omega - \int_{\partial_r \Omega} \mathbf{t}^* \cdot \mathbf{u} d\Gamma \quad (2.8)$$

where displacements and stresses are independent variables. The HW and the HR principles are referred to as mixed variational principles since they involve an additional field to the displacement one in the continuum as a variable. When a mixed variational principle is employed to derive the governing equations of a structural problem, a mixed formulation is obtained. Since in mixed formulations the secondary fields are computed explicitly, one can think of mixed formulations as an alternative method for secondary-field recovery. Then, a natural manner to fulfill the C_z^0 -Requirements of multilayered composite structures is to assume both displacements and stresses as unknown variables. The computational cost involved in using mixed approaches can be prohibitive for practical problems. Fulfillment of the C_z^0 -Requirements can also be achieved at a reduced computational cost by employing the partial mixed variational equation proposed by Reissner (1984, 1986), namely Reissner's Mixed Variational Theorem (RMVT). RMVT can be simply interpreted as a particular case of the HW and HR mixed variational principles in which only compatibility of the transverse strains is enforced using Lagrange multipliers which, in this case, turn out to be the transverse stresses. For multilayered structure analyses it is sufficient to restrict the mixed assumptions to transverse stresses since only for such stresses is an independent field required a priori to completely fulfill the C_z^0 -Requirements.

2.3.3 Multilayered Form Description: Classical Equivalent Single Layer Theories and their Refinements

Equivalent Single Layer (ESL) laminated theories are those in which a heterogeneous laminate is treated as a statically equivalent single layer having complex constitutive behaviour, reducing the 3D continuum problem to a 2D problem. ESL theories are developed by assum-

ing that the displacement field is at least C^1 -continuous, i.e. the function and its derivative are continuous, through the thickness of the laminate. In Cartesian rectangular coordinates, the general form of the assumed displacement field is a linear combination of unknown functions and the thickness coordinate

$$\varphi_i(x, y, z) = \sum_{j=0}^N (z)^j \varphi_i^j(x, y) \quad (2.9)$$

where φ_i is the i th component of displacements, (x, y) the in-plane coordinates, z the thickness coordinate, and φ_i^j are functions to be determined. The governing equations in two dimensions are obtained by integrating the virtual work statement, usually the PVD (2.4), through the laminate thickness. Classifications and reviews concerning ESL theories for multilayered composite plates and shells are addressed in Whitney (1969), *et al.* Noor and Burton (1989, 1990), Jones (1999), Carrera (1999a, 2002), Reddy and Robbins (1994), Reddy (2004), and will be briefly summarized below.

The simplest ESL laminated theory is the *Classical Lamination Theory* (CLT). The CLT is an application, to multilayered structures, of the Kirchhoff-Love theory (Noor and Burton, 1990) developed for single-layer isotropic structures, and, in the case of plate geometries, i.e. Classical Laminated Plate Theory (CLPT), it is based on the following displacements assumptions Carrera (2002); Jones (1999); Reddy (2004):

$$\begin{aligned} u_i(x, y, z) &= u_i^0(x, y) - z u_{i,z}(x, y) \quad i = 1, 2 \\ u_3(x, y, z) &= u_3^0(x, y) \end{aligned} \quad (2.10)$$

where (x, y) are the in-plane coordinates of the reference plate surface, and commas denotes partial derivatives while apexes 0 denotes displacement components of a point on the reference surface of the plate, see figure 2.4. The displacement field (2.10) implies that straight lines normal to the 12-plane before deformation remain straight and normal to the midsurface after deformation. This assumption amounts to neglect of both transverse shear and transverse normal effects, meaning that deformation is due entirely to bending and in-plane stretching. The CLT is intended for use with thin homogeneous plates, however, composite laminates have relatively low transverse shear stiffnesses compared to in-plane stiffnesses, and therefore the neglect of transverse shear deformation precludes failures due to transverse stresses (Reddy and Robbins, 1994). Curvatures terms appear in the case of shell structures (Kraus, 1967).

The kinematic of the CLT is extended in the *First Order Shear Deformation Theory* (FSDT), where a transverse shear deformation is included in its kinematic assumptions. In the case of plate geometries, the FSDT is based on the following displacement field Carrera (2002); Jones (1999); Reddy (2004); Whitney (1969):

$$\begin{aligned} u_i(x, y, z) &= u_i^0(x, y) + z \phi_i(x, y) \quad i = 1, 2 \\ u_3(x, y, z) &= u_3^0(x, y) \end{aligned} \quad (2.11)$$

where ϕ_i denotes the rotation around the in-plane axe orthogonal to the i -esima direction, as shown in figure 2.5. The FSDT can be written in a similar form for shell geometries (Kraus, 1967; Noor and Burton, 1990). Using these kinematic assumptions, the transverse shear

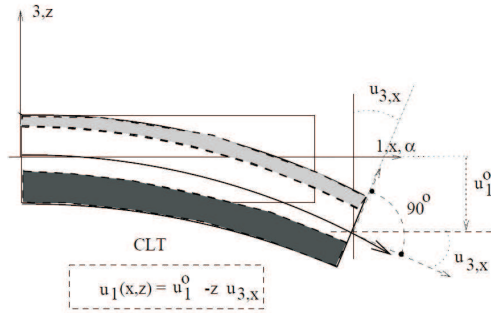


Figure 2.4: CLT assumptions in one-dimensional case (courtesy of Carrera (2002)).

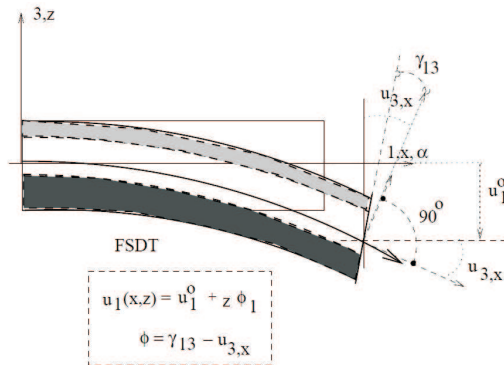


Figure 2.5: FSDT assumptions in one-dimensional case (courtesy of Carrera (2002)).

strain is assumed to be constant with respect to the thickness coordinate. This generates transverse shear stresses that are also constant. It is well known from elementary theory that in composite laminated beams and plates, the transverse shear stresses vary at least quadratically through layer thickness (Reddy, 2004). The discrepancy between the actual stress states and the predicted constant one is often corrected by multiplying the transverse shear force resultants with a parameter K , called *shear correction factor*, which is difficult to determine for arbitrary laminated composite structures (Reddy, 2004). It is important to emphasize that any refinement of the CLT should take into account Koiter's recommendation (Koiter, 1959). Koiter's recommendation, formulated for isotropic structures and based on energy considerations, states that a refinement of the Kirchoff-Love's theory, the CLT in presence of multilayered composite structures, is in general meaningless unless the effects of transverse shear and normal stresses are simultaneously taken into account. These recommendation can be fulfilled by including both transverse shear and normal strains in the FSDT as done in the work of Hildebrand et al. (1938) where the displacement model is written as follows:

$$\begin{aligned}
 u_i(x, y, z) &= u_i^0(x, y) + z\phi_i(x, y) \\
 u_3(x, y, z) &= u_3^0(x, y) + z\phi_3 + z^2\varphi_3
 \end{aligned}
 \tag{2.12}$$

where additional variables with respect to FSDT are introduced in the transverse displacement expansion. Type of refinements of FSDT such as the displacement model (2.12) are known as Higher Order Theories (HOT) (Reddy, 2004). In general, HOT are based on displacement models of the following type,

$$u_i(x, y, z) = u_i^0(x, y) + zu_{i1} + z^2u_{i2} + \dots + z^{N_i}u_{iN_i}, \quad i = 1, 2, 3 \quad (2.13)$$

where N_i are the order of the expansions used for the displacement variables. The additional unknowns in the expansion are often difficult to interpret in physical terms. In this context, the third order theory with transverse inextensibility of Reddy (2004) is of particular interest. This theory is based on a displacement field that provides quadratic variation of transverse shear strains, and hence stresses, and the disappearance of transverse shear stresses at the top and bottom of a general composite laminate. Thus there is no need to use shear correction factors, however, Koiter's recommendation is not taken into account since the transverse normal stresses are not refined compared to CLT.

Two-dimensional plate/shell multilayered elements are usually derived by introducing finite element approximations which correspond to the reference surface, as showed in figure 2.6 for a classical two-dimensional quadratic shell element. Detailed overviews con-

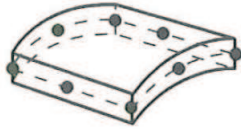


Figure 2.6: Classical two-dimensional quadratic shell element: nodes located on the reference middle surface.

cerning finite elements implementations of the aforementioned ESL theories are given in the works of Reddy (2004); Reddy and Robbins (1994), Kant and Swaminathan (2000), and Carrera (2002). It can be concluded from the aforementioned works that although the CLT yields finite element models that are economical in terms of the number of degrees of freedom used, these models require C^1 continuity of the transverse displacement, which complicates the development of conforming elements and inhibits the use of these elements with other commonly used finite elements. In contrast, FEs based on the FSDT have the advantage of requiring only C^0 continuity of all primary variables, however, early FSDT plate type elements showed severe stiffening for thin laminates. Such a numerical mechanism, known as shear locking, can be contrasted using reduced/selective integration schemes or by using higher order elements, but sometimes at the expense of rate of convergence (Reddy, 2004). Although the reduced/selective integration solution is the most economical alternative among the techniques mentioned above to contrast shear locking, the process may generate hourglass mechanisms from spurious energy modes which can be introduced by using these sub-integration techniques. The mixed interpolation of tensorial components technique is usually implemented to alleviate this mechanisms (Carrera, 2002). Locking phenomena are even more emphatic in shell finite elements due to the bending-stretching coupling of such structures, and membrane locking may occur in addition to shear locking for thin shell structures (Chapelle and Bathe, 2003). Additional difficulties may arise in

the case of finite rotations in non-linear analyses of shell structures since complex update algorithms for finite rotations may be required (Vu-Quoc and Tan, 2003a). A large variety of plate/shell finite element implementations of HOT are also proposed in the literature. A comprehensive discussion of HOT type theories and related finite element suitability is given in Tessler (1991).

Shell finite elements based on ESL theories can also be developed using the degenerated shell concept (Bischoff et al., 2004; Carrera, 2002; McNeal, 1998). In this concept, the idea of developing shell finite elements via degeneration means switching the sequence of dimensional reduction and discretization. Thus, the starting point is a finite element discretization of the three-dimensional continuum. Shell elements based on the degenerated solid approach are therefore also denoted continuum-based shell elements (Bischoff et al., 2004). The continuum based shell element is degenerated from a 3D isoparametric description element by imposing two-dimensional hypotheses as constraint equations using Lagrange multiplier. A schematic representation of the degeneration procedure from a 20 node solid element to an 8 node shell element is given in figure 2.7. Enforcing the

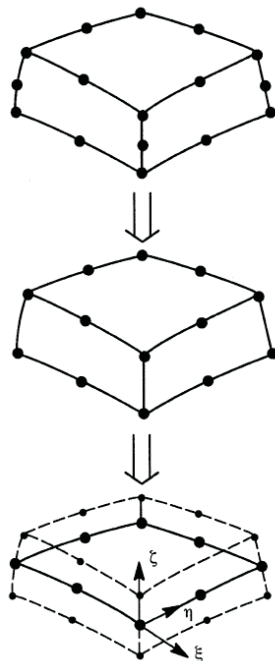


Figure 2.7: Degeneration of a twenty-node brick element into an eight-node shell element (McNeal, 1998).

same assumptions made for the FSDT would involve the following three steps: (i), nodes in the middle plane are removed assuming constant transverse strain, (ii), opposite nodes are linked by assuming equal displacements and assigning two rotational degrees of freedom to each pair of nodes, and (iii), the motion of each straight line is described using five degrees of freedom in one node, lying in the reference surface. The degeneration approach

is appealing since it potentially enhances the capabilities of the resulting shell elements in the thick shell range and it offers an alternative way for imposing shell assumptions without having to discretize the governing shell equations as in traditional shell elements. However, the degenerated approach needs modifications since it can present two shortcomings: one, bending cannot be represented properly because of the presence of artificial normal stresses in the thickness direction, i.e. thickness locking, and two, conditioning of the corresponding element stiffness matrices is much worse than in conventional 5-parameter shell elements due to the extremely high stiffness in the transverse normal direction (Bischoff et al., 2004).

Finite element models based on ESL theories are often able to provide a sufficiently accurate description of the global response of thin to moderately thick laminates, e.g. gross deflections, critical buckling loads, fundamental vibration frequencies and associated mode shapes. In particular, finite element models based on FSDT appear to provide the best compromise of solution accuracy, solution economy, model simplicity and compatibility with other displacement finite element models (Reddy and Robbins, 1994). However, ESL models have several limitations that prevent them from being used to solve the whole spectrum of composite laminate problems. One, the accuracy of the global response deteriorates as the laminate becomes thicker. Two, ESL theories are often incapable of accurately describing the state of stress at the ply level near geometric and material discontinuities, where a three dimensional stress state is generally achieved, or near regions of intense loading. In these cases, the transverse stresses calculated using the constitutive relations can be inaccurate (Carrera, 2001; Reddy, 2004). The reason of such inaccuracies is that these theories are 'kinematically homogeneous' in the sense that the kinematic is insensitive to individual layers (Carrera, 2003a). Then, ESL theories lack to fulfill the C_z^0 -Requirements since ZZ and IC are not imposed in their theoretical foundations. It has been shown that better transverse stresses can be obtained by integrating three-dimensional 3D equilibrium equations rather than using Hooke's law (Jones, 1999; Pagano, 1969), however, this alternative procedure, which provides reasonably accurate predictions of the transverse stresses for closed form analytic solutions, in finite element procedures require appropriate strain gradients evaluations whose recovery from the finite element shape functions is known to be inferior compared to the accuracy reached in the displacement field. In any case the accuracy of the obtained transverse stress distributions cannot be guaranteed (Carrera, 2002).

An alternative approach to improve the stress field calculations obtained using ESL theories is to employ full mixed and partially mixed formulations. Compared to the displacement type of finite element formulations, mixed formulations demand less stringent admissible requirements on continuity and offer the flexibility to deal with a greater variety of problems. One of the aims of mixed finite elements is to relax formulations that otherwise would be overconstrained giving rise to phenomena such as locking (Reddy, 2002; Zienkiewicz and Taylor, 2000). Moreover, since the secondary fields are computed explicitly, one can think of mixed formulations as an alternative method for secondary-field recovery or smoothing. Then, a natural manner to fulfill the C_z^0 -Requirements of multilayered composite structures is to assume both displacements and stresses as unknown variables. Full mixed methods have been developed which make use of mixed variational statements where all six stress components and the three displacements are assumed to be unknown variables of the structural problem (Carrera, 2002; Pagano, 1978). However, the computational cost involved when using full mixed approaches can be prohibitive for practical problems. An interesting discussion on possible ways to improve of FSDT type models by using mixed and partially

mixed formulation is given in Auricchio and Sacco (2001). The Hellinger-Reissner mixed principle (2.8) is employed in Auricchio and Sacco's work, and two FSDT type models, both describing transverse shear stresses as independent variables, were discussed. Auricchio et al. (2001) have developed mixed finite elements for laminated composite plates based on Auricchio and Sacco's work (Auricchio and Sacco, 2001) in subsequent work.

2.3.4 Layer-Wise Theories

When a detailed response of individual layers is required to include a highly accurate assessment of the stress state of localized regions, especially if significant variations in displacements gradients between layers exist as in the case of local phenomena descriptions, a possible manner of including the ZZ effect in the framework of ESL models can be obtained by applying CLT, FSDT or HOT at layer level. That is, each layer is seen as an independent plate and compatibility of displacement components is imposed as a constraint at each interface. In these cases Layer-Wise, LW, models are obtained (Carrera, 2003a; Reddy, 2004). In contrast to ESL theories, LW theories are developed by assuming that the displacement fields exhibits only C^0 continuity through the laminate thickness. Then, displacement components are continuous through the laminate thickness, but the derivatives of the displacements with respect to the thickness coordinate may be discontinuous at various points through the thickness, thus allowing for the possibility of continuous transverse stresses at interfaces separating dissimilar materials. Such theories are also able to represent the ZZ behaviour of the displacement fields required by C_z^0 -Requirements by allowing the displacements to vary in a layerwise manner through the thickness of the laminate.

A detailed overview of available LW theories in the open literature is given in Reddy (2004). Other relevant examples of these type of theories are those found in the articles by Srinivas (1973), who uses CLT in each layer, and by Cho et al. (1991), who use the HOT developed by Lo et al. (1977) where the in-plane and normal displacements are, respectively, approximated by third and second order functions of the thickness coordinate in each layer. The aforementioned procedures require the inclusion of constraint conditions to enforce the compatibility conditions at each interface. Carrera (2000) has shown that a layer-wise approach employing a third or four order displacement fields in each layer can provide accurate displacements and stresses descriptions, both in-plane and transverse components, directly by using Hooke's law. Generalizations on LW types of theories are given in Nosier et al. (1993) and in Reddy (2004) where the displacement variables of the k -th layer in the thickness direction are expressed in terms of Lagrange polynomials as follows:

$$u^k(x, y, z) = L_1(z_k)u_{i(h_k/2)}^k + L_2(z_k)u_{i(-h_k/2)}^k + L_3(z_k)u_{i2}^k + \dots + L_N(z_k)u_{iN}^k \quad (2.14)$$

$$i = 1, 2, 3 \quad k = 1, N_l$$

where the adopted notation is introduced in figure 2.8, N_l is the number of layers, and interface values of the displacements at the top of the k -th layer $u_{i(h_k/2)}^k$ and at the bottom of the k -th layer $u_{i(-h_k/2)}^k$ are used as unknown variables, thus permitting an easy linkage for applying compatibility conditions at each interface. This is because L_1, L_2 coincide with linear Lagrangian polynomials while L_3, \dots, L_N should be an independent base of polynomials which start from the parabolic L_3 . Reddy extended this theory to the finite element framework by representing the transverse variation of the displacement components in terms

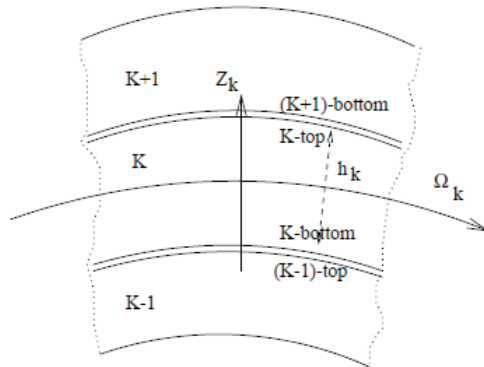


Figure 2.8: Notation used for multilayered plates/shells (courtesy of Carrera (2002)).

of one-dimensional Lagrangian finite elements (Reddy, 2004). This layer-wise field is very general in that any desired number of layers, distribution of layers and order of interpolation can be achieved simply by specifying a particular mesh of one-dimensional finite elements through the thickness.

The aforementioned LW models based on displacement formulations show acceptable accuracy with respect to three-dimensional analyses, but these models do not a priori and completely fulfill the C_z^0 -Requirements since transverse stress interlaminar continuity is not accounted for a priori. Applications of LW models based on displacement formulations require a posteriori recovery of transverse stresses. Carrera (1996a, 1998, 1999c, 2002) have developed mixed LW theories for laminated plates analysis to a priori fulfill the continuity of transverse shear and normal stress components at the interface between two adjacent layers. This was achieved by employing the Reissner Mixed Variational Theorem (RMVT) (Reissner, 1984, 1986) to derive the governing equations in terms of introduced transverse stress and displacement variables. In Carrera's theories, two independent fields are assumed in the thickness direction, linear, up-to fourth order, for the displacements and transverse stresses unknowns similar to those used in Reddy's theory (2.14), but Legendre polynomials are used as base functions. Legendre polynomials, like Lagrange polynomials, offer an easy linkage to impose compatibility of the displacements and equilibrium for the transverse stress components at each layer interface. However, as opposed to Lagrange polynomials, the use of Legendre polynomials permits the thickness interpolation to be spanned by a hierarchical basis, where each additional base function is orthogonal to, or at least linearly independent of, the previous ones. Standard Lagrange polynomials are neither hierarchic nor orthogonal. Thus, increasing the order of interpolation requires a complete new set of shape functions (Bischoff et al., 2004). Carrera (1999a,b) uses mixed layerwise shell theories for analyses of multilayered, double curved shells made of orthotropic laminae in linear static cases, and he provides a unified compact formulation (UF) that can be used to assess multilayered ESL/LW plate and shell theories based on displacement and mixed variational statements (Carrera, 2002). Carrera and Demasi (2002a,b) have developed and compared multilayered plate elements based upon the PVD and the RMVT, see section 2.3.2 for both equivalent single-layer, see section 2.3.3, and layer-wise multilayered form descriptions using Carrera's UF. In this context, a generalization of Carrera's UF (GUF) has been developed

for plate theories by Demasi (2008). In Demasi's GUF each variable, in the most general case each displacement and each transverse stress, can be independently expanded along the thickness leading to a wide variety of new displacement and mixed ESL/LW plate theories. Now, each variable can be expanded in different forms by simply changing the order of the polynomial used in the expansion along the thickness of the laminate.

Highly accurate models based on a Layer-Wise laminate theory are computationally expensive and sometimes impractical to run, especially in geometrically nonlinear cases. To capture the localized 3-D stress fields in a tractable manner, it is usually necessary to resort to Multiple Methods (Noor, 1986), i.e. simultaneous and sequential multiple methods techniques, in which different subregions of the structure are described using different types of mathematical models based on physical characteristics, applied loading, expected behaviour and level of solution accuracy desired. For instance, LW models are generally used in regions of a structure where an accurate description is required, whereas ESL models are employed in less critical areas of the structure. The actual implementation of such a technique is complicated and cumbersome, due mainly to the need to maintain displacement continuity across subregion boundaries separating incompatible subdomains. Established methods of achieving displacement continuity between incompatible regions can be found in the work of Reddy and Robbins (1994).

Compared to 3-D finite element models, layer-wise elements have some analysis advantages over the conventional 3-D elements. The layer-wise format maintains a 2-D type data structure similar to finite element models for 2-D ESL theories. This provides several advantages over conventional 3-D finite element models. One, the volume of the input data is reduced. Two, the in-plane 2-D mesh and the transverse 1-D mesh of the discretized structure can be refined independently without having to reconstruct a 3-D finite element mesh. The 2-D type data structure also allows efficient formulation of the element stiffness matrices of the structural problem (Reddy, 2004). However, a 3-D finite element model is more general than a layer-wise finite element model: the latter represents a special case of the former. This is because a layer-wise model assumes that the displacements, material properties and element geometry of the discretized structure can be approximated by a sum of separable 3-D interpolation functions, where each 3-D interpolation function can be written as the product of an in-plane 2-D interpolation function and a through the thickness 1-D interpolation function. However, the modeling capabilities of the two methods are essentially the same. In this context, a detailed investigation on the similarities and differences between layer-wise and 3-D finite element models is given in Reddy (2004).

2.3.5 Zig-Zag Theories

Within both frameworks of the ESL and LW variable descriptions there is a need to try to develop theories which fulfill *a priori* the C_z^0 -Requirements. Due to the form of the required displacement field in the thickness direction of the laminate, these type of theories are referred to as Zig-Zag theories. The fundamental idea in developing Zig-Zag theories is an assumption that a certain displacement and/or stress model is available for each layer, and the number of the unknown variables is reduced using compatibility and equilibrium conditions at the interfaces between the layers. For the clarity, a one dimensional flat case is considered as an example, where a piecewise, continuous, linear displacement field is considered, see figure 2.9. The origin of the thickness coordinates is at the bottom surface

of the laminate. The displacement field u in each layer of the laminate can be first written

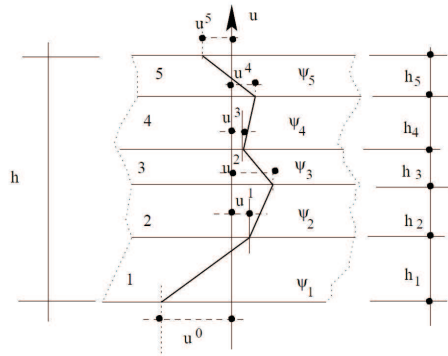


Figure 2.9: Geometry and notation employed to introduce Zig-Zag theories (courtesy of Carrera (2002)).

using displacement values at the interfaces. For instance, for the first and last layers one gets:

$$\begin{aligned} u^1(z) &= u^0 + z\psi_1, & 0 \leq z \leq h_1 \\ u^{N_l}(z) &= u^{N_l-1}(h_{N_l-1}) + (z - h_{N_l-1})\psi_{N_l}, & h_{N_l-1} \leq z \leq h_{N_l} \end{aligned} \quad (2.15)$$

where N_l is the number of layers, u^0 and u^{N_l} are, respectively, the values of the displacement u at the bottom and top surfaces of the laminate, $u^k(h_k)$ are the interface value of u with $k = 1, (N_l - 1)$, and ψ_k are the rotations in the layers with $k = 1, N_l$. The generic displacement interface value can be re-written as follows:

$$u^k(h_k) = u^0 + \sum_{k=1}^{N_l-1} (h_k - h_{k-1})\psi_k, \quad h = 1, N_l \quad (2.16)$$

Using compatibility and equilibrium conditions at the interfaces, the displacement u can be written in a form which is formally not affected by k :

$$u(z) = u^0 + \sum_{k=1}^{N_l-1} (z - z_{k-1})\psi_k H(z - z_k) \quad (2.17)$$

where H is a Heavieside step function defined as follows:

$$H(z - z_k) = \begin{cases} 0 & z \leq z_k \\ 1 & z \geq z_k \end{cases} \quad (2.18)$$

or

$$u(z) = u^0 + \sum_{k=1}^{N_l-1} (z - z_{k-1})a_k\psi_k H(z - z_k) \quad (2.19)$$

since it is possible to express the N_l rotations ψ_k of each layer of the laminate in terms of one of them, for instance the rotation in the bottom layer ψ_1 , by imposing the $N_l - 1$ interlaminar continuity conditions for the transverse shear stress, from which the following relation is obtained:

$$\psi_k = a_k \psi_1, \quad k = 2, N_l - 1 \quad (2.20)$$

where a_k are layer constants defined by the interlaminar transverse stresses. The complete procedure retrieving the equation (2.19) can be found in Carrera (2002). The assumed linear piece-wise form of the displacement u leads to layer continuity stiffnesses a^k that are independent of z . In this case, top-bottom homogeneous conditions can not be imposed. Assuming a^k as a cubic functions of z , as in the works done by Whitney (1969) and Ambartsumian (1969), allows homogeneous transverse shear stress conditions to be imposed on the top and bottom plate/shell surfaces.

An accurate historical review of Zig-Zag theories for multilayered plates and shells is given in Carrera (2002, 2003b), where references to complete reviews of several approaches, computational techniques and numerical assessment are also reported. The Zig-Zag theories that have provided the most outstanding contributions to FE applications are summarized below. The first, and most relevant work, is that of Lekhnitskii (1935), who has developed an elegant approach for beam geometries which describes interlaminar continuous transverse shear stress and zigzag effects of the displacement components. Ambartsumian (1962, 1969) further has developed this work and applied it to plates and shells structures. Another pioneering analysis is presented in Yu (1959), where zigzag effects of the in-plane displacement components and transverse continuity of the shear stress components in correspondence of each layer interface of a sandwich plate were both fulfilled. Particular mention should be made of the work of Ren (1986a,b), who has extended the early work of Lekhnitskii on beam geometries to anisotropic plates, and Whitney (1969), who has extended Ambartsumian's theory (Ambartsumian, 1962, 1969) to unsymmetric cases, this has been extended to shell geometries by Rath and Das (1973). Rath and Das's theory has been extended further by Cho and Permerter (1993) who have developed a theory for arbitrary laminated plates including zigzag effects of the in-plane displacement components, and capable of satisfying the continuity of the transverse shear stress components in correspondence of each layer interface and shear free surface conditions at the top/bottom of the plate. It should be noted that, because of the intrinsic material couplings between the transverse normal and in-plane components of the stress field, all the theories discussed above generate difficulties in dealing with the extension of the zigzag forms to the transverse displacement component or in accounting for the interlaminar continuity of the transverse normal stress. As a consequence, all of the related results have shown deficiencies in analysing problems in which transverse normal stress plays a determinant role, as for instance in the stress analysis of thick composite laminates and in areas where a 3-D stress state needs to be determined, i.e. stresses near holes, cut-outs and traction free edges (Carrera, 1998).

Procedures formulated using only displacement unknowns cannot *a priori* be used to describe interlaminar equilibrium IC for the transverse stresses, meaning that C_z^0 requirements cannot be completely fulfilled. Zig-Zag theories employing the RMVT (Reissner, 1984, 1986) have been developed to fulfill the C_z^0 requirements better (Carrera, 2002, 2003b). Murakami and Toledano (Murakami, 1986; Toledano and Murakami, 1987a,b) were the first to develop a plate theory for specially orthotropic laminated plates on the basis of RMVT in

the framework of ESL models. Rao and Meyer-Piening (1990) have extended the Toledano-Murakami's theory to the case of generally laminated orthotropic plates. Rao and Meyer-Piening's theory has been used by the same authors to develop plate finite element for the analysis of laminated plates composed of arbitrary oriented layers. Of particular interest is the work done by Bhaskar and Varadan (1992) and by Jing and Tzeng (1993) who have extended a particular case of the Toledano and Murakami type theory to cylindrical shells, and by Carrera (2002) who has presented a systematic manner of using RMVT to develop ESL plate and shell theories, including Zig-Zag theories, along with finite elements for statics and dynamics and linear and nonlinear problems. In this context, Carrera (1996b) has extended the standard Reissner-Mindlin model to multilayered plate structures in such a way that, compared to models based on the FSDT (2.11), ZZ effects and IC for the transverse shear stresses were also considered. In Carrera's work (Carrera, 1996b), Murakami's theory (Murakami, 1986) is employed and multilayered plate finite elements are developed. Later on, Brank and Carrera (2000) have extended Carrera's work (Carrera, 1996b) to shell geometries, and they implemented an assumed shear strain concept to eliminate shear locking mechanisms and to prevent spurious modes which are typical of alternative sub-integration techniques. Within the RMVT framework, although in most of the references mentioned above the C_z^0 -Requirements have been a priori and completely included, the results have been very poor when it comes to treating arbitrarily laminated plate and shell structures (Carrera, 1998).

2.4 Conclusions

An appropriate computational strategy for the analysis of variable stiffness panels require an efficient modeling strategy able to detect the local three-dimensional stress states generated during the manufacturing process. A strategy can only be developed if it is fully understood how conventional composite laminates function. In particular, multilayered plate and shell structures require appropriate models to handle the complicated effects arising from their intrinsic in-plane and out-of-plane anisotropy. Complicated effects, such as high transverse deformability, zig-zag effects and interlaminar continuity, have been discussed and summarized by the acronym C_z^0 -Requirements. It is necessary to handle C_z^0 requirements well to obtain accurate descriptions of the stress and strain fields in the analysis of multilayered composite structures. Accurate analyses can be performed by adopting models based on 3D brick elements, however, three dimensional modeling is generally computationally expensive, thus often too time consuming and costly for practical use. Two-dimensional, 2D, modeling can be a valuable alternative, and an overview of common two-dimensional plate/shell axiomatic theories used for composite, multilayered structures is given above.

Axiomatic theories are developed by making an appropriate choice for which unknown variables to use for a structural problem, whether to use displacement or mixed formulation, and which multilayer form description to adopt, ESL or LW model. Models based on ESL theories are often able to provide a sufficiently accurate description of the global response of thin to moderately thick plate/shell structures. In particular, finite element models based on FSDT appear to provide the best compromise to obtain solution accuracy, solution economy, model simplicity and compatibility with other displacement finite element models. However, ESL models do not permit the description of zig-zag effects of the displacement fields

and interlaminar continuity of transverse stresses. Although improved transverse stress distributions can be obtained by integrating the three-dimensional 3D equilibrium equations or by assuming mixed formulations rather than using Hooke's law, ESL models generally lead to unsatisfactory results in the evaluation of the global response of thick plate/shell structures, and in the evaluation of the state of stress at the ply level near geometric and material discontinuities.

Complete fulfillment of the C_z^0 requirements can be achieved by employing Zig-Zag theories combined with mixed formulations, but these theories give generally inaccurate results when treating arbitrarily laminated plates and shells. In this case, the use of a Layer-Wise description becomes mandatory to obtain an accurate evaluation of the stress fields in plate/shell composite structures. Within a LW multilayered form description, accurate transverse stresses can be computed directly from Hooke's law if an adequate expansion is used in each layer for the displacement components. Compared to 3-D finite element models, layer-wise elements have some analysis advantages over the conventional 3-D elements. The layer-wise format maintains a 2-D type data structure similar to finite element models of 2-D ESL theories. This provides several advantages over conventional 3-D finite element models. Although a layer-wise finite element model represents a special case of a 3-D finite element model, the modeling capabilities of the two methods are essentially the same. Highly accurate, models based on a Layer-Wise laminate theory are computationally expensive and sometimes impractical, especially in geometrically nonlinear cases. Multiple Methods can be employed to capture the localized 3-D stress fields in a tractable manner. However, the actual implementation of such methods is generally complicated and cumbersome.

Chapter 3

Stress Recovery Techniques

3.1 Introduction

Beside an appropriate modeling theory, appropriate stress analyses of variable stiffness panels also required an appropriate stress recovery procedure. In particular, the three-dimensional stress states arising at regions such as tow-drop and/or tow-overlaps require an accurate evaluation of the interlaminar stresses. An appropriate stress recovery procedure can only be developed if a proper overview and understanding of conventional stress recovery techniques are, respectively, provided and achieved. Moreover, comparisons between different procedures commonly used to make stress calculations will give a better understanding of the appropriate technique to use in terms of consistency and accuracy of the recovered stress fields, and in terms of computational effort involved in using a particular procedure.

The selection of the best procedure to use to recover accurate stress field measurements strongly depends on the variational formulation used to obtain the governing equations of the structural problem. Although the displacement finite element method has generally been shown to be a very attractive structural analysis method, it is also known to have certain shortcomings, for instance, its lower accuracy for predicting strains and stresses compared to displacements. The reason for this lack of accuracy when predicting stresses are well understood (Jones, 1999; Reddy, 2004). Since in a displacement based variational formulation the displacements are assumed as unknowns variables of the problem, the displacements are imposed to be interelement continuous, whereas the stresses are generally obtained as derivatives of the displacements, resulting in a lower degree of approximation. This lack of accuracy leads to an additional shortcoming, that displacement based formulations give a bad approximation of the stresses at nodes which are generally the most interesting points for stress recovery. For instance, in problems involving determination or estimation of stresses and high stress gradients at the boundary or a bi-material interface of an object, nodes are the most useful output locations for stresses.

Enhancement procedures aimed at making the stress fields obtained using displacement models competitive with refined models, such as those based on mixed approaches which do not suffer from the above deficiencies, have been explored from the beginning by those working on the finite element method (Zienkiewicz and Taylor, 2000). A review of com-

monly used displacement based methods is provided in section 3.2 where the advantages and shortcomings of these procedures are discussed. Since mixed finite element formulations give rise to improved methods for stress calculation, stress recovery expressions based on hybrid formulations of the Hellinger-Reissner- and the Hu-Washizu-functional are derived and compared in section 3.3 with commonly used stress recovery techniques for displacements models. Stress recovery expressions of enhanced hybrid formulations are also discussed in this section to compare the different methods. The chapter ends with a number of conclusions.

3.2 Stress Recovery Techniques for Displacement Based Finite Elements

Finite element models based on displacement approximations are widely used for structural analyses, and a common deficiency of these models is their low level of accuracy for predicting local quantities in structures such as stresses and strains compared to displacements. An obvious and consistent approach to calculating the stresses resulting from a displacement finite element approximation is to differentiate the finite element solution directly and evaluate the stresses at points of interest in a structure using the appropriate constitutive relations. This direct calculation results in lower order, discontinuous stress measurements with inferior accuracy at the boundary of the elements and at the interelement nodes, places where accurate values are usually desired such as the tow-drop and tow-overlap regions of tow-placed layups. This problem has motivated the development of stress recovery techniques aimed at replacing the stress field results deduced directly from constitutive equations, referred to as conventional stress field, with a technique that is more accurate for predicting a stress field. This field is called a recovered stress field.

There are points within an element, for certain classes of finite elements and interpolation functions, at which the rate of convergence for stresses is exceeded by one order compared to other locations, i.e. Barlow or superconvergent points (Barlow, 1976). Proof of superconvergence at Gauss-Legendre points for the gradient of the Dirichlet problem exists for the Serendipity (Zlamal, 1977) and Lagrangian (Lesaint, 1979) class of elements. The existence of these optimal sampling points within an element provides a sound basis for extrapolation techniques from such points to the boundaries of the element domain, resulting in improved nodal values. In the past, in the case of discontinuous stress distributions, it was handled by assigning the conventional stresses from the respective closest superconvergent points to the common node of the two elements. However, these superconvergent point assigned values could be inaccurate in cases where stress gradients at the bi-material interface were high. In the case of continuous stress distributions, superconvergent point conventional stress values were assigned to the common node of the two elements and then averaged. In this case where the superconvergent point stress values were averaged, the distances of the superconvergent points from the nodes were often not taken into account resulting in inaccurate estimates of stresses (Chen et al., 1996). Later, as an alternative strategy to that discussed above, conventional least-square smoothing was adopted. In this procedure, discrete conventional stress data obtained from finite element superconvergent points are smoothed and extrapolated to the boundaries of the element domain. This is achieved by defining a smooth polynomial from the discrete data distribution. However,

Hinton and Irons (1968) have indicated that such polynomials tend to behave erratically near areas where stress concentrations occur.

In virtue of the shortcomings of the above procedures, the conventional stress field is now generally evaluated at superconvergent points and it is then assumed that, throughout the element, the stresses of the recovered stress field $\bar{\sigma}$ can be obtained by interpolation in the same manner as the displacements are interpolated throughout the element. The following equation is used:

$$\bar{\sigma} = \psi^k \bar{\sigma}^k \quad k = 1, N_k \quad (3.1)$$

where $\bar{\sigma}^k$ are the stresses evaluated at superconvergent points, N_k is the number of superconvergent points for the stress field within an element, and ψ^k are the C^r -continuous interpolation functions that have continuous first r derivatives. This technique can be enhanced further by using a *stress smoothing* technique such as the one proposed by Hinton (1974), i.e. the local projection method, where an error function is defined as the difference between the recovered stress field and a smoothed stress field. The value of this error function is minimized, usually by using a least-squares approach. The underlying assumption in these kind of methods is that an average of the conventional stress field is more accurate than the conventional stress field itself. *Stress smoothing* may be local, at the element level, or global: for local smoothing, the smoothed stress field within an element is also given by (3.1) where N_k now represents the number of nodes for the recovered stress field. Following Hinton (1974) the error function can be generalized as:

$$\chi = \int_{\Omega_e} \mathbf{e} : \mathbf{e} d\Omega, \quad \mathbf{e} = \boldsymbol{\sigma} - \bar{\boldsymbol{\sigma}} = \boldsymbol{\sigma} - \psi^k \bar{\boldsymbol{\sigma}}^k \quad (3.2)$$

where $d\Omega$ is a differential element of volume and $\boldsymbol{\sigma}$ are the recovered stresses. The recovery expression for the smoothed stress field is obtained in the following form by minimizing χ with respect to $\bar{\boldsymbol{\sigma}}$ (Mota and Abel, 2000):

$$\bar{\boldsymbol{\sigma}} = \boldsymbol{\Psi} \cdot \mathbf{H}^{-1} \cdot \boldsymbol{\Sigma}, \quad \mathbf{H} := \int_{\Omega_e} \boldsymbol{\Psi} \otimes \boldsymbol{\Psi} d\Omega, \quad \boldsymbol{\Sigma} := \int_{\Omega_e} \boldsymbol{\Psi} \otimes \boldsymbol{\sigma} d\Omega \quad (3.3)$$

where the vector of interpolation functions $\boldsymbol{\Psi}$ is introduced. Using this technique, the smoothed stress field is interelement discontinuous. In engineering practice it is customary to average the contributions of contiguous elements at common nodes in the case of continuous stress distributions. A continuous smooth stress field can also be obtained in a more computationally expensive manner by assembling each H and Σ in (3.3) into corresponding global tensors, in a process analogous to the assembly of the global stiffness. In this case, since C^0 -continuous interpolation functions are normally used for stress recovery, variations in global stress smoothing include the introduction of a penalty term in the error function that enforce C^1 -continuity of the recovered stress field (Riggs et al., 1997). Hinton and Campbell propose using the *stress smoothing* technique for linear least square fit of reduced integrated elements. Chen et al. (1996) extended this procedure to quadratic least-square smoothing for both two- and three-dimensional cases showing that the quadratic extrapolation is more effective than the linear extrapolation of reduced integrated elements for estimating the nodal stress values of composite laminates. An equivalent relation to (3.3) for the smooth stress field is also obtained by defining an error function as (Mota and Abel,

2000):

$$\Psi := \int_{\Omega_e} (\boldsymbol{\sigma} - \bar{\boldsymbol{\sigma}}) : (\boldsymbol{\epsilon} - \bar{\boldsymbol{\epsilon}}) d\Omega \quad (3.4)$$

where a recovered strain field $\bar{\boldsymbol{\epsilon}} = \psi^L \bar{\boldsymbol{\epsilon}}^L$ is introduced, in which ψ^L are interpolation functions for the recovered strain field related to the L number of interpolation points, and the strain-displacement operator is:

$$\mathbf{u} = N^I \mathbf{u}^I, \quad \boldsymbol{\epsilon} = \mathcal{B}^I \cdot \mathbf{u}^I, \quad \mathcal{B}^I := \mathcal{G} \cdot \nabla N^I \quad (3.5)$$

where N^I are the interpolation functions for the displacement field, \mathbf{u}^I is the nodal displacement vector, \mathcal{G} is a fourth-order tensor such that $\mathcal{G} : \mathbf{A} = \frac{1}{2}(\mathbf{A} + \mathbf{A}^T) \equiv \text{symm}(\mathbf{A})$ for any second order tensor \mathbf{A} , with $\nabla(\cdot) := [\partial(\cdot)/\partial \mathbf{x}]^T$, in which $\mathbf{x} := (x^1, x^2, x^3) \in \mathbb{R}^3$ is a material point (Mota and Abel, 2000). The stress recovery expression (3.3) is easily derived with the additional recovery expression for the strain by minimizing Ψ with respect to $\bar{\boldsymbol{\sigma}}$ and $\bar{\boldsymbol{\epsilon}}$ to obtain the optimality conditions:

$$\bar{\boldsymbol{\epsilon}} = \boldsymbol{\Psi} \cdot \mathbf{H}^{-1} \cdot \mathbf{E}, \quad \mathbf{E} := \int_{\Omega_e} \boldsymbol{\Psi} \otimes \boldsymbol{\epsilon} d\Omega \quad (3.6)$$

The L_2 global projection method (Oden and Brauchli, 1971) is a considerably more costly process of recovering accurate nodal values. In this procedure it is initially assumed a C_0 continuous interpolation of the recovered stress field values of the same form as that used for the displacements interpolation, and the nodal values of the global smoothed stress field are then determined by a least square fit of the recovered stresses. This is achieved by assuming the interpolation functions for the smooth stress fields to be biorthogonal with respect to the interpolation functions of the displacement field of the entire domain. For example, the L_2 global projection method applied to a single element, thus recovering a local, interelement discontinuous, stress field, allows the strains and the recovered stresses to be assumed in the following form

$$\boldsymbol{\epsilon} = \Psi^K \boldsymbol{\epsilon}^K, \quad \boldsymbol{\sigma} = \Phi^L \boldsymbol{\sigma}^L \quad (3.7)$$

where Ψ^K and Φ^L are the interpolation functions, respectively, for the conventional strains and recovered stresses field. Since stresses and strains are work conjugate, the interpolation functions are also required to satisfy conjugacy in the sense that

$$\int_{\Omega_e} \boldsymbol{\Psi} \otimes \boldsymbol{\Phi} d\Omega = \mathbf{I} \quad (3.8)$$

which is achieved by defining

$$\boldsymbol{\Phi} := \boldsymbol{\Psi} \otimes H^{-1}, \quad H := \int_{\Omega_e} \boldsymbol{\Psi} \otimes \boldsymbol{\Psi} d\Omega, \quad \boldsymbol{\Sigma} := \int_{\Omega_e} \boldsymbol{\Psi} \otimes \boldsymbol{\sigma} d\Omega \quad (3.9)$$

The recovery expression for stresses (3.3) is then obtained by introducing (3.9) into (3.7).

Zienkiewicz and Zhu (1992a,b) made a significant breakthrough towards an efficient post-processing technique when they proposed the Superconvergent Patch Recovery (SPR) procedure. In the SPR technique a single and continuous polynomial expansion of the

function describing the recovered stresses is used on an element patch surrounding the nodes at which recovery is desired. The continuous polynomial expansion is assumed to be of the same order p as that used for the displacements over the element patch considered. The patch represents a union of elements having in common an assembly node at which recovery is desired. For the sake of simplicity, typical patches for one and two dimensional elements are shown in figure 3.1 and 3.2. The polynomial expansion of each recovered

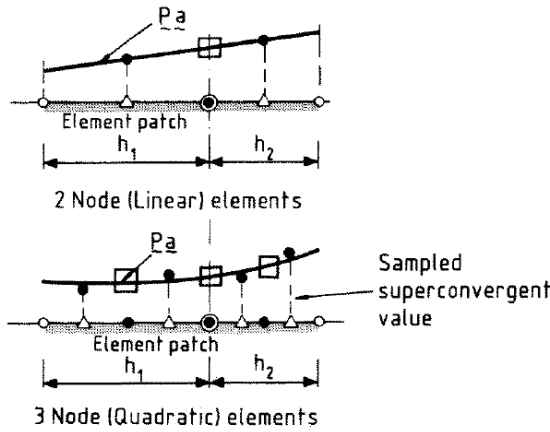


Figure 3.1: Typical one dimensional element patches showing the least square fit to sampled superconvergent Gauss point values: \triangle superconvergent Gauss points, \square nodal values determined using the recovery procedure, \odot Patch assembly point (Zienkiewicz and Zhu (1992a,b)).

stress component is assumed in the following form:

$$\sigma_p^* = \mathbf{P}\mathbf{a} \quad (3.10)$$

where \mathbf{P} contains the appropriate polynomial terms and \mathbf{a} is a set of unknown parameters. For instance, for one dimensional elements of order p it is possible to assume:

$$\mathbf{P} = [1, x, x^2, \dots, x^p], \quad \mathbf{a} = [a_1, a_2, a_3, \dots, a_{p+1}]^T \quad (3.11)$$

The recovery can be continuous or discrete, although only in the discrete case is the method known as SPR. The continuous patch recovery technique is a variant of the local L_2 projection method, and hence, of the stress smoothing technique applied on an element patch $\Omega_s = \bigcup_{j=1}^m \Omega_j$, where m is the number of elements in the patch. Then, (3.2) and (3.3) are applied by substituting Ω_s in place of Ω_e .

The determination of the unknown parameters a is made by ensuring a least square fit of the conventional stress field evaluated at superconvergent points in the case of discrete

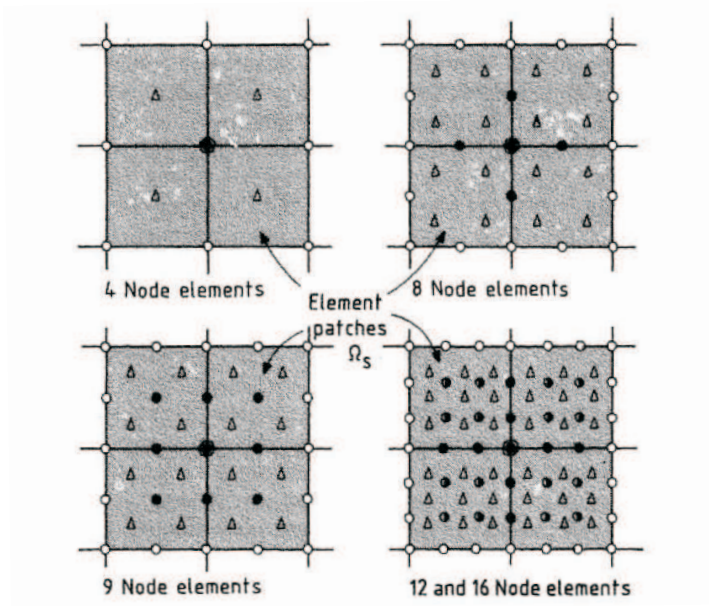


Figure 3.2: Computation of superconvergent nodal values for linear, quadratic and cubic lagrangian quadrilateral elements: \triangle superconvergent Gauss points, \bullet nodes at which stresses are recovered, \bullet Patch assembly point (Zienkiewicz and Zhu (1992a,b)).

SPR. This is done by minimizing the functional:

$$F(\mathbf{a}) = \sum_{i=1}^n (\sigma_h(x_i, y_i) - \sigma_p^*(x_i, y_i))^2 = \sum_{i=1}^n (\sigma_h(x_i, y_i) - \mathbf{P}(x_i, y_i)\mathbf{a})^2 \quad (3.12)$$

where (x_i, y_i) are the coordinates of the superconvergent points, $n = mk$ is the total number of superconvergent points and k is the number of superconvergent points on each element m_j ($m_j = 1, 2, \dots, m$) of the element patch $\Omega_s = \bigcup_{j=1}^m \Omega_j$, see figure 3.1 and 3.2.

Once the parameters a are determined, the stresses are calculated at the nodes inside the patch by the insertion of appropriate coordinates into the expression (3.10). The procedure is simply illustrated in figure 3.1 where one dimensional linear and quadratic elements are considered, and the appropriate fit of linear and quadratic polynomials over an element patch is indicated. It is clear from the procedure that element patches will overlap for internal midside nodes and nodes in the element interior. This means that such recovered nodal values are frequently evaluated from two patches, and for such nodes, an average value is used. A more difficult situation arise at the domain boundary where a local patch may involve only one or two elements, as shown in figure 3.3: for the one element solution (corner node) the size of the patch is insufficient for the determination of the parameters

a and the corner node values are determined from an interior patch. The standard manner is usually adopted for two element patches although all the boundary nodes values can be determined using interior patches (Zienkiewicz and Zhu, 1992a,b).

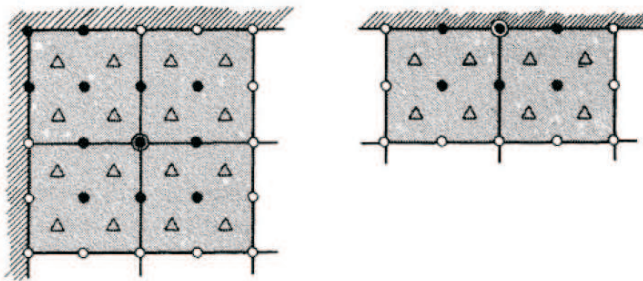


Figure 3.3: Boundary nodal recovery. Element patches: \triangle Sampling point; \bullet Nodal values determined using the recovery procedure; \odot Patch assembly point (Zienkiewicz and Zhu (1992a,b)).

Many investigators have modified the Zienkiewicz and Zhu's procedure by increasing the functional in such a way that the least square fit is performed to include satisfaction of boundary conditions (Blacker, 1994; Lee et al., 1997; Wiberg et al., 1994). In particular, Tessler et al. (1998) have developed the Smoothing Element Analysis (SEA) procedure based on a variational principle which combines the discrete-least-squares and penalty-constraint functionals in a single variational form. This approach produces smooth C^1 -continuous fields from any type of discrete data. Then, strain gradients can be properly recovered, and the interlaminar stresses in laminated composite plate/shell analysis that are obtained by integrating the gradients of stress (strain) quantities, as, for instance, when either the *Classical Lamination Theory* (CLT) (2.10) or the *First Shear Deformation Theory* (FSDT) (2.11) is adopted as the modeling theory, are readily computed.

Later, other viable alternatives to SPR have been considered. One of these is the Recovery by Equilibrium in Patches (REP) procedure, comparable in performance to SPR but taking into account a more simple and feasible implementation (Boroomand, 1997a,b). The REP method is based on recovering stresses by imposing equilibrium in a weak form over patches of elements. The resultant equations are obtained by projecting the error between new and original stresses into the finite element strain space over the patch and are solved using a least-squares scheme. There is also the Recovery of stresses by Compatibility in Patches (RCP) procedure presented by Ubertini (2004). The basic idea of RCP lies in observing that the finite element solution of displacement based models is obtained by imposing the equilibrium equations in a weak form among a set of kinematically admissible displacements. Thus, compatibility is always ensured while equilibrium is generally not. Then, RCP consists of recovering equilibrated stress fields over each patch by relaxing compatibility, that is by imposing compatibility in a weak form. To this purpose, the patch is considered to be a separate system on which finite element displacements are prescribed along the boundaries. Stresses are then recovered by minimizing the complementary energy

functional associated with such a separate patch system, over a set of stress fields which satisfy a priori interior equilibrium within the patch. The resultant equations are obtained by projecting the error between the finite element compatible strain and the strain coming from the equilibrated stresses into the new stress space over the patch. The RCP method can be viewed as dual to REP but, compared to REP, it gives more accurate and effective results especially in the case of arbitrarily generated meshes or in presence of severe element distortions. Ubertini concluded that RCP is competitive with the popular SPR procedure.

One desirable feature of all the aforementioned methods is that they can be applicable regardless of the governing constitutive behaviour, however, these recovery procedures depend crucially on the consistency of the conventional stress field evaluated within elements. In addition to the poor accuracy of stress measurements at the interelement boundaries and the consequent need for enhanced nodal stress recovery procedures, stress fields deduced directly using constitutive relations can show spurious oscillations due to the retention of higher order (inconsistent) terms which do not contribute to the determination of the displacements and then the strains, but get reflected as extraneous stress oscillations (Prathap and Naganarayana, 1990, 1995). These oscillations have been found in problems involving prescribed initial stresses or strains, or varying rigidities over the element domain (De Miranda and Ubertini, 2002). For instance, in thermoelastic analyses, compatible finite elements may predict oscillating stresses if the temperature distribution is not coherent with the element strain coming from the assumed displacement approximation. The problem of generating spurious stress oscillations can be further exacerbated due to element geometry distortions in parametric formulations (De Miranda and Ubertini, 2001). This local erratic behaviour of the conventional stress distribution generally implies that superconvergent points are no longer points for optimal stress recovery since the spurious stress oscillations do not generally vanish at these points. Then, the standard stress recovery procedures presented above could be not suitable for eliminating the spurious outcomes due to the lack of consistency of the recovered stresses. Prathap and Naganarayana (1990, 1995) have outlined the origin of such unreliable responses and introduced the notion of consistency within stress fields evaluations.

In order to recover consistent stress fields within elements other approaches to the conventional stress recovery have been proposed, and consistent stress distributions can be obtained in a variationally correct manner by employing integrated procedures (Argyris and Willam, 1974; Dakshina Moorthy and Reddy, 1999). In this context, De Miranda and Ubertini (2002) have proposed an integrated procedure defined at element level, where Prathap and Naganarayana's notion of consistency (Prathap and Naganarayana, 1990, 1995) is formalized in a condition involving each stress component being dealt with independently. This procedure is developed within a general weighted residual approach, and a systematic and effective procedure for recovering consistent stress distributions has been established. It should be remarked that variationally consistent stress recovery procedures are not an alternative for stress recovery but complementary to the standard stress recovery procedures presented above. In this respect, the consistent stress distribution should be reconstituted first and subsequently used for a reliable recovery of a smooth stress field.

Numerous approaches have been proposed as a means to obtain accurate analyses of laminated composite structures. Assessments of the various approaches can be found in (Kant and Swaminathan, 2000; Noor and Malik, 2000; Reddy and Robbins, 1994) and the

references contained therein. Economical finite element models as such adopting plate or shell elements based on either first-order or higher-order shear deformation theories are often combined for geometrically linear composite structures with post-processing procedures incorporating the through-the thickness integration of the three dimensional equilibrium equations performed using consistent in-plane stresses calculations based on superconvergent recovery. This procedure, which is not entirely consistent with the assumptions of the multilayer description form, provides improved stress distributions in the analysis of both thin and moderately thick structures. However, to evaluate accurate transverse shear and normal stresses these procedures require an accurate evaluation of in-plane strain gradients with respect to the in-plane coordinates, the recovery of which from the finite element shape functions is known to be inferior. In this context, it is worth mentioning the stress recovery procedures of (i) Tessler et al. (1998) based on the Smoothing Element Analysis (SEA) previously presented in the context of superconvergent stress recovery procedures on patches of elements, and (ii) the two-phase predictor-corrector postprocessing (PCP) scheme based on the *First Shear Deformation Theory* (2.11) used by Noor et al. (1994) and Park and Kim (1999) for geometrically linear composite structures under static loads.

Within the PCP procedure, accurate transverse shear stresses are predicted using thickness-wise integration of the equilibrium equations performed using in-plane stresses obtained by the SPR technique proposed by Zienkiewicz and Zhu (1992a). The accuracy of transverse normal stresses, displacements, and in-plane stresses are enhanced during the corrector phase by using the results from the finite element analysis and the predictor phase. This procedure has been enhanced further by Park and Kim (2003) who incorporated a mesh superposition technique for the local mesh refinement in the in-plane directions in the region where the evaluation of the stresses is needed. Stress recovery can not be conducted via direct integration of the equilibrium equations for geometrically nonlinear cases. Accordingly, non-linear predictor-corrector approaches which accurately computes transverse stresses for composite and sandwich panels undergoing geometrically non-linear deformations were introduced by Park and Kim (2003) and Lee and Lee (2003).

Procedures adopting economical finite elements combined with post-processing procedures incorporating the through-the-thickness integration of the three-dimensional equilibrium equations have considerable economical merits compared to full three dimensional finite element analyses or two-dimensional finite element analyses using Layer-Wise multilayer form descriptions. These procedures are widely used when the main emphasis of the analysis is to determine the global response, i.e. gross deflections, critical buckling loads, fundamental vibrations frequencies, of thin to moderately-thick structures, as for instance secondary structural components. However, when the emphasis of the analysis is the study of failure and failure modes or the modeling of delamination between layers of primary critical structural components these methods are, in general, inaccurate (Reddy, 2004): most primary structural components are considerably thicker than secondary components. Then, the assumption that a heterogeneous laminate is treated as a statically equivalent single layer would not be able to satisfy properly the C_z^0 requirements of multilayered composite structures, addressed in section 2.2, leading to inaccurate responses even in the evaluation of the global response. Moreover, the assessment of localized regions of potential damage initiation begins with an accurate determination of the three-dimensional state of stress at the ply level. Laminated composites often exhibit interlaminar stress failure due to transverse stress concentrations near geometric and material discontinuities, i.e. free edges, cut-outs,

leading to damage in the form of delamination. This also means that accurate evaluations of transverse stresses are specially required at the interelement nodes as opposed to superconvergent points. Then, the analysis of primary composite structural components generally require the use of either a Layer-Wise laminate theory that contains full 3-D kinematics and constitutive relations, or 3-D elasticity theory. Moreover, Layer-Wise and 3-D elasticity theories can model the kinematics of delamination.

In the context of studying delamination in multilayered composites, the interlaminar stress recovery procedure developed by Dakshina Moorthy and Reddy (1999) for 3-D finite element formulations becomes important. In their approach, each ply is modelled as a separate body and the interlaminar boundary is treated as a contact surface. The interlaminar forces are obtained using an interface model based on the penalty method. The interlaminar stresses are recovered using these contact loads. The recovery procedure partitions the contact surface into a set of non-overlapping patches corresponding to groups of elements. The traction distribution is interpolated over each patch in terms of nodal values. Static equivalence between the tractions and the contact forces is used to calculate the nodal value of the tractions, hence the interlaminar stresses. The procedure was found in practice to lead to oscillatory interlaminar stresses. Thus, a final step is to apply a smoothing technique to obtain more physically meaningful interlaminar stresses. This procedure provides transverse stress values directly at nodes without relying on extrapolation techniques from superconvergent points, thus leading to faster convergence. This suggests that transverse stresses obtained from interlaminar forces using static equivalence can represent a valuable method to recover accurate interlaminar stress distributions without requiring demanding computational resources.

3.3 Mixed Formulations as Stress Recovery Techniques

Compared to displacement type of finite element formulations, mixed formulations demand less stringent admissible requirements on continuity and offer flexibility to deal with a greater variety of problems. One of the aims of mixed finite elements is to relax formulations that otherwise would be overconstrained, giving rise to phenomena such as locking. This is achieved by assuming the independence of one or more secondary fields, e.g. stresses or strains or both, with respect to the displacement field. Then, mixed formulations compute the displacement field and the secondary fields from the finite element solution. Since the secondary fields are computed explicitly, one can think of mixed formulations as an alternative method for secondary-field recovery or smoothing.

3.3.1 Hellinger-Reissner Functional

Mixed finite element equations can be established using the Hellinger-Reissner (HR) functional:

$$\Pi_{HR}(\mathbf{u}, \bar{\boldsymbol{\sigma}}) := \int_{\Omega} \bar{\boldsymbol{\sigma}} : \boldsymbol{\epsilon} d\Omega - \int_{\Omega} w_c(\bar{\boldsymbol{\sigma}}) d\Omega + \Pi_{ext}(\mathbf{u}) \quad (3.13)$$

as presented in section (2.3.2), where only the stress $\bar{\boldsymbol{\sigma}}$ is introduced as an additional variable to the displacement \mathbf{u} . The optimality conditions for the HR functional are obtained using

the following two conditions:

$$\begin{aligned} D\Pi_{HR}(\mathbf{u}, \bar{\boldsymbol{\sigma}}) \cdot \delta \mathbf{u} &= \int_{\Omega} \bar{\boldsymbol{\sigma}} : \delta \boldsymbol{\epsilon} d\Omega + D\Pi_{ext}(\mathbf{u}) \cdot \delta \mathbf{u} = 0 \\ D\Pi_{HR}(\mathbf{u}, \bar{\boldsymbol{\sigma}}) : \delta \bar{\boldsymbol{\sigma}} &= \int_{\Omega} \boldsymbol{\epsilon} : \delta \bar{\boldsymbol{\sigma}} d\Omega - \int_{\Omega} \frac{\partial w_c}{\partial \bar{\boldsymbol{\sigma}}} : \delta \bar{\boldsymbol{\sigma}} d\Omega = 0 \end{aligned} \quad (3.14)$$

where $\delta \mathbf{u}$ and $\delta \bar{\boldsymbol{\sigma}}$ are, respectively, variations in the displacement and stress fields. A finite-dimensional discretization for both the displacement and stress tensor fields in the element domain is introduced as:

$$\begin{aligned} \delta \mathbf{u} &= N^I \delta \mathbf{u}^I, \quad \mathbf{u} = N^J \mathbf{u}^J \\ \delta \bar{\boldsymbol{\sigma}} &= \Psi^K \delta \bar{\boldsymbol{\sigma}}^K, \quad \bar{\boldsymbol{\sigma}} = \Psi^L \bar{\boldsymbol{\sigma}}^L \end{aligned} \quad (3.15)$$

where $I, J \in \{1, \dots, N_u\}$ and $K, L \in \{1, \dots, N_\sigma\}$, with N_u and N_σ the number of interpolation points for, respectively, the displacement and the stress field within an element Ω_e , N^I and N^J are the interpolation functions for the displacement field, Ψ^K and Ψ^L are the interpolation functions for the stress field. Using this discretization, the discrete form at the element level of the variational statement (3.14) is obtained as:

$$\begin{aligned} \mathbf{R}_u^I(\mathbf{u}) &:= \int_{\Omega_e} \bar{\boldsymbol{\sigma}} : \mathcal{B}^I d\Omega - \int_{\Omega_e} N^I \mathbf{b} d\Omega - \int_{\partial_t \Omega_e} N^I \mathbf{t} d\Gamma = \mathbf{0} \\ \mathbf{R}_\sigma^K(\bar{\boldsymbol{\sigma}}) &:= \int_{\Omega_e} \Psi^K (\boldsymbol{\epsilon} - \bar{\boldsymbol{\epsilon}}) d\Omega = \mathbf{0} \end{aligned} \quad (3.16)$$

where \mathbf{R}_u^I and \mathbf{R}_σ^K , the residual forces, are zero for an equilibrium configuration, $\bar{\boldsymbol{\epsilon}} := \partial W_c / \partial \bar{\boldsymbol{\sigma}}$, and $\bar{\boldsymbol{\epsilon}}$ is the strain-displacement operator (3.5). Within the context of Newton-Kantorowitch type numerical solution procedures, the discrete variational statement (3.16) needs to be linearized with respect to an increment in both the displacement and stress fields as:

$$\begin{aligned} D\mathbf{R}_u^I(\mathbf{u}) : \Delta \boldsymbol{\sigma} &= \mathcal{H}_{u\sigma}^{IL} : \Delta \bar{\boldsymbol{\sigma}}^L \\ D\mathbf{R}_\sigma^K(\bar{\boldsymbol{\sigma}}) \cdot \Delta \mathbf{u} &= \mathcal{H}_{\sigma u}^{KJ} \cdot \Delta \mathbf{u}^J \\ D\mathbf{R}_\sigma^K(\bar{\boldsymbol{\sigma}}) : \Delta \bar{\boldsymbol{\sigma}} &= \mathcal{H}_\sigma^{KL} : \Delta \bar{\boldsymbol{\sigma}}^L \end{aligned} \quad (3.17)$$

where the nodal stiffness contributions are:

$$\begin{aligned} (\mathcal{H}_{\sigma u}^{LI})^T &= \mathcal{H}_{u\sigma}^{IL} := \int_{\Omega_e} \Psi^L \mathcal{B}^I d\Omega \\ \mathcal{H}_\sigma^{KL} &:= - \int_{\Omega_e} \Psi^K \Psi^L \mathcal{E} d\Omega \end{aligned} \quad (3.18)$$

in which $\mathcal{E} := \partial^2 w_c / \partial \bar{\boldsymbol{\sigma}}^2$ is the compliance tensor.

A mixed formulation offers several possibilities as far as the treatment of stress variables is concerned: (i) stress variables can be retained and a full mixed implementation is then obtained. Thus, a post-processing recovery procedure is not required since stresses are determined *a priori* and stress continuity between adjacent elements is guaranteed directly. The shortcoming is represented by the great added burden of solving the governing equations

simultaneously for both stress and displacement degrees of freedom; (ii) stress variables can be expressed in terms of the displacement ones, i.e. the *static condensation technique* (Zienkiewicz and Taylor, 2000), thus reducing the computational cost involved. Formulations that involve a multi-variable variational principle but the resulting matrix equations at global level consist only of the nodal displacement values as unknowns are referred to as *hybrid* formulations. From the numerous possibilities to derive *hybrid* stress (HS) elements, in the context of this thesis HS refer to the version based on the HR functional. If the HS formulation is adopted, the independent stress tensor at the element level can be retrieved using the following relation (Mota and Abel, 2000):

$$\Delta \bar{\boldsymbol{\sigma}} = \boldsymbol{\Psi} \cdot \mathbf{H}^{-1} \cdot \int_{\Omega^e} \boldsymbol{\Psi} \otimes \Delta \boldsymbol{\epsilon} d\Omega \quad (3.19)$$

where the vector of interpolation functions $\boldsymbol{\Psi}$ is introduced, and with

$$\mathbf{H} := \int_{\Omega^e} \boldsymbol{\Psi} \otimes \mathcal{L} \otimes \boldsymbol{\Psi} d\Omega \quad (3.20)$$

Mixed finite element equations can also be established using the Reissner's Mixed Variational Theorem (RMVT) (Reissner, 1984, 1986) which allows one to assume two independent fields for displacements and the transverse stress variables only. Carrera and Demasi (2002a,b) have developed and compared multilayered plate elements based upon the *Principle of Virtual Displacements* (PVD), see the relation (2.4), and the RMVT for both equivalent single-layer (see section 2.3.3) and layer-wise (see section 2.3.4) multilayered form descriptions. The authors found RMVT formulated finite elements superior to those related to PVD in fulfilling the C_z^0 requirements of multilayer composite structures, addressed in section 2.2. Carrera (2000) has also compared different ways of computing transverse stresses, that is, stresses from an assumed model, *a priori*, were compared to those calculated *a posteriori*, i.e. from Hooke's law and by integration of three-dimensional indefinite equilibrium equations. In further research, an interesting analysis concerning the treatment of stress variables within the RMVT formulation is addressed by Demasi (2006). In particular, stress fields obtained using a full RMVT formulation and an *hybrid* formulation based on the *static condensation technique* are compared. In addition to the classical *static condensation technique*, an hybrid formulation based on the RMVT can also be obtained using the Weak Form of Hooke's Law (WFHL) proposed by Carrera (1996a). The WFHL, which was completely inspired by RMVT, permits one to express, in a weak sense, transverse stress variables in terms of the displacement variables.

3.3.2 Hu-Washizu Functional

The mixed Hu-Washizu (HW) functional as presented in section (2.3.2)

$$\Pi_{HW}(\mathbf{u}, \bar{\boldsymbol{\epsilon}}, \bar{\boldsymbol{\sigma}}) := \int_{\Omega} w(\bar{\boldsymbol{\epsilon}}) d\Omega + \int_{\Omega} \bar{\boldsymbol{\sigma}} : (\boldsymbol{\epsilon} - \bar{\boldsymbol{\epsilon}}) d\Omega + \Pi_{ext}(\mathbf{u}) \quad (3.21)$$

can also be employed for deriving mixed finite element equations, where the stress $\bar{\boldsymbol{\sigma}}$ and the strain $\bar{\boldsymbol{\epsilon}}$ are introduced as an additional variable to the displacement \mathbf{u} . In this case, the

optimality conditions are:

$$\begin{aligned}
D\Pi_{HW}(\mathbf{u}, \bar{\boldsymbol{\epsilon}}, \bar{\boldsymbol{\sigma}}) \cdot \delta \mathbf{u} &= \int_{\Omega} \bar{\boldsymbol{\sigma}} : D\boldsymbol{\epsilon} \cdot \delta \mathbf{u} d\Omega + D\Pi_{ext}(\mathbf{u}) \cdot \delta \mathbf{u} = 0 \\
D\Pi_{HW}(\mathbf{u}, \bar{\boldsymbol{\epsilon}}, \bar{\boldsymbol{\sigma}}) : \delta \bar{\boldsymbol{\epsilon}} &= \int_{\Omega} (\boldsymbol{\sigma} - \bar{\boldsymbol{\sigma}}) : \delta \bar{\boldsymbol{\epsilon}} d\Omega = 0 \\
D\Pi_{HW}(\mathbf{u}, \bar{\boldsymbol{\epsilon}}, \bar{\boldsymbol{\sigma}}) : \delta \bar{\boldsymbol{\sigma}} &= \int_{\Omega} (\boldsymbol{\epsilon} - \bar{\boldsymbol{\epsilon}}) : \delta \bar{\boldsymbol{\sigma}} d\Omega = 0
\end{aligned} \tag{3.22}$$

where $\boldsymbol{\sigma} := \partial w / \partial \boldsymbol{\epsilon}$, and $\delta \mathbf{u}$, $\delta \bar{\boldsymbol{\sigma}}$, and $\delta \bar{\boldsymbol{\epsilon}}$ are, respectively, variations in the displacement, stress, and strain fields. Assuming a finite-dimensional discretization of the displacement and stress fields as (3.15), and the following one for the strain field:

$$\delta \bar{\boldsymbol{\epsilon}} = \Psi^K \delta \bar{\boldsymbol{\epsilon}}^K, \quad \bar{\boldsymbol{\epsilon}} = \Psi^L \bar{\boldsymbol{\epsilon}}^L, \tag{3.23}$$

the discrete form of the variational statement (3.22) is now:

$$\begin{aligned}
\mathbf{R}_u^I(\mathbf{u}) &:= \int_{\Omega_e} \bar{\boldsymbol{\sigma}} : \mathcal{B}^I d\Omega - \int_{\Omega_e} N^I \mathbf{b} d\Omega - \int_{\partial_t \Omega_e} N^I \mathbf{t} d\Gamma = \mathbf{0} \\
\mathbf{R}_{\bar{\boldsymbol{\epsilon}}}^K(\bar{\boldsymbol{\epsilon}}) &:= \int_{\Omega_e} \Psi^K (\boldsymbol{\sigma} - \bar{\boldsymbol{\sigma}}) d\Omega = \mathbf{0} \\
\mathbf{R}_{\bar{\boldsymbol{\sigma}}}^K(\bar{\boldsymbol{\sigma}}) &:= \int_{\Omega_e} \Psi^K (\boldsymbol{\epsilon} - \bar{\boldsymbol{\epsilon}}) d\Omega = \mathbf{0}
\end{aligned} \tag{3.24}$$

The linearization of the discrete variational statement (3.24) with respect to increments of the displacement, stress and strain gives:

$$\begin{aligned}
D\mathbf{R}_u^I(\mathbf{u}) : \Delta \bar{\boldsymbol{\sigma}} &= \mathcal{H}_{u\bar{\boldsymbol{\sigma}}}^{IL} : \Delta \bar{\boldsymbol{\sigma}}^L \\
D\mathbf{R}_{\bar{\boldsymbol{\epsilon}}}^K(\bar{\boldsymbol{\epsilon}}) \cdot \Delta \mathbf{u} &= \mathcal{H}_{\sigma u}^{KJ} \cdot \Delta \mathbf{u}^J, \quad D\mathbf{R}_{\bar{\boldsymbol{\sigma}}}^K(\bar{\boldsymbol{\sigma}}) : \Delta \bar{\boldsymbol{\epsilon}} = \mathcal{H}_{\sigma \bar{\boldsymbol{\epsilon}}}^{KL} : \Delta \bar{\boldsymbol{\epsilon}}^L \\
D\mathbf{R}_{\bar{\boldsymbol{\sigma}}}^K(\bar{\boldsymbol{\sigma}}) : \Delta \bar{\boldsymbol{\epsilon}} &= \mathcal{H}_{\sigma \bar{\boldsymbol{\epsilon}}}^{KL} : \Delta \bar{\boldsymbol{\epsilon}}^L, \quad D\mathbf{R}_{\bar{\boldsymbol{\sigma}}}^K(\bar{\boldsymbol{\sigma}}) : \Delta \bar{\boldsymbol{\sigma}} = \mathcal{H}_{\sigma \bar{\boldsymbol{\sigma}}}^{KL} : \Delta \bar{\boldsymbol{\sigma}}^L
\end{aligned} \tag{3.25}$$

with all the other contributions being zero, and in which the nodal stiffness contributions are:

$$\begin{aligned}
(\mathcal{H}_{\sigma u}^{LI})^T &= \mathcal{H}_{u\bar{\boldsymbol{\sigma}}}^{IL} := \int_{\Omega_e} \Psi^L \mathcal{B}^I d\Omega \\
(\mathcal{H}_{\sigma \bar{\boldsymbol{\epsilon}}}^{LK})^T &= \mathcal{H}_{\sigma \bar{\boldsymbol{\epsilon}}}^{KL} := - \int_{\Omega_e} \Psi^K \Psi^L \mathcal{F} d\Omega \\
\mathcal{H}_{\bar{\boldsymbol{\sigma}}}^{KL} &:= \int_{\Omega_e} \Psi^K \Psi^L \mathcal{C} d\Omega
\end{aligned} \tag{3.26}$$

An hybrid formulation based on the HW functional is obtainable using the *static condensation* technique. In this case, the independent tensor fields at element level can be written as:

$$\bar{\boldsymbol{\epsilon}} = \boldsymbol{\Psi} \cdot \mathbf{H}^{-1} \cdot \mathbf{E}, \quad \bar{\boldsymbol{\sigma}} = \boldsymbol{\Psi} \cdot \mathbf{H}^{-1} \cdot \boldsymbol{\Sigma} \tag{3.27}$$

where

$$\mathbf{H} := \int_{\Omega_e} \boldsymbol{\Psi} \otimes \boldsymbol{\Psi} d\Omega, \quad \mathbf{E} := \int_{\Omega_e} \boldsymbol{\Psi} \otimes \boldsymbol{\epsilon} d\Omega, \quad \boldsymbol{\Sigma} := \int_{\Omega_e} \boldsymbol{\Psi} \otimes \boldsymbol{\sigma} d\Omega \tag{3.28}$$

which shows that the recovery expressions for the strain and stress fields are independent from the constitutive relations, in contrast with the stress field obtained using the HS formulation which involves the compliance tensor (3.19). This means that the HW functional may be applied for any constitutive relationship that admits a stored energy function.

The relationship between the stresses recovered using various implementations of the HW formulation and some of the stress recovery techniques presented in section 3.2 is elucidated by Mota and Abel (2000) using the concept of projection operators. At the local level, the stress recovery expressions for the HW formulation, stress smoothing, L_2 projection are equivalent. Identical stresses are obtained only when the derivatives of displacement interpolation functions can be represented exactly by the stress and strain interpolation functions selected for the HW formulation. At global level, the recovery expressions for the HW formulation, stress smoothing, and L_2 projection are also equivalent. The SPR expression is a discrete analogue of the recovery expressions for the HW formulation. At the global level and at the patch level, although these methods share analogous stress recovery expressions, the recovered stress fields are different since the stiffnesses are not equivalent. This suggests that the HW formulation with stiffnesses not equivalent with respect to the classical formulation and with appropriate choices of the secondary fields interpolation may present the opportunity for still more accurate stress and strains calculations to be made.

3.3.3 Enhanced Assumed Strain Method

Simo and Rifai (1990) have presented a class of mixed assumed strain methods, called the Enhanced Assumed Strain (EAS) method, which allows the systematic development of low order elements with enhanced accuracy for coarse meshes. The EAS method was originally classified as a hybrid formulation based upon the HW functional, although due to the structure of the variational problem and its related element matrices, classification as a modified displacement model is more appropriate. Within the EAS three-field mixed finite element framework, the classical method of incompatible displacement modes proposed by Taylor et al. (1976), who also conceived this idea with the purpose to develop low order elements with enhanced performance in coarse meshes, is obtained as a special case of the EAS method. The key point of the EAS method lies in the strain field that is composed of the compatible strain field $\bar{\epsilon}^c$, expressed in relation (3.5), and the enhanced strain field $\bar{\epsilon}^e$:

$$\bar{\epsilon} = \underbrace{\mathcal{B}^I \cdot \mathbf{u}^I}_{\bar{\epsilon}^c} + \bar{\epsilon}^e \quad (3.29)$$

Including the strain field (3.29) in the HW functional (3.21) gives the following functional:

$$\Pi_{EAS}(\mathbf{u}, \bar{\epsilon}, \bar{\sigma}) := \int_{\Omega} w(\bar{\epsilon}^c(\mathbf{u}) + \bar{\epsilon}^e) d\Omega - \int_{\Omega} \bar{\sigma} : \bar{\epsilon}^e d\Omega + \Pi_{ext}(\mathbf{u}) \quad (3.30)$$

In order to reduce the computational cost, Simo and Rifai (1990) have proposed eliminating the stresses from the variational formulation by choosing the enhanced strain field $\bar{\epsilon}^e$ to be orthogonal to the stress field $\bar{\sigma}$:

$$\int_{\Omega} \bar{\sigma} : \bar{\epsilon}^e d\Omega = 0 \quad (3.31)$$

Then, the number of independent variables in the functional Π_{EAS} is reduced to two, respectively, the displacement \mathbf{u} and the enhanced strain $\bar{\boldsymbol{\epsilon}}^e$. For a typical element, the displacement and the enhanced strain field are approximated as:

$$\mathbf{u} = \mathbf{N}\mathbf{u}_e, \quad \bar{\boldsymbol{\epsilon}}^e = \mathbf{G}\boldsymbol{\alpha}_e \quad (3.32)$$

where N is the matrix containing the standard isoparametric shape functions, \mathbf{u}_e is the vector of the nodal displacements, \mathbf{G} an interpolation matrix containing the enhanced modes, and $\boldsymbol{\alpha}_e$ the vector of internal strain parameters. The strain parameters are local for each individual element and can be eliminated at the element level from the final algebraic equations using a *static condensation technique*. Hence, due to the structure of the variational problem and its related element matrices, the EAS formulation can be classified as a modified displacement model.

It is interesting to note that not all types of elements can be enhanced by using assumed strains or incompatible modes. Reddy and Simo (1995) have shown that enhancement procedures do not work for triangles. Thus only quadrilaterals can be enhanced. For obvious reasons, the question arises whether a similar relation between EAS- and HS-models can be found. An important relation between the HW principle and the HR principle has been established by Stolarsky and Belytschko (1987), i.e. the first limit principle, which states that the HW principle is equivalent to the HR principle if an inclusion relation between the spaces of the stresses and the strains is satisfied. When the element Jacobian is constant, this principle can explain the equivalence between the EAS- and the HS-method, but the equivalence is not justified when the element Jacobian is not constant. Andelfinger and Ramm (1993) proposed equivalence between some EAS- and HS-elements, but this equivalence was proved only by inspection of the numerical results and was generalized for linear elastic problems. However, they could not base this equivalence on a theoretical foundation. While in the work of Andelfinger and Ramm only the equivalence of stiffness matrices is considered, Yeo and Lee (1996) have also considered the equivalence of the stresses with a more rigorous theoretical foundation. For a constant element Jacobian, Yeo and Lee concluded that the EAS- and the HS-method are equivalent. This means that, in addition to displacements, the consistent stresses of the EAS-elements are identical to those of the corresponding HS-elements at every point of the element, provided that the following orthogonality condition (3.33) and inclusion condition (3.34) are satisfied:

$$\mathcal{E}^\sigma \cap \mathcal{E}^e = 0 \quad (3.33)$$

$$\mathcal{E}^\sigma \oplus \mathcal{E}^e \subseteq \mathcal{E}^c \quad (3.34)$$

where \mathcal{E}^c is the compatible strain space derived from the admissible displacement field, \mathcal{E}^e is the space of admissible enhanced strain, and \mathcal{E}^σ is the stress-driven strain space associated with the admissible stress field. Thus, the *exact equivalence* is constructed. If the element Jacobian is not constant, a *weak equivalence* between the EAS- and the HS method is achieved, that is the displacements of the two methods are identical redundant and the consistent stresses are identical only at integration points provided that the orthogonality condition (3.33) and an additional condition of invertibility of the admissible enhanced strain and stress-driven strain tensors are satisfied. Using a different concept, Bischoff et al. (1999) have confirmed the conclusions drawn by Yeo and Lee although the equivalence conditions

are expressed in terms of stresses instead of strains. Based on these stress conditions of equivalence, Bischoff et al. (1999) were able to derive trial functions for equivalent EAS- and HS-elements in a straightforward manner, and a class of equivalent elements could be defined with polynomials of arbitrary order. The conditions of equivalence need to be combined with other conditions for convergence and stability of the EAS-method, this is well described in Simo and Rifai (1990).

In the EAS-method, the stresses are introduced as primary independent field in the beginning. However, the stresses cannot be retrieved directly by solving the system of governing equations since the stresses are eliminated from the formulation. Although stress recovery via the constitutive relation is simple, the stresses of the EAS-elements based on the strains are inaccurate since, in general, they are not variationally consistent (Yeo and Lee, 1996). Thus, it is necessary to devise a stress recovery procedure that is variationally consistent and efficient. From the procedure outlined above it is clear that the EAS formulation can be classified as a modified displacement model. Then, all the stress recovery procedures derived and conclusions drawn in section 3.2 are also valid for stress recovery of EAS finite element models. For instance, Simo and Rifai (1990) have proposed a least-squares type stress recovery procedure for the infinitesimal theory, similar to (3.4), based on the minimization of the following error function:

$$L(\bar{\boldsymbol{\sigma}}, \bar{\boldsymbol{\epsilon}}^e) = \int_{\Omega_e} [\bar{\boldsymbol{\sigma}} - \mathbf{C}(\bar{\boldsymbol{\epsilon}}^c + \bar{\boldsymbol{\epsilon}}^e)]^T : [\bar{\boldsymbol{\epsilon}}^\sigma - (\bar{\boldsymbol{\epsilon}}^c + \bar{\boldsymbol{\epsilon}}^e)] d\Omega \quad (3.35)$$

where \mathbf{C} is the elasticity tensor. Based on the enhanced assumed Green-Lagrangian strains, the recovery procedure proposed by Simo and Rifai has been extended to the geometrically non-linear case by Klinkel and Wagner (1997). If equivalence between the EAS and the HS method is achieved, this equivalence can be exploited to develop stress recovery procedures in which features known from one of both methods can be transferred directly to the other one, at least in the geometrically linear case. For instance, once the nodal displacements are known, a sound stress recovery procedure for EAS-elements can be taken directly from the corresponding HS element (Andelfinger and Ramm, 1993). The procedures of Simo and Rifai, Klinkel and Wagner and Andelfinger and Ramm require time-consuming matrix inversion operations. In this context, the equivalence between the EAS and the HS method has also been exploited by Yeo and Lee (1996) where a computationally efficient calculation of the stresses for EAS formulations not involving matrix inversion operations is derived.

In order to further improve the basic idea of Simo and Rifai in terms of range of applicability and numerical efficiency of enhanced strain elements, many different formulations have been developed over the past years in both the linear (Andelfinger and Ramm, 1993; Wriggers and Korelc, 1996) and the non-linear cases (Klinkel and Wagner, 1997; Simo and Armero, 1992; Slavkovic et al., 1994; Vu-Quoc and Tan, 2003a,b). From these papers, it can be concluded that EAS formulation present, in general, several remarkable properties. For instance, these elements do not involve any reduced or selective integration techniques to avoid locking phenomena. This means that rank deficiency, leading to the presence of zero energy modes in excess of the three rigid body motions, i.e hourglassing, does not occur. Moreover, good performances are generally obtained in bending dominated situations and in the case of incompressibility. Comparisons to other element formulations show a very

good coarse mesh accuracy and distortion insensitivity properties. It is generally accepted that an important number of enhanced modes is usually required to have an element free of locking, especially in three dimensional analysis. Thus, the EAS formulation can become extremely inefficient. In this context, Vu-Quoc and Tan (2003a,b) have developed a non-linear eight node solid-shell element based on an optimal combination of the Assumed Natural Strain (ANS) method (Bathe and Dvorkin, 1985; MacNeal, 1978; Simo and Hughes, 1986), and the minimal number of EAS parameters required to pass both the membrane and the bending patch test. This formulation resulted in seven optimal EAS parameters making the procedure numerically efficient.

3.4 Conclusions

One common deficiency of the displacement finite element method concerns the lower accuracy in predicting stresses and strains compared to displacements. This lack of accuracy directly affects structural design and failure predictions. A review of customary enhancement procedures aimed at replacing the consistent stress field by a more accurate one was presented in this chapter. These procedures are applicable regardless of the governing constitutive behaviour but depend crucially on the consistency of the stress field initially evaluated at superconvergent points within elements. Although recovery of stress data via the constitutive relation is relatively simple and widely adopted to compute the consistent stress field, this method may lead to the generation of spurious oscillations due to a lack of consistency. Other techniques were reviewed and a consistent stress field free of spurious oscillations can be obtained using integrated procedures. Economical finite element models as such adopting plate or shell elements based on either first-order or higher-order shear deformation theories are often combined with post-processing procedures incorporating the through-the thickness integration of the three-dimensional equilibrium equations performed using consistent in-plane stresses based on superconvergent recovery. However, when the emphasis of the analysis is the assessment of localized regions of potential damage initiation, this class of methods results to be inaccurate since an accurate determination of the three-dimensional state of stress at the ply level is required. In this case it becomes necessary to use either a Layer-Wise laminate theory that contains full 3-D kinematics and constitutive relations or 3-D elasticity theory.

Some of the stress recovery expressions obtained using the reviewed customary enhancement procedures have been compared with stress recovery expressions obtained using more refined methods, such as mixed/hybrid formulations based on the Hellinger-Reissner (HR)- and the Hu-Washizu (HW)-functional. The hybrid-HW formulation leads to stress recovery expressions that do not involve the compliance tensor, in contrast with the HS formulation where the compliance tensor is involved. This means that the HW functional may be applied for any constitutive relationship that admits a stored energy function, thus allowing for a direct analogy to stress recovery techniques of displacement models. Various implementations of the HW formulation give rise to stress recovery expressions analogous to customary stress recovery techniques of displacement models, but in most of the cases the stiffnesses obtained are not equivalent. This suggests that the HW formulation with stiffnesses that are not equivalent to the stiffnesses obtained using displacement formulations, and with an appropriate choice of the secondary fields interpolation, may present the

opportunity for still more accurate stress calculations.

An enhancement of the HW formulation is obtained by adopting an Enhanced Assumed Strain (EAS) formulation: EAS-elements do not generally present any rank deficiency, perform well in bending situations, and show a very good coarse mesh accuracy and distortion insensitivity properties compared to other element formulations. Moreover, EAS-Lagrangian elements can provide, in addition to equivalent displacements, consistent stresses that are *exactly equivalent*, in the case of a constant element Jacobian, or *weakly equivalent*, in the case of non-constant element Jacobian, to those of the HS counterparts. This is achievable if certain conditions between the enhanced assumed strain and assumed stress fields are satisfied. The EAS-elements are also preferred to HS-elements for non-linear analysis since EAS-elements do not involve inverse constitutive relations which are generally not available. Using a combination of the EAS- and ANS-method, procedures based on EAS formulations can also be made numerically efficient compared to displacement finite element formulations.

Chapter 4

A Finite Element Procedure for Interlaminar Stress Analyses

4.1 Introduction

The prevention of failure in composite material laminates requires an accurate and reliable procedure for the recovery of stress fields generated in response to operational loads and boundary conditions that are applied to such structures. Composites are prone to delamination when subjected to high interlaminar stresses. Commonly once the interlaminar stress fields are evaluated, the location of cracks and their form are usually assumed in advance in most theoretical studies on the characterization of delamination onset and growth in composite laminates (Coutellier et al., 2006; O'Brien, 1982). In particular, a variable stiffness panel has, by definition, a nonuniform in-plane stiffness distribution that might result in large in-plane stress gradients (Lopes, 2009). Such gradients contribute to the amplification of the interlaminar stresses, as demonstrated in Saeger et al. (2002), and possibly to render delamination the dominant failure mode in these configurations. Furthermore, variable stiffness panels have manufacturing characteristics, such as course edges, tow-drops and overlaps, as described in section 1.4, which may act as discontinuities and stress concentration zones that locally excite the interlaminar stresses further. This supports the need for an appropriate method that can be used to evaluate interlaminar stresses, and it will be crucial for accurate prediction of failure mechanisms in composite laminates.

Customary finite element models, such as the ones adopting plate or shell elements based on either first-order or higher-order shear deformation theories, are often combined with post-processing procedures incorporating through-the thickness integration of the 3D equilibrium equations. However, this class of methods gives inaccurate results when the emphasis of the analysis is the assessment of localized regions of potential damage initiation. This is because an accurate determination of the 3D state of stress at the ply level is required. Then, it becomes necessary to use either a Layer-Wise laminate theory that contains full 3D kinematics and constitutive relations or 3D elasticity theory, as explained in detail in chapter 2.

Customary stress recovery procedures are able to generate reliable interlaminar stress

distributions, i.e. accurate nodal stress values satisfying the C_2^0 -Requirements, see section 2.2, only by employing refined meshes requiring demanding computational resources. Interlaminar stresses are continuous both across and along layer interfaces. Nonetheless, the continuity of interlaminar stresses is difficult to enforce in C^0 interpolated elements. This is because in customary stress recovery procedures the nodal values of the stresses are usually retrieved using extrapolation techniques from super-convergent points inside the element, e.g. Gauss points for Lagrangian class of elements. Thus, refined meshes need to be used to achieve interlaminar continuity of the transverse stresses, especially in the presence of high out-of-plane stress gradients.

The Enhanced Assumed Strain (EAS) method can generate consistent stress distributions that are as much accurate as those produced using stress based hybrid formulations 3.3.3. This is generally achieved at a reduced computational cost, and without the need to employ inverse constitutive relations. However, difficulties arise using conventional three-dimensional procedures in the development of a finite element model that is able to capture properly all the locations of interest within the complete variable stiffness panel, even resorting to refined finite element models. Then, the purpose of this chapter is to present a three-dimensional finite element procedure based on the EAS method able to perform reliable future stress analyses of variable stiffness panels. Moreover, the procedure has to overcome the problems that would arise in the modeling and analysis of such laminates using customary procedures.

The starting point of the proposed procedure, explained in detail in section 1.6, is to partition a variable stiffness laminate in such a way that every ply can be considered to be an independent subdomain. In this way the user would be able to either mesh properly each course by simulating the procedure followed during the manufacturing process by the tow-placement machine's head, or to mesh the complete ply using a reliable mesh generator tool. However, the compatibility between the plies has to be reestablished subsequently by imposing adequate interfacial conditions between the plies. Once the finite element model is generated, a procedure for distributed computing generally employed in domain decomposition methods, i.e. the finite element tearing and interconnecting method, was employed to solve the system of algebraic equations. A post-processing recovery procedure able to recover accurate interlaminar stress distributions using less demanding computational resources compared to customary procedures was also developed. Moreover, the post-processing stress recovery procedure had to be conceived such that the stress states generated can be combined with three-dimensional failure criteria commonly used for delamination initiation. The complete stress states was obtained using a variational consistent procedure for the recovery of the in-plane stress distributions. The complete procedure was developed within the MATLABTM framework and it is presented in this chapter. The reliability of the approach was tested analysing several benchmark problems concerning multilayered conventional straight-fiber plates of various geometries.

4.2 Finite Element Model

Customary shell element formulations are, in general, developed within the context of the degenerated shell concept and the classical shell theory, thus based on the common kinematic assumption of inextensibility in the thickness direction of the shell and the zero trans-

verse normal-stress condition, see section 2.3.3 for a detailed overview. Using these approximations several difficulties can arise, and these difficulties are briefly summarized here: (i), in the case of complex 3-D material models, the zero transverse normal-stress condition must be imposed, (ii), in finite rotations complex update algorithms for finite rotations may be required with consequent high computational costs, (iii), the accuracy of the global response deteriorates as the laminate becomes thicker, (iv), the description of the state of stress at the ply level near geometric and material discontinuities is often inaccurate since a 3D stress state is generally achieved or near regions of intense loading, (v), the combination of these approximations with regular solid elements requires transition elements to connect rotational and displacement degrees of freedom.

Although finite element models based on a Layer-Wise theories can be suitable for the purpose of this thesis as shown in Dakshina Moorthy and Reddy (1999), see also section 2.3.4, the procedure developed and discussed in this thesis uses the simple low-order solid-shell element formulation presented by Vu-Quoc and Tan (2003a,b) for accurate analyses of large deformable multilayer shell structures. This is because Vu-Quoc and Tan's formulation (VTF) is based on the class of mixed assumed strain methods presented by Simo and Rifai (1990), i.e. the EAS formulation, see section 3.3.3, which allows the systematic development of low order elements with enhanced accuracy for coarse meshes. Compared to the customary shell element formulations mentioned above, VTF does not require complex finite-rotation updates and transition elements to connect solid-shell elements to regular solid elements. In fact, Vu-Quoc and Tan describe the kinematic of deformation using the position vectors of a pair of material points at the top and at the bottom of the shell surface using the same displacement degrees of freedom as found in the regular linear brick solid element. In their kinematic description, a straight transverse fiber before deformation remains straight after deformation, but it does not need to be normal to the shell mid-surface before deformation and after deformation. The kinematics of deformation in curvilinear coordinates of VTF is described in detail in (Vu-Quoc and Tan, 2003a). It is worth mentioning that in VTF all the stress and strain components are accounted for, thus allowing for an implementation of unmodified 3-D non linear constitutive laws, without the need to apply the plane-stress constraint. Thanks to an optimal combination of the EAS method and the Assumed Natural Strain (ANS) method (Bathe and Dvorkin, 1985; MacNeal, 1978; Simo and Hughes, 1986), VTF is also computationally efficient, and shows accurate in-plane and out-of-plane bending behaviour especially in refined analyses of composite structures involving a large number of high aspect-ratio layers (Vu-Quoc and Tan, 2003a).

In this section, attention will be paid to the derivation of the finite element governing equations based on the VTF. The point of departure is the Fraeijs de Veubeke-Hu-Washizu three-field functional (Felippa, 2000), that assumes the following form in the case of static analyses:

$$\begin{aligned} \Pi(\mathbf{u}, \mathbf{E}, \mathbf{S}) := & \int_{\Omega_0} w(\mathbf{E}) d\Omega + \int_{\Omega_0} \mathbf{S} : (\mathbf{E}^c(\mathbf{u}) - \mathbf{E}) d\Omega + \\ & \int_{\partial_u \Omega_0} (\mathbf{u}^* - \mathbf{u}) \cdot \mathbf{t} d\Phi - \int_{\partial_t \Omega_0} \mathbf{u} \cdot \mathbf{t}^* d\Gamma \end{aligned} \quad (4.1)$$

where the displacement boundary conditions are introduced in the Hu-Washizu variational functional (3.21) as an additional condition of constraint through a Lagrange multiplier,

which turns out to be the surface traction, $\partial_u \Omega$ is the part of $\partial \Omega$ on which the boundary displacement \mathbf{u}^* is specified. In the equation above \mathbf{t} is the traction vector, \mathbf{E} is the Green-Lagrange strain tensor, \mathbf{S} is the second Piola-Kirchhoff stress tensor, and \mathbf{E}^c is the compatible part of the Green-Lagrange strain tensor define as follows:

$$E_{ij}^c = \frac{1}{2} \left(\mathbf{G}_i \cdot \frac{\partial \mathbf{u}}{\partial \xi^i} + \frac{\partial \mathbf{u}}{\partial \xi^i} \cdot \mathbf{G}_j + \frac{\partial \mathbf{u}}{\partial \xi^i} \cdot \frac{\partial \mathbf{u}}{\partial \xi^j} \right), \quad (4.2)$$

with

$$\mathbf{G}_i(\boldsymbol{\xi}) = \frac{\partial \mathbf{X}(\boldsymbol{\xi})}{\partial \xi^i}, \quad i = 1, 2, 3 \quad (4.3)$$

where $\mathbf{X}(\boldsymbol{\xi})$ is the mapping from the biunit cube, parameterized by the material convective coordination (ξ^1, ξ^2, ξ^3) , to the initial configuration. All variables are expressed in the initial configuration Ω_0 . The extension of the EAS method to geometrically non-linear problems can also be done by enhancing the deformation gradient, as done by Simo and Armero (1992). However, Vu-Quoc and Tan (2003a,b) have showed that, from a computational standpoint, enhancing the Green-Lagrange strain tensor is simpler and more efficient, even though their numerical analyses indicated that both methods lead to the same numerical results when the same EAS parameters are used.

The next step in the EAS method is to introduce an enhancement to the compatible part of the Green-Lagrange strain \mathbf{E}^c :

$$\mathbf{E} = \mathbf{E}^c + \tilde{\mathbf{E}}. \quad (4.4)$$

By introducing (4.4) in (4.1), the following functional is obtained:

$$\begin{aligned} \Pi(\mathbf{u}, \tilde{\mathbf{E}}, \mathbf{S}) = & \int_{\Omega_0} w(\mathbf{E}^c(\mathbf{u}) + \tilde{\mathbf{E}}) d\Omega - \int_{\Omega_0} \mathbf{S} : \tilde{\mathbf{E}} d\Omega \\ & + \int_{\partial_u \Omega_0} (\mathbf{u}^* - \mathbf{u}) \cdot \mathbf{t} d\Phi - \int_{\partial_t \Omega_0} \mathbf{u} \cdot \mathbf{t}^* d\Gamma. \end{aligned} \quad (4.5)$$

Thus, the variation of Π in (4.5) with respect to the displacement \mathbf{u} is:

$$D\Pi(\mathbf{u}, \tilde{\mathbf{E}}, \mathbf{S}) \cdot \delta \mathbf{u} = \int_{\Omega_0} \frac{\partial w}{\partial \mathbf{E}} : \left(\frac{\partial \mathbf{E}^c(\mathbf{u})}{\partial \mathbf{u}} \cdot \delta \mathbf{u} \right) d\Omega - \int_{\partial_u \Omega_0} \delta \mathbf{u} \cdot \mathbf{t} d\Gamma - \int_{\partial_t \Omega_0} \delta \mathbf{u} \cdot \mathbf{t}^* d\Gamma, \quad (4.6)$$

the variation of Π in (4.5) with respect to $\tilde{\mathbf{E}}$ is:

$$D\Pi(\mathbf{u}, \tilde{\mathbf{E}}, \mathbf{S}) : \delta \tilde{\mathbf{E}} = \int_{\Omega_0} \left(\frac{\partial w}{\partial \tilde{\mathbf{E}}} - \mathbf{S} \right) : \delta \tilde{\mathbf{E}} d\Omega, \quad (4.7)$$

and the variation of Π in (4.5) with respect to \mathbf{S} is:

$$D\Pi(\mathbf{u}, \tilde{\mathbf{E}}, \mathbf{S}) : \delta \mathbf{S} = \int_{\Omega_0} \delta \mathbf{S} : \tilde{\mathbf{E}} d\Omega + \int_{\partial_u \Omega_0} (\mathbf{u}^* - \mathbf{u}) \cdot \delta \mathbf{t} d\Phi. \quad (4.8)$$

By designing the approximation for the stress field \mathbf{S} and the approximation for the enhanc-

ing strain field $\tilde{\mathbf{E}}$ such that the following orthogonality condition holds

$$\int_{\Omega} \mathbf{S} : \tilde{\mathbf{E}} d\Omega = 0, \quad (4.9)$$

the number of independent variables in the functional (4.5) is reduced to two, i.e.,

$$\Pi(\mathbf{u}, \tilde{\mathbf{E}}) = \int_{\Omega_0} w(\mathbf{E}^c(\mathbf{u}) + \tilde{\mathbf{E}}) d\Omega + \int_{\partial_u \Omega_0} (\mathbf{u}^* - \mathbf{u}) \cdot \mathbf{t} d\Phi - \int_{\partial_t \Omega_0} \mathbf{u} \cdot \mathbf{t}^* d\Gamma, \quad (4.10)$$

leading to the following total variation and equilibrium condition:

$$\delta \Pi(\mathbf{u}, \tilde{\mathbf{E}}) = \delta \Pi_{stiff}(\mathbf{u}, \tilde{\mathbf{E}}) + \delta \Pi_{ext}(\mathbf{u}) = 0, \quad (4.11)$$

where:

$$\begin{aligned} \delta \Pi_{stiff}(\mathbf{u}, \tilde{\mathbf{E}}) &= \int_{\Omega_0} (\delta \mathbf{E}^c(\mathbf{u}) + \delta \tilde{\mathbf{E}}) : \frac{\partial}{\partial \mathbf{E}} w(\mathbf{E}^c(\mathbf{u}) + \tilde{\mathbf{E}}) d\Omega \\ \delta \Pi_{ext} &= - \int_{\partial_t \Omega_0} \delta \mathbf{u} \cdot \mathbf{t}^* d\Gamma. \end{aligned} \quad (4.12)$$

The finite element discretization is then introduced by discretizing the initial configuration Ω_0 into a number of non-overlapping elements, *nel*, such that $\Omega \approx \cup_{e=1}^{nel} \Omega_0^{(e)}$, where the displacement \mathbf{u} , its variation $\delta \mathbf{u}$, and increment $\Delta \mathbf{u}$ are interpolated in the element domain as follows:

$$\mathbf{u} = \mathbf{N}(\boldsymbol{\xi}) \mathbf{d}^{(e)}, \quad \delta \mathbf{u} = \mathbf{N}(\boldsymbol{\xi}) \delta \mathbf{d}^{(e)}, \quad \Delta \mathbf{u} = \mathbf{N}(\boldsymbol{\xi}) \Delta \mathbf{d}^{(e)} \quad (4.13)$$

where \mathbf{N} is a matrix containing the basis linear 3D isoparametric shape functions restricted to element $\Omega_0^{(e)}$, and $\mathbf{d}^{(e)}$ is a matrix containing the nodal displacements. Within an element (*e*), the variation and the increment of the compatible Green-Lagrange strain \mathbf{E}^c is related to the variation and the increment of displacement as follows:

$$\{\delta E_{ij}^c\}_{6 \times 1} = \mathbf{B}(\mathbf{d}^{(e)}) \delta \mathbf{d}^{(e)}, \quad \{\Delta E_{ij}^c\}_{6 \times 1} = \mathbf{B}(\mathbf{d}^{(e)}) \Delta \mathbf{d}^{(e)}, \quad (4.14)$$

where the components of E_{ij}^c are arranged into a 6×1 column matrix according to the Voigt ordering (Vu-Quoc and Tan, 2003a)

$$\{E_{ij}^c\} = \{E_{11}^c, E_{22}^c, 2E_{12}^c, E_{33}^c, 2E_{23}^c, 2E_{13}^c\}^T, \quad (4.15)$$

and \mathbf{B} is the deformation dependent displacement-to-strain operator, which detailed expression is given in (Vu-Quoc and Tan, 2003b). As far as the enhanced Green-Lagrange strain tensor $\tilde{\mathbf{E}}$ is concerned, Vu-Quoc and Tan (2003a) denote with $\delta \boldsymbol{\alpha}^{(e)}$ the admissible variation of the element EAS-parameter column-matrix $\boldsymbol{\alpha}^{(e)} \in \mathbb{R}^{neas}$ associated with the enhancing strain $\{E_{ij}\}$, where *neas* is the number of EAS parameters. Then, the components of the enhancing strain $\tilde{\mathbf{E}}$ are expressed as a product of an enhancing strain interpolation matrix \mathfrak{S} and the element EAS parameters $\boldsymbol{\alpha}^{(e)}$; the same interpolation applies to the variation and the increment of $\tilde{\mathbf{E}}$, i.e.,

$$\{\tilde{E}_{ij}\}_{6 \times 1} = \mathfrak{S}(\boldsymbol{\xi}) \boldsymbol{\alpha}^{(e)}, \quad \{\delta \tilde{E}_{ij}\}_{6 \times 1} = \mathfrak{S}(\boldsymbol{\xi}) \delta \boldsymbol{\alpha}^{(e)}, \quad \{\Delta \tilde{E}_{ij}\}_{6 \times 1} = \mathfrak{S}(\boldsymbol{\xi}) \Delta \boldsymbol{\alpha}^{(e)}. \quad (4.16)$$

The enhancing strain interpolation matrix \mathfrak{S} is defined in (Vu-Quoc and Tan, 2003a) as follows:

$$\mathfrak{S} = \frac{1}{J} \mathbf{T}_0^{-T} \mathbf{M}(\xi) \quad (4.17)$$

where \mathbf{T}_0 is a matrix that transform the strain components relative to the covariant basis calculated in the element center to those components relative to the covariant basis calculated in a generic point, J is the determinant of the element Jacobian matrix of the mapping from the iso-parametric space to the initial configuration of the element, and \mathbf{M} is the interpolation matrix that has to be chosen in such a way that the enhanced strain field satisfies the orthogonality condition (4.9) for a generic α .

Two ANS modifications on the compatible covariant strains are employed by Vu-Quoc and Tan (2003a) to eliminate the locking effects resulting from the use of the compatible low-order interpolations (Chapelle and Bathe, 2003). The ANS interpolation is the most successful tool to use to overcome the *shear locking* effect in the four-node displacement-based shell elements, even for initially distorted meshes (Bathe and Dvorkin, 1985; Mac-Neal, 1978; Simo and Hughes, 1986). In this context, Vu-Quoc and Tan apply a linear interpolation of the compatible transverse shear strain E_{13}^c and E_{23}^c evaluated at the four mid-points A, B, C, D of the element edges, at $\xi^3 = 0$, see figure 4.1, as follows:

$$\begin{Bmatrix} E_{13}^{ANS} \\ E_{23}^{ANS} \end{Bmatrix} = \begin{Bmatrix} (1 - \xi^2)E_{13}^c(\xi_A) + (1 + \xi^2)E_{13}^c(\xi_C) \\ (1 - \xi^1)E_{23}^c(\xi_D) + (1 + \xi^1)E_{23}^c(\xi_B) \end{Bmatrix} \quad (4.18)$$

where the coordinates of points A, B, C, D are $\xi_A = (0, -1, 0)$, $\xi_B = (1, 0, 0)$, $\xi_C = (0, 1, 0)$,

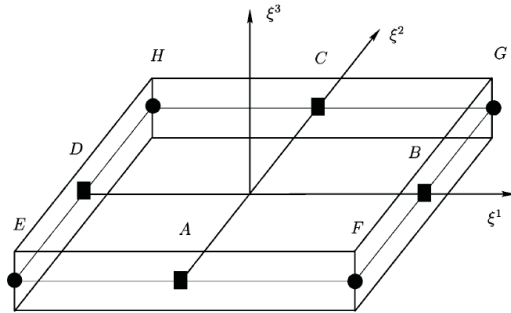


Figure 4.1: Eight-node solid shell element in isoparametric coordinates: sampling points for ANS interpolations for transverse shear strains (A, B, C, D), and for transverse normal strain (E, F, G, H) (Vu-Quoc and Tan, 2003a).

$\xi_D = (-1, 0, 0)$, respectively. The above interpolation on the transverse shear strains eliminates the *shear locking* problem, and allows for pure bending deformation without parasitic transverse shear strains. In the case of curved thin shell structures or in non-linear analyses, there is another locking effect, i.e. *curvature thickness locking* (Bischoff and Ramm, 2000), which is also known as *trapezoidal locking*. To circumvent this locking effect from parasitic transverse normal strain, Vu-Quoc and Tan employ a bilinear interpolation for the covariant component E_{33}^c of the compatible Green-Lagrangian strain tensor, sampled at the

four corners E, F, G, H of the element midsurface, see figure 4.1, as follows:

$$E_{33}^{ANS} = \sum_{i=1}^4 N_i(\xi^1, \xi^2) E_{33}^c(\xi_i), \quad (4.19)$$

with $N_i = (\frac{1}{4})(1 + \xi_i^1 \xi^1)(1 + \xi_i^2 \xi^2)$, $\xi_1 = \xi_E = (-1, -1, 0)$, $\xi_2 = \xi_F = (1, -1, 0)$, $\xi_3 = \xi_G = (1, 1, 0)$, and $\xi_4 = \xi_H = (-1, 1, 0)$.

To incorporate 3-D constitutive laws in shell formulations, the transverse normal strain must have at least a linear distribution over the shell thickness, otherwise, an additional locking effect, i.e. the *Poisson-thickness locking*, will occur (Bischoff and Ramm, 2000; Zienkiewicz and Taylor, 2000). Two methods have been proposed in the literature to alleviate this effect: one, assumes a quadratically distributed displacement field over the shell thickness (Parish, 1995), and then introduces an additional kinematic parameter; the other, uses the EAS method to enhance the transverse normal strain (Bucher et al., 1994). Vu-Quoc and Tan (2003a) enhance the transverse normal strain using the EAS method to include the bilinear terms $\xi^1 \xi^3$ and $\xi^2 \xi^3$ in terms of material coordinates. Vu-Quoc and Tan also enhance the membrane strains to improve the membrane behaviour. These enhancements are achieved by selecting the following interpolation matrix

$$\mathbf{M} = \begin{bmatrix} \xi^1 & 0 & 0 & 0 & 0 & 0 & 0 \\ 0 & \xi^2 & 0 & 0 & 0 & 0 & 0 \\ 0 & 0 & \xi^1 & \xi^2 & 0 & 0 & 0 \\ 0 & 0 & 0 & 0 & \xi^3 & \xi^1 \xi^3 & \xi^2 \xi^3 \end{bmatrix}, \quad (4.20)$$

enhancing, respectively, the membrane strains $[E_{11}, E_{22}, 2E_{12}]$ and the transverse normal strain E_{33} , leading to an optimal number of EAS parameters, seven, that in combination with the ANS method described above make the VTF able to pass both the membrane and the bending patch test. Thus, a complete free of locking solid-shell element is obtained, without resorting to reduced or selective integration techniques to avoid locking phenomena. This means that rank deficiency, leading to hourglass mechanisms from spurious energy modes, does not occur (Reddy, 2004). Vu-Quoc and Tan (2003a) have justified, through numerical analyses, the relative importance of the separate use of the EAS method and the ANS method, compared to the pure displacement formulation, and more importantly, the combined use of both the EAS method and the ANS method for obtaining accurate results for plate bending problem over a large range of aspect ratios. It is also worth mentioning that the strain-driven character of the VTF also makes it easier to implement non-linear constitutive models, when compared to hybrid finite-element formulation where the stress field is involved.

The following expression at the element level is obtained by applying a standard finite-element procedure to discretize the total variation (4.11):

$$\delta \Pi^{(e)} = \delta \Pi_{stiff}^{(e)} + \delta \Pi_{ext}^{(e)}(\mathbf{u}) = 0, \quad (4.21)$$

with

$$\begin{aligned}\delta\Pi_{stiff}^{(e)} &= \int_{\Omega_0^{(e)}} \delta \{ \mathbf{E}_{ij}^c \}^T \{ S_{ij} \} d\Omega + \int_{\Omega_0^{(e)}} \delta \{ \tilde{\mathbf{E}}_{ij} \}^T \{ S_{ij} \} d\Omega, \\ \delta\Pi_{ext} &= - \int_{\partial_t \Omega_0^{(e)}} \delta \mathbf{u} \cdot \mathbf{t}^* d\Gamma,\end{aligned}\quad (4.22)$$

where the following symbol definition is used to alleviate the notation

$$\mathbf{S} := \frac{\partial w}{\partial \mathbf{E}}, \quad (4.23)$$

which corresponds to the second Piola-Kirchoff stress, and where the column matrix $\{S^{ij}\}$ has its coefficients arranged in the same Voigt ordering as in (4.15)

$$\{S^{ij}\} = [S^{11}, S^{22}, S^{12}, S^{33}, S^{23}, S^{13}]. \quad (4.24)$$

The linearization of the discrete weak form (4.21) can be accomplished using the truncated Taylor series about the k th iterate $(\mathbf{u}_{(k)}, \tilde{\mathbf{E}}_{(k)})$:

$$\begin{aligned}\delta\Pi(\mathbf{u}_{(k+1)}, \tilde{\mathbf{E}}_{(k+1)}) &\approx \delta\Pi(\mathbf{u}_{(k)}, \tilde{\mathbf{E}}_{(k)}) + \left. \frac{\partial(\delta\Pi)}{\partial(\mathbf{u}, \tilde{\mathbf{E}})} \right|_{(\mathbf{u}=\mathbf{u}_{(k)}, \tilde{\mathbf{E}}=\tilde{\mathbf{E}}_{(k)})} \cdot (\Delta\mathbf{u}, \Delta\tilde{\mathbf{E}}) \\ &= \delta\Pi(\mathbf{u}_{(k)}, \tilde{\mathbf{E}}_{(k)}) + D(\delta\Pi)(\mathbf{u}_{(k)}, \tilde{\mathbf{E}}_{(k)}) \cdot (\Delta\mathbf{u}, \Delta\tilde{\mathbf{E}}),\end{aligned}\quad (4.25)$$

where $\Delta\mathbf{u} = \mathbf{u}_{(k+1)} - \mathbf{u}_{(k)}$, $\Delta\tilde{\mathbf{E}} = \tilde{\mathbf{E}}_{(k+1)} - \tilde{\mathbf{E}}_{(k)}$. Note: to alleviate the notation, henceforward the subscript k designating the iterative index will be omitted. Using the approximations (4.13), (4.14), and (4.16) in (4.25), the increments $\Delta\mathbf{d}^{(e)}$ and $\Delta\boldsymbol{\alpha}^{(e)}$ can be computed in the Newton's solution process by setting the expression (4.25) equal to zero. Thus, the following relation is obtained:

$$\begin{aligned}D(\delta\Pi^{(e)})(\mathbf{d}^{(e)}, \boldsymbol{\alpha}^{(e)}) \cdot (\Delta\mathbf{d}^{(e)}, \Delta\boldsymbol{\alpha}^{(e)}) &= \frac{\partial(\delta\Pi_{stiff}^{(e)} + \delta\Pi_{ext}^{(e)})}{\partial(\mathbf{d}^{(e)}, \boldsymbol{\alpha}^{(e)})} \cdot (\Delta\mathbf{d}^{(e)}, \Delta\boldsymbol{\alpha}^{(e)}) \\ &= \frac{\partial(\delta\Pi_{stiff}^{(e)})}{\partial(\mathbf{d}^{(e)}, \boldsymbol{\alpha}^{(e)})} \cdot (\Delta\mathbf{d}^{(e)}, \Delta\boldsymbol{\alpha}^{(e)}) = -(\delta\Pi_{stiff}^{(e)} + \delta\Pi_{ext}^{(e)}),\end{aligned}\quad (4.26)$$

in which the variation $\delta\Pi_{stiff}^{(e)}$ and $\delta\Pi_{ext}^{(e)}$ in (4.22) now take, respectively, the following form:

$$\begin{aligned}\delta\Pi_{stiff}^{(e)}(\mathbf{d}^{(e)}, \boldsymbol{\alpha}^{(e)}) &= \delta\mathbf{d}^{(e)T} \mathbf{f}_{stiff}^{(e)} + \delta\boldsymbol{\alpha}^{(e)T} \mathbf{f}_{EAS}^{(e)} \\ \text{with } \mathbf{f}_{stiff}^{(e)} &= \int_{\Omega_0^{(e)}} \mathbf{B}^T \{S^{ij}\} d\Omega, \quad \mathbf{f}_{EAS}^{(e)} = \int_{\Omega_0^{(e)}} \mathfrak{S}^T \{S^{ij}\} d\Omega, \\ \delta\Pi_{ext}^{(e)}(\mathbf{d}^{(e)}) &= -\delta\mathbf{d}^{(e)T} \mathbf{f}_{ext}^{(e)}, \\ \text{with } \mathbf{f}_{ext}^{(e)} &= \int_{\Omega_0^{(e)}} \mathbf{N}^T \mathbf{t}^* d\Omega.\end{aligned}\quad (4.27)$$

Thus, the left hand side of (4.26) becomes:

$$\begin{aligned}
D(\delta\Pi_{stiff}^{(e)})(\Delta\mathbf{d}^{(e)}, \Delta\boldsymbol{\alpha}^{(e)}) &= \frac{\partial(\delta\Pi_{stiff}^{(e)})}{\partial\mathbf{d}^{(e)}} \cdot \Delta\mathbf{d}^{(e)} + \frac{\partial(\delta\Pi_{stiff}^{(e)})}{\partial\boldsymbol{\alpha}^{(e)}} \cdot \Delta\boldsymbol{\alpha}^{(e)} \\
&= \left[\delta\mathbf{d}^{(e)T} \mathbf{k}_{uu}^{(e)} + \delta\boldsymbol{\alpha}^{(e)T} \mathbf{k}_{\alpha u}^{(e)} \right] \cdot \Delta\mathbf{d}^{(e)} + \left[\delta\mathbf{d}^{(e)T} \mathbf{k}_{u\alpha}^{(e)} + \delta\boldsymbol{\alpha}^{(e)T} \mathbf{k}_{\alpha\alpha}^{(e)} \right] \cdot \Delta\boldsymbol{\alpha}^{(e)} \quad (4.28) \\
&= \delta\mathbf{d}^{(e)T} \left[\mathbf{k}_{uu}^{(e)} \Delta\mathbf{d}^{(e)} + \mathbf{k}_{u\alpha}^{(e)} \Delta\boldsymbol{\alpha}^{(e)} \right] + \delta\boldsymbol{\alpha}^{(e)T} \left[\mathbf{k}_{\alpha u}^{(e)} \Delta\mathbf{d}^{(e)} + \mathbf{k}_{\alpha\alpha}^{(e)} \Delta\boldsymbol{\alpha}^{(e)} \right].
\end{aligned}$$

Let the fourth-order constitutive tensor be defined as follows:

$$\mathbf{C} = \left[C^{ijkl} \right] := \left[\frac{\partial S^{ij}}{\partial E_{kl}} \right] \in \mathbb{R}^{6 \times 6}, \quad (4.29)$$

where C^{ijkl} are the components of the constitutive tensor \mathbf{C} in the convected basis arranged according to the ordering of the strain components in (4.15), and of the stress components in (4.24). Then, the following expressions are obtained in (4.28):

$$\begin{aligned}
\mathbf{k}_{uu}^{(e)} &= \frac{\partial \mathbf{f}_{stiff}^{(e)}}{\partial \mathbf{d}^{(e)}} = \int_{\Omega_0^{(e)}} (\mathbf{G}^T \mathbb{S} + \mathbf{B}^T \mathbf{C} \mathbf{B}) d\Omega, \\
\mathbf{k}_{u\alpha}^{(e)} &= \frac{\partial \mathbf{f}_{stiff}^{(e)}}{\partial \boldsymbol{\alpha}^{(e)}} = \int_{\Omega_0^{(e)}} \mathbf{B}^T \mathbf{C} \mathbb{Z} d\Omega, \\
\mathbf{k}_{\alpha u}^{(e)} &= \frac{\partial \mathbf{f}_{EAS}^{(e)}}{\partial \mathbf{u}^{(e)}} = \left[\mathbf{k}_{u\alpha}^{(e)} \right]^T = \int_{\Omega_0^{(e)}} \mathbb{Z}^T \mathbf{C} \mathbf{B} d\Omega, \\
\mathbf{k}_{\alpha\alpha}^{(e)} &= \frac{\partial \mathbf{f}_{EAS}^{(e)}}{\partial \boldsymbol{\alpha}^{(e)}} = \int_{\Omega_0^{(e)}} \mathbb{Z}^T \mathbf{C} \mathbb{Z} d\Omega,
\end{aligned} \quad (4.30)$$

where the matrix \mathbf{G}

$$\mathbf{G} := \frac{\partial \mathbf{B}(\mathbf{d}^{(e)})}{\partial \mathbf{d}^{(e)}}, \quad (4.31)$$

and the stress matrix \mathbb{S} , which is related to the matrix $\{S^{ij}\}$ in (4.24), have their detailed expressions given in (Vu-Quoc and Tan, 2003b). It follows from (4.26), (4.27), and (4.28) that the discrete linearized system of equations to solve for the increments $\Delta\mathbf{d}^{(e)}$ and $\Delta\boldsymbol{\alpha}^{(e)}$ is given by the following expressions:

$$\mathbf{K}_{uu}^{(e)} \Delta\mathbf{d}^{(e)} + \mathbf{K}_{u\alpha}^{(e)} \Delta\boldsymbol{\alpha}^{(e)} = \mathbf{f}_{ext}^{(e)} - \mathbf{f}_{stiff}^{(e)} \quad (4.32)$$

$$\mathbf{K}_{\alpha u}^{(e)} \Delta\mathbf{d}^{(e)} + \mathbf{K}_{\alpha\alpha}^{(e)} \Delta\boldsymbol{\alpha}^{(e)} = -\mathbf{f}_{EAS}^{(e)}, \quad (4.33)$$

or in a matrix form as:

$$\begin{bmatrix} \mathbf{K}_{uu}^{(e)} & \mathbf{K}_{u\alpha}^{(e)} \\ \mathbf{K}_{\alpha u}^{(e)} & \mathbf{K}_{\alpha\alpha}^{(e)} \end{bmatrix} \begin{Bmatrix} \Delta\mathbf{d}^{(e)} \\ \Delta\boldsymbol{\alpha}^{(e)} \end{Bmatrix} = \begin{Bmatrix} \mathbf{f}_{ext}^{(e)} - \mathbf{f}_{stiff}^{(e)} \\ -\mathbf{f}_{EAS}^{(e)} \end{Bmatrix}. \quad (4.34)$$

Since the enhanced strain field $\tilde{\mathbf{E}}$ is chosen to be discontinuous across the element bound-

aries, the EAS parameters increments $\Delta\alpha^{(e)}$ are eliminated at element level before proceeding to assemble the element matrices into global matrices. Solving equation (4.33) for the increment $\Delta\alpha^{(e)}$ as follows

$$\Delta\alpha^{(e)} = -[\mathbf{K}_{\alpha\alpha}^{(e)}]^{-1} (\mathbf{f}_{EAS}^{(e)} + \mathbf{K}_{\alpha u}^{(e)} \Delta\alpha^{(e)}), \quad (4.35)$$

and then substituting (4.35) into (4.32), gives the following condensed symmetric element stiffness matrix $\mathbf{K}_T^{(e)}$, and the element residual force vector $\mathbf{r}^{(e)}$, respectively (4.36) and (4.37):

$$\mathbf{K}_T^{(e)} = \mathbf{K}_{uu}^{(e)} - [\mathbf{K}_{\alpha u}^{(e)}]^T [\mathbf{K}_{\alpha\alpha}^{(e)}]^{-1} \mathbf{K}_{\alpha u}^{(e)}, \quad (4.36)$$

$$\mathbf{r}^{(e)} = \mathbf{f}_{ext}^{(e)} - \mathbf{f}_{stiff}^{(e)} + [\mathbf{K}_{\alpha u}^{(e)}]^T [\mathbf{K}_{\alpha\alpha}^{(e)}]^{-1} \mathbf{f}_{EAS}^{(e)}. \quad (4.37)$$

An assembly of the element matrices $\mathbf{K}_T^{(e)}$ and $\mathbf{r}^{(e)}$ leads to the global system:

$$\mathbf{K}_T \Delta\mathbf{d} = \mathbf{R} \quad (4.38)$$

with

$$\mathbf{K}_T = \mathbb{A}_{e=1}^{nel} \mathbf{K}_T^{(e)}, \quad \mathbf{R} = \mathbb{A}_{e=1}^{nel} \mathbf{r}^{(e)} \quad (4.39)$$

where \mathbb{A} denotes the finite-element assembly operator. Thus, the time required for calculation is now comparable to models based on displacement formulations. Note: for details of the iterative procedure used see (Vu-Quoc and Tan, 2003b).

4.3 Parallel Computing

The solution of systems of linear algebraic equations such as (4.38) is one of the basic components of the numerical methods used in mathematical physics and it generally represents the most demanding part of dealing with the algorithms. In particular, the high level of accuracy required for an appropriate modeling of a variable stiffness panel, especially close to tow-drops and tow/overlaps areas, lead to a finite element model involving a large number of degrees of freedom. Therefore, appropriate attention should be paid to the development of solvers.

Sparse direct solvers, which have been for a long time as the main procedure used in commercial finite element software to solve system of equations, continue to play an important role in these numerical simulation codes. However, the pressing need for higher-fidelity 3D finite element structural models with millions of degrees of freedom, and the extreme demanding computer resources required by direct solvers for such large problems have led to the employment of supercomputing systems, i.e. *parallel computing*, such as those that are obtained by teaming together several computing units to increase the computing power. The idea of connecting computers has proved to be less complicated than the development of faster and more efficient single processors. In particular, the evolution of PC clusters, i.e. using ordinary PCs connected using a suitable network, is expected to be almost unlimited.

Solving large systems of equations on parallel computers has been, and still is, a challenging research field since algorithms that are highly efficient for sequential machines usually perform poorly on parallel computers (Rixen, 2001; Rixen and Magoulès, 2007). Parallel solvers can be constructed in different ways: (i) by re-organizing classical factorization

methods, i.e. direct solvers, (ii) by applying iterative solvers. Considering the system of equations (4.38), a direct solver would usually be used to perform the factorization of \mathbf{K}_T , e.g. Gaussian factorization, and forward/backward substitutions to find $\Delta\mathbf{d}$. The looping sequence on rows and columns within the factorization and substitutions can be organized to maximize the amount of independent, i.e. parallel, tasks. However, as the number of processors increases, the parallel efficiency becomes very poor due to the large amount of communications required by the sequential factorization and substitution algorithm (Rixen, 2001). A better alternative is to first subdivide the problem into a certain number of connected subparts, i.e. *substructures* or *subdomains* as in Fig.4.2, by ordering the matrix to bordered block diagonal form. A direct solver can then be applied in parallel to each of

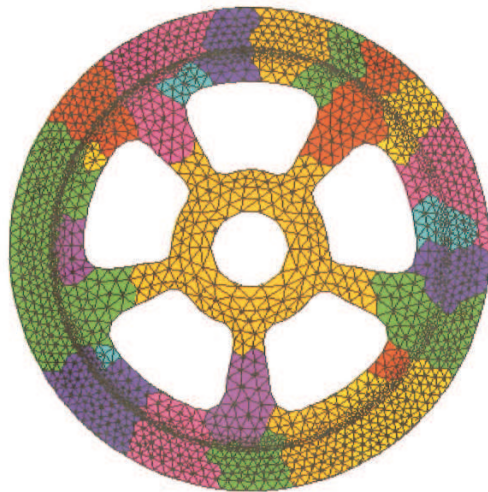


Figure 4.2: Wheel: mesh of a structure subdivided in different connected subdomains (Kruis (2007)).

the subdomains since the internal stiffness matrices of every subdomain can be factorized independently. Once all possible eliminations for the subdomains have been performed, there remains an interface problem, i.e. *condensed interface* (CI) problem, which is smaller than the original system. The interface solution is used to complete the solution of the subdomains. More details about this procedure can be found in (Rixen, 2001). Although very robust, this approach is efficient on a small number of processors but it does not scale up well for massive parallel computers set ups since the CI problem can not be efficiently factorized in parallel and its size increases as the decomposition is refined.

Factorization schemes are inherently sequential since they are based on Gaussian elimination where the solution is obtained for one variable after the other. For this reason, a large segment of the computational mechanics community, including software development houses, is increasingly investigating the adoption of iterative solvers (Farhat et al., 2000b). Iterative solvers search for approximations of all unknowns simultaneously and involve simple matrix operations. Thus, they are naturally parallel. Since a large class of structural and solid mechanics applications generate systems of equations that are symmetric positive definite or semi-definite, the conjugate gradient method (Hestnes, 1952) has always been

an iterative method of choice among computational structural mechanics. In structural analysis, direct solvers have been favored for their robustness compared to iterative methods where fast convergence can be difficult to achieve in practice (Rixen, 2001). With the advent of parallel computing iterative methods have gained a new momentum. Conjugate gradient based iterative methods applied to a structure subdivided into different connected subdomains as shown in Fig.4.2, also known as *domain decomposition* (DD) methods (Kruis, 2007), have emerged as powerful contenders on both sequential and parallel computing platforms. In particular, most efficient and useful parallel solvers rely on DD methods that use a blend of direct solvers to solve independent local problems and iterative solvers to solve the globally coupled CI problem. When equipped with an appropriate subdomain level preconditioner, a DD method can be numerically scalable with respect to the mesh size, or number of elements, of the given problem. In order to be also numerically scalable with respect to the subdomain size, or number of subdomains, it must be equipped with a preconditioner whose mathematical foundation is similar to that encountered in multigrid methods (Farhat et al., 2000b).

4.3.1 FETI Method

The *Finite Element Tearing and Interconnecting* (FETI) method, introduced in (Farhat, 1991) and (Farhat and Roux, 1991), is among the first non-overlapping DD methods that have demonstrated numerical scalability with respect to the mesh and subdomain sizes, for both second-order elasticity and fourth-order plate and shell problems. In particular, the parallel scalability of the FETI method and its ability to outperform several popular direct and iterative algorithms on both sequential and parallel computers have been extensively demonstrated (Farhat et al., 2000b). For the reasons mentioned above, the FETI method has been employed to solve the system of governing equations (4.38) in the developed finite element procedure. In order to understand better how the FETI method is conceived, the following system of linear algebraic equations is considered:

$$\mathbf{K}\mathbf{d} = \mathbf{f}. \quad (4.40)$$

where \mathbf{K} is the stiffness matrix of the structure, \mathbf{d} and \mathbf{f} are, respectively, the nodal displacement and the nodal load vectors. Once the domain of the structure under consideration is decomposed into a certain number of subdomains, the initial problem (4.40) can be expressed in the following equivalent form by introducing the Lagrange multipliers λ to enforce the compatibility constraints between the subdomains:

$$\begin{bmatrix} \mathbf{K}^{(1)} & \mathbf{0} & \dots & \mathbf{B}^{(1)T} \\ \mathbf{0} & \ddots & & \vdots \\ & & \mathbf{K}^{(N_s)} & \mathbf{B}^{(N_s)T} \\ \mathbf{B}^{(1)} & \dots & \mathbf{B}^{(N_s)} & \mathbf{0} \end{bmatrix} \begin{bmatrix} \mathbf{d}^{(1)} \\ \vdots \\ \mathbf{d}^{(N_s)} \\ \lambda \end{bmatrix} = \begin{bmatrix} \mathbf{f}^{(1)} \\ \vdots \\ \mathbf{f}^{(N_s)} \\ \mathbf{0} \end{bmatrix}, \quad (4.41)$$

where $\mathbf{K}^{(s)}$, $\mathbf{B}^{(s)}$, $\mathbf{d}^{(s)}$ and $\mathbf{f}^{(s)}$ are respectively the stiffness matrix, the Boolean matrices, the displacements, and load vectors of every subdomain.

In order to find the *condensed interface* (CI) problem, the linear system (4.60) is solved

for the local degrees of freedom

$$\mathbf{d}^{(s)} = \mathbf{K}^{(s)+} \left(\mathbf{f}^{(s)} - \mathbf{B}^{(s)T} \boldsymbol{\lambda} \right) - \mathbf{R}^{(s)} \boldsymbol{\alpha}^{(s)}, \quad (4.42)$$

where $\mathbf{K}^{(s)+}$ is the inverse of $\mathbf{K}^{(s)}$ for sub-domains with no unconstrained rigid modes, or a generalized inverse if sub-domain (s) is floating, in which case $\mathbf{R}^{(s)}$ contains in columns the rigid body motions of the subdomain, and $\boldsymbol{\alpha}^{(s)}$ contains the coefficients of linear combinations (Kruis, 2007; Rixen, 2001). By substituting in the following compatibility conditions

$$\sum_{s=1}^{N_s} \mathbf{B}^{(s)} \mathbf{d}^{(s)} = \mathbf{0} \quad (4.43)$$

the expression (4.42) of $\mathbf{d}^{(s)}$ in terms of $\boldsymbol{\lambda}$, and taking into account that the forces applied to a floating sub-domain must be in self-equilibrium, namely

$$\mathbf{R}^{(s)T} \left(\mathbf{f}^{(s)} - \mathbf{B}^{(s)T} \boldsymbol{\lambda} \right) = \mathbf{0}, \quad (4.44)$$

we obtain the following CI problem

$$\begin{bmatrix} \mathbf{F}_I & \mathbf{G}_I \\ \mathbf{G}_I^T & \mathbf{0} \end{bmatrix} \begin{bmatrix} \boldsymbol{\lambda} \\ \boldsymbol{\alpha} \end{bmatrix} = \begin{bmatrix} \mathbf{d} \\ \mathbf{e} \end{bmatrix}, \quad (4.45)$$

with

$$\begin{aligned} \mathbf{F}_I &= \sum_{s=1}^{N_s} \mathbf{B}^{(s)} \mathbf{K}^{(s)+} \mathbf{B}^{(s)T}, \\ \mathbf{d} &= \sum_{s=1}^{N_s} \mathbf{B}^{(s)} \mathbf{K}^{(s)+} \mathbf{f}^{(s)}, \\ \mathbf{G}_I &= \left[\mathbf{B}^{(1)} \mathbf{R}^{(1)} \quad \dots \quad \mathbf{B}^{(N_s)} \mathbf{R}^{(N_s)} \right], \\ \boldsymbol{\alpha} &= \begin{bmatrix} \boldsymbol{\alpha}^{(1)} \\ \vdots \\ \boldsymbol{\alpha}^{(N_s)} \end{bmatrix} \quad \text{and} \quad \mathbf{e} = \begin{bmatrix} \mathbf{R}^{(1)T} \mathbf{f}^{(1)} \\ \vdots \\ \mathbf{R}^{(N_s)T} \mathbf{f}^{(N_s)} \end{bmatrix}, \end{aligned}$$

where \mathbf{F}_I is the interface flexibility operator, \mathbf{d} is the interface gap created by the applied loads, \mathbf{G}_I is the restriction of the rigid modes on the interface, \mathbf{e} is the default of equilibrium of the applied loads, and $\boldsymbol{\alpha}$ collects the modal amplitudes. The CI problem (4.45) expresses that the connecting forces should be such that they fill the interface gap created by the external loads, and such that, together with the applied loads, they are in equilibrium with respect to the local rigid modes (self-equilibrium). The problem (4.45) is also called the *dual interface* problem because it is expressed in terms of the dual variables $\boldsymbol{\lambda}$ representing the interface connecting forces. The solution to the system of equations (4.45) is identical to the problem of minimising the quadratic form

$$\Phi = \frac{1}{2} \boldsymbol{\lambda}^T \mathbf{F} \boldsymbol{\lambda} - \boldsymbol{\lambda}^T \mathbf{g}, \quad (4.46)$$

with the additional condition:

$$\mathbf{G}^T \boldsymbol{\lambda} = \mathbf{e}. \quad (4.47)$$

It is appropriate to use the conjugate gradient method (Hestnes, 1952) for the solution of this problem, however, the classical method can not be used because it is derived for systems with symmetric positive definite matrices and the matrix \mathbf{F} does not fulfill this requirement since it is symmetric but not positive definite. Then, the system of equations (4.45) is solved iteratively using a modified conjugate-gradient method (Kruis, 2007). Upon convergence the interior subdomain states are recovered from (4.42) using direct solvers to solve the independent local problems.

The behaviour of the iterative methods used for the solution of reduced problems can be improved by suitable preconditioning. There are two popular pre-conditioners commonly adopted: lumped and Dirichlet (Kruis, 2007; Rixen, 2001). For second-order elasticity and fourth-order plate and shell problems, the Dirichlet preconditioner ensures scalability with respect to the mesh size. The lumped preconditioner is a more economical version of the Dirichlet preconditioner that, for many second-order elasticity problems, delivers superior computational performance since it reduces the overall computing time, although it yields slower convergence of the iterations on the interface problem. Both the lumped and Dirichlet preconditioners can be used in the finite element procedure developed in this thesis.

The FETI method has been applied in many areas; i.e. in applications to non-conforming interfaces using multi-point constraints (Farhat et al., 1998), geometrically non linear problems (Farhat et al., 2000a), and to analyses of layered structures (Kruis and Matous, 2002). The FETI method has also inspired many variants, extensions, and applications, and detailed overviews of these variations are provided in (Farhat et al., 2000b; Kruis, 2007).

4.4 Variationally Consistent Stress Recovery Procedure

It is apparent from the finite element procedure derived in section 4.2 that the stress field does not enter explicitly into the determination of the nodal displacements \mathbf{d} , and the enhanced strain parameters $\boldsymbol{\alpha}$. A consistent recovery procedure for the stress field from the nodal displacements \mathbf{d} is then required. An obvious approach to calculating the stresses resulting from a displacement finite element approximation is to differentiate the finite element solution directly and evaluate the stresses at superconvergent points within an element using the appropriate constitutive relations. However, stress fields deduced directly using constitutive relations can show spurious oscillations due to the retention of higher order (inconsistent) terms which do not contribute to the determination of the displacements and then the strains, but get reflected as extraneous stress oscillations, see section 3.2. In order to recover consistent stress fields other approaches to the conventional stress recovery have been proposed, and consistent stress distributions can be obtained in a variationally correct manner by employing integrated procedures, see section 3.2. In this regard, an appropriate procedure in the context of a class of assumed strain methods is presented for the infinitesimal theory in Simo and Rifai (1990). This procedure, which does not involve the enhanced strain field, has been extended to the geometrical non-linear case using the enhanced assumed Green-Lagrangian strains in Klinkel and Wagner (1997), and the complete procedure is reported below.

Since the displacement field is retrieved once the system of governing equations (4.38) is solved, the following least-square functional can be adopted in the procedure with the intention to minimize the stress error (Klinkel and Wagner, 1997; Simo and Rifai, 1990):

$$L(\tilde{\mathbf{E}}, \mathbf{S}) := \int_{\Omega_0} [\mathbf{C}(\mathbf{E}^c + \tilde{\mathbf{E}}) - \mathbf{S}] : \mathbf{C}^{-1} : [\mathbf{C}(\mathbf{E}^c + \tilde{\mathbf{E}}) - \mathbf{S}] d\Omega, \quad (4.48)$$

where Ω_0 is the volume of the initial configuration, \mathbf{E}^c is the compatible part of the Green-Lagrange strain tensor defined in (4.2), $\tilde{\mathbf{E}}$ is the stress tensor enhancing \mathbf{E}^c , \mathbf{S} is the second Piola-Kirchhoff stress tensor, and \mathbf{C} is the fourth order constitutive tensor defined in (4.29). Then, it is assumed that the least-squares minimization problem,

$$L(\tilde{\mathbf{E}}, \mathbf{S}) = \text{MIN}[L(\delta\tilde{\mathbf{E}}, \delta\mathbf{S})], \quad (4.49)$$

defines the correct enhanced strain $\tilde{\mathbf{E}}$ and stress \mathbf{S} fields. Considering that the first variation of $L(\tilde{\mathbf{E}}, \mathbf{S})$ has to be zero for equilibrium, the following two independent equations are obtained:

$$\begin{aligned} \int_{\Omega_0} \delta\tilde{\mathbf{E}} : [\mathbf{C} : (\mathbf{E}^c + \tilde{\mathbf{E}}) - \mathbf{S}] d\Omega &= 0, \\ \int_{\Omega_0} \delta\mathbf{S} : [(\mathbf{E}^c + \tilde{\mathbf{E}}) - \mathbf{C}^{-1} : \mathbf{S}] d\Omega &= 0. \end{aligned} \quad (4.50)$$

The stress tensor \mathbf{S} defined in (4.23) implies that $\partial w / \partial \mathbf{E}$ is equal to $\mathbf{C}(\mathbf{E}^c + \tilde{\mathbf{E}})$. Then, the equation (4.50)₁ in the case of balance is satisfied, meaning that the correct values of the enhanced strain parameters $\alpha^{(e)}$ are obtained. The second condition (4.50)₂ contains new information, from which the stress field is recovered. First, an interpolation scheme for the element stresses $\mathbf{S}^{(e)}$ has to be chosen. This interpolation scheme is assumed to be the following:

$$\mathbf{S}^{(e)} = \mathbf{G}_s \boldsymbol{\beta}^{(e)}, \quad (4.51)$$

with

$$\mathbf{G}_s = \mathbf{T}_0 \mathbf{G}(\boldsymbol{\xi}), \quad (4.52)$$

where \mathbf{T}_0 is the transformation matrix introduced in the interpolation scheme of the enhanced strain tensor \mathfrak{S} defined in (4.17), \mathbf{G} is the interpolation matrix that needs to be properly defined, $\boldsymbol{\beta}^{(e)}$ is the stress-parameters column-matrix, and $\boldsymbol{\xi} = [\xi^1, \xi^2, \xi^3]$ is the material convective coordination parameterizing the element isoparametric space. Due to the orthogonality condition (4.9) the stress field $\mathbf{S}^{(e)}$ has to be orthogonal to the enhanced strain field $\tilde{\mathbf{E}}^{(e)}$. Then, from the orthogonality condition (4.9), by substituting the interpolation scheme adopted for the enhanced strain field $\tilde{\mathbf{E}}^{(e)}$ (4.16) and the stress field $\mathbf{S}^{(e)}$ (4.51), the following expression at element level is obtained:

$$\int_{\Omega_0^{(e)}} \delta\boldsymbol{\beta}^{(e)T} \mathbf{G}_s^T \mathfrak{S} \boldsymbol{\alpha}^{(e)} \det \mathbf{J} d\xi^1 d\xi^2 d\xi^3 = 0, \quad (4.53)$$

where $\det \mathbf{J}$ is the determinant of element Jacobian matrix of the mapping from the isoparametric space to the initial configuration $\Omega_0^{(e)}$ of element (e) . Thus, the following condition

between the enhanced strain and stress interpolation matrices has to be satisfied:

$$\int_{\Omega_0^{(e)}} \mathbf{G}^T(\boldsymbol{\xi}) \mathbf{M}(\boldsymbol{\xi}) d\xi^1 d\xi^2 d\xi^3 = 0. \quad (4.54)$$

The interpolation matrix \mathbf{G} which is orthogonal to \mathbf{M} (4.20) has been investigated in An-delfinger and Ramm (1993), and assumes the following form:

$$\mathbf{G} = \begin{bmatrix} 1 & \xi^2 & \xi^3 & \xi^2 \xi^3 & 0 & 0 & 0 & 0 & 0 & 0 & 0 & 0 & 0 & 0 \\ 0 & 0 & 0 & 0 & 1 & \xi^1 & \xi^3 & \xi^1 \xi^3 & 0 & 0 & 0 & 0 & 0 & 0 \\ 0 & 0 & 0 & 0 & 0 & 0 & 0 & 0 & 1 & \xi^3 & 0 & 0 & 0 & 0 \\ 0 & 0 & 0 & 0 & 0 & 0 & 0 & 0 & 0 & 0 & 1 & \xi^1 & \xi^2 & \xi^1 \xi^2 \end{bmatrix}. \quad (4.55)$$

By inserting equation (4.52) in (4.50)₂ the following optimal stress field in the sense of least-squares minimization is obtained:

$$\mathbf{S}^{(e)} = \mathbf{G}_s \mathbf{H}_s^{-1} \boldsymbol{\Gamma}_s, \quad (4.56)$$

with

$$\begin{aligned} \mathbf{H}_s &= \int_{\Omega_0^{(e)}} \mathbf{G}_s^T \mathbf{C}^{-1} \mathbf{G}_s \det \mathbf{J} d\xi^1 d\xi^2 d\xi^3, \\ \boldsymbol{\Gamma}_s &= \int_{\Omega_0^{(e)}} \mathbf{G}_s^T \mathbf{E}^c(\xi^1, \xi^2, \xi^3) \det \mathbf{J} d\xi^1 d\xi^2 d\xi^3, \end{aligned} \quad (4.57)$$

where \mathbf{E}^c is the compatible part of the Green-Lagrange strain tensor evaluated for each Gauss point $(\xi_p^1, \xi_p^2, \xi_p^3)$. The compatible strains expression (4.2) can be reformulated as following:

$$\mathbf{E}^c(\xi^1, \xi^2, \xi^3) = \frac{1}{2} [\text{Grad} \mathbf{u}^T \text{Grad} \mathbf{u} + \text{Grad} \mathbf{u}^T + \text{Grad} \mathbf{u}], \quad (4.58)$$

where the displacement field \mathbf{u} is defined in (4.13), and the operator $\text{Grad} \mathbf{u}$ is then a function of ξ^1, ξ^2, ξ^3 :

$$\text{Grad} \mathbf{u} = \sum_{I=1}^{Nnodes} \begin{bmatrix} \mathbf{N}_{I,x} & 0 & 0 \\ 0 & \mathbf{N}_{I,y} & 0 \\ 0 & 0 & \mathbf{N}_{I,z} \\ \mathbf{N}_{I,y} & \mathbf{N}_{I,x} & 0 \\ \mathbf{N}_{I,z} & 0 & \mathbf{N}_{I,x} \\ 0 & \mathbf{N}_{I,z} & \mathbf{N}_{I,y} \end{bmatrix} \mathbf{d}_I. \quad (4.59)$$

with $Nnodes$ defining the number of nodes within an element.

This procedure will be adopted in this thesis to only recover in-plane stress distributions. This is because although consistent stress states can be retrieved at superconvergent points within the elements using this recovery procedure, when the emphasis of the analysis is the prediction of interlaminar stress failure initiation it is necessary to have accurate interlaminar stresses on these interfaces as opposed to Gauss points. Then, the stresses evaluated at superconvergent points are usually extrapolated to the boundaries of the element domain using sophisticated extrapolation techniques, as explained in detail in section 3.2. However, in presence of high in-plane and out-of-plane stress gradients, accurate nodal

stress values can only be obtained by resorting to meshes requiring demanding computational resources (Dakshina Moorthy and Reddy, 1999). In particular, the interlaminar continuity of the transverse stresses required by the C_z^0 -Requirements, as opposed to the in-plane stresses as explained in section 2.2, is difficult to achieve without resorting to refined meshes through-the-thickness of the laminate, especially in displacement based formulations in which the order of the polynomial describing the through-the-thickness variation of the transverse stresses is one order less compared to both the in-plane stress and displacement polynomials. Moreover, a coarse mesh through the thickness of the laminate in 3D formulations may lead to the possibility of thickness locking if the Poisson effect through the thickness is not correctly represented. The enhanced strain method used to derive the finite element model in section 6.1 was conceived to overcome the thickness locking, thus allowing the use of coarse meshes through the thickness of the laminate. Then, a recovery procedure able to provide accurate interlaminar stresses and not requiring demanding computational resources was developed, and is presented in the next section.

4.5 Interlaminar Stress Recovery Procedure

The present procedure is an extension of the interlaminar stress recovery procedure developed by Dakshina Moorthy and Reddy (1999) in the context of studying delamination in multilayered composites. In their approach, each ply is modeled as a separate body, and the interlaminar forces are obtained using an interface model that involves the selection of an interface in the laminate a priori and modeling it as an adhesive contact zone between portions of the laminate separated by this interface. The adhesive contact between portions of the laminate at its interface is enforced by a penalty function method, and the contact load that satisfies the equilibrium at the interface is used to evaluate the interlaminar stresses. The recovery procedure partitions the contact surface into a set of non-overlapping patches corresponding to groups of elements. The traction distribution is interpolated over each patch in terms of nodal values. Static equivalence between the tractions and the contact forces is used to calculate the nodal values of the traction, hence the interlaminar stresses. Dakshina Moorthy and Reddy showed that the procedure lead in practice to oscillatory interlaminar stress distributions. A final step in their procedure is the application of a smoothing technique to obtain more physically meaningful interlaminar stress distributions.

The procedure discussed in this thesis extends the procedure of Dakshina Moorthy and Reddy in two ways. One, each ply is still modeled separately but the compatibility between the plies is enforced using the FETI domain decomposition method introduced in section 4.3.1. Thus, connecting forces are obtained without resorting to a penalty formulation. Two, the traction distribution is interpolated over the complete interlaminar surface. Thus, the full distribution of interlaminar stresses is obtained simultaneously. More details of the proposed formulation are provided below.

Consider a typical interface between two plies as shown in figure 4.3. The system of linear equilibrium equations and compatibility conditions can be written as (4.40)

$$\begin{bmatrix} \mathbf{K}^{(1)} & 0 & \mathbf{B}^{(1)T} \\ 0 & \mathbf{K}^{(2)} & \mathbf{B}^{(2)T} \\ \mathbf{B}^{(1)} & \mathbf{B}^{(2)} & 0 \end{bmatrix} \begin{bmatrix} \mathbf{d}^{(1)} \\ \mathbf{d}^{(2)} \\ \lambda \end{bmatrix} = \begin{bmatrix} \mathbf{f}^{(1)} \\ \mathbf{f}^{(2)} \\ 0 \end{bmatrix}, \quad (4.60)$$

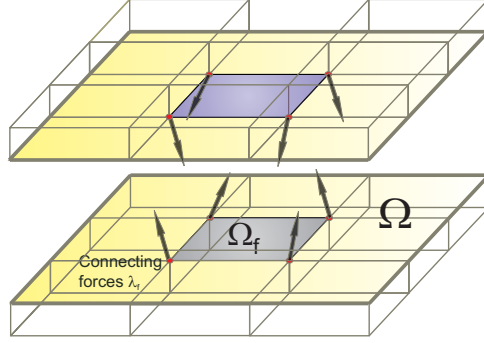


Figure 4.3: Connecting forces λ_f at the interfacial nodes of each element obtained using the FETI method.

where $\mathbf{K}^{(1)}$ and $\mathbf{K}^{(2)}$ are the stiffness matrices of the two plies, $\mathbf{u}^{(1)}$ and $\mathbf{u}^{(2)}$ the displacement vectors of the two plies, $\mathbf{f}^{(1)}$ and $\mathbf{f}^{(2)}$ the load vectors of the two plies, $\mathbf{B}^{(1)}$ and $\mathbf{B}^{(2)}$ are the Boolean matrices providing the equality conditions between displacements of the two plies, and λ are the Lagrange multipliers (interlaminar forces) introduced to enforce the compatibility constraints between the plies. Solving the system of equations (4.60), the interlaminar forces between the plies are obtained as are the displacements. Then, the traction distribution \mathbf{t}_{Ω_f} over the surface Ω_f is interpolated using C^0 iso-parametric shape functions:

$$\mathbf{t}_{\Omega_f} = \mathbf{N} \mathbf{t}_f, \quad (4.61)$$

where \mathbf{t}_f is the vector of the nodal traction values and \mathbf{N} is the matrix of C^0 shape functions. The displacement distribution \mathbf{u}_{Ω_f} over the surface Ω_f is interpolated using the same C^0 iso-parametric shape functions used for the traction distribution

$$\mathbf{u}_{\Omega_f} = \mathbf{N} \mathbf{d}_f, \quad (4.62)$$

where \mathbf{d}_f is the vector of the nodal displacements. Thus, the internal work W_{in} done by the tractions over the element surface can be written as:

$$W_{in} = \int_{\Omega_f} \underbrace{(\mathbf{t}_f \mathbf{N})^T}_{\mathbf{t}_{\Omega_f}^T} \underbrace{\mathbf{N} \delta \mathbf{d}_f}_{\mathbf{u}_{\Omega_f}} d\Omega_f = \mathbf{t}_f^T \mathbf{M}_f \delta \mathbf{d}_f, \quad (4.63)$$

where \mathbf{M}_f is the matrix of areas:

$$\mathbf{M}_f = \int_{\Omega_f} \mathbf{N}^T \mathbf{N} \partial \Omega_f. \quad (4.64)$$

Then, the matrices of areas of all the elements on the interlaminar surface Ω are assembled in a matrix \mathbf{M} :

$$\mathbf{M} = \mathbb{A}_{e=1}^{nel} \mathbf{M}_f, \quad (4.65)$$

where \mathbb{A} denotes the finite-element assembly operator. The elements connectivity on the

surface Ω is directly inherited from the solid element faces. Considering the static equivalence between the tractions and the connecting forces:

$$\mathbf{t}^T \mathbf{M} \delta \mathbf{d} = \boldsymbol{\lambda}^T \delta \mathbf{d}, \quad (4.66)$$

where \mathbf{d} and \mathbf{t} are, respectively, the global vector of nodal displacements and nodal tractions on the surface Ω , the following relation is obtained:

$$\mathbf{M} \mathbf{t} = \boldsymbol{\lambda} \Rightarrow \mathbf{t} = \mathbf{M}^{-1} \boldsymbol{\lambda}, \quad (4.67)$$

which allows to retrieve the interlaminar stress distributions over the surface Ω . The process is repeated for every interlaminar surface of interest.

It is worth mentioning that the present procedure can be easily combined with the Mortar method for the analysis of plies with non-conforming meshes. The Mortar method was introduced in the early 1990s (Puso, 2004) to formulate weak continuity conditions at the interfaces of subdomains in which different variational approximations are used. Relaxing the constraint on the boundaries of the interfaces using Lagrange multipliers provides the standard framework within which the method is normally used (Hauret and Ortiz, 2006). Then, in the case of non-conforming meshes between the plies, the Boolean matrices in equation (4.60) can be simply replaced with \mathbf{B} matrices obtained using the Mortar method. The accuracy of the present approach is demonstrated in the next section.

4.6 Numerical Results

4.6.1 Simply Supported Plate Subjected to Bisinusoidal Pressure Load

The procedure discussed and developed in this thesis was validated considering a benchmark problem analysed in Pagano (1970), where 3D exact elasticity solutions of idealised simply supported cross-ply $[0^\circ/90^\circ/0^\circ]$, square plates under bisinusoidally distributed pressure load of intensity p_z , are provided. The length and thickness of the plate is denoted by a and H respectively. The laminate is made of material plies that are idealized to be homogeneous, elastic and orthotropic. The following material properties are used: $E_{11} = 25 \text{ GPa}$, $E_{22} = E_{33} = 1 \text{ GPa}$, $G_{12} = G_{13} = 0.5 \text{ GPa}$, $G_{23} = 0.2 \text{ GPa}$, and $\nu_{12} = \nu_{13} = \nu_{23} = 0.25$. Subscripts 1,2 and 3 denote the fibre, transverse and thickness directions, respectively. The rectangular Cartesian coordinate system used is such that the origin is located in the middle of the laminate at one of the side corners, see figure 4.4. Stresses are normalized according to the following formulae,

$$\begin{aligned} (\tau'_{xz}, \tau'_{yz}) &= \frac{1}{p_z S} (\tau_{xz}, \tau_{yz}), \quad \sigma'_{zz} = \frac{1}{p_z} \sigma_{zz}, \\ (\sigma'_{xx}, \sigma'_{yy}, \tau'_{xy}) &= \frac{1}{p_z S^2} (\sigma_{xx}, \sigma_{yy}, \tau_{xy}) \end{aligned}$$

where the S is the laminate length to thickness ratio $S = a/H$.

Laminates of length to thickness ratios $S = 20, 50, 100$ were analysed to demonstrate the accuracy of the present procedure in analysing moderately-thick/thin composite struc-

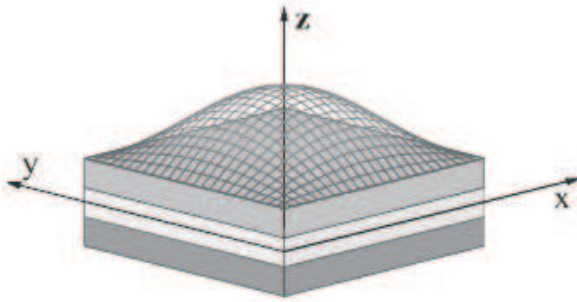


Figure 4.4: Bisinusoidal pressure load

tures. Particular attention was paid to the recovery of the interlaminar stress fields. This is because an appropriate level of accuracy of the transverse stress fields that is able to fulfill the C_z^0 -Requirements, see section 2.2, usually represents the aspect, the achievement of, which demands accurate and computationally expensive finite element models. One solid-shell element was adopted in the through-the-thickness mesh of each ply in the laminate. Convergence analyses of the interlaminar transverse stresses evaluated at the $[0^\circ/90^\circ]$ interface between the top and middle plies, i.e. $z/H=0.1666$, were performed using different in-plane meshes. This interface is the one with maximum interlaminar stresses due to the mismatch of the material properties (0° and 90° plies). The results for the performed convergence analyses are presented in figures 4.5 and 4.6 for, respectively, values of length to thickness ratios $S = 20$ and $S = 100$. Referring to the scheme reported in figure 4.3, interlaminar transverse stress distributions were obtained using a linear interpolation for the traction distribution over the surface Ω_f . This was achieved by adopting the same classical linear isoparametric shape functions assumed for the displacement field. Excellent agreement with Pagano's exact solution and fast convergence were obtained for both moderately thick laminates, i.e. $S = 20$, and thin laminates, i.e. $S = 100$. This fast convergence is due to the fact that the present procedure provides the transverse stresses directly at nodes using equilibrium considerations, thus interlaminar continuity of the transverse stresses was easily satisfied, and accurate interlaminar transverse stress distributions with respect to the exact solutions could be obtained using an in-plane coarse mesh of 12×12 elements. However, in figure 4.5₁ it can be seen that the value of the transverse normal stress σ'_{zz} at the boundary of the laminate, i.e. $y/a = 0$, does not converge exactly to zero by refining the mesh, as it should be, but a stress state of compression or tension is generated depending on the sign of the pressure load considered. Boundary stress states were generated at the boundaries of the laminate where idealised simply supported boundary conditions were applied in the 3D finite element model.

The appropriate level of accuracy reached in the evaluation of the interlaminar stress fields is further shown in table 4.2, where transverse stress values evaluated at the $(0^\circ/90^\circ)$ interface at points of major interest, labeled as EQUILIBRIUM, are reported for different values of length to thickness ratio S of the laminate. The percentage errors with respect to Pagano's exact solutions, labeled as EXACT, are also reported in brackets. The percentage errors obtained were always less than 1.3%, confirming that accurate evaluations of the

interlaminar stresses were obtained in these locations for both moderately-thick and thin laminates by adopting an in-plane mesh of 12×12 elements.

Table 4.1: Comparison between interlaminar transverse stress values evaluated at points of major interest on the $(0^\circ/90^\circ)$ interface of a $[0^\circ/90^\circ/0^\circ]$ laminate using the proposed procedure and Pagano's exact solution (Pagano, 1970).

S		$\tau'_{xz}(0, \frac{a}{2}, \frac{1}{6})$	$\tau'_{yz}(\frac{a}{2}, 0, \frac{1}{6})$	$\sigma'_{zz}(\frac{a}{2}, \frac{a}{2}, \frac{1}{6})$
20	EXACT	0.3804	0.0374	0.7398
	EQUILIBRIUM	0.3825 (0.55%)	0.0375 (0.27%)	0.7483 (1.15%)
50	EXACT	0.3892	0.0341	0.7406
	EQUILIBRIUM	0.3914 (0.57%)	0.0342 (0.29%)	0.7496 (1.22%)
100	EXACT	0.3905	0.0336	0.7407
	EQUILIBRIUM	0.3926 (0.54%)	0.0337 (0.3%)	0.7498 (1.23%)

The excellent level of smoothness reached in the recovered interlaminar transverse stress distributions is shown in figures 4.7 and 4.8 which show, respectively, the surface plots at the $(0^\circ/90^\circ)$ interface of the interlaminar transverse shear stress τ'_{yz} and normal stress σ'_{zz} for $S = 20$, and the surface plot of the interlaminar transverse shear stress τ'_{xz} for $S = 100$. The maximum value and the location where the maximum value is reached is also highlighted for each surface plot. The boundary stress states mentioned above, and generated at the locations where the idealised simply supported boundary conditions were imposed, are also evident in the surface plot of the transverse shear stress τ'_{yz} in figure 4.5₂ at the locations $x/a = 0$ and $x/a = 1$.

Based on the considerations formulated above, henceforth the in-plane mesh in the finite element model will consist of 12×12 elements unless differently stated. As far as the through-the-thickness mesh is concerned, from figure 4.9(a) one can see the surface plot of the interlaminar shear stress τ'_{xz} distribution at the $(0^\circ/90^\circ)$ interface for a laminate of length to thickness ratios $S = 50$ obtained considering no fictitious interfaces within the plies, while in figure 4.9(b) it is shown the same surface plot obtained when one fictitious interface located in the middle of every ply is considered. The difference between the two analyses in the maximum value of the transverse shear stress τ'_{xz} obtained, and highlighted in the plots, is 0.0357%. Moreover, in both the analyses the difference with respect to the exact solution is less than 0.5%. Similar results were obtained considering laminates of length to thickness ratios $S = 20$ and $S = 100$. Then, the minimum required number of elements in the thickness direction was three. While this is sufficient for accurate interlaminar stresses, it does not allow the detailed evaluation of the through the thickness variation of the transverse stresses. To also provide transverse stress distributions in the middle of every layer, three more mathematical interfaces are required in these locations to give a total number of six elements through the thickness.

The same laminate is analysed in Dakshina Moorthy and Reddy (1999) where two different values of length to thickness ratios $S = 10, 100$ are considered. The rectangular Cartesian coordinate system used in their work is such that the origin is located at the center of the bottom surface of the plate. Regarding the structural symmetry, only a quarter of the

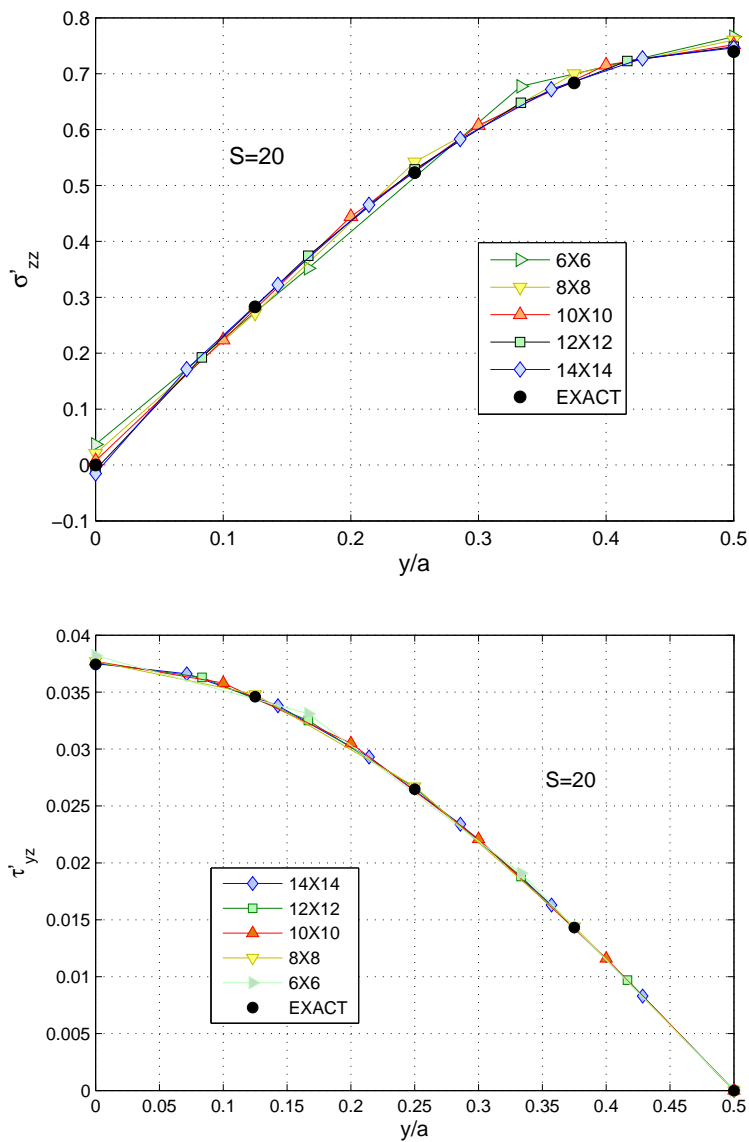


Figure 4.5: Convergence analyses concerning the transverse normal stress σ'_{zz} and the transverse shear stress τ'_{yz} at the $(0^\circ/90^\circ)$ interface of a $[0^\circ/90^\circ/0^\circ]$ laminate considering different in-plane meshes; $x/a = 0.5$, $S = 20$.

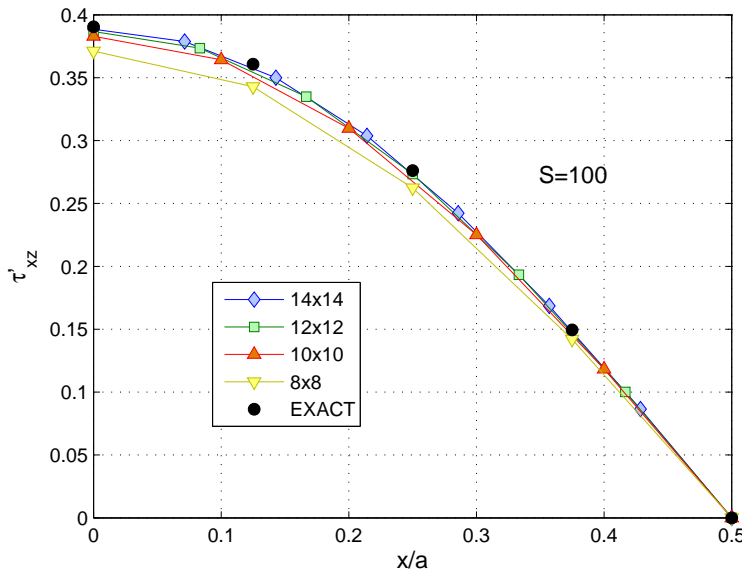
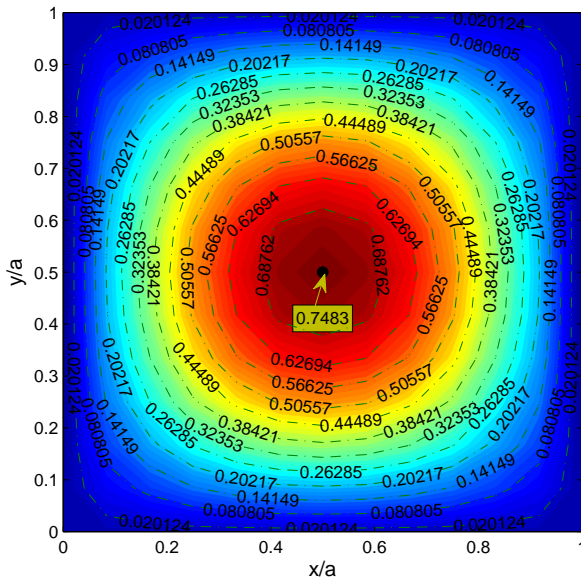


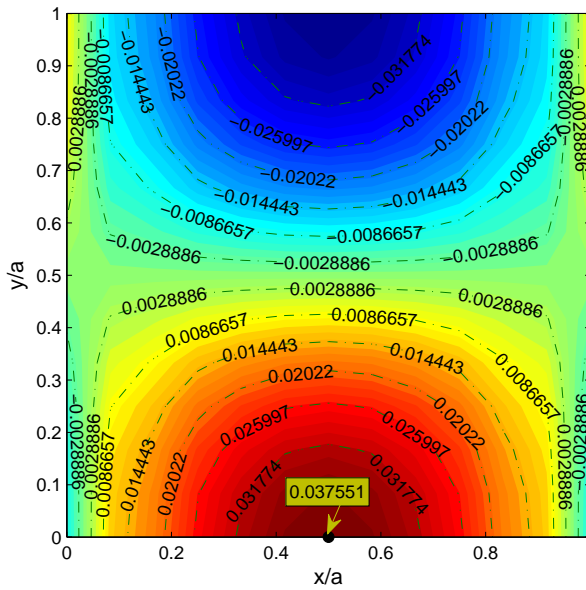
Figure 4.6: Convergence analysis concerning the transverse shear stress τ'_{xz} at the $(0^\circ/90^\circ)$ interface of a $[0^\circ/90^\circ/0^\circ]$ laminate considering different in-plane meshes; $y/a = 0.5$, $S = 100$.

plate is taken into account. Then, the computational domain of the quarter plate model is $0 \leq x \leq a/2; 0 \leq y \leq a/2; 0 \leq z \leq H$. An in-plane mesh of $[8 \times 8]$ nine-node quadratic elements and a mesh of linear Lagrange elements through the thickness of the laminate is considered. For their study of interlaminar stresses, Dakshina-Moorthy and Reddy selected the $(0^\circ/90^\circ)$ interface between the top and middle plies. The interlaminar stresses are calculated and compared using three different approaches: (1) their equilibrium based stress recovery procedure, at nodes; (2) from constitutive relations, at integration points; and (3) variationally optimal stress recovery procedure, at integration points. Dakshina-Moorthy and Reddy's interlaminar stress distributions for the transverse normal stresses σ'_{zz} and τ'_{xz} are reported in figure 4.10. The stresses computed using the last two approaches were not single valued at the interface. These approaches were then used by Dakshina-Moorthy and Reddy to evaluate interlaminar stresses at the integration Gauss points within each element. Their equilibrium based stress recovery procedure could be used to compute interlaminar stresses at the nodes on the interface.

The distribution of the interlaminar normal stress σ'_{zz} for a laminate with thickness to length ratio $S = 10$ is shown in figure 4.10₁. It can be noted that σ'_{zz} obtained from the equilibrium is very close to the exact solution. The approach based on the constitutive relations overpredicts the transverse normal stresses, and the variationally optimal stress recovery procedure produces a distribution of stress that is constant within an element and not much different from that obtained using constitutive relations. Although less accurate compared to equilibrium, transverse normal stress distributions recovered using constitutive relations show qualitatively the correct distribution. However, for very thin plates, i.e. $S =$



(a) Surface plot concerning the interlaminar transverse normal stress σ_{zz}^I .



(b) Surface plot concerning the interlaminar transverse normal stress τ_{yz}^I .

Figure 4.7: Surface plots concerning the recovered interlaminar transverse stresses at the $(0^\circ/90^\circ)$ interface of a $[0^\circ/90^\circ/0^\circ]$ laminate, $S = 20$.

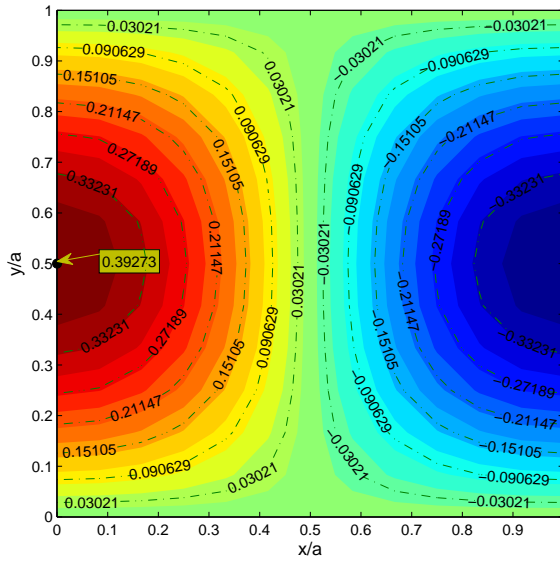


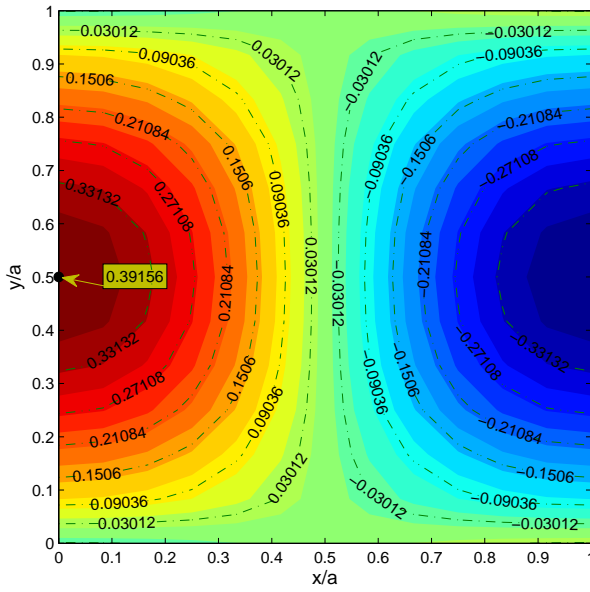
Figure 4.8: Surface plot concerning the recovered interlaminar transverse shear stress τ'_{xz} at the $(0^\circ/90^\circ)$ interface of a $[0^\circ/90^\circ/0^\circ]$ laminate, $S = 100$.

100, Dakshina-Moorthy and Reddy have shown that constitutive relation-based transverse normal stresses were very inaccurate near the edges of the plate.

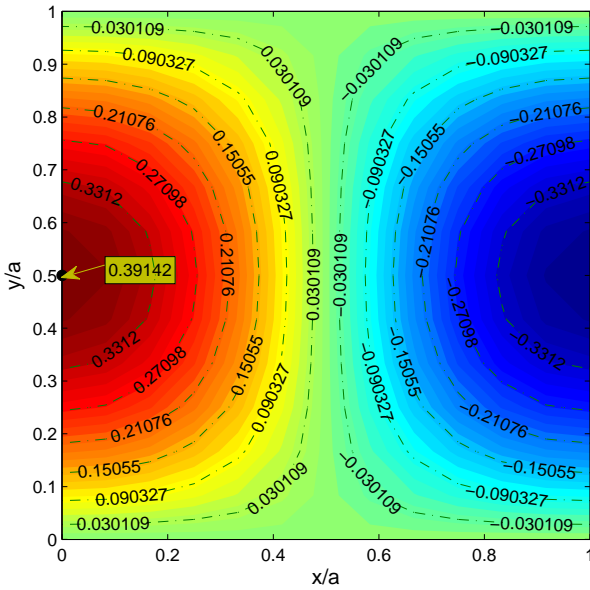
The distribution of τ'_{xz} for $S = 100$ is reported in figure 4.10₂. The stresses from the constitutive relations and that from variationally recovery procedures are less accurate when compared to the equilibrium-based stress recovery procedure. It can also be noted that the variationally optimal stress distribution is extremely close to that obtained from constitutive relations both in terms of distribution and value.

One undesirable feature of the stress recovery procedures mentioned above is the presence of oscillations in the transverse stress distributions, especially for thin plates. These oscillations were found to be severe in transverse shear stresses. The amplitudes of oscillations for equilibrium-based stresses were found to be comparable to that in constitutive relation-based stresses. Further, it was noted that these oscillations tend to increase in amplitude as the laminate gets thinner. Then, either a refinement of the mesh or the employment of smoothing techniques is usually required, however, the computational cost involved increases significantly. Comparing these distributions with the ones obtained using the present procedure and shown in figure 4.5, it can be stated that the present procedure is able to circumvent the shortcomings of the recovery procedures developed by Dakshina-Moorthy and Reddy by employing much coarser meshes compared to their model, and without the need to resort to the use of smoothing techniques to obtain accurate and smooth interlaminar stress fields.

The same laminate was also analysed using the layer-wise mixed theories proposed by Carrera and Demasi (2002a,b). In their work, quadrilateral multilayered four-, eight-, and



(a) Surface plot obtained without the introduction of mathematical interfaces.



(b) Surface plot obtained introducing one mathematical interface in the middle of each ply.

Figure 4.9: Surface plots concerning the recovered interlaminar transverse shear stress τ'_{xz} at the $(0^\circ/90^\circ)$ interface of a $[0^\circ/90^\circ/0^\circ]$ laminate, $S = 50$.

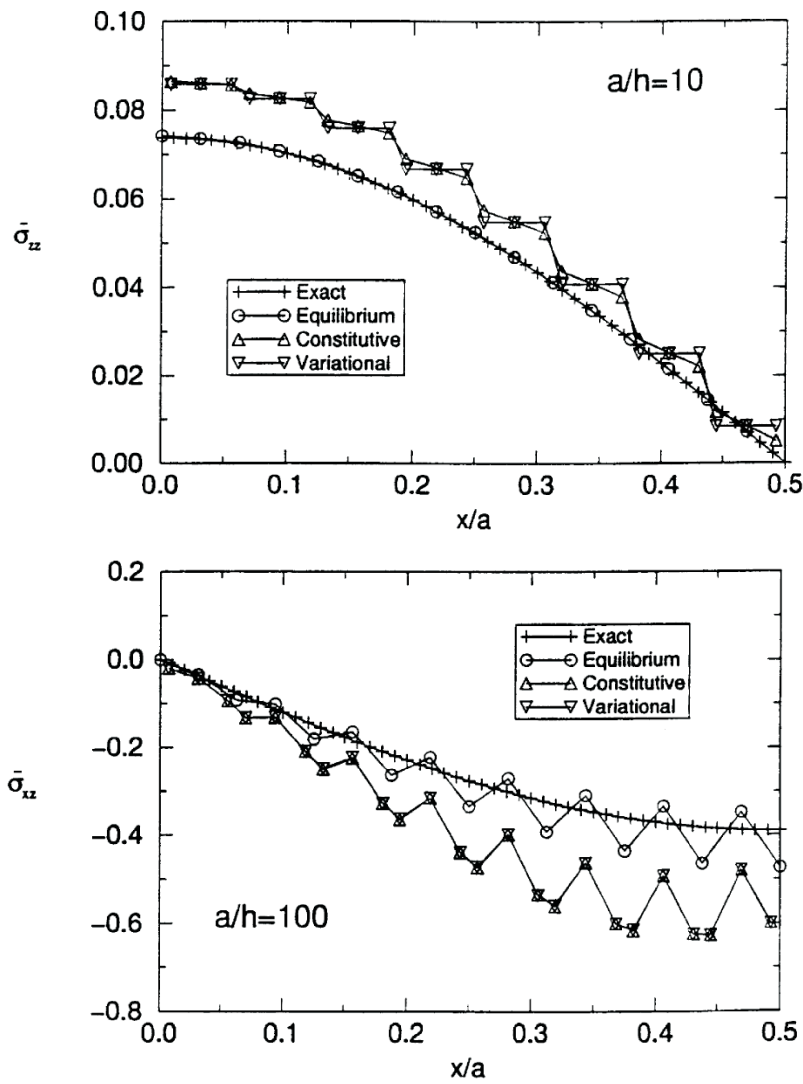


Figure 4.10: Transverse normal stress $\bar{\sigma}_{zz}$ (σ'_{zz} in the present convention) and transverse shear stress $\bar{\sigma}_{xz}$ (τ'_{xz}) distributions obtained in Dakshina Moorthy and Reddy (1999) at the interlaminar surface ($0^\circ/90^\circ$) of a $[0^\circ/90^\circ/0^\circ]$ laminate using different approaches, and different length to thickness ratios S ; $y/a = 0.5$ with reference to the present cartesian coordinate system.

nine-noded plate elements are developed based upon the Reissner's Mixed Variational Theorem (RMVT) (Reissner, 1984, 1986), which allows one to assume two independent fields for displacements and the transverse stress variables. Layer-wise modeling, see section 2.3.4, and equivalent single-layer modeling, see section 2.3.3, are considered on the framework of the RMVT. Linear and higher-order, up to fourth order, expansion in the through-the-thickness direction of the laminate are implemented for both displacements and transverse stresses. In this thesis, attention will be restricted to those elements assuming a layer-wise multilayered form description through-the-thickness of the laminate. These elements are denoted using the acronym LMn, where n is the order of expansion assumed for both the displacements and transverse stresses polynomials along the thickness direction of every ply. The LMn's distributions showed below were obtained without the introduction of fictitious interfaces within the plies, and the final system of algebraic equations was solved for both displacements and transverse stress variables. Thus, the transverse stresses were obtained directly at nodes, and accurate and continuous interlaminar stress distributions could be generated without the employment of a post-processing recovery procedure, as opposed to conventional displacement based formulations.

Through-the-thickness distributions of the transverse stresses were obtained at locations in the $x-y$ plane of major interest using the multilayered nine-noded plate elements developed in Carrera and Demasi (2002a,b). These distributions are shown in figure 4.11 for, respectively, the transverse shear stresses τ'_{xz} and τ'_{yz} , and in figure 4.12 for the transverse normal stress σ'_{zz} . In these plots, Carrera and Demasi's distributions are compared with the ones obtained using the procedure presented in this thesis, and Pagano's exact solutions. A laminate with a value of length to thickness ratios $S = 20$ is considered to highlight the accuracy obtained by the present procedure in the analysis of moderately-thick composite laminates. An in-plane mesh of 12×12 elements was adopted in all the cases. Among the considered Carrera and Demasi's multilayered nine-noded plate elements, accurate transverse stress distributions with respect to the exact solutions were obtained by assuming at least a third order polynomial through-the-thickness of each ply, i.e. LM3, for the transverse stress approximations. A third order of approximation is particularly required by the transverse shear stress distributions due to the presence of higher through-the-thickness gradients compared to the transverse normal stress σ'_{zz} distribution. In fact, by analysing more in detail the transverse shear stress τ'_{yz} distribution in figure 4.11, a quadratic order of interpolation for the assumed transverse stresses, i.e. LM2, generates a percentage error with respect to the exact solution of 3.76% at the point of maximum value, i.e. $z/H=0$, and at the $(0^\circ/90^\circ)$ interface, i.e. $z/H= 0.1666$, a percentage error of 25.13%. Moreover, inaccurate values are obtained at the boundaries, i.e. top and bottom of the laminate. The percentage errors in these locations is reduced to less than 1.5% using LM3. A similar response is obtained for the transverse shear stress τ'_{xz} , whereas a quadratic order of interpolation is enough to generate an accurate distribution for the assumed transverse normal stress σ'_{zz} , as shown in figure 4.12. Thus, a system of algebraic equations with 37500 unknowns needs to be solved using Carrera and Demasi's formulation for appropriate evaluations of the interlaminar stresses.

The percentage error with respect to the exact solution generated using the present procedure for the evaluation of the transverse shear stress τ'_{yz} at the point of maximum value, i.e. $z/H=0$, is of 0.53%, and at the $(0^\circ/90^\circ)$ interface, i.e. $z/H= 0.1666$, the percentage error is of 0.27%. A similar response is obtained for both the transverse shear stress τ'_{xz} and the transverse normal stress σ'_{zz} . This means that the present procedure obtains accurate values

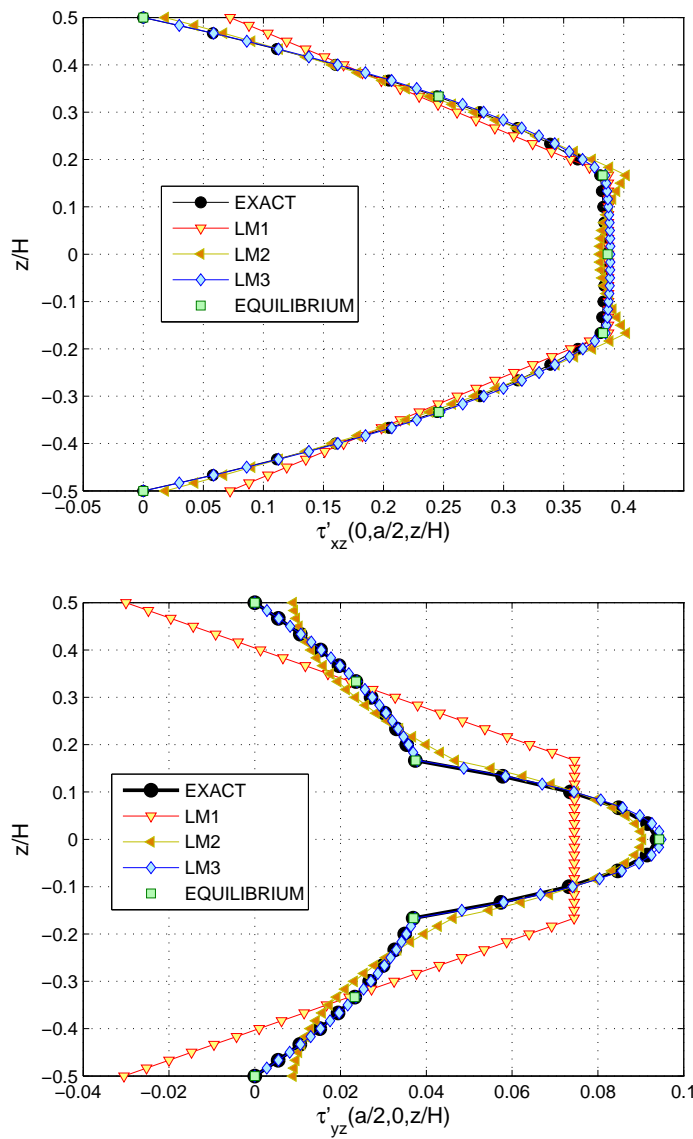


Figure 4.11: Comparisons between the through-the-thickness distributions of the transverse shear stresses obtained at locations in the $x-y$ plane of major interest using different approaches, $S=20$.

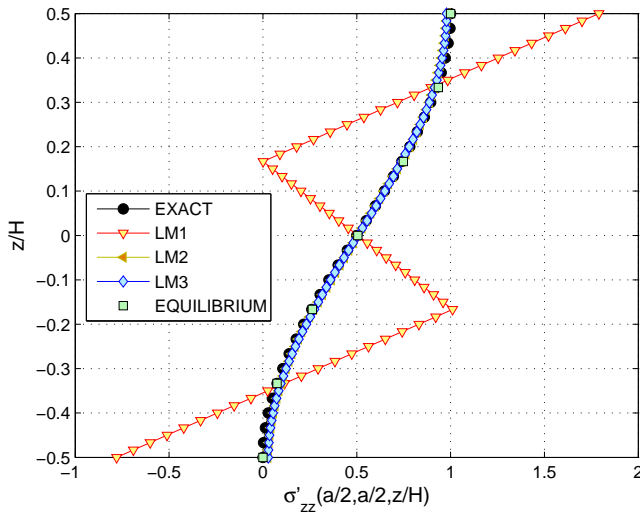


Figure 4.12: Comparisons between the through-the-thickness distributions of the transverse normal stress σ'_{zz} obtained in the middle of the laminate using different approaches, $S=20$.

of the transverse stresses by solving a system of algebraic equations with 8619 unknowns, although a fictitious interface was introduced in the middle of each ply to recover intralaminar values of the transverse stresses. This means that the present procedure is able to generate a percentage reduction of 72% in the total number of degrees of freedom required to achieve accurate distributions of the interlaminar stresses compared to Carrera and Demasi's formulation. For the sake of completeness, it is worth remarking that in analyses requiring accurate evaluation of the intralaminar transverse stresses, as for instance in cases where intralaminar failure initiation is more likely to occur than interlaminar failure, the present procedure may be as much computationally expensive as stress-based formulations since additional fictitious interfaces would be required in the locations of interest.

Comparisons between the through-the-thickness distributions of the in-plane stresses at points of major interest are shown in figure 4.13. In this case the comparisons are between the plots obtained using the proposed variational consistent procedure, labeled as VARIATIONAL, the ones obtained using Carrera and Demasi's multilayered nine-noded plate elements and based on the constitutive relations, and Pagano's exact solutions. Accurate distributions were obtained in all the cases. By using the proposed variational consistent recovery procedure, in plane stresses are evaluated at the integration points within each element, and the retrieved values are extrapolated to the element nodes using the shape functions. Then, the values at the common nodes between the elements are obtained averaging all the contributions. Additional in-plane stress values obtained at points of major interest using the present procedure are reported in table 4.2 for different values of length to thickness ratios S . In this case, the percentage error of the recovered in-plane stress values with respect to the exact solutions is always less than 1.6%.

A comparison between convergence analyses of the interlaminar transverse stress τ'_{yz}

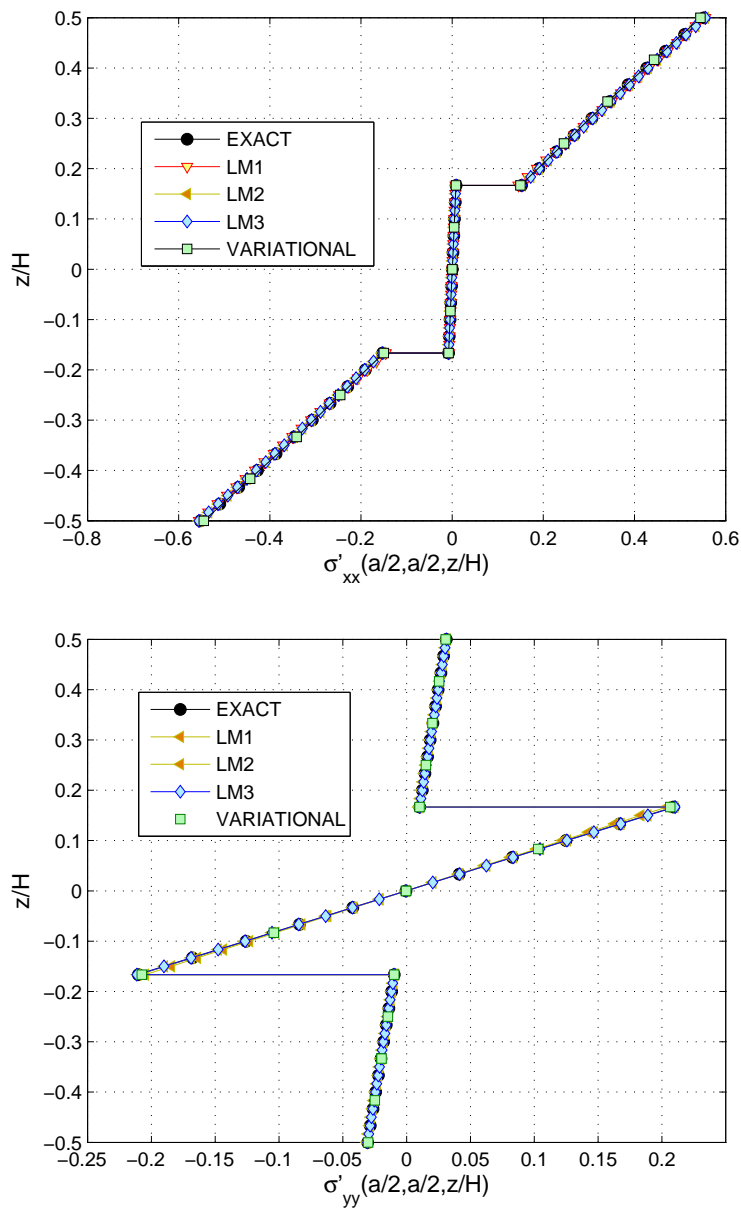


Figure 4.13: Comparisons between the through-the-thickness distributions of the in-plane normal stresses obtained in the middle of the laminate using different approaches, $S=20$.

Table 4.2: Comparison between in-plane stress values evaluated at points of major interest using the proposed procedure and Pagano's exact solution (Pagano, 1970).

S		$\sigma'_{xx}(\frac{a}{2}, \frac{a}{2}, \pm\frac{1}{2})$	$\sigma'_{yy}(\frac{a}{2}, \frac{a}{2}, \pm\frac{1}{6})$	$\tau'_{xy}(0, 0, \pm\frac{1}{2})$
20	EXACT	± 0.5524	± 0.2092	∓ 0.0234
	VARIATIONAL	$\pm 0.5450(1.34\%)$	$\pm 0.2062(1.45\%)$	$\mp 0.0230(1.52\%)$
50	EXACT	± 0.5409	± 0.1845	∓ 0.0216
	VARIATIONAL	$\pm 0.5338(1.33\%)$	$\pm 0.1820(1.37\%)$	$\mp 0.0213(1.41\%)$
100	EXACT	± 0.5393	± 0.1808	∓ 0.0213
	VARIATIONAL	$\pm 0.5326(1.26\%)$	$\pm 0.1786(1.23\%)$	$\mp 0.02102(1.33\%)$

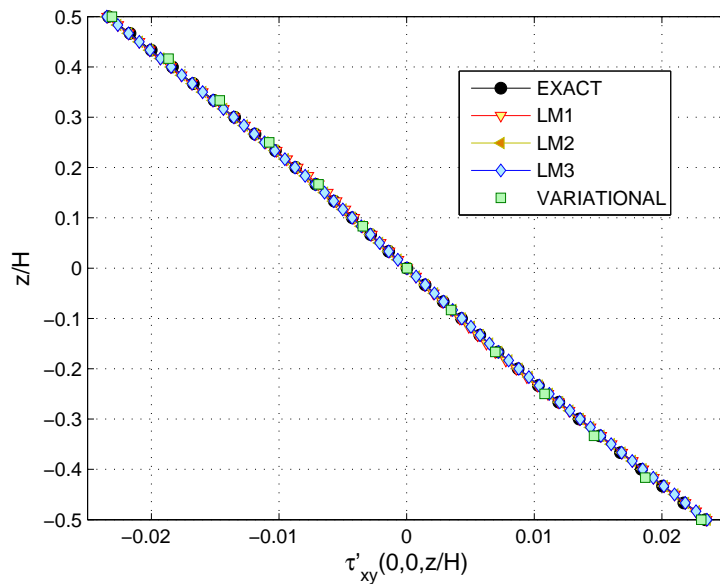


Figure 4.14: Comparisons between the through-the-thickness distributions of the in-plane shear stress τ'_{xy} obtained at the in-plane location $x = 0, y = 0$ using different approaches, $S=20$.

performed considering different in-plane meshes, and obtained at the point of maximum value is shown in figure 4.15(a). These analyses were carried on using the proposed procedure, and Carrera and Demasi's multilayered four- and nine-noded *LM3* plate elements, respectively labeled Q4 and Q9, and shown in figure 4.15(a). In these plots Ne represents the number of elements along each side of the plate. A laminate of thickness to length ratio $S = 20$ was considered. The proposed procedure produces a slope similar to the one obtained using the *LM3 Q9* plate element, but a faster convergence to the exact solution is achieved. Similar slopes were obtained for the interlaminar transverse shear stress τ'_{xz} and transverse normal stress σ'_{zz} . These plots again confirm the excellent level of accuracy and efficiency of the proposed procedure since these results were obtained using a significant reduction in the number of degrees of freedom involved compared to other approaches. A similar analysis, but concerning the in-plane stress σ'_{xx} , is shown in figure 4.15(b). In this case, the slope followed by the proposed procedure is similar to the one obtained using the *LM3 Q4* plate element, but with a slightly slower convergence due to the different order of interpolation adopted through the thickness of the laminate. This similarity was expected since variationally consistent recovery procedures usually provides distributions that are extremely close to that obtained from constitutive relations both in terms of distribution and value, as shown in figure 4.10, provided that the stress distributions obtained from the constitutive relations are consistent with the finite element model. Similar trends were obtained for the in-plane stresses σ'_{yy} and τ'_{xy} .

From the comparisons made above it is clear that the procedure presented in this thesis is able to provide data on stress fields as accurate as Carrera and Demasi's stress based formulation, even in the range from thick to moderately-thick laminates, i.e. $S = 20$, but with a significant reduction in the computational cost involved and faster overall performances. This is particularly remarkable in the recovery of the interlaminar stress fields, although in Carrera and Demasi's procedure a post-processing stress recovery technique is not required. For the sake of completeness, it is worth to say that the computational cost involved in Carrera and Demasi's stress based formulation can be reduced using a generalization of this approach proposed by Demasi (2008), where each variable, in the most general case each displacement and each transverse stress, can be independently expanded along the thickness of the laminate based on the order of approximation required. For instance, in the case under consideration the through-the-thickness distribution of the σ'_{zz} would require a quadratic order of interpolation and not a third order as for the transverse shear stress distributions.

4.6.2 Stress Analyses of Laminated Composite Plates with Open Hole Subjected to Uniaxial Tension

Stress concentration phenomena play an important role in the design of layered structures. A well known stress concentration problem is the problem of a plate loaded in-plane and containing a circular open hole. This problem combines strong in-plane stress gradients with free edge effects and is characterized by the occurrence of strongly 3D singular stress fields at the free edges in the interface between two layers of composite laminates. As a consequence, stress calculation at the interlaminar surfaces in the vicinity of the hole edge is a difficult problem.

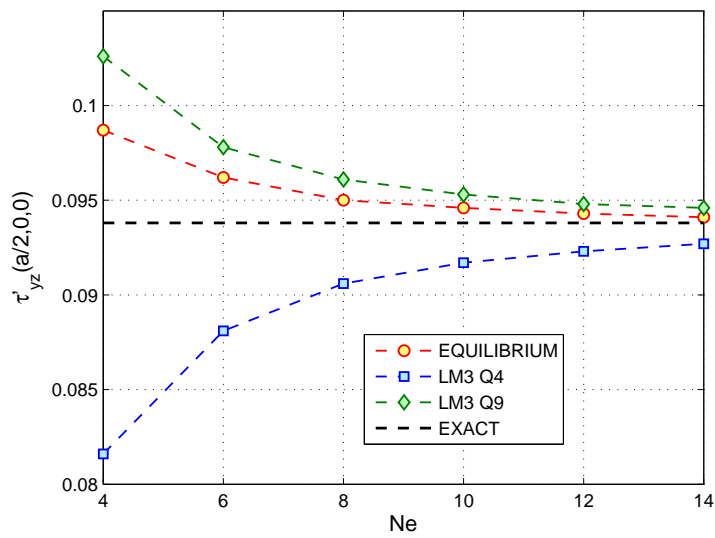
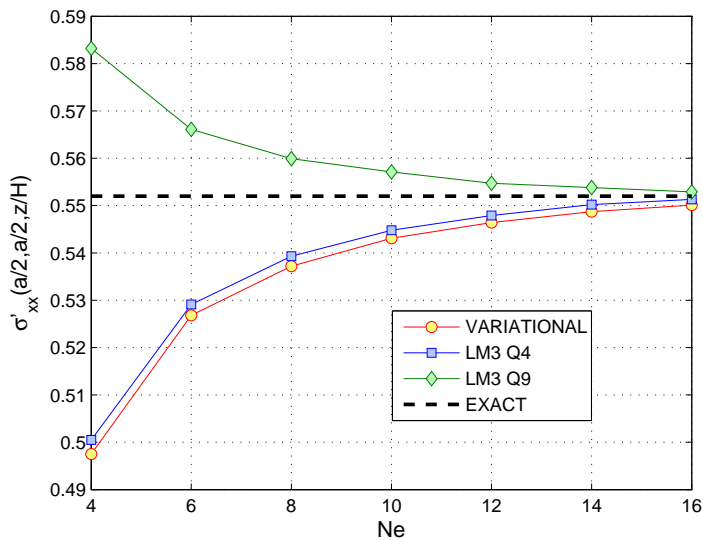
(a) Convergence analysis of the transverse shear stress τ'_{yz} .(b) Convergence analysis of the in-plane normal stress σ'_{xx} .

Figure 4.15: Convergence analyses concerning some recovered stresses at points of maximum values, and performed considering different in-plane meshes and different approaches; $S = 20$.

The accuracy of the recovery procedure presented in this thesis was tested examining a square $[45^\circ/-45^\circ]_s$ plate with a circular hole as shown in figure 4.16. The laminate con-

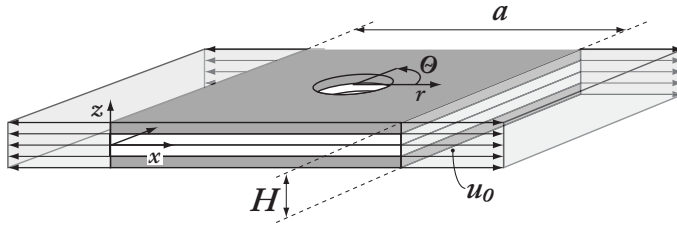


Figure 4.16: Laminate plate with hole.

sist of the planar dimensions $a = 508\text{ mm}$, diameter of the hole $D = 50.8\text{ mm}$, coordinate of the hole center $x_c = y_c = a/2$, ply thickness $h = 2.54\text{ mm}$. Each ply is treated as an homogeneous, elastic and orthotropic material with the following properties: $E_{11} = 138\text{ GPa}$, $E_{22} = E_{33} = 14.5\text{ GPa}$, $G_{12} = G_{13} = G_{23} = 5.86\text{ GPa}$, and $\nu_{12} = \nu_{13} = \nu_{23} = 0.21$. The uniaxial loading $u_0/a = 0.001$ is applied via displacement boundary conditions at the lateral sides ($x = 0, a$),

$$-u_x(0, y, z) = u_x(a, y, z) = u_0, u_y(0, y, z) = u_y(a, y, z) = 0. \quad (4.68)$$

The averaged applied stress is calculated as:

$$\sigma_0 = \frac{1}{aH} \int_0^a \int_0^H \sigma_{xx}(a, y, z) dy dz \quad (4.69)$$

where H is the complete laminate thickness.

This problem is analysed in Iarve (1996) where an independent polynomial spline approximation of displacement and interlaminar tractions is proposed for accurate stress analysis of multilayer composite laminates with open hole, and a three-dimensional full field solution is obtained. Spline approximation is able to eliminate the inter-element compatibility problems leading to unsatisfactory finite element results in the presence of field singularities. Moreover, spline approximation offers continuity of displacement, strain and stress fields within homogeneous domains simultaneously preserving the advantages of local approximation, such as sparsity of the resulting system of equations. In the work of Iarve (1996) the system of equations allowing for the calculation of the displacement spline approximation coefficients under given surface tractions is obtained using the minimum potential energy principle. A closed form asymptotic solution, valid in the vicinity of the hole edge at the interface of two orthotropic plies of arbitrary thickness, is also developed in Iarve (1996) to verify the spline approximation. Good agreement was observed between the asymptotic solution and Iarve's spline approximation for distances up to $H/4$ from the hole edge for all stress components. However, the procedure was shown to be detrimental for accurate interlaminar stress calculation within approximately one half-ply thickness from the singular point. In order to provide accurate stress fields also in the singular neighborhood of the ply interface and the hole edge, the procedure is improved in Iarve and Pagano (2001) using a superposition approach of an hybrid and displacement approximation based on the

Reissner's variational principle Reissner (1984, 1986). The approximation of displacement is still based on the polynomial B-spline functions, but the hybrid stress functions are derived using the asymptotic solution carried on in Iarve (1996). Iarve and Pagano (2001) show converged interlaminar stress components, including their singularities, as a function of the distance from the hole edge. Then, the interlaminar stress distributions obtained in Iarve and Pagano (2001) were taken as benchmark solutions to validate the recovery procedure presented in this thesis.

In the present analysis, given the symmetry of loading and lay-up, only half of the total thickness of the laminate was modelled. An example of the in-plane mesh adopted is shown in figure 4.17. Henceforth, the designation $[ner/rsr-net]$ denotes a mesh where: ner is the number of elements extending in the radial direction from the hole edge to the end of the circular region, i.e. $r = 80\text{mm}$, rsr is the radial spacing ratio of the elements in the refined circular region in which the interval size increases in geometric progression beginning at the hole edge, and net is the number of elements through the half thickness of the complete laminate. For instance, the mesh denoted as $24/30-2$ adopts two elements in the thickness direction, that is one solid-shell element is assumed through-the-thickness of each ply. In the present analysis a refinement of the mesh in the thickness direction was obtained by introducing the necessary fictitious interfaces in each ply. Thus, the final number of plies increased, and the interlaminar stress recovery procedure presented in section 4.5 could also be adopted at every fictitious interface to provide intralaminar transverse stress values. When introduced, the fictitious interfaces were equally spaced within each ply, and one solid-shell element was still considered through-the-thickness of each ply. The number of solid-shell elements adopted around a quarter of the hole edge was 36.

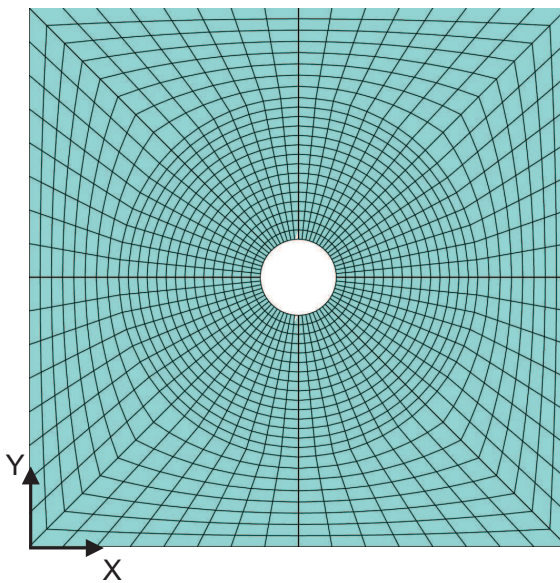


Figure 4.17: Example of the adopted mesh

Interlaminar transverse normal stress σ_{zz} distributions along the radial r coordinate at

$\theta = 90^\circ$, evaluated in a cylindrical coordinate system r, θ, z with the origin in the center of the plate, are shown in figure 4.18 considering different meshes. These distributions are plotted starting from the hole edge up to one laminate thickness $r = H + D/2$, at the $[45^\circ/-45^\circ]$ interface, and compared with the stress fields provided in Iarve and Pagano (2001) (not reported) in the singular neighborhood of the ply interface and the hole edge. The present procedure shows excellent agreement with Iarve and Pagano's distributions for distances up to approximately one half-ply thickness from the singular point for all the mesh considered. The mesh denoted as $24/30-2$ does not employ fictitious interfaces, and involves 51840 degrees of freedom in the circular refined region. However, a mesh-dependent influence of the stress singularity was encountered instead within approximately one half-ply thickness from the singular point. This behaviour is shown in figure 4.18₁ where different through-the-thickness meshes are considered, and an in-plane mesh of $24/30-n$ is assumed. A better agreement is obtained compared to the $24/30-2$ mesh with Iarve and Pagano's distribution by introducing fictitious interfaces in the laminate, e.g. the mesh denoted as $24/30-4$ introduce one fictitious interface in the middle of every layer. However, the influence of the stress singularity is not reduced further by introducing additional fictitious interfaces. An analysis of the influence of different in-plane meshes on the stress singularity is shown in figure 4.18₁. A fictitious interface is adopted in the middle of every layer. The influence of the stress singularity is reduced, and a smooth distribution in excellent agreement with the one shown in Iarve and Pagano (2001) is obtained by refining the mesh close to the hole edge, i.e. using the mesh $30/120-4$.

Interlaminar transverse shear stress $\tau_{\theta z}$ distributions are reported in figure 4.19. A similar behaviour to the interlaminar transverse normal stress σ_{zz} is encountered within approximately one half-ply thickness from the singular point. However, a refinement of the in-plane mesh close to the hole edge in this case only reduced the influence of the stress singularity but did not completely smoothed out the distribution obtained. This is because a even more refined mesh is required in this area due to the high in-plane gradient encountered. The in-plane mesh could be refined further but attention has to be paid to both the aspect ratio and distortion level that would be achieved in the solid-shell elements close to the singularity point. Interlaminar transverse shear stress τ_{rz} distributions obtained considering different through-the-thickness meshes are shown in figure 4.20. In this case a smooth and accurate distribution is obtained close to the singularity point by introducing two fictitious interfaces equally spaced within each ply. However, a good distribution is also obtained using the mesh $24/30-4$.

In order to understand the mesh-dependent behaviour of the stress singularities encountered close to the hole edge in the previous analysis better, a further analysis was also carried out. A symmetric cross ply $[90^\circ/0^\circ]_s$ laminate similar to the previous one and subjected to an uniaxial tensile load σ_0 was considered. This laminate has been analysed by Hu et al. (1997) using a 3D finite-element (FE) analysis based on a displacement formulation employing a curved isoparametric 20-node element. The total length of the panel is 60 mm, the total width 30 mm, the hole radius R is 2.5 mm, and the ply thickness h is equal to 0.125 mm. The material properties are the same as those used for the $[45^\circ/-45^\circ]_s$ square laminate previously analysed.

Given the symmetry of loading, hole location and lay-up, only one-eighth of the laminate was modeled. The in-plane mesh structure was the same as the one used in the $[45^\circ/-45^\circ]_s$

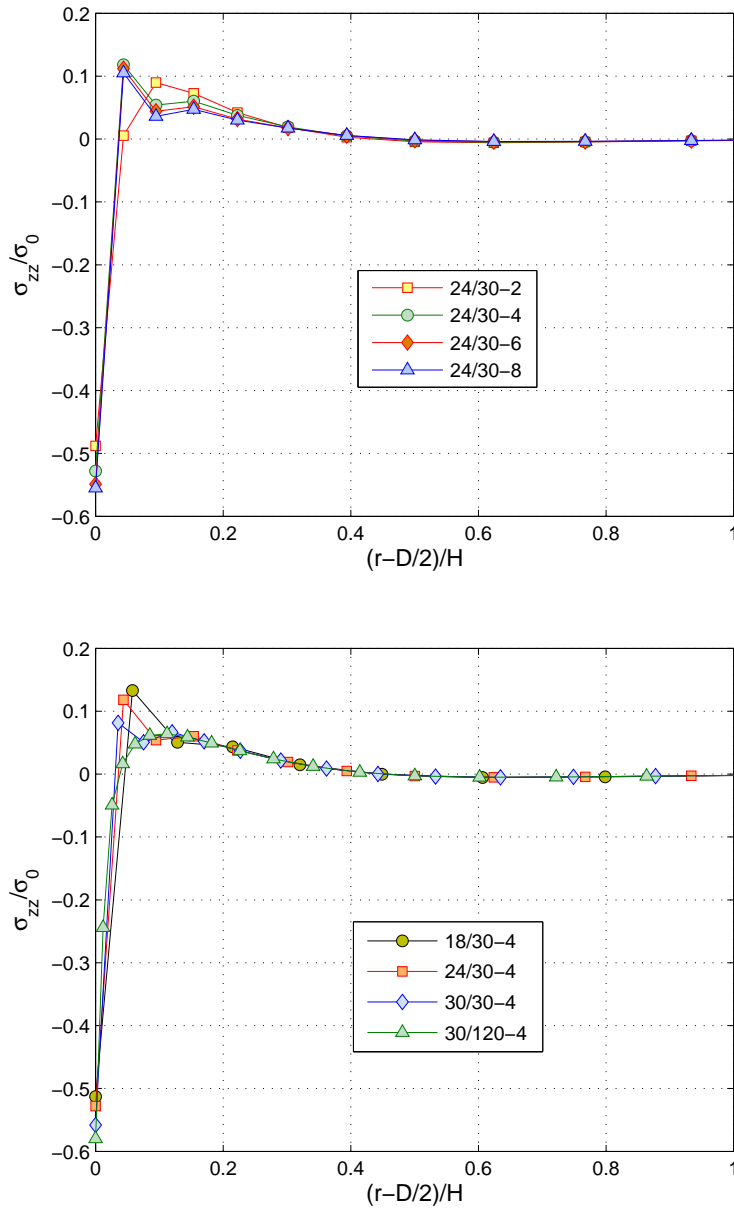


Figure 4.18: Interlaminar transverse normal stress σ_{zz} distributions from the hole edge up to one laminate thickness at the $(45^\circ / -45^\circ)$ interface of a $[45^\circ / -45^\circ]_s$ laminate considering different meshes, $\theta = 90^\circ$.

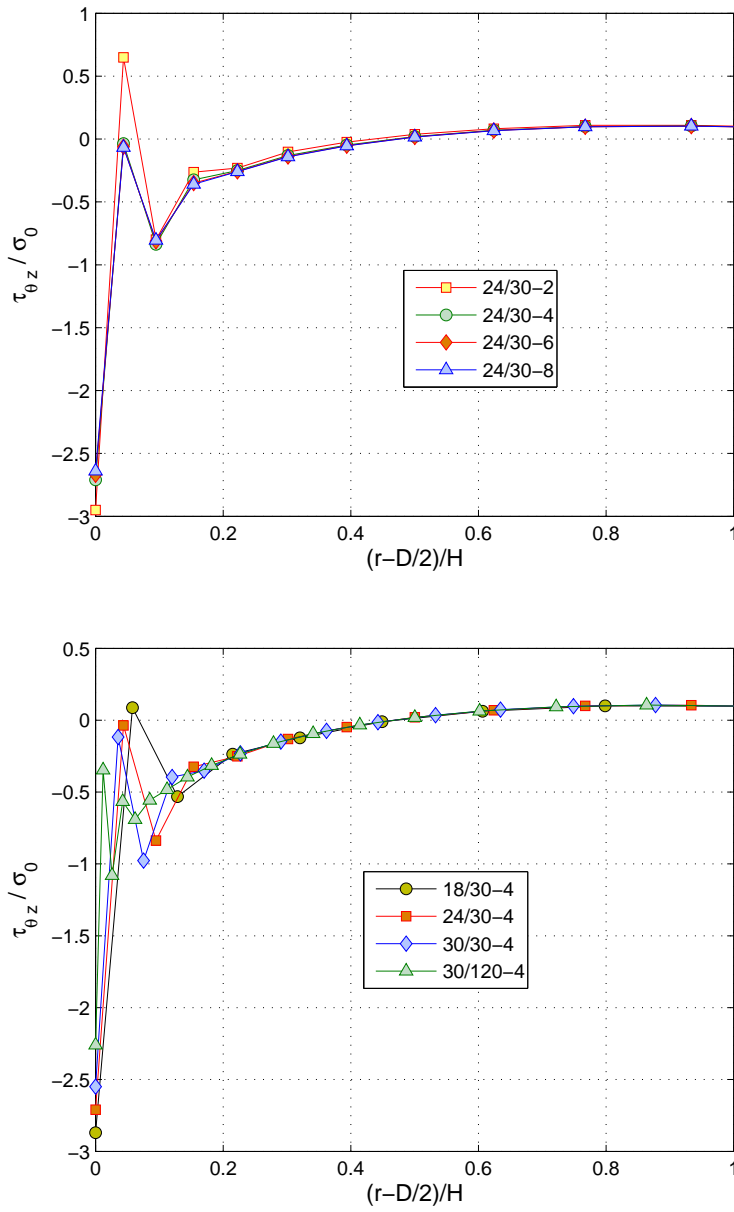


Figure 4.19: Interlaminar transverse shear stress $\tau_{\theta z}$ distributions from the hole edge up to one laminate thickness at the $(45^\circ / -45^\circ)$ interface of a $[45^\circ / -45^\circ]_s$ laminate considering different meshes, $\theta = 90^\circ$.

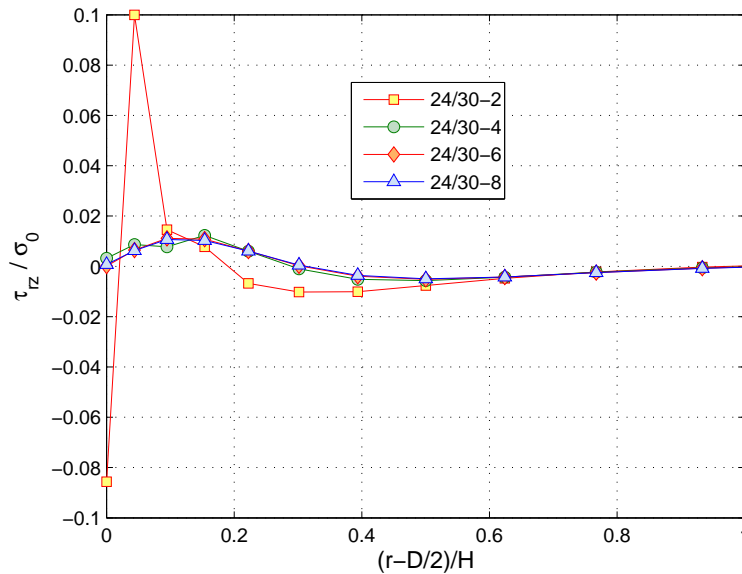


Figure 4.20: Interlaminar transverse shear stress τ_{rz} distributions from the hole edge up to one laminate thickness at the $(45^\circ / -45^\circ)$ interface of a $[45^\circ / -45^\circ]_s$ laminate considering different meshes, $\theta = 90^\circ$.

square laminate previously analysed, with the addition of a coarse part extended in the x direction since the laminate is not anymore square. The through-the-thickness mesh adopted was similar to the one adopted in Hu et al. (1997), see figure 4.21. Thus, the interlaminar stress recovery procedure presented in section 4.5 could only be applied at the $(90^\circ / 0^\circ)$ interface of the laminate. The selected mesh gives 43200 unknowns in the final system of governing equations, with approximately a second order difference between the sizes of the elements along the in-plane directions and the bigger ones in the thickness direction. This mesh was selected in the present analysis because it allows a comparison in point of interest with the distributions reported in Hu et al. (1997), and it is also the minimum required to generate appropriate values of both aspect ratio and distortion level of the elements close to the hole edge. In their work, Hu *et al.* adopt a FE model that consists of 4000 elements, and leading to 56000 unknowns in the final system of governing equations. This means that their procedure employ a percentage increment of 23% in the total number of degrees of freedom compared to the proposed procedure. They provide stress distributions along radial lines away from the hole and around the hole at the $90^\circ / 0^\circ$ interface, obtained by averaging the 90° and 0° ply values at the interface, a customary finite element practice. These distributions are obtained near but not at the hole edge because of the mathematical interlaminar stress singularity. Hu et al. (1997) obtained good agreement with respect to other finite element approaches, then their distributions are taken as benchmark solutions in the present analysis.

Normalized radial distributions of the transverse normal stress σ_{zz} away from the hole at three angular positions $\theta = 0^\circ, 45^\circ, 90^\circ$ obtained using the present procedure are presented

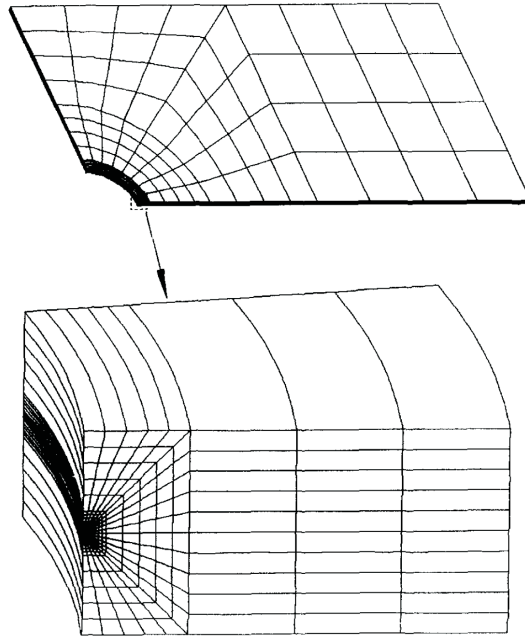
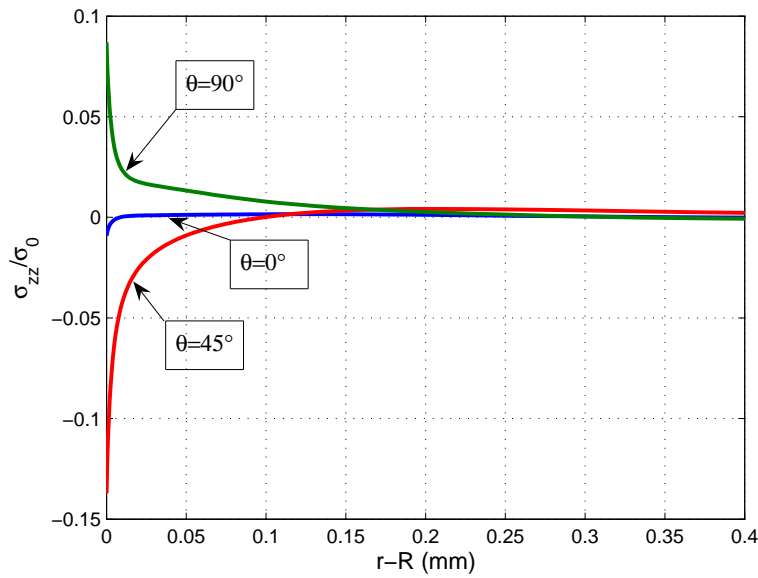


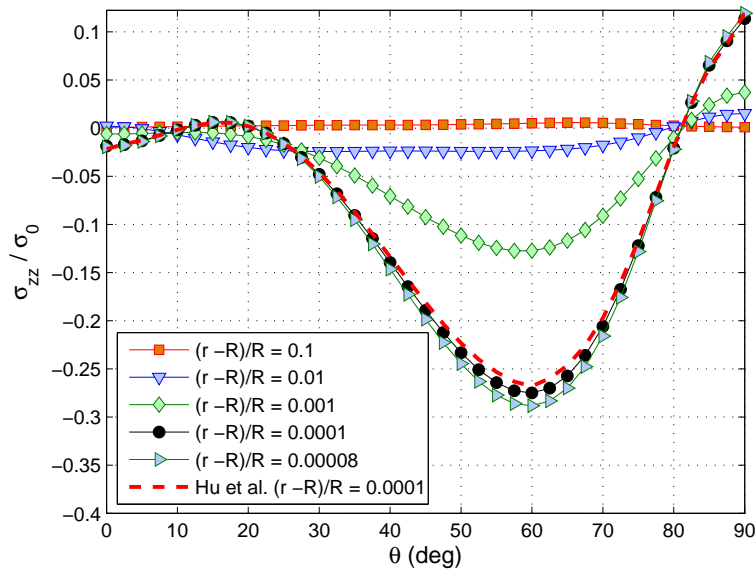
Figure 4.21: Three-dimensional finite element mesh for one-eighth of the laminate (Hu *et al.*, 1997).

in figure 4.22(a). The σ_{zz} distributions have step gradients near the hole edge and approach to zero within a ply thickness from the hole. Smooth distributions were generated close to the hole edge due to the refined mesh adopted in this area. However, a behaviour similar to the one encountered in the square $[45^\circ/-45^\circ]_s$ plate previously analysed was also encountered in this case. These distributions are in excellent agreement with the results (not reported) of Hu *et al.* (1997). Normalized interlaminar normal stress distributions at the $(90^\circ/0^\circ)$ ply interface around the hole at different radial distances from the hole edge are shown in figure 4.22(b). As a mathematical interlaminar stress singularity exists at the free edge between the 90° and 0° plies, the computed stresses are presented near but not at the hole boundary. As the distance from the edge $(r-R)$ increases, the interlaminar stress σ_{zz} rapidly decreases. When $(r-R) = 0.1R$, i.e. two-ply thickness away from the hole boundary, σ_{zz} becomes almost zero. σ_{zz} is compressive for most of the region around the hole with a small tensile region near $\theta = 90^\circ$. The largest compressive σ_{zz} occurs at about 60° from the loading axis. The distribution obtained by Hu *et al.* at $(r-R)/R = 0.0001$ is also plotted for comparison. The maximum difference between the two distributions is less than 3% at the point of maximum value, i.e. $\theta = 60^\circ$.

Normalized radial variations of the transverse shear stress $\tau_{\theta z}$ at $\theta = 10^\circ, 45^\circ, 75^\circ$ are shown in figure 4.23(a). The decay ratio to zero varies with θ ; the maximum decay ratio is at $\theta = 75^\circ$, and, despite the refined mesh adopted, oscillations are still present very close to the hole edge for all the distributions, although more negligible compared to the $[45^\circ/-45^\circ]_s$ plate previously analysed. This means that a further refinement of the mesh



(a) Normalized interlaminar normal stress distributions in the radial directions $\theta = 0^\circ, 45^\circ$ and 90° .



(b) Normalized interlaminar normal-stress distributions around the hole.

Figure 4.22: Normalized interlaminar normal stress distributions σ_{zz}/σ_0 at the $(90^\circ/0^\circ)$ interface of a $[90^\circ/0^\circ]_s$ symmetric laminate.

is required to smooth the distributions out completely. A further refinement of the mesh in the through-the-thickness direction of the laminate, up to the point where the size of the element in the through-the-thickness direction is of the same order as the size in the plane of the laminate, led to smoother distributions having negligible oscillations. However, these distributions are in very good agreement with the ones obtained by Hu *et al.* Normalized circumferential interlaminar shear stress distributions $\tau_{\theta z}$ at various distances, $(r-R)/R$, from the hole boundary are shown in figure 4.23(b). Similar to the normal stress, σ_{zz} , the interlaminar shear stress $\tau_{\theta z}$ decreases as the distance $(r-R)$ from the hole boundary increases and becomes small within two-ply thickness ($0.25mm$) from the hole. The maximum value is obtained at approximately $\theta = 75^\circ$ from the loading axes and is $1.75\sigma_0$ which is about seven times as large as the largest σ_{zz} value computed for the same distance $r/R = 0.000082$ from the hole. This comparison indicates that, in this case, the interlaminar shear stress $\tau_{\theta z}$ is mainly responsible for the onset of delamination in the laminate. The distribution obtained by Hu *et al.* at $(r-R)/R = 0.0001$ is also plotted for comparison. The maximum difference between the two distributions is within 4% at the point of maximum value, i.e. $\theta = 75^\circ$. Distributions concerning the shear stress component τ_{rz} are not reported since τ_{rz} is very small compared to $\tau_{\theta z}$ and thus can be neglected. The minimum distance $r/R = 0.000082$ from the hole to report the circumferential interlaminar stress distributions was selected based on the consideration that stress oscillations begin after the considered point and a certain error in the distributions can be introduced. To verify if these oscillations effect the prediction of delamination initiation, a stress failure criteria needs to be selected.

From the literature (Brewer and Lagace, 1988) it can be seen that the approach for predicting failure in such laminates has been that of averaging the interlaminar stresses over a distance from the hole edge, suggesting that the exact values of the stresses at the free edge are not too important. Since it is assumed that the delamination initiation is mainly attributed to interlaminar stress effects, the Chang and Springer (1986) criterion was assumed as a failure stress criterion, in which only the interaction between the three out-of-plane stress components is considered. Moreover, since the interlaminar shear stress τ_{rz} can be neglected compared to $\tau_{\theta z}$, the Chang-Springer criterion in a cylindrical coordinate system can be simplified as:

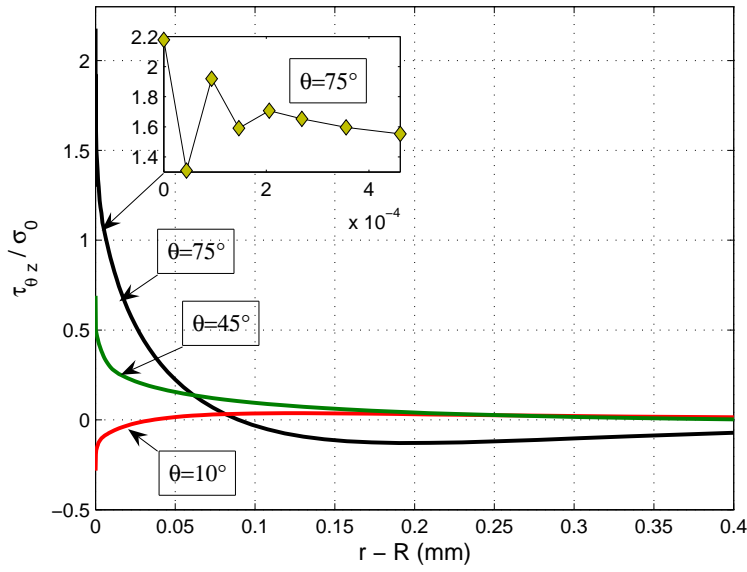
$$\left(\frac{\sigma_{zz}}{Z}\right)^2 + \left(\frac{\tau_{\theta z}}{S}\right)^2 = e^2 \begin{cases} e < 1 \text{ no failure} \\ e > 1 \text{ failure} \end{cases} \quad (4.70)$$

where Z is the interlaminar normal strength and S is the interlaminar shear strength. For positive interlaminar normal stress σ_z the uniaxial tensile strength Z_t should be used while for negative σ_z the compressive strength Z_c should be employed.

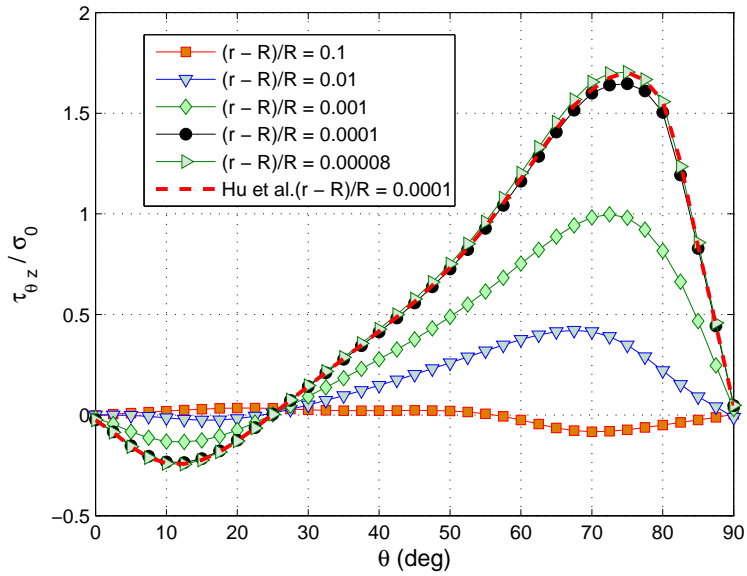
The average stress failure criteria assumes that delamination initiates when the stresses at a characteristic distance a_0 from the discontinuity meet the failure criteria (4.70). The characteristic distance a_0 is experimentally determined and can vary with lay-up and hole size. The average of a stress component is defined as:

$$\bar{\sigma}_{ij} = \frac{1}{a_0} \int_R^{R+a_0} \sigma_{ij} dr. \quad (4.71)$$

The following strength properties, $Z_t = 50.6MPa$, $Z_c = 200MPa$ and $S = 103MPa$, were



(a) Normalized interlaminar shear stress distributions at different angular positions.



(b) Normalized interlaminar shear stress distributions around the hole.

Figure 4.23: Normalized interlaminar shear stress distributions $\tau_{\theta z} / \sigma_0$ at the $(90^\circ / 0^\circ)$ interface of a $[90^\circ / 0^\circ]_s$ symmetric laminate.

used for the carbon fiber-epoxy laminates. e -index distributions obtained around the hole assuming different values of a_0 are shown in figure 4.24. The maximum value of e varies with a_0 and occurs in the region $\theta = 67.5^\circ - 75^\circ$ to the loading direction, indicating that these are the critical locations for delamination growth. e -indexes distributions obtained by Hu *et al.* are also reported for comparison. Slightly different values of the failure index e are obtained assuming $a_0 = 0.0005$ between 70° and 80° , but the percentage difference is always within 3%. Then, the oscillations of the interlaminar shear stress $\tau_{\theta z}$ close to the hole edge do not seem to influence the failure index distribution. A refinement of the global mesh produces negligible variations on the results, indicating that convergence has already been reached. Convergence of every single transverse stress component was also checked and achieved. Then, the proposed procedure seems to be adequate to be combined with failure stress criteria commonly used in the open literature to predict onset of delamination in presence of curved free edges and stress concentrations (Brewer and Lagace, 1988; Coutellier *et al.*, 2006; O'Brien, 1982). Additional analyses should be done in the future to validate the proposed procedure for laminated composite plates with open hole subjected to different loading cases, and employing different failure criteria available in the open literature.

The above analysis does not take into account matrix cracking, which may influence the delamination onset load, and does not attempt to relate the adjustable characteristic length used in the quadratic failure criterion to any micromechanical feature. Moreover, it is worth to mention that average stress failure criteria are appropriate for predicting onset of delamination, but they are not suitable for failure analysis of composites for which fracture mechanics based methods are required such as the one proposed in Kashtalyan (2001, 2002).

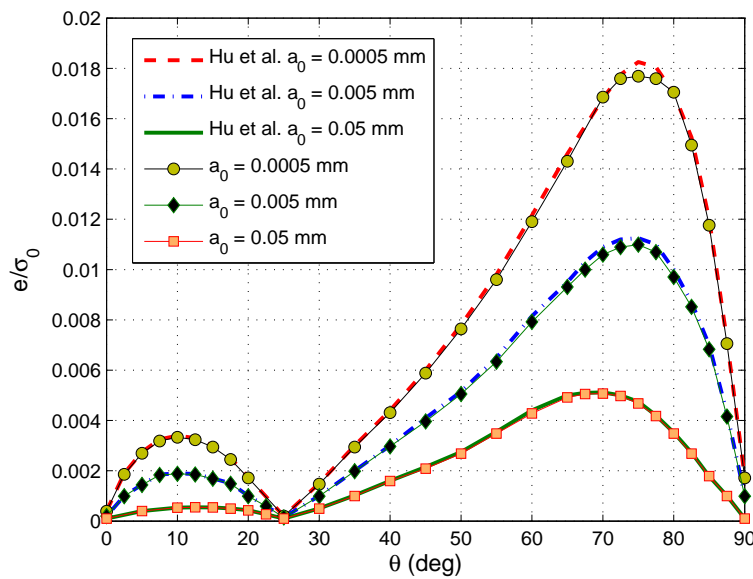


Figure 4.24: e -index distributions at the $(90^\circ/0^\circ)$ interface of a $[90^\circ/0^\circ]_s$ laminate obtained near the hole edge, and determined using an average stress criterion.

4.7 Conclusions

An efficient three-dimensional finite element procedure conceived to be suitable to perform reliable future stress analyses of variable stiffness panels was presented in this chapter. Although the finite element model was generated using a simple low-order solid-shell element, the procedure was conceived to be applicable to general 3D finite element formulations. In order to broaden the range of applications of the present procedure, the Finite Element Tearing and Interconnecting method, conceived for parallel computing, was employed to solve the system of governing equations obtained from the finite element model. A post-processing procedure for appropriate recovery of stress distributions was also developed. In particular, an interlaminar stress recovery procedure conceived for 3D finite element formulations was proposed. The complete stress states were obtained by employing a variational consistent recovery procedures for the recovery of the in-plane stress distributions. The proposed stress recovery procedure can be applied independently at every interlaminar surface of interest. It is based on equilibrium considerations, and interlaminar stress values are retrieved directly at the element's nodes. Thus, stress continuity at the inter-element boundary is automatically satisfied. Moreover, the accuracy of the recovered interlaminar stresses is neither dependent on the knowledge of superconvergent point nor it is sensitive to the stress recover method employed to obtain element stress distributions, as opposed to commonly used stress recovery procedures.

The accuracy of the present procedure was validated by analysing moderately-thick/thin composite plates of various geometries. The results were compared with available exact and finite element solutions. These comparisons indicated that excellent agreement was obtained with exact solutions, and that convergence was reached using considerably fewer degrees of freedom compared to other finite elements procedures, thus making the procedure more suitable for design purposes. The proposed procedure was able to generate a minimum percentage reduction of 72% in the total number of degrees of freedom required to achieve accurate interlaminar stress distributions compared to other finite element formulations. In particular, the procedure was also as much accurate as assumed stress methods without the need to include stress degrees of freedoms in the solution process. It was also shown that smooth distributions are easily generated without the need to employ smoothing techniques, as usually required instead using customary stress recovery procedures. Thus, the proposed procedure was able to overcome the problem of severe oscillations of stress distributions, especially for thin laminates, usually encountered using customary procedures.

Special emphasis was placed on the problem of a loaded plate with an open circular hole. Despite the presence of oscillations encountered close to the hole edge in the interlaminar stress distributions, the present procedure could be used to produce convergent averaged interlaminar stresses over a distance from the hole edge. Then, the procedure could be effectively combined with an average failure stress criterion available in the open literature to predict delamination initiation in presence of curved free edges and stress concentrations. In this case, the minimum percentage reduction in the total number of degrees of freedom required to achieve accurate interlaminar stress distributions was reduced to around 23% compared to other finite element formulations. However, this analysis did not look at matrix cracking, which may influence the delamination onset load, and no attempt was made to relate the adjustable characteristic length used in the quadratic failure criterion to any micromechanical feature.

Chapter 5

Interlaminar Stress Analyses of Multilayered Laminates having Non-Conforming Meshes between the Plies

5.1 Introduction

An efficient three-dimensional finite element procedure conceived to be suitable to perform reliable future stress analyses of variable stiffness panels was presented in the previous chapter. Keeping in mind that the aim of the present thesis is to develop a procedure that is suitable for appropriate analysis of variable stiffness panels having various geometries, the applicability of the method also had to be validated for general 3-D shell type structures. Moreover, by restricting attention to variable stiffness panels with tow-drops, failure initiation may be primarily due to delamination at the tow-drop resin-rich areas, meaning that this locations need to be modeled accurately.

The triangular shape of the tow-drop locations, known from the procedure developed in Blom et al. (2009), can be modeled properly using triangular prism elements. Assuming that brick elements are the best option for modeling the courses of a variable stiffness panel, the procedure presented in the previous chapter needed to be tested while considering types of mesh in the plies obtained as a combination of both brick and triangular prism elements. The fact that when using the proposed procedure every ply is considered to be an independent subdomain gives the user more freedom in their selection of the proper mesh to be adopted in each ply. This means, for instance, that the final mesh of the complete laminate for a variable stiffness panel may be obtainable by simulating the procedure followed during the manufacturing process by the tow-placement machine's head, as explained in detail in section 1.6. However, the approach of having an independent mesh in every ply leads inevitably to have non conforming meshes between the subdomains, i.e. the plies. A schematic example of non-conforming meshes between the courses of two different plies

of a variable stiffness panel with tow-drops is shown in figure 5.1. For the sake of clarity, a mesh composed of triangular prism elements is not reported in the tow-drops areas. Non-matching node locations at the interface of two adjacent plies might lead to interfacial data distributions, i.e. connecting force distributions, presenting oscillatory behaviours, and thus providing inaccurate nodal input for the developed post-processing procedure. Then, an averaging technique able to smooth out the obtained distributions needed to be provided.

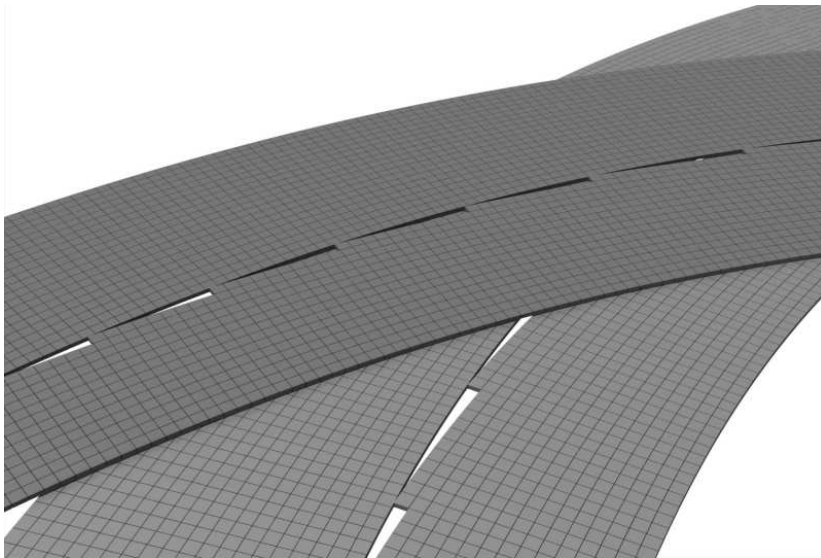


Figure 5.1: Schematic example of non-conforming meshes between the courses of two different plies of a variable stiffness panel with tow-drops.

In this chapter, the proposed post-processing procedure is combined with the commercial finite element software ABAQUS 6.8TM with the aim of broadening the applicability of the method to general 3-D shell type structures. Moreover, the user would be also enabled to use tools and features already developed within ABAQUS framework. Non conforming meshes between the layers, obtained as a combination of both brick elements and triangular prism elements, are also considered. Benchmark problems concerning conventional straight fibers multilayered composite plates and shell structures are analysed, and comparisons with ABAQUS' built-in recovery procedures and available solutions in the literature are also reported.

5.2 Interlaminar Stress Recovery Procedure

The post-processing stress recovery technique developed in the previous chapter was combined with the commercial finite element software ABAQUS 6.8TM. A flow chart of the procedure is given in figure 5.2. A summary of the different steps of the flow chart is provided below.

The first step is to implement a discrete model in ABAQUS/Standard. Within multilayered laminates, each ply is modelled as a separate body using linear brick elements and/or linear triangular prism elements, and the interlaminar boundary is treated as a contact surface. The interlaminar boundary is modelled as a contact zone because the connecting forces required by the developed interlaminar stress recovery procedure, see section 4.5, can only be obtained from a contact formulation, and not for instance, using a tie constraints formulation, which ties two surfaces together for the duration of the simulation, and the nodes in the pair are constrained to have the same motion. Once the analysis is performed, the interlaminar contact forces are retrievable as part of ABAQUS's nodal variables output, as opposed to the connecting tie-constrain forces that are not retrievable as part of ABAQUS 6.8TM's nodal variables output. Abaqus/Standard offers several contact formulations (ABAQUS, 2005). Discretization of the contact pair is of primary importance once the master surface and the slave surface are assigned in the contact pair, because conditional constraints at various locations on each surface are applied to simulate contact conditions. A surface-to-surface contact discretization is used because the contact conditions are enforced in an average sense over the slave surface, rather than at discrete points, such as at slave nodes, as in the case of node-to-surface discretization. This gives a more accurate contact pressure accuracy. The mechanical contact properties are defined using a tied contact formulation, i.e. tied contact. The tied contact formulation ties two surfaces forming a contact pair together for the duration of a simulation, and constrains only translational degrees of freedom in mechanical simulations. This mechanical constraint enforcement is obtained using a direct Lagrange multiplier method.

The second step is the recovery, from the ABAQUS's output database file, of the input variables required by the variational consistent stress recovery procedure for the in-plane stresses presented in section 4.4, and the interlaminar stress recovery procedure presented in section 4.5, i.e. nodal contact loads, element connectivity, nodal coordinates, and nodal displacements. These parameters are retrieved using the Abaqus Scripting Interface, an application programming interface to the models and data used by ABAQUS, based on the Python object-oriented programming language ABAQUS (2005).

In the third step, using the retrieved data, interlaminar stresses are recovered from the contact loads that satisfy force equilibrium at the interface between two adjacent plies. In-plane stress distributions are retrieved using the developed variational stress recovery procedure. The complete procedure is implemented within the MATLAB framework.

In the fourth step, once the interlaminar and in-plane stress fields are obtained, the data are sent back to the Output Database File of ABAQUS using the Abaqus Scripting Interface. As a final step, the retrieved stress distributions are visualized in the updated Output Database File.

To speed up the complete process, the procedure can be completely implemented within ABAQUS environment using the Abaqus Scripting Interface. This can be achieved using NumPy, a package of numerical extensions for Python that introduces a multidimensional array type and a rich set of matrix operations and mathematical functions. If the user wishes to take advantage of some MATLAB's additional functions, i.e. plotting interface, the PyMat package can be incorporated. The PyMat module acts as an interface between NumPy arrays in Python and a MATLAB engine session, allowing arrays to be passed back and forth, and arbitrary commands to be executed in the MATLAB workspace (Python, 2006).

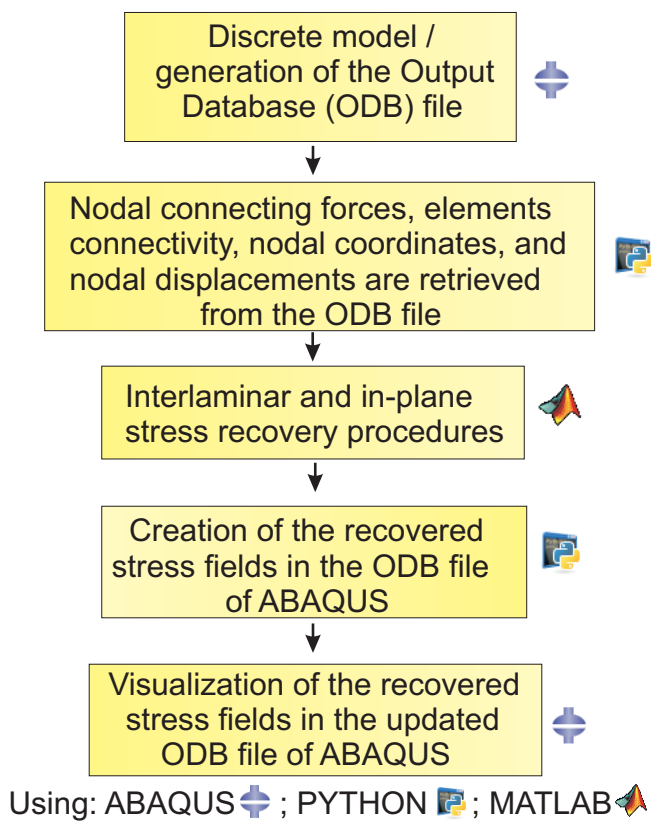


Figure 5.2: Flow chart of the complete process.

5.3 Numerical Results

5.3.1 Simply Supported Plates Subjected to Bisinusoidal Pressure Load

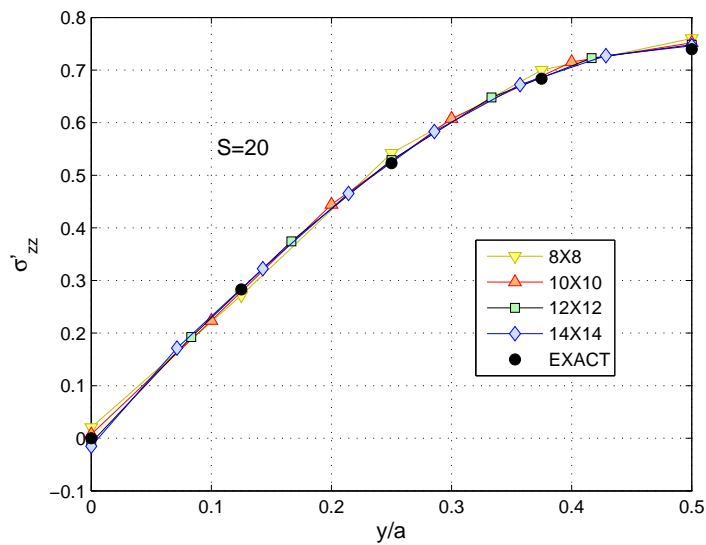
The present procedure was validated using the benchmark problem analysed by Pagano (Pagano, 1970), where three dimensional exact elasticity solutions of idealised simply supported cross-ply $[0^\circ/90^\circ/0^\circ]$ square laminates under bisinusoidally distributed pressure load of intensity p_z are provided. This problem was also analysed in section 4.6.1 using the proposed procedure developed completely within the MATLAB framework. The length and thickness of the plate is denoted by a and H respectively. The laminate is made of material plies that are idealized to be homogeneous, elastic and orthotropic. The following material properties are used: $E_{11} = 25 \text{ GPa}$, $E_{22} = E_{33} = 1 \text{ GPa}$, $G_{12} = G_{13} = 0.5 \text{ GPa}$, $G_{23} = 0.2 \text{ GPa}$, and $\nu_{12} = \nu_{13} = \nu_{23} = 0.25$. Subscripts 1,2 and 3 denote the fibre, transverse and thickness directions, respectively. The rectangular Cartesian coordinate system used is the same assumed in section 4.6.1, see figure 4.4. Stresses are normalized according to the following formulae,

$$\begin{aligned} (\tau'_{xz}, \tau'_{yz}) &= \frac{1}{p_z S} (\tau_{xz}, \tau_{yz}), \quad \sigma'_{zz} = \frac{1}{p_z} \sigma_{zz}, \\ (\sigma'_{xx}, \sigma'_{yy}, \tau'_{xy}) &= \frac{1}{p_z S^2} (\sigma_{xx}, \sigma_{yy}, \tau_{xy}) \end{aligned}$$

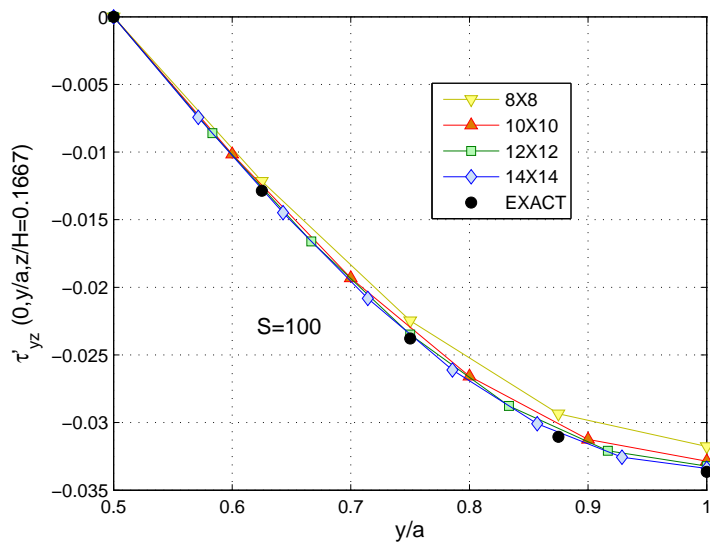
where the S is the laminate length to thickness ratio, $S = a/H$.

The discrete model is obtained using an 8-node linear brick incompatible modes element, i.e. (C3D8I). Within the built-in elements of ABAQUS this element was chosen because it possesses good coarse mesh and distortion insensitivity properties for a large range of length to thickness ratios of the laminate. Moreover, this element has very similar properties to the solid-shell element developed in section 6.1. This is because the class of mixed assumed strain methods encompass, as a particular case, the classical method of incompatible modes. Unless differently stated, the in-plane mesh consists of 12×12 elements for each ply. Conforming meshes are initially considered. The minimum required number of elements in the thickness direction of the laminate is three. While this is sufficient for accurate interlaminar stresses, it does not allow detailed evaluation of their through-the-thickness variation, as shown in section 4.6.1. The values of transverse stresses in the middle of every layer are also reported in the case under consideration and, as a consequence, three more mathematical interfaces are required in these locations to give a total number of six elements through-the-thickness of the laminate.

Laminates of length to thickness ratios $S = 20, 50, 100$ were analysed and the results calculated at several points of interest are reported in table 5.1. Compared to Pagano's exact solutions, excellent agreement was obtained for all the considered cases. The percentage error of the recovered stress values with respect to the exact solution is always less than 1.3%. Convergence analyses of the interlaminar stresses σ'_{zz} and τ'_{yz} at the $[0^\circ/90^\circ]$ interface obtained considering laminates of length to thickness ratio $S = 20$ and 100 are shown in figure 5.3. Excellent agreement with Pagano's exact solution, smoothness and fast convergence were obtained. A laminate of length to thickness ratio $S = 50$ was also considered to demonstrate the accuracy of the proposed procedure for analyzing moderately thick lam-



(a) Convergence of the interlaminar normal stress σ'_{zz} with different in-plane meshes; $S = 20$.



(b) Convergence of the interlaminar shear stress τ'_{yz} with different in-plane meshes, $S = 100$.

Figure 5.3: Convergence analyses of the recovered interlaminar transverse stresses at the $[0^\circ/90^\circ]$ interface of a $[0^\circ/90^\circ/0^\circ]$ laminate obtained considering different length to thickness ratio S .

Table 5.1: Recovered stress fields considering different values of length to thickness ratio S .

S		$\tau'_{xz}(0, \frac{a}{2}, 0)$	$\tau'_{yz}(\frac{a}{2}, 0, 0)$	$\sigma'_{zz}(\frac{a}{2}, \frac{a}{2}, H/6)$
20	EXACT	0.3846	0.0938	0.7398
	EQUILIBRIUM	0.3844	0.0937	0.7488
50	EXACT	0.3934	0.0842	0.7406
	EQUILIBRIUM	0.3930	0.0841	0.7491
100	EXACT	0.3946	0.0828	0.7407
	EQUILIBRIUM	0.3931	0.0822	0.7481

inates. Through-the-thickness distributions of the interlaminar transverse shear and normal stresses obtained using the proposed method, labelled as EQUILIBRIUM, were compared with Pagano's exact solution at points of major interest, see respectively figures 5.4 and 5.5. Excellent agreement and fast convergence were achieved in all the distributions. Through-the-thickness distributions obtained using different ABAQUS's built-in solid elements and associate post-processing procedures are also reported for comparison. The adopted elements were respectively, the 8-node linear brick incompatible modes $C3D8I$, that is the same adopted in the proposed procedure, the 20-node quadratic brick $C3D20R$, and the linear 8-node $C3D8R$. Stresses are recovered at integration points using constructive models derived from either variational principles or other energy laws in the post-processing procedures of ABAQUS associated with each element (ABAQUS, 2005). Then, stresses evaluated at the integration points are extrapolated at the element's nodes using the shape functions. Neither the linear $C3D8R$ nor the $C3D8I$ elements provided single valued results at the interfaces, meaning that a through-the-thickness refinement of the mesh was required. It is worth pointing out that the proposed procedure was able to improve considerably the accuracy of the response obtained using the built-in $C3D8I$ element compared to ABAQUS's built in stress recovery procedure. The distributions obtained using the $C3D8I$ element also explains the reason why the variational consistent stress recovery procedure developed in section 4.4 was only adopted for the recovery of the in-plane stress distributions. This is because the recovery of the transverse stress distributions in low-order formulations based on mixed assumed strain methods obtained using customary procedures, i.e. constitutive relations or variational procedures, can lead to inaccurate distributions, as shown clearly in figure 5.5, i.e. ABAQUS / $C3D8I$. It is also worth to highlight that the stress recovery procedure associated with the 8-node linear brick incompatible modes $C3D8I$ element in the ABAQUS framework is the approach successfully used by Simo and Armero (1992) in which an enhanced displacement gradient is assumed, as opposed to the variational procedure adopted in the present thesis which is based on the enhanced assumed Green-Lagrangian strains. This means that for linear analyses, such as the present one, both procedures are exactly equivalent. Since in this chapter only linear analyses are considered, henceforth the in-plane stress distributions are retrieved in the proposed procedure using the built-in post-processing procedure of ABAQUS associated with the adopted $C3D8I$ element to reduce the computational time. The quadratic $C3D20R$ element did not produce an accurate estimation of the transverse shear stress τ'_{yz} . The percentage error at the point of maximum values, i.e. $z = 0$, compared to the exact solution was 9.46%. An appropriate

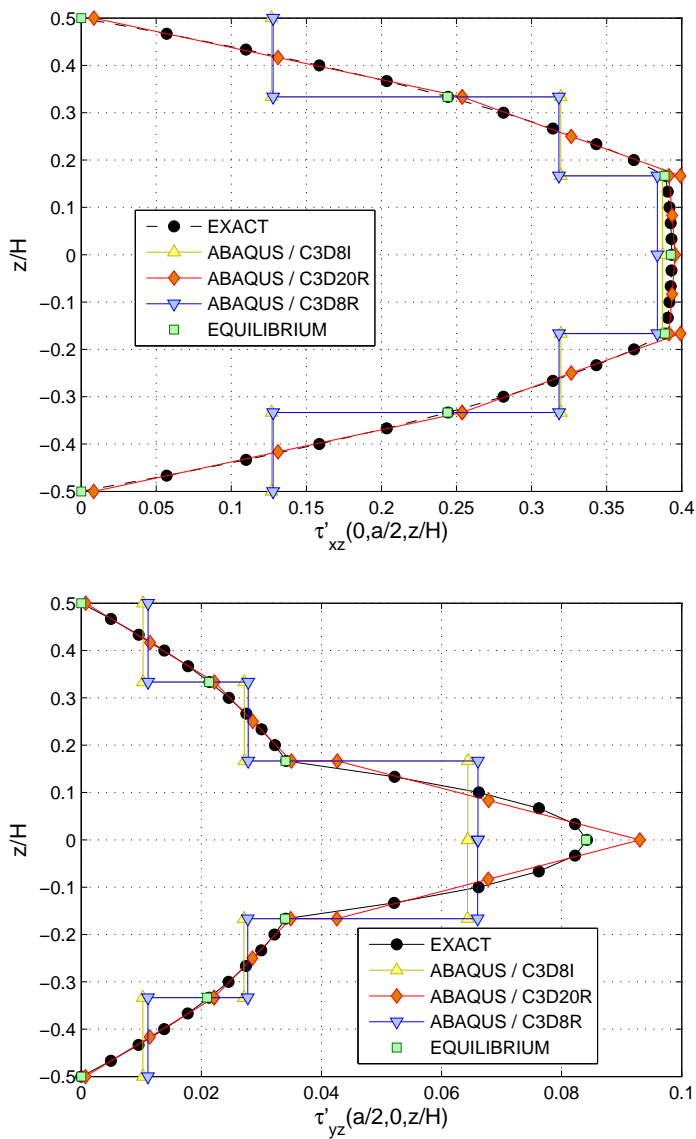


Figure 5.4: Comparisons of the through-the-thickness distributions between the interlaminar shear stresses obtained using the proposed procedure, using different ABAQUS's built-in elements and associate post-processing procedures, and Pagano's exact solution, $S = 50$.

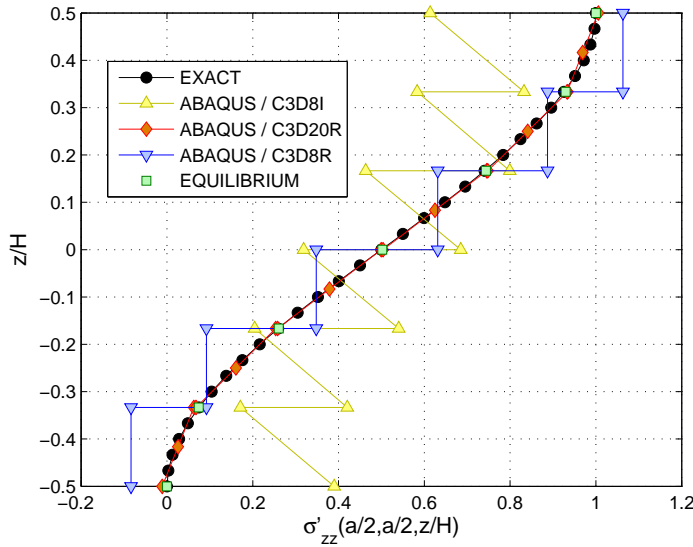


Figure 5.5: Comparisons of the through-the-thickness distributions between the interlaminar normal stress σ'_{zz} obtained using the proposed procedure, using different ABAQUS's built-in elements and associate post-processing procedures, and Pagano's exact solution, $S = 50$.

response was obtained instead for the interlaminar shear τ'_{xz} and normal σ'_{zz} stresses. Identical in plane stress distributions to the ones shown in section where obtained. Hence, these distributions are not shown in the present analysis.

The aforementioned results were obtained by adopting one additional mathematical interface in the middle of every ply to also provide intralaminar stress values at these points. However, these mathematical interfaces were not required to achieve convergence in the retrieved interlaminar stress distributions, as already shown in section 4.6.1. The proposed procedure uses a model with 4050 degrees of freedom and attains converged results, whereas the ABAQUS model, using quadratic elements, has 17595 degrees of freedom but still obtains inaccurate interlaminar stress distributions. This means that the proposed procedure was able to generate a percentage reduction of 77% in the total number of degrees of freedom required to achieve accurate interlaminar stress distributions compared to ABAQUS's quadratic formulation that still fails to converge.

Analysis considering Non-Conforming Meshes between the Plies

Non-conforming meshes were also considered for a $[0^\circ/90^\circ/0^\circ]$ square laminate of length to thickness ratio $S = 50$. One fictitious interface was considered in the middle of every ply, thus giving a total number of six plies. An example of the meshes adopted in two adjacent plies is shown in figure 5.6. Assuming that the count of the layers starts from the bottom of the laminate, a regular mesh composed of rectangular C3D8I elements is adopted in layers 2, 4 and 6. A mesh obtained as a combination of linear brick C3D8I elements

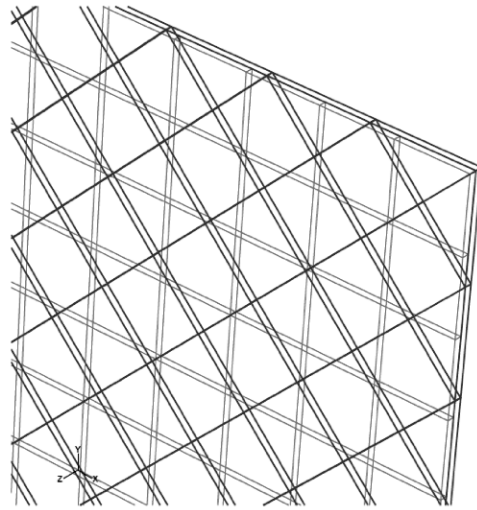


Figure 5.6: An example of non-conforming meshes adopted in two adjacent plies.

and linear triangular prism *C3D6* elements is assumed in layers 1, 3 and 5. This kind of mesh was selected to simulate the tow-cut in the areas close to the sides and corners of a variable stiffness panel, which makes triangular prism elements suitable for a reliable finite element model. Moreover, the adopted mesh schematically represents, without considering tow-drops or tow-overlaps regions, possible courses in a variable stiffness ply oriented at 90, or 0 = , i.e. layers 2, 4 and 6, in contact with courses oriented at 45, i.e. layers 1, 3 and 5. However, in layers 1, 3 and 5, although the courses can be thought to be oriented at 45 with respect to layers 2, 4 and 6, the material properties considered were still the ones with fiber orientation of 90 to compared the results with the available exact solutions. This does not affect the reliability of the approach since the only differences with respect to future variable stiffness panels analyses are the material properties at the integration points. In a real variable stiffness panel, plies having the same orientation will also have conforming meshes at their interface. However, to validate the method, stress distributions will be shown at $z = 0$, that is the location where maximum values of the interlaminar shear stresses are achieved. In order to show that the proposed procedure works properly at the location of major interest, i.e. $z = 0$, non-conforming meshes were adopted in layer 3 and 4, regardless of the material orientation. Resin-rich areas in tow-steered laminates have to be modeled using triangular shape elements, as explained in section 1.6. The selected meshes also help us to understand if ABAQUS's triangular prism *C3D6* element is suitable for being combined with ABAQUS's linear brick *C3D8I* element, in particular close to areas where the boundary conditions are applied.

Distribution concerning the transverse shear stress τ'_{xz} and the transverse normal stress σ'_{zz} obtained at $z = 0$ and $x/a = 0.5$ are shown in figure 5.7. Different meshes are considered in the plots: e.g the label *ENC - 20/28* denotes non conforming meshes between the plies, where 20 indicates the number of triangular prism *C3D6* elements adopted in each side of

the layers 1,3 and 5, and 28 indicates the number of linear brick *C3D8I* elements adopted in each side of the layers 2,4 and 6. The label *EC-40X40* denotes conforming meshes between the plies where 40 linear brick *C3D8I* elements are assumed on each side of all the six plies. In all the contact pairs it is assumed that the master surface adopts the mesh with all brick elements. Then, layers 2, 4 and 6 have to adopt a coarser mesh compared to the other layers for accurate contact simulations (ABAQUS, 2005).

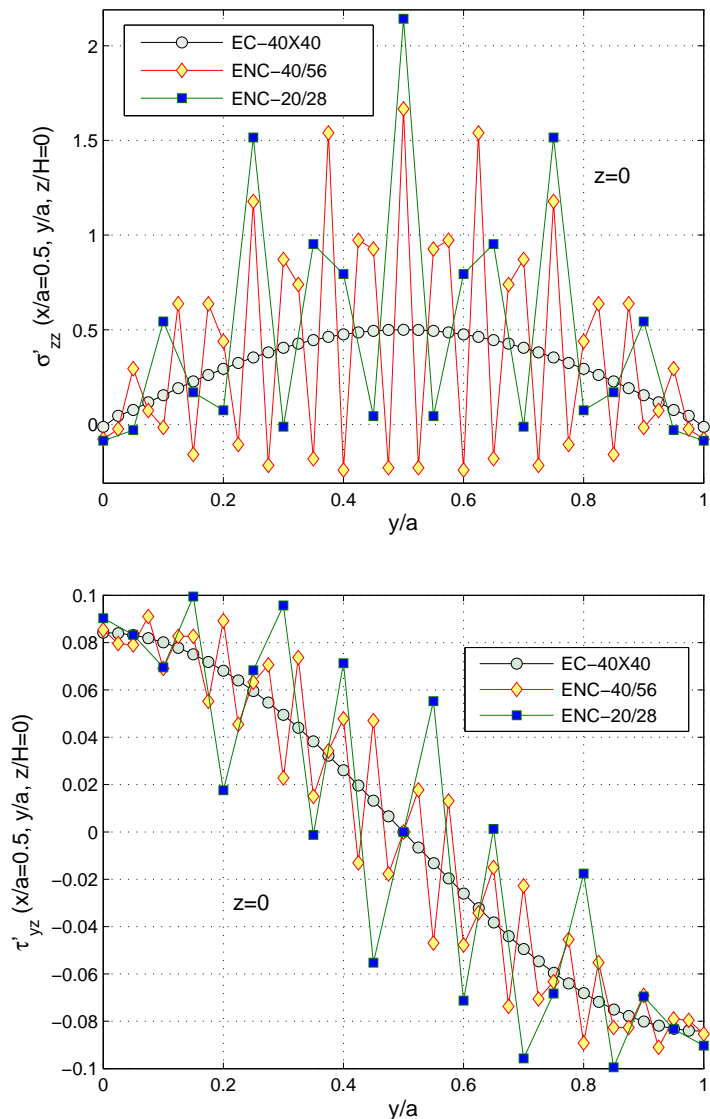


Figure 5.7: Transverse stress distributions obtained considering both conforming and non-conforming meshes between the plies.

From the plots reported in figure 5.7 it is clear that oscillatory behaviours were encountered in the retrieved transverse stress distributions when non-conforming meshes between the plies were adopted, thus leading to inaccurate results. However, these oscillations seem to have the same trends as the distributions obtained using the conforming meshes, used as reference solutions. Then, an averaging technique was developed to smooth out these distributions. The developed technique consists of averaging the stress values obtained in each node with the stress values obtained in the nodes of the surrounding elements sharing the node under consideration. The stress averaging is described in the following paragraph.

Consider a corner section of the layer where a mix of rectangular and triangular elements are used, see fig. 5.8. By assuming that f_9 is the nodal component of the stress that has to be averaged, the averaged stress component f_{9avg} is obtained as follows:

$$f_{9avg} = \frac{f_2 A_2 w_t + f_8 A_2 w_t + f_9 A_2 w_t + f_2 A_3 w_t + f_4 A_3 w_t + f_9 A_3 w_t + f_4 A_5 w_s + f_5 A_5 w_s}{A_{tot}} + \frac{f_6 A_5 w_s + f_9 A_5 w_s + f_6 A_6 w_s + f_7 A_6 w_s + f_8 A_6 w_s + f_9 A_6 w_s}{A_{tot}}, \tag{5.1}$$

where w_t is the weight of the nodal components on the triangular element areas, equal to $\frac{1}{3}$, w_s is the weight of the nodal components on the square element areas, obtained as $\int_{A_i} N_i dA_i$ where N_i is the isoparametric shape function associated with the node under consideration and A_i is the element area, and A_{tot} is the total area of the elements surrounding the node in which the averaging procedure is applied. This procedure can be iteratively used until the level that proper distributions are achieved.

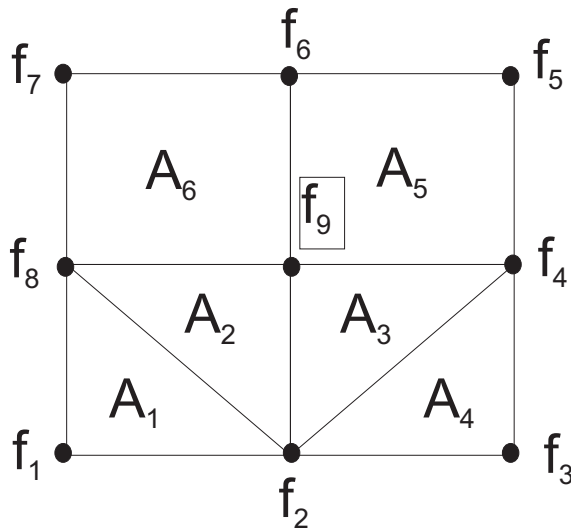


Figure 5.8: Convention used in the adopted averaging technique.

The validity of the developed averaging procedure is shown in figure 5.9, where the distributions shown in figure 5.7 are now averaged using the proposed technique. These interlaminar transverse stress distributions were obtained using a linear interpolation for the trac-

tion distribution over the surface under consideration for both triangular and quad elements. This was achieved by adopting the classical linear isoparametric shape functions assumed for the displacement field on the triangular areas and quadrilateral areas. In these plots the label $ENC-20/28-nl$ still denotes the case in which non-conforming meshes between the plies are adopted, with the additional parameter nl denoting the number of iterations performed using the proposed averaging technique. The proposed averaging technique was able to generate smooth distributions in excellent agreement with the ones obtained in the case of conforming meshes, i.e. $EC-40X40$ within three/four iterations, depending on the mesh assumed. For instance, the percentage difference at points of major interest with respect to the distributions $EC-40X40$ obtained using the mesh $ENC-20/28-n3$ or $ENC-20/24-n4$ was always within 3%. The percentage difference was reduced when refined meshes were considered, and dropped to less than 0.5% using the mesh $ENC-40/56-n3$. However, much more refined meshes had to be adopted compared to conforming meshes between the plies, and inaccurate stress values were generated in the case of high gradients close to the boundaries of the laminate due to the iterations performed, as shown in figure 5.9₁. An improvement close to the boundary was obtained using the refined mesh $ENC-40/56-n3$ compared to both the meshes $ENC-20/28-n3$ and $ENC-20/24-n4$, but the percentage difference at $y/a = 0$ was still not negligible. Then, more refined meshes were required to obtain appropriate values of the transverse normal stress σ'_{zz} also close to the boundaries of the laminate.

Similar trends in the transverse stress distributions were obtained using the ABAQUS' built-in variational recovery post-processing procedure, combined with the developed averaging technique, as shown in figure 5.10, i.e. $ENC-40/56-n3-ABAQUS$. Although the trends of these distributions were similar to the distributions reported in figure 5.9, a refinement of the mesh was still required to achieve convergence of the retrieved transverse stress values. These distributions were not as much accurate as the ones obtained using the proposed interlaminar stress recovery procedure, and this is because stress recovery procedures adopting extrapolation techniques from superconvergent points required much more refined meshes through-the-thickness of the laminate to provide accurate interlaminar stresses (Dakshina Moorthy and Reddy, 1999).

The in-plane stress σ'_{yy} distribution obtained at the ($0^\circ/90^\circ$) interface, i.e. $z/H = 0.1666$, using the proposed procedure combined with the developed averaging technique is shown in figure 5.11. In this case a good distribution was obtained using the mesh $ENC-20/28-n0$ that does not employ the developed averaging technique. The percentage difference with respect to $EC-40X40$ at points of major interest was always less than 2%.

5.3.2 Varadan and Bhaskar's Cylindrical Shells

Three dimensional elasticity solutions for finite length cross-ply laminated cylindrical shells have been considered by Varadan and Bhaskar (1991), see figure 5.12, with simply supported ends subjected to transverse sinusoidal pressure at the internal surface:

$$P_{zb1}^* = P_{zb1} \sin \frac{m\pi z}{L} \cos n\theta, \quad (5.2)$$

where $m = 1$ and $n = 4$. Varadan and Bhaskar's solutions were taken as benchmark solutions to validate the proposed procedure for cylindrical shell geometries. In this regard, the

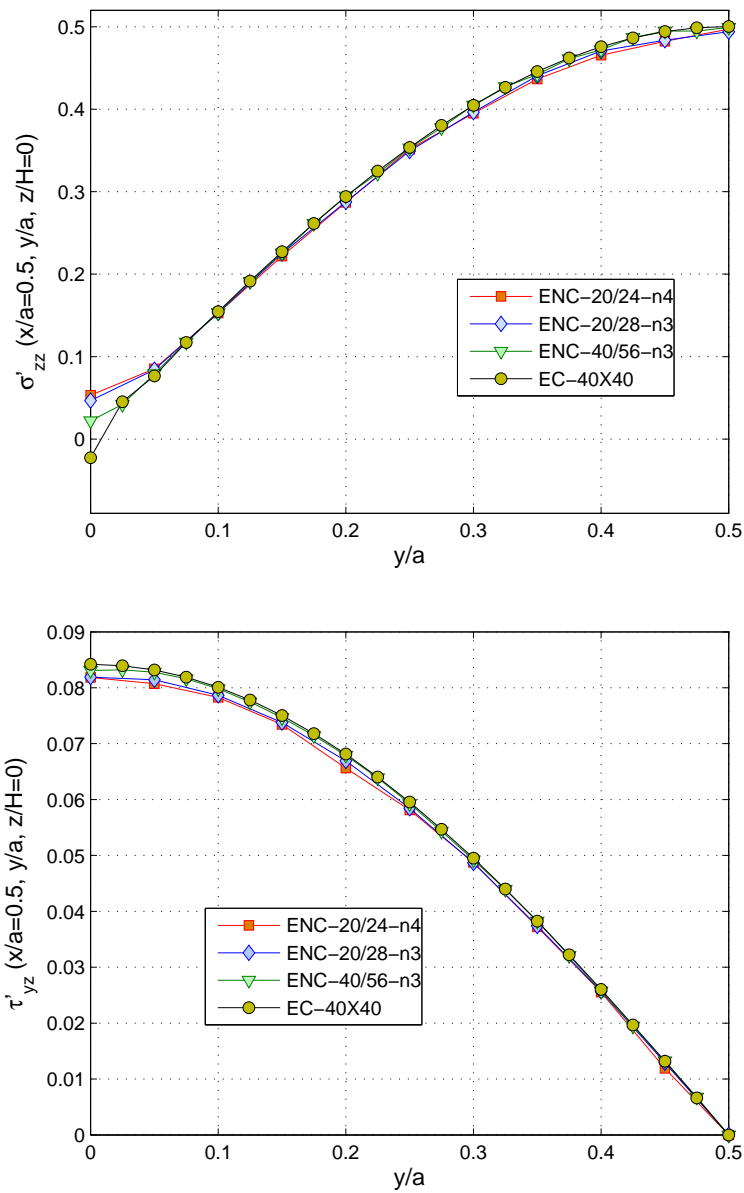


Figure 5.9: Transverse stress distributions obtained using the developed averaging technique.

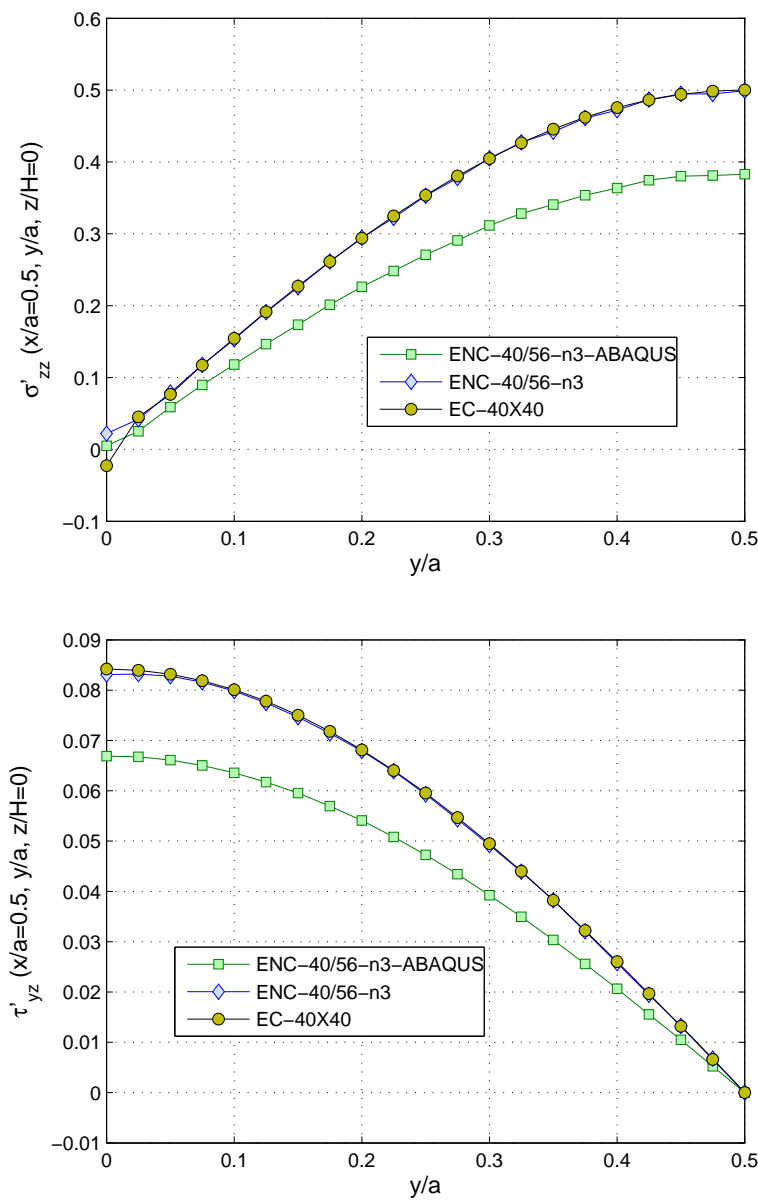


Figure 5.10: Transverse stress distributions obtained using the ABAQUS's built-in variational recovery post-processing procedure combined with the developed averaging technique.

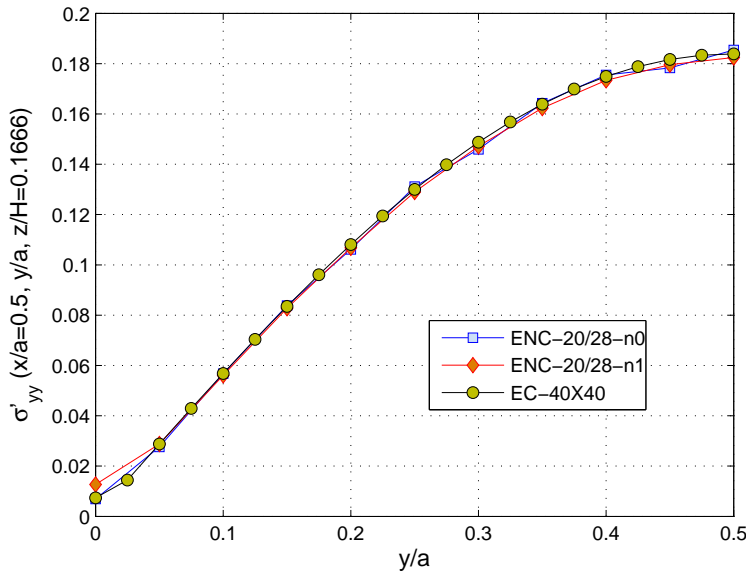


Figure 5.11: In-plane stress σ'_{yy} distribution obtained at the $(0^\circ/90^\circ)$ interface, i.e. $z/H=0.1666$, using the developed averaging technique.

following lamination schemes are considered in detail below: a two-layered $[90/0]$ shell, 90° for the outer layer and 0° for the inner layer, and a three-layered $[90/0/90]$ shell. The individual plies are taken to be of equal thickness. Length to mean radius of the cylindrical shell is $L/R_0 = 4$. The mechanical data are $E_L/E_T = 25$, $G_{LT}/E_T = 0.5$, $G_{TT}/E_T = 0.2$, $\nu_{LT} = \nu_{TT} = 0.25$. A non-dimensional transverse coordinate ξ varying from -0.5 at the inner surface to 0.5 at the outer surface is defined for convenience. The value $\xi = 0$ refers to the geometric middle surface.

Regarding the structural symmetry only an octant of the cylindrical shell was modeled in the finite element analysis. The discrete model was obtained using the 8-node linear brick incompatible modes element, i.e. $(C3D8I)$. The deformed and undeformed configurations of the adopted model are reported in figure 5.13. The in-plane mesh consists of 30 elements along the cylindrical coordinate θ and of 20 elements along the longitudinal coordinate z for each ply. Conforming meshes between the plies were considered initially. The mesh in the through-the-thickness direction of the laminate is the minimum required to apply the procedure at the points of interest. As for the simply supported plate previously analyzed, one mathematical interface was introduced in the middle of every layer to provide measures of intralaminar transverse stresses, thus leading to four layers of mesh for the first layup and six for the second.

Stress distributions are presented for values of $S = R_0/h = 50$ and 100 according to the following formulae,

$$\sigma'_r = \sigma_r/P_{zb^1}, \quad (\tau'_{rz}, \tau'_{r\theta}) = (10/P_{zb^1}S)(\tau_{rz}, \tau_{r\theta}),$$

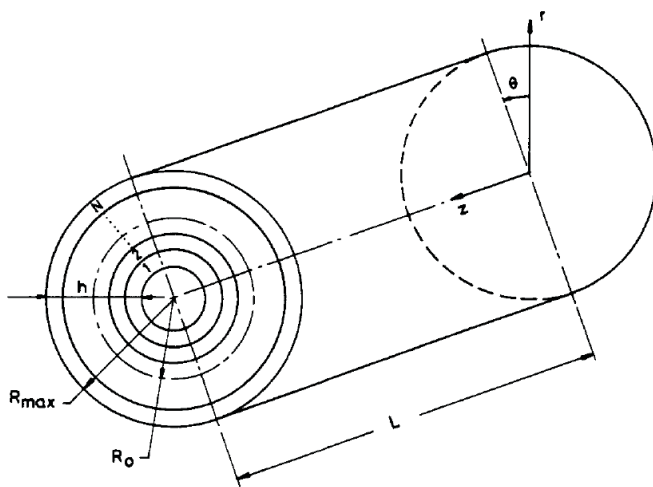


Figure 5.12: Varadan and Bhaskar's circular cylindrical shell.

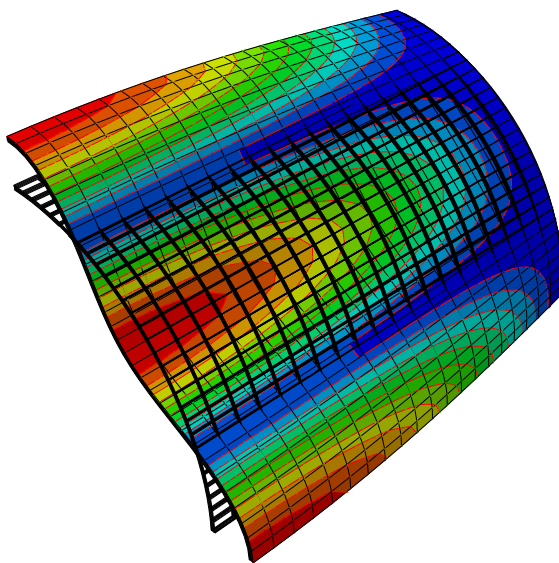


Figure 5.13: Adopted model: an octant of the cylindrical shell.

$$\tau'_{\theta z} = (10/P_{zb}S^2)\tau_{\theta z}, \quad (\sigma'_\theta, \sigma'_z) = (10/P_{zb}S^2)(\sigma_\theta, \sigma_z).$$

A three-layered [90/0/90] shell of value $S = 100$ is first taken into consideration. Comparisons between the through-the-thickness variation of the transverse shear and normal stress fields and the exact solution obtained at points of major interest are shown, respectively, in figure 5.14 and 5.15. Through-the-thickness distributions obtained using different built-in solid elements of ABAQUS with associated post-processing procedures are also reported for comparison. As for the simply supported plate analysed in section 5.3.1, the adopted elements were the 8-node linear brick incompatible modes *C3D8I*, the 20-node quadratic brick *C3D20R*, and the linear 8-node *C3D8R*. Neither the linear *C3D8R* nor the *C3D8I* elements provided single valued results at the interfaces, meaning that a through-the-thickness refinement of the mesh was required. It is clear from these plots that the proposed procedure was able to improve considerably the accuracy of the transverse stress states obtained using the ABAQUS' built-in *C3D8I* element. The percentage difference between the stress states obtained using the proposed procedure, i.e. EQUILIBRIUM, and the exact solution at the points reported on the plots of figure 5.14 and 5.15 was always less than 1%.

The ABAQUS's quadratic *C3D20R* element produced a good overall response, but it was less accurate compared to the response obtained using the proposed procedure combined with the built-in *C3D8I* element. This is because an overestimation of the transverse normal stress σ'_r was encountered, meaning that a refinement of the mesh through-the-thickness of the laminate was still required. Moreover, oscillations leading to inaccurate results were encountered in areas where boundary conditions are applied. This is shown in figure 5.16 which shows the circumferential plot of the transverse normal stress σ'_r starting from $\theta = 0^\circ$ up to $\theta = 45^\circ$ at the [90/0] interface and $z = L/2$ of the cylindrical shell.

The accuracy of the interlaminar stress fields obtained using the built-in formulations and stress recovery procedures of ABAQUS was reduced significantly when a two-layered [90/0] shell of value $S = 100$ was considered, see figures 5.17 and 5.18. The quadratic *C3D20R* element produced a distribution of the transverse shear stress $\tau'_{r\theta}$ that was not as accurate as that for the three-layered cylindrical shell previously analyzed, and in particular highly inaccurate results were obtained for the transverse normal stress σ'_r . This means that a more refined mesh had to be adopted in the present analysis to achieve numerical convergence of the recovered stress fields compared to the three-layered cylindrical shell previously analysed. This is due to the higher transverse stress gradients achieved along the through-the-thickness direction of the laminate in the present analysis. More demanding computational resources were required, as opposed to the proposed procedure which was able to generate excellent results compared to the exact solution, completely overlapping with the exact solution at most of the points shown in figure 5.17 and 5.18, using the same mesh adopted for the three-layered cylindrical shell.

Additional results obtained at points of maximum value using the proposed procedure are reported in table 5.2, where results for cylindrical shells of value $S = 50$ are also shown. Excellent agreement with available exact solutions were obtained indicating that an appropriate response is also generated in the case of moderately-thick structures. The aforementioned results were obtained by adopting one additional mathematical interface in the middle of every ply. However, as for the simply supported plates analysed in section 5.3.1, these mathematical interfaces were not required to have accurate interlaminar stress distributions. In-plane stress values for cylindrical shells of value $S = 50$ and $S = 100$ are reported in

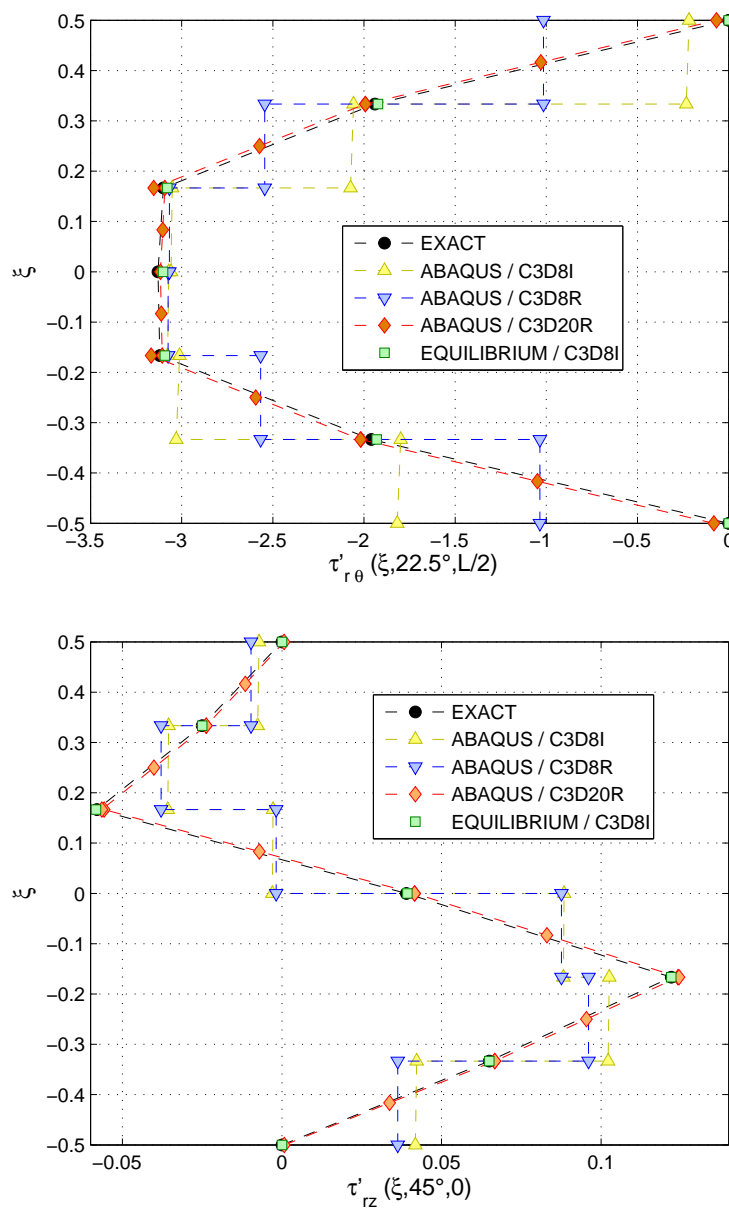


Figure 5.14: Comparison between the through-the-thickness distributions of the transverse shear stresses obtained using different approaches and the exact solution, three-layered $[90/0/90]$ shell, $S = 100$.

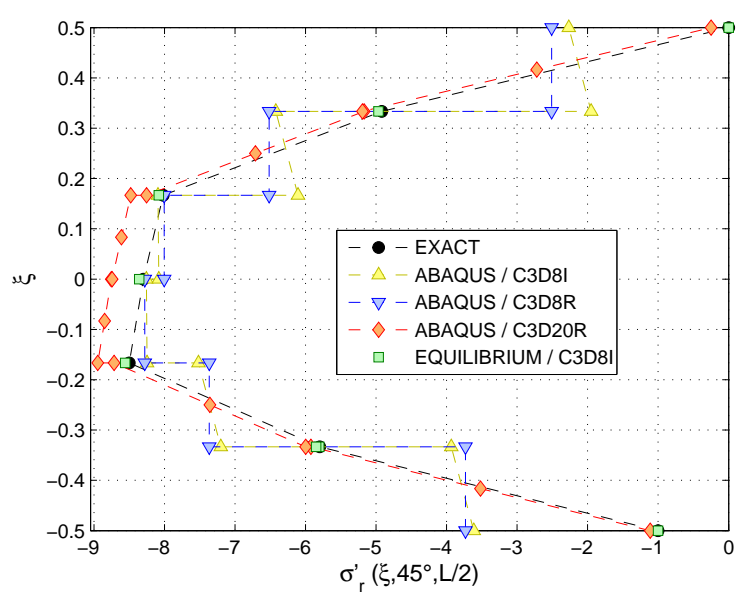


Figure 5.15: Comparison between the through-the-thickness distributions of the transverse stress σ'_r obtained using different approaches and the exact solution, three-layered $[90/0/90]$ shell, $S = 100$.

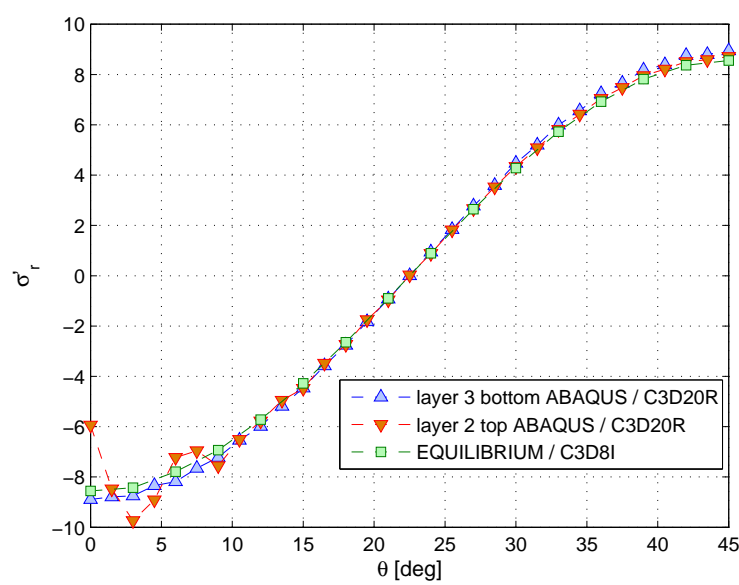


Figure 5.16: Circumferential plot of the transverse normal stress σ'_r at the $[90/0]$ interface and $z = L/2$, three-layered $[90/0/90]$ shell, $S = 100$.

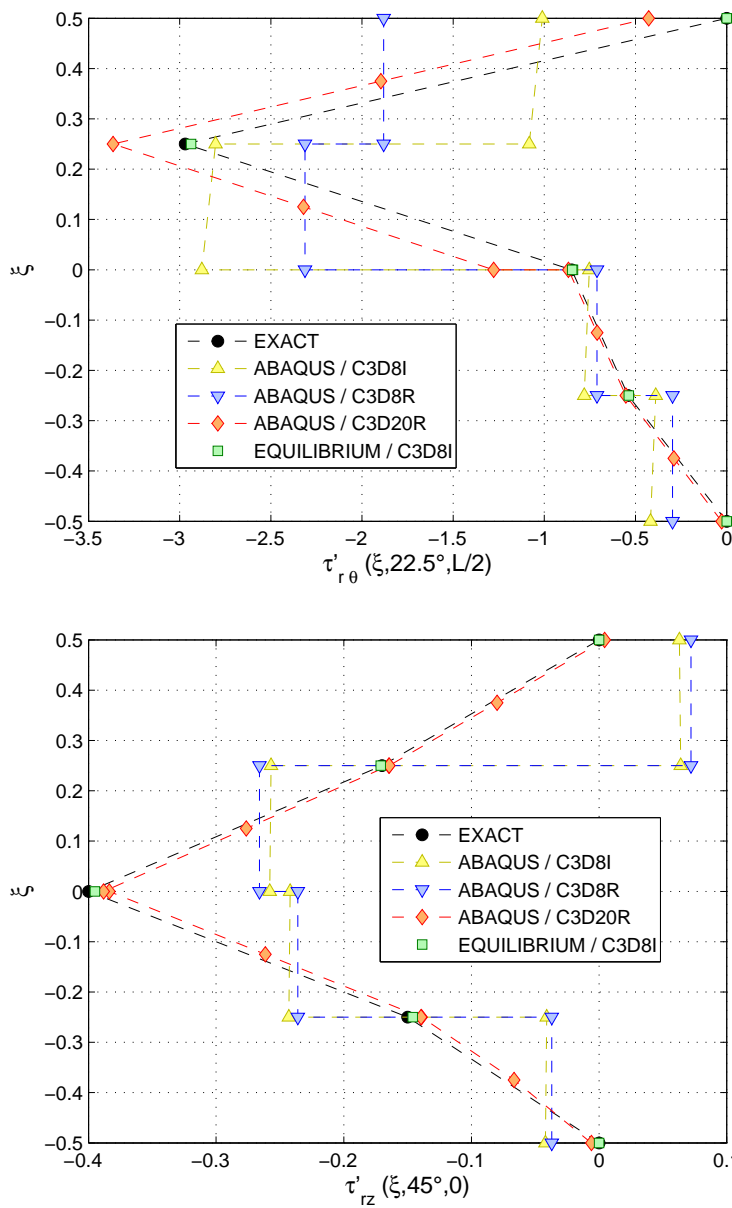


Figure 5.17: Comparison between the through-the-thickness distributions of the transverse shear stresses obtained using different approaches and the exact solution, two-layered [90/0] shell, $S = 100$.

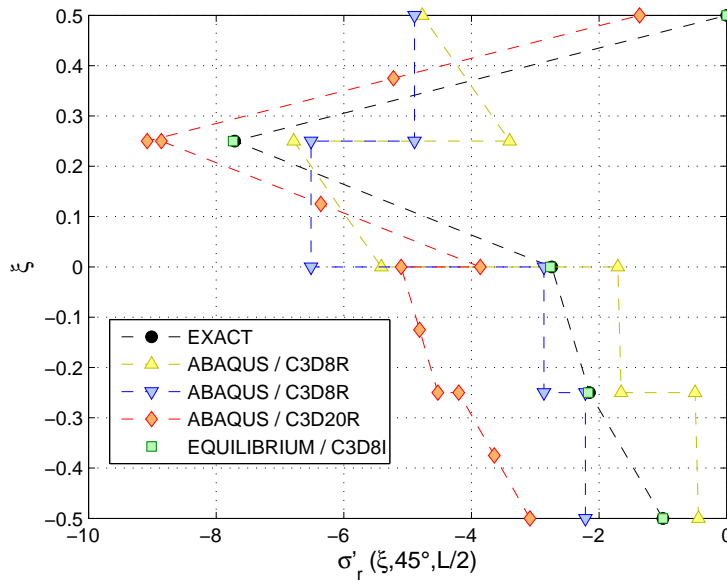


Figure 5.18: Comparison between the through-the-thickness distributions of the transverse normal stress σ'_r obtained using different approaches and the exact solution, two-layered $[90/0]$ shell, $S = 100$.

table 5.3. These results also confirmed the accuracy achieved by the proposed procedure in recovery appropriate stress states in multilayer composite laminates.

Table 5.2: Recovered transverse stress fields using different lamination schemes and values of mean radius to thickness ratio S .

S		τ'_{rz}	$\tau'_{r\theta}$	σ'_r
		$(\xi = -\frac{1}{6}, 45^\circ, 0)$	$(\xi = 0, 22.5^\circ, L/2)$	$(\xi = 0, 45^\circ, L/2)$
50	$[90/0/90]$			
	EXACT	0.0894	-3.491	-4.85
	EQUILIBRIUM	0.0897	-3.466	-4.88
100	EXACT	0.1223	-3.127	-8.30
	EQUILIBRIUM	0.1220	-3.102	-8.35
50	$[90/0]$			
	EXACT	0.0448	-4.785	-6.29
	EQUILIBRIUM	0.0449	-4.736	-6.32
100	EXACT	-0.1512	-2.972	-7.71
	EQUILIBRIUM	-0.1496	-2.937	-7.74

Three-layered $[90/0/90]$ cylindrical shells were also analysed using non conforming meshes between the plies created in the same manner as done for the simply supported plate, see figure 5.6, analysed in the previous section. Transverse stress distributions along

Table 5.3: Recovered in-plane stress fields using different lamination schemes and values of mean radius to thickness ratio S .

S		σ'_θ	σ'_z	$\tau'_{\theta z}$
		$(\xi = \mp \frac{1}{5}, 45^\circ, L/2)$	$(\xi = \mp \frac{1}{5}, 45^\circ, L/2)$	$(\xi = \mp \frac{1}{5}, 22.5^\circ, 0)$
50	[90/0/90]			
	EXACT	-3.987	-0.0225	-0.0760
	EQUILIBRIUM	-3.930	0.0712	-0.0118
		-3.940	-0.0229	-0.0754
100	EQUILIBRIUM	-3.892	0.0705	-0.0117
	EXACT	-3.507	0.0018	-0.1038
	EQUILIBRIUM	3.507	0.0838	-0.0478
-3.478		0.00187	-0.1030	
50	[90/0]			
	EXACT	-0.9670	1.610	-0.3449
	EQUILIBRIUM	8.937	0.2189	-0.0784
		-0.9583	1.6125	-0.339
100	EQUILIBRIUM	8.856	0.2145	-0.0773
	EXACT	-0.5759	2.30	-0.3452
	EQUILIBRIUM	5.560	0.1871	-0.1819
-0.572		2.298	-0.340	
		5.497	0.185	-0.179

the tangential direction at $\xi = 0$ and $z = L/2$ are shown in figure 5.19. The same kind of non-conforming meshes between the plies used for the simply supported plate analysed in the previous section were adopted, i.e. figure 5.6. Assuming that the count of the layers starts from the bottom of the cylindrical shell, a regular mesh composed of $C3D8I$ elements is adopted in layers 2, 4 and 6, and a mesh obtained as a combination of linear brick $C3D8I$ elements and linear triangular prism $C3D6$ elements is assumed in layers 1, 3 and 5. The plots in the figure are labeled using the same convention introduced in section 5.3.1 to denote conforming and non-conforming meshes.

As for the simply supported plate analyses reported in the previous section, oscillatory behaviours were encountered in the retrieved transverse stress distributions when non-conforming meshes were adopted, thus leading to inaccurate results. Then, the averaging technique introduced in the previous section was applied to the retrieved distributions. A smooth distribution for the transverse normal stress σ'_r , almost coincident with the one obtained using conforming meshes, is obtained using the mesh $ENC-40/56-n2$, i.e. figure 5.19₁. In the plot concerning the transverse shear stress $\tau'_{r\theta}$, i.e. figure 5.19₂, a smooth distribution in excellent agreement with the one obtained using a conformed mesh was obtained without the use of the averaging technique, i.e. $ENC-40/56-n0$. However, if the averaging technique, that needs to be adopted for smoothing out the transverse normal stress σ'_r distributions, is applied to all the transverse stress components, an error would be introduced in the transverse shear stress $\tau'_{r\theta}$ distribution $ENC-40/56-n0$ close to the boundaries of the laminate, i.e. $\theta = 0$ and $\theta = 90$, due to the high stress gradients achieved in these areas.

Transverse normal stress σ'_r distributions along the longitudinal direction at $\xi = 0$ and

$\theta = 45$ are shown in figure 5.20. In this case the developed averaging technique has to be adopted, and a smooth distribution is obtained using two iterations of the averaging technique, i.e. $n2$. However, the distribution obtained using the mesh $ENC-40/56-n2$ has in some of the points shown a percentage differences of 3.5% compared to the distribution obtained using the conforming mesh $EC-20 \times 30$. Then, a refinement of the mesh should be considered to reduce the percentage difference between the two distributions.

5.3.3 Spherical Curved Surfaces

Analyses concerning the recovery of interlaminar stress distributions in double curved laminates subjected to mechanical loadings are not quite addressed in the open literature due to the intrinsic difficulty associated with producing analytical solutions for such structures. Simply supported square spherical curved surfaces are considered in this section to provide reference solutions for future analyses of such laminates. An example of spherical curved surface and the adopted spherical coordinate system are shown in figure 5.21. The length to thickness and shell radii to thickness ratios evaluated on the mean reference surface of the spherical panel are denoted, respectively, by a_0/h and R_0/h .

The mechanical data are $E_L/E_T = 25$, $G_{LT}/E_T = 0.5$, $G_{TT}/E_T = 0.2$, $\nu_{LT} = \nu_{TT} = 0.25$. A three-layered $[0/90/0]$ lamination scheme is considered. The 0° fiber orientation is aligned with the spherical coordinate “ Th ”. The individual plies are assumed to be of equal thickness. These panels are subjected to a harmonic distribution of pressure applied in correspondence of the external surface, having the following equation:

$$P_{zb^1}^* = P_{zb^1} \sin \frac{\pi Th}{a_{top}} \sin \frac{\pi P}{a_{top}}. \quad (5.3)$$

The discrete model is obtained using the 8-node linear brick incompatible modes $C3D8I$ element of ABAQUS. Unless differently stated, the in-plane mesh consists of 30×30 elements for each ply. Conforming meshes between the plies are considered. As for both the plates and cylinders analysed in the previous sections, one mathematical interface was introduced in the middle of every ply to provide also intralaminar transverse stresses, thus leading to six layers of mesh.

The results are presented for values of $S = a_0/h = 50$ in terms of the following non-dimensional parameters:

$$(\tau'_{r\theta}, \tau'_{rp}) = \frac{1}{P_{zb^1} S} (\tau_{r\theta}, \tau_{rp}), \quad \sigma'_r = \frac{\sigma_r}{P_{zb^1}}, \quad \sigma'_\theta = \frac{\sigma_\theta}{P_{zb^1} S^2}.$$

For the reader's benefit, a non-dimensional through-the-thickness coordinate ξ varying from -0.5 at the inner surface to 0.5 at the outer surface is introduced to show through-the-thickness transverse stress distributions. The length and radii shell of the generic interface under consideration are defined, respectively, as a_ξ and R_ξ . Since the most severe effects due to shell curvature are encountered for the transverse shear stress τ'_{rp} , particular attention was paid to this component.

Plots of τ'_{rp} evaluated at points of major interest on different interfaces are presented in figure 5.22. Values of $R_0/a_0 = 20$ and 2 are taken into consideration. Similar transverse

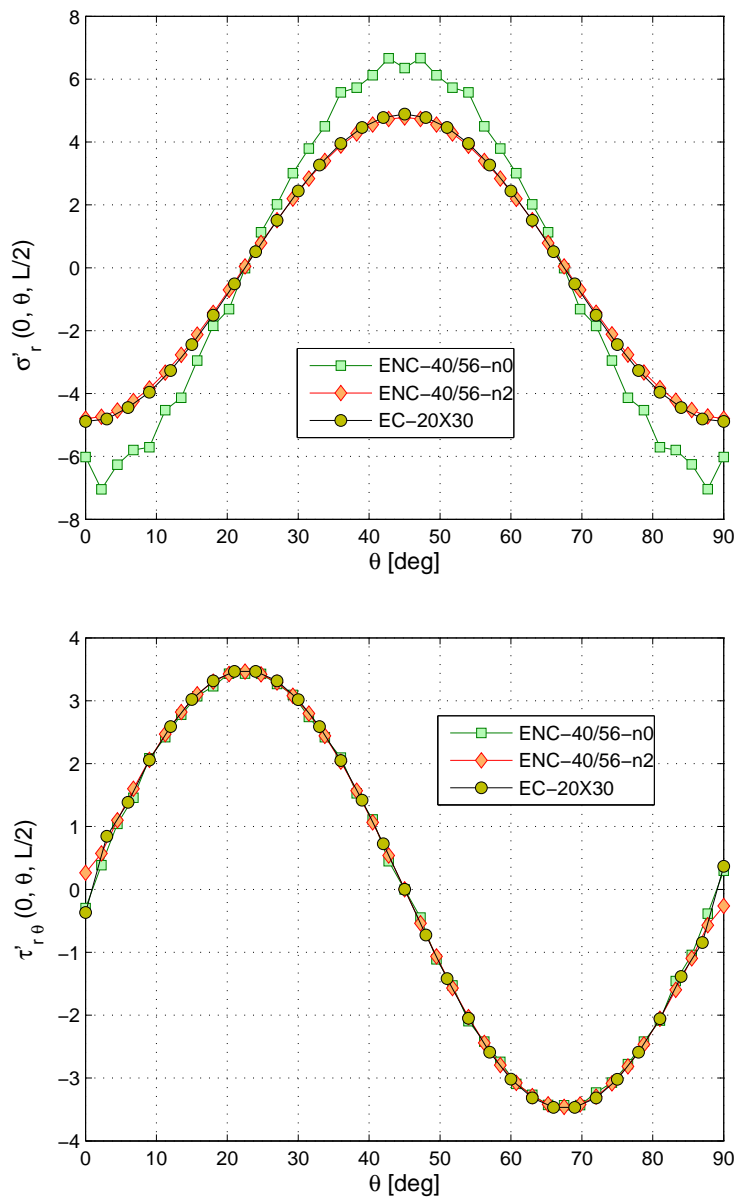


Figure 5.19: Transverse stress distributions obtained along the tangential direction of the cylindrical shell at $\xi = 0$ and $z = L/2$.

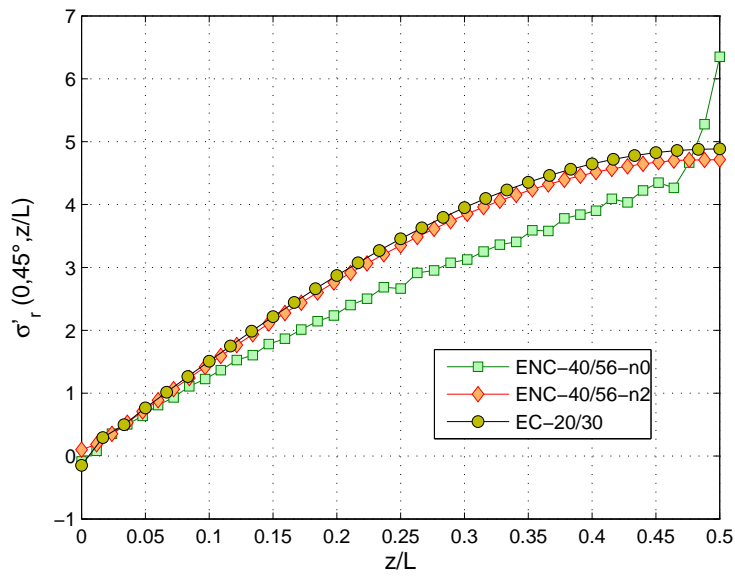


Figure 5.20: Transverse normal stress σ'_r distributions obtained along the longitudinal direction at $\xi = 0$ and $\theta = 45$.

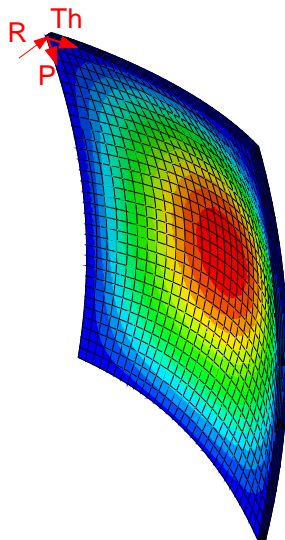


Figure 5.21: Spherical curved surface with the assumed spherical coordinate system.

shear stress distributions to the ones obtained in section 5.3.1 for the simply supported plate were obtained for $R_0/a_0 = 20$. These distributions are shown in figure 5.22₁, where a similar behaviour between the interfaces without the occurrence of severe in-plane stress gradients is encountered. These distributions were clearly affected by the shell curvature when a value of $R_0/a_0 = 2$ is considered. In this case, different behaviours and stress states were obtained on the different interfaces. The occurrence of higher in-plane stress

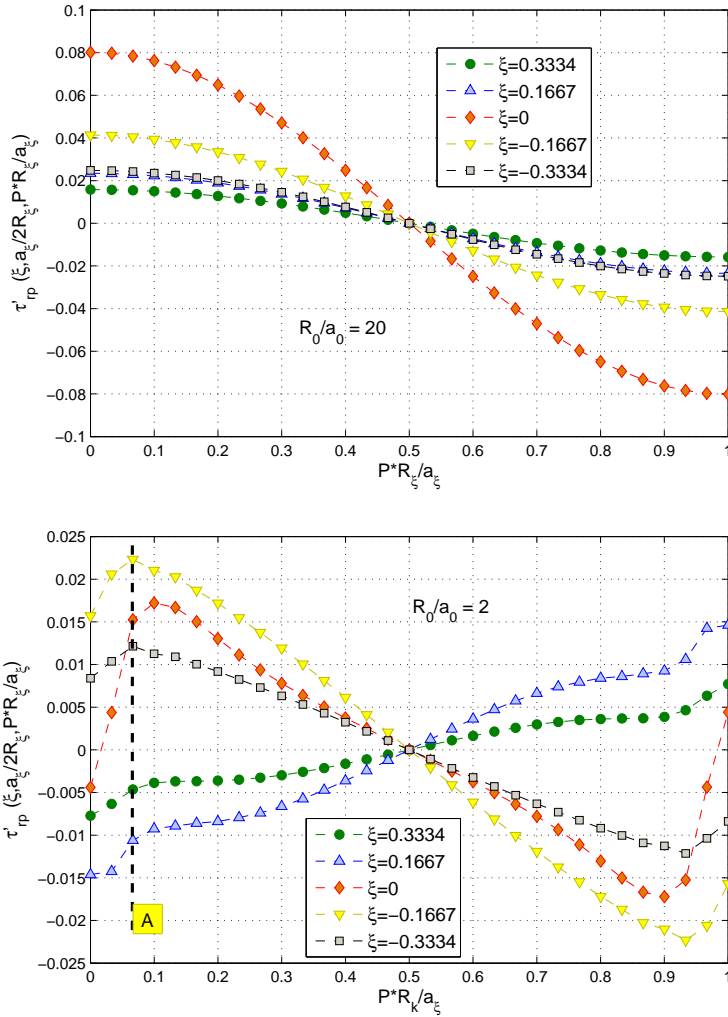


Figure 5.22: Transverse shear stress τ'_{rp} distributions obtained on different interfaces at points of major interest for $R_0/a_0 = 2$ and $R_0/a_0 = 20$.

gradients especially close to boundaries, as shown in figure 5.23 where the contour plot of the in-plane stress σ'_θ is reported, leads to severe gradients for the transverse stresses in both in-plane and out-of-plane directions. The effects of these severe in-plane stress gradients

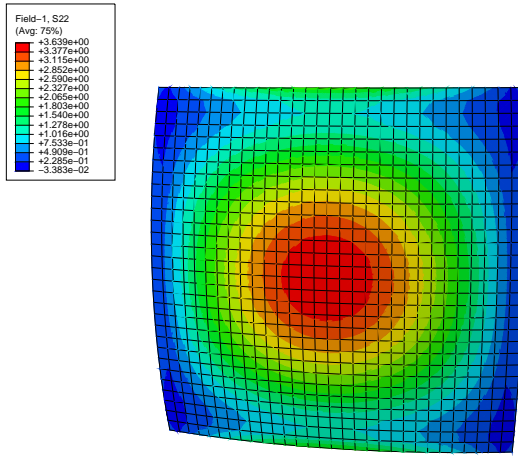


Figure 5.23: Contour plot of the in-plane stress σ'_θ at $\xi = 0$, $R_0/a_0 = 2$.

are considered in figure 5.24 where the through-the-thickness variation of the interlaminar shear stress τ'_{rp} is shown at section A, defined previously in figure 5.22. It can be seen from figure 5.24 that the accuracy of the distributions along the thickness of the spherical shell is not affected when additional mathematical interfaces are introduced. In this case three fictitious interfaces for every layer were introduced for a total number of 12 layers of mesh. This means that the present procedure does not require refined meshes along the thickness direction of the spherical shell to reach convergence, even in presence of severe gradients, as instead required using customary stress recovery procedures.

A convergence analysis of the transverse stress τ'_{rp} at $\xi = 0$ and $Th = a_0/2R_0$, that is the location where the most severe in-plane gradient is encountered, was also done and the results are shown in figure 5.25. It can be stated that a smooth distribution is obtained using an in-plane mesh of 28×28 , although a converging distribution can be reached only using an in-plane mesh of 30×30 , i.e. $PR/a = 0$. Through-the-thickness variations of the transverse shear stresses $\tau'_{r\theta}$ and τ'_{rp} and the transverse normal stress σ'_r taking into account different values of R_0/a_0 , are shown, respectively, in figures 5.26 and 5.27 at points of major interest. Confirmation of the accuracy of the model is obtained by increasing the value of R_0/a_0 . This is because the distributions obtained in figures 5.4 and 5.5 for the simply supported plate are retrieved also in this case by decreasing, using the parameter R_0/a_0 , the curvature of the laminate.

Non conforming meshes were taken in consideration also in this case. The same kind of non-conforming meshes between the plies used for the simply supported plate and cylindrical shell analysed in the previous sections were adopted, i.e. figure 5.6. Compared to the transverse stress distributions shown in figure 5.9 for the simply supported plate case, the same conclusions can be drawn also in this case concerning the transverse normal stress distribution σ'_r . As opposed to the simply supported plate case, the increment in the value of R_0/a_0 , i.e. the curvature of the spherical curved surface, introduce in-plane transverse shear stress distributions that present higher gradients close to the boundaries of the laminate,

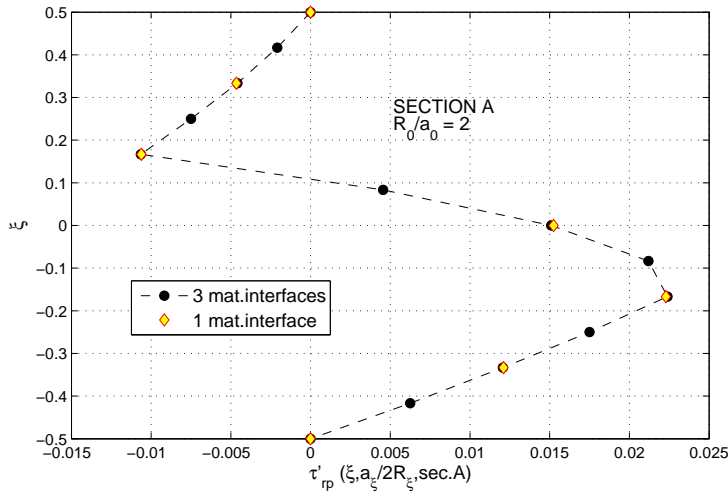


Figure 5.24: Through-the-thickness plot and convergence analysis for the transverse shear stress τ'_{rp} evaluated in section A, i.e. figure 5.22.

as shown in figure 5.22. This means that, although smooth distributions are obtained also in this case using the proposed averaging technique within three-four iterations, depending on the mesh adopted, compared to the simply supported plate case, inaccuracy was encountered also for the transverse shear stress components close to the boundary of the cylindrical shells, similarly to what happen for the transverse normal stress component σ'_r , see figure 5.9₁.

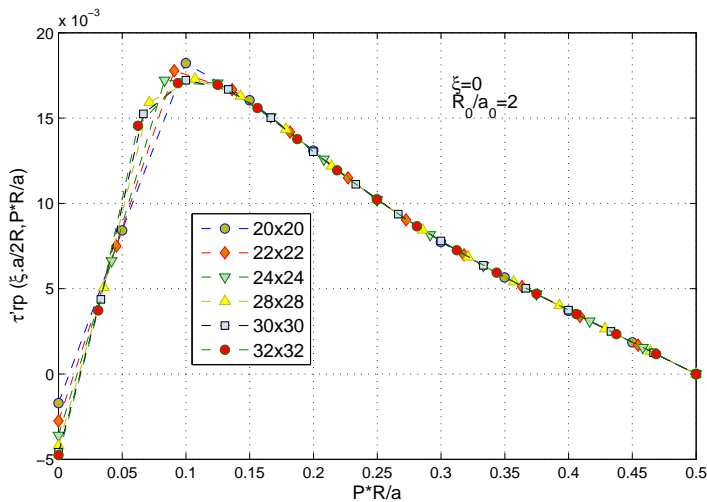


Figure 5.25: Convergence analysis of the transverse shear stress τ'_{rp} .

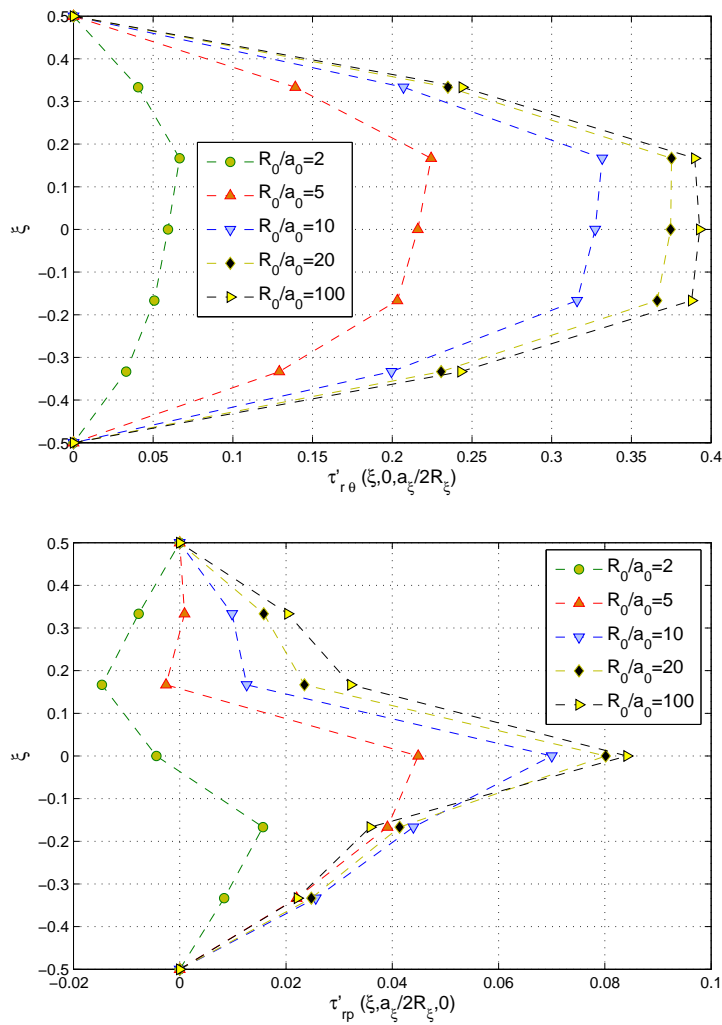


Figure 5.26: Through-the-thickness distributions of the recovered transverse shear stresses $\tau'_{r\theta}$ and τ'_{rp} obtained at points of major interest considering different values of R_0/a_0 .

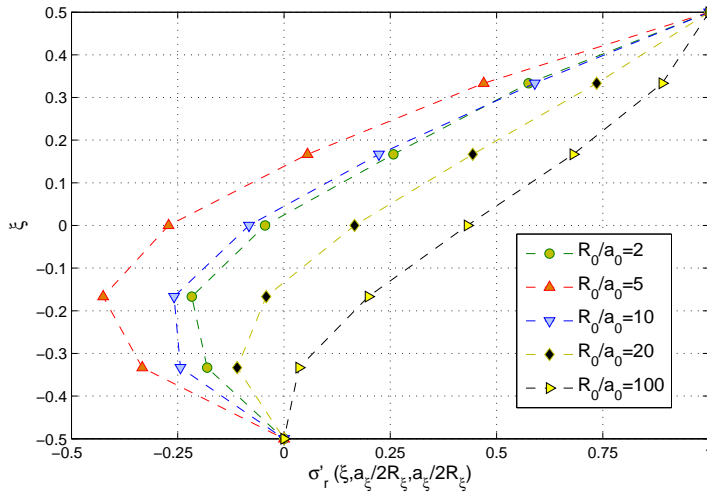


Figure 5.27: Through-the-thickness distributions of the recovered transverse normal stress σ'_r obtained at points of major interest considering different values of R_0/a_0 .

5.4 Conclusions

The efficient three-dimensional finite element procedure presented in chapter 4 was combined with the commercial Finite Element software ABAQUS 6.8TM with the aim of broadening the applicability of the method to general 3-D shell type structures. Particular attention was paid to the recovery of the interlaminar stresses. Benchmark problems concerning conventional straight fibers multilayered composite plates and shell laminates were analysed. In the finite element model each ply was modeled as a separate layer of elements, and the interlaminar boundary was treated as a contact surface. The interlaminar boundary was modelled as a contact zone because the connecting forces required by the developed interlaminar stress recovery procedure can only be obtained in ABAQUS 6.8TM using a contact formulation, and not, for instance, using tie constraints. Conforming meshes between the plies were initially considered, and the finite element model was obtained using the ABAQUS's built-in solid *C3D8I* element. The results were compared with ABAQUS's built in solid elements and associate post-processing procedures. ABAQUS's post-processing procedures are based either on stress recovery from the constitutive relations or on variational consistent recovery. This depends on the element's formulation. The proposed procedure was able to improve considerably the accuracy of the response obtained using the ABAQUS's built-in *C3D8I* element compared to ABAQUS's built-in stress recovery procedure. Smooth and accurate interlaminar stress distributions were obtained using a considerable reduced number of degrees of freedom, especially for multilayered shell structures, even compared to quadratic formulations. The proposed procedure was able to generate a minimum percentage reduction of 77% in the total number of degrees of freedom required to achieve accurate interlaminar stress distributions compared to ABAQUS's formulations that still failed to converge. Moreover, interlaminar continuity of the interlaminar stresses was directly satisfied without the need to employ a refined mesh through-the-thickness of

the laminate, as usually required using customary procedures. The reliability of the procedure was also validated by comparing the results with exact solutions available in the open literature.

Non conforming meshes between the plies were also considered. Plies with a regular mesh composed of *C3D8I* elements were alternated at plies having a mesh obtained as a combination of linear brick *C3D8I* elements and linear triangular prism *C3D6* elements. The triangular prism *C3D6* element was employed because it might be suitable for modeling both the areas close to the sides of a variable stiffness panel and the resin-rich areas generated during the manufacturing procedure of a variable stiffness panel. Then, the *C3D6* element needed to be tested in combination with ABAQUS's *C3D8I* element, that was shown to be a sound element for modeling composite laminates elsewhere. Oscillatory behaviours were encountered in the retrieved transverse stress distributions for both plate and shell laminates. Thus, inaccurate nodal values of the interlaminar transverse stresses were obtained. However, these oscillations showed the same trends of the distributions obtained using conforming meshes, that were taken as reference solutions. Then, an iterative averaging technique was developed to smooth out the distributions obtained.

The developed averaging technique consists in averaging the stress values obtained in each node with the stress values obtained in the nodes of the surrounding elements sharing the node under consideration. In general, smooth and accurate distributions were obtained using the proposed averaging technique within three-four iterations for both plates and shell laminates. However, much more refined meshes had to be adopted compared to the cases having conforming meshes between the plies. Moreover, inaccuracies in the retrieved transverse stress distributions were generated close to the boundaries of the laminates. This means that the proposed procedure needs to be improved for analyses employing non-conforming meshes between the plies of conventional composite laminates. It is extremely necessary to pay attention to this aspect before moving to the analysis of variable stiffness panels. In fact, the demanding computational resources required, and the inaccuracies generated close to the boundaries of conventional laminates make the proposed procedure not enough accurate for reliable interlaminar stress analyses of variable stiffness panels. Moreover, the number of iterations that would be required to smooth out the interlaminar stress distributions obtained in the analyses of variable stiffness panels can not be directly deduced from the analyses reported in this chapter. Then, interlaminar stress analyses of variable stiffness panels would not bring in at this stage of the work any additional understanding concerning the accuracy of the procedure in the analysis of such laminates. This is also because no comparison with available interlaminar stress data can be made.

Chapter 6

Recommendations and Future Developments

This thesis covers the structural analysis of conventional straight-fiber plate and shell laminates performed using a three-dimensional finite element computational procedure developed to perform reliable future stress analyses of variable stiffness panels. This is because an accurate finite element modeling that supports appropriate analyses of such laminates would be extremely difficult to obtain using customary procedures. In particular, variable stiffness panels have manufacturing characteristics, such as course edges, tow-drops and overlaps, that lead to amplification of the interlaminar stresses at the interface between the plies, and that possibly causes delamination to be the dominant failure mode in these configurations. Particular attention was paid to accurate interlaminar stress recovery of conventional composite laminates. Although a direct analysis of a variable stiffness panel was not performed during the research reported in the present thesis, several aspects concerning conventional composite laminates were considered to validate the procedure. Additional aspects arising for a proper modeling of variable stiffness laminates were also taken into account. The lessons learned, recommendations, and future challenges in this line of research are presented in the following paragraphs.

6.1 Pre-Processing Procedures

Two finite element pre-processing procedures were developed based on the idea of modeling a variable stiffness laminate by simulating the procedure followed during the manufacturing process by the tow-placement machine's head. The first procedure was developed within the MATLAB framework and was validated by analysing multilayered composite plate laminates. The second was developed within the ABAQUS framework with the aim of broadening the applicability of the method to general 3-D shell type structures. The second procedure was conceived such that it also enables the user to use tools and features already developed within the ABAQUS framework. Both the procedures were based on finite element models adopting linear solid elements. In particular, a simple low-order solid-shell element formulation based on the class of mixed assumed strain methods presented by Simo

and Rifai (1990), i.e. EAS formulation, was used in the pre-processing procedure developed within the MATLAB framework. This element was selected because it has an enhanced accuracy for coarse meshes and distortion insensitivity properties for a large range of length to thickness ratios of the laminate. Moreover, locking phenomena are solved without the employment of reduced or selective integration techniques. This is remarkable because low order reduced-integration elements may show hourglass mechanisms from spurious energy modes due to rank deficiency, thus leading to inaccurate results. This kind of element was not available in the library of ABAQUS's built-in elements. In the ABAQUS's framework the discrete model was obtained using an 8-node linear brick incompatible modes element, i.e. (*C3D8I*). This element was chosen because the class of mixed assumed strain methods encompass, as a particular case, the classical method of incompatible modes. However, enhanced assumed strain methods are recommended for a larger variety of problems compared to elements based on the method of incompatible modes. Future developments in this area might be addressed towards the implementation of the element based on the assumed enhanced strain method and presented in section in the library of ABAQUS's built-in elements.

Both the procedures were developed in such a way that any three-dimensional formulation for the through-the-thickness form description can be adopted in the finite element model. This means that models based on more advanced theories, i.e. the Layer-Wise theories or quadratic three-dimensional formulations, can also be adopted. For instance, in the research reported in this thesis particular attention was paid to develop models for accurate interlaminar stress recovery. Intralaminar stress values were also retrieved by introducing fictitious interfaces in the locations of interest. However, higher order solid elements or Layer-Wise formulations may be adopted in analyses of multilayer composite laminates requiring more accurate estimations of intralaminar stress distributions.

Non-conforming meshes between the plies were also considered in the ABAQUS's pre-processing procedure. Plies with a regular mesh composed of *C3D8I* elements were alternated at plies with a mesh obtained as a combination of linear brick *C3D8I* elements and linear triangular prism *C3D6* elements. It is worth to underline that the *C3D8I* element and the *C3D6* element are based on different formulations. This is because the *C3D6* element is not based on the classical method of incompatible modes, and the reduced integration technique is adopted to eliminate locking. Although the combined used of these elements led to accurate results in the mechanical analyses performed in section 5.3, it is recommended to validate the procedure further considering different kinds of analyses. For instance, different loadings, i.e. thermal loadings, and different combination of non-conforming meshes may be considered for additional verification. Non-linear analyses should also be addressed in the future.

The compatibility between the plies of the composite plies analysed were imposed using different methods in the two pre-processing procedures. In the procedure developed within the MATLAB framework, compatibility between the subdomains was reestablished using Lagrange multipliers. Then, the final system of governing equations was solved using a procedure for distributed computing generally employed in domain decomposition methods, i.e. the finite element tearing and interconnecting (FETI) method. The simultaneous use of multiple compute resources to solve a computational problem, i.e. parallel computing, definitely broaden the range of applications of the proposed procedure in numerical simulations. In particular, the choice to implement the FETI method was due to its parallel scalability and

its ability to outperform several popular direct and iterative algorithms on both sequential and parallel computers. This method was tested by analysing plate laminates with different geometries and conforming meshes between the plies. Smooth and accurate stress fields were obtained. This procedure is also easily extendible to non-conforming meshes by replacing the Boolean matrices appearing in the final system of governing equations (4.60) with, for instance, matrices obtained using the Mortar finite element method (Puso, 2004). Further research on this aspect is highly recommended for future developments in the field of non-conforming meshes between the plies of multilayer composite laminates.

An alternative procedure to the previous one was developed within the ABAQUS framework. In this case compatibility was enforced using a contact formulation between the plies. Excellent stress fields were obtained for both plates, these were almost identical to the results obtained using the first pre-processing procedure, and shell laminates in the case of conforming meshes between the plies. However, oscillatory behaviours were encountered in the retrieved stress distributions, in particular the transverse stress distributions, in the case of non-conforming meshes between the plies. Thus, inaccurate nodal values of the stresses fields were obtained. An averaging technique was developed to smooth out the stress fields distributions. In general, smooth and accurate distributions were obtained by using the proposed averaging technique within three-four iterations for both plates and shell laminates. However, much more refined meshes had to be adopted in the finite element model compared to the conforming meshes between the plies, and inaccuracies in the retrieved transverse stress distributions were generated close to the boundaries of the laminates for some of the transverse stress components. This means that further research should be addressed towards improving ABAQUS's contact formulation. An improvement may be obtained, for instance, by using a Mortar's contact formulation (Laursen, 2003). Another option would be to also implement the complete first pre-processing procedure within ABAQUS framework. In this case a tie-constrain formulation can be adopted ABAQUS (2005), and the FETI method could also be implemented within ABAQUS to perform parallel computing. Moreover, parallel computing is strongly recommended in the analyses of variable stiffness panels since appropriate stress analyses of such laminates require accurate modeling. This leads to finite element models having a large number of degrees of freedom. Both the procedures outlined in this thesis could then be tested and compared for different kind of laminate configurations, loadings, etc.

The idea of meshing in a variable stiffness laminate every single course using solid-brick elements, and both the tow-drop/tow-overlaps locations and the final part of the courses close to the edges of the laminate using triangular prism elements requires a reliable mesh generator to be developed. The mesh generator has to provide the required mesh for any kind of configuration. Then, a mesh can be inherently adopted in each course lied-down by the tow-placement machine's head based on the assumed construction method. Thus, the mesh of the complete laminate can be obtained by simulating the procedure followed by the tow-placement machine's head during the manufacturing process. Within the ABAQUS framework it is possible to import the geometry of each ply using the partition method (ABAQUS, 2005). Then, it is possible to control the mesh in the desired manner by using ABAQUS's mesh generator, i.e. hex-dominated element shape and structured mesh control (ABAQUS, 2005). However, ABAQUS's mesh generator has to be tested with different variable stiffness panel configurations since numerical issues could arise. Future research should be also addressed at the development of a reliable mesh generator, designed specifi-

cally for the procedure proposed in this thesis.

6.2 Post-Processing Procedure

In this thesis attention was also paid to develop an accurate post-processing procedure for accurate interlaminar stress recovery. The proposed interlaminar stress recovery procedure has shown several advantages compared to customary procedures. For instance, this procedure does not rely on extrapolation techniques from super-convergent or integration points, as usually done using customary procedures. Interlaminar stress values are retrieved directly at nodes and stress continuity at the inter-element boundary is automatically satisfied. Excellent agreements were obtained in the retrieved interlaminar stress distributions with exact solutions for both plate and shell structures. Convergence was reached using considerably fewer degrees of freedom compared to other finite elements procedures, thus making the procedure more suitable for the design of such laminates. It was also shown that smooth interlaminar stress distributions were easily generated without the need to employ smoothing techniques, as usually required when using customary stress recovery procedures. Moreover, the procedure was shown to be as accurate as commonly used assumed stress methods using coarser meshes, and without the need to include stress degrees of freedoms in the solution process. This is definitely a plus compared to stress based formulations which involve inverse constitutive relations that are generally not available in the case of non-linear analyses. The procedure could be also effectively combined with an average failure stress criterion to predict delamination initiation in presence of curved free edges and stress concentrations, i.e. laminated composite plates with open hole subjected to uniaxial tension. However, it is recommended to run additional analyses in the future to validate the proposed procedure for laminated composite plates with open hole subjected to different loading cases, and employing different failure criteria available in the open literature.

Oscillatory behaviours were encountered in the retrieved transverse stress distributions using the pre-processing procedure developed within the ABAQUS framework in the case of non-conforming meshes between the plies. The developed averaging technique was able to smooth out the distributions obtained. However, much more refined meshes had to be adopted compared to the ones employed in the case of conforming meshes between the plies. Moreover, inaccuracies in the retrieved transverse stress distributions were generated close to the boundaries of the laminates. This technique might be improved in the future by considering in the averaging procedure not only the nodes of the surrounding elements sharing the node under consideration, but also the nodes of the elements sharing the surrounding nodes of the node under consideration. This would allow a better estimation of the averaged nodal value to be obtained since more nodes would be involved in the averaging procedure. Other possible options are (i) to implement a different averaging technique, for instance one among the procedures presented in section 3.2, (ii) to improve ABAQUS's contact formulation, as mentioned in the previous section, (iii) to implement within ABAQUS the FETI method in combination with the Mortar method, and enforce the compatibility between the plies using tied constraints. These are three suggestions that have to be considered before moving to perform analyses of variable stiffness panels.

The pre-processing procedure developed within the ABAQUS framework was combined with the post-processing procedure developed within the MATLAB framework. This proce-

cedure could be also implemented entirely within the ABAQUS environment using the Abaqus Scripting Interface to speed up the process. This can be achieved using NumPy, a package of numerical extensions for Python that introduces a multidimensional array type and a rich set of matrix operations and mathematical functions. In case the user wishes to take advantage of some MATLAB's additional functions, i.e. plotting interface, the PyMat package can be incorporated. The PyMat module acts as an interface between NumPy arrays in Python and a MATLAB engine session, allowing arrays to be passed back and forth, and arbitrary commands to be executed in the MATLAB workspace (Python, 2006).

6.3 Future Challenges

The three-dimensional finite element computational strategy developed in this thesis was validated for conventional composite laminates. However, this procedure can be also used in the analysis of variable stiffness panels with tow-drops, although certain features in the procedure have to be further validated and improved, as suggested in the previous sections. Regarding the analysis of variable stiffness panels with tow-drops, the results reported in the work of Blom et al. (2009) can be taken as reference solutions for additional validation of the procedure. Both linear and non-linear analyses of such laminates should be considered for different kind of loads. For instance, thermal loadings may be taken into consideration to simulate the curing process of variable stiffness panels. In this manner it would be possible to evaluate the impact of the residual stresses in the structural performances of such laminates.

The proposed procedure might also be easily extendible to the analysis of variable stiffness panels with overlaps. This is because the tow-overlaps areas can be meshed using triangular prism elements, but oriented differently compared to the orientation that the triangular prism elements assume in the model of the tow-drops areas. A typical ply drop-off is shown in figure 6.1. However, the method should be validated first considering benchmark prob-

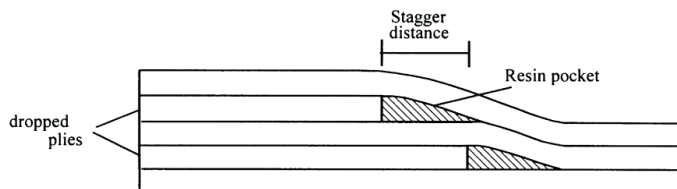


Figure 6.1: A typical ply drop-off (Mukherjee and Varughese (2001)).

lems concerning ply drop-off areas of laminated composite laminates subjected to different loads. Then, the results should be compared with available solutions in the open literature (Harrison and Johnson, 1996; Mukherjee and Varughese, 2001). The proposed procedure combined with integrating geometric design tools such as CATIA and fiber placement simulation software might be the right tool for an accurate design of a variable stiffness laminate.

Bibliography

Ingersoll machine tools. <http://www.ingersoll.com>.

Inc. ABAQUS. *Abaqus Analysis User's Manual-Abaqus Version 6.8*. Pawtucket, RI, USA, 2005.

M. M. Abdalla, Z. Gürdal, and G. F. Abdelal. Thermo-mechanical response of variable-stiffness composite panels. *Journal of Thermal Stresses*, 32:187–208, 2009.

A. Alhajahmad. *Design Tailoring of Panels for Pressure Pillowing Using Tow-Placed Steered Fibers*. PhD thesis, Delft University of Technology, The Netherlands, December 2008.

A. Alhajahmad, M. M. Abdalla, and Z. Gürdal. Optimal design of tow-placed fuselage panels with cutouts for maximum strength and buckling performance. In *Proceedings of the 2nd International Conference on Multidisciplinary Design Optimization and Applications*, Gijon, Spain, 2008a.

A. Alhajahmad, M.M. Abdalla, and Z. Gürdal. Design tailoring for pressure pillowing using tow-placed steered fibers. *Journal of Aircraft*, 45(2):630–640, 2008b.

S. A. Ambartsumian. Contributions to the theory of anisotropic layered shells. *Applied Mechanics Review*, 15:245–249, 1962.

S. A. Ambartsumian. *Theory of anisotropic plates*. J.E. Ashton Tech. Pub. Co., 1969.

U. Andelfinger and E. Ramm. Eas-elements for two dimensional, three dimensional, plate and shell structures and their equivalence to hr-elements. *International Journal for Numerical Methods in Engineering*, 36:1311–1337, 1993.

J. H. Argyris and K. J. Willam. Some considerations for the evaluation of finite element models. *Nuclear Engineering and Design*, 28(1):76–96, 1974.

F. Auricchio and E. Sacco. Partial-mixed formulation and refined models for the analysis of composites laminated within fsdt. *Composite Structures*, 46:103–113, 2001.

F. Auricchio, C. Lovadina, and E. Sacco. Analysis of mixed fibite elements for laminated composite plates. *Comput. Methods Appl. Mech. Engrg*, 190:4767–4783, 2001.

N. V. Banichuk. Optimal orientation of orthotropic materials for plates designed against buckling. *Structural Optimization*, 10:191–196, 1995.

- J. Barlow. Optimal stress locations in finite element models. *International Journal for Numerical Methods in Engineering*, 10(2):243–251, 1976. 10.1002/nme.1620100202.
- N. V. Bath and P. A. Lagace. An analytical method for the evaluation of interlaminar stresses due to material discontinuities. *Journal of Composite Materials*, 28:190–210, 1994.
- K. J. Bathe and E. N. Dvorkin. A four-node plate bending element based on mindlin/reissner plate theory and a mixed interpolation. *International Journal for Numerical Methods in Engineering*, 21(2):367–383, 1985.
- K. Bhaskar and T. K. Varadan. Reissner’s new mixed variational principle applied to laminated cylindrical shells. *Journal of Pressure Vessel Technology*, 114:115–119, 1992.
- S. B. Biggers and S. S. Pageau. Shear buckling response of tailored rectangular composite plates. *AIAA J.*, 32(5):1100–1103, 1994.
- S. B. Biggers and S. Srinivasan. Compression buckling response of tailored rectangular composite plates. *AIAA J.*, 31(3):590–596, 1993.
- M. Bischoff and E. Ramm. Shear deformable shell element for large strains and rotations. *Int. J. Numer. Methods. Engrg.*, 40(23):4427–4449, 2000.
- M. Bischoff, E. Ramm, and D. Braess. A class of equivalent enhanced assumed strain and hybrid stress finite elements. *Computational Mechanics*, 22:443–449, 1999.
- M. Bischoff, W. A. Wall, K. U. Bletzinger, and E. Ramm. Models and finite elements for thin-walled structures. *Encyclopedia of Computational Mechanics*, 2, 2004.
- T. Blacker, T. Belytschko. Superconvergent patch recovery with equilibrium and conjoint interpolant enhancements. *International Journal for Numerical Methods in Engineering*, 37(3):517–536, 1994.
- A. W. Blom, S. Setoodeh, J. M. A. M. Hol, and Z. Gürdal. Design of variable-stiffness conical shells for maximum fundamental eigenfrequency. *Computers and Structures*, 86(9):870–878, 2008a.
- A. W. Blom, B. F. Tatting, J. M. A. M. Hol, and Z. Gürdal. Path definitions for elastically tailored conical shells. *Composites part B: engineering*, 2008b. doi:10.1016/j.physletb.2003.10.071.
- A. W. Blom, C. S. Lopes, P. J. Kromwijk, Z. Gürdal, and Camanho P.P. A theoretical model to study the influence of tow-drop areas on the stiffness and strength of variable-stiffness laminates. *Journal of Composite Materials*, 43(5):403–425, 2009.
- O. C. Boroomand, B. Zienkiewicz. Recovery by equilibrium in patches (rep). *International Journal for Numerical Methods in Engineering*, 40(1):137–164, 1997a.
- O. C. Boroomand, B. Zienkiewicz. An improved rep recovery and the effectivity robustness test. *International Journal for Numerical Methods in Engineering*, 40(17):3247–3277, 1997b.

- B. Brank and E. Carrera. Multilayered shell finite element with interlaminar continuous shear stresses: A refinement of the reissner-mindlin formulation. *International Journal of Numerical Methods in Engineering*, 48:843–874, 2000.
- J. C. Brewer and P. A. Lagace. Quadratic stress criterion for initiation of delamination. *Journal of Composite Materials*, 22(12):1141–1155, 1988.
- F. Brezzi and M. Fortin. *Mixed and Hybrid Finite Element Methods*. Springer-New York, 1991.
- N. Buchter, E. Ramm, and Roehl. D. Three-dimensional extension of nonlinear shell formulation based on the enhanced assumed strain concept. *Int. J. Numer. Methods. Engrg.*, 37(15):2551–2568, 1994.
- F. Bullock, S. Kowalski, and R. Young. Automated prepreg tow-placement for composite structures. In *35th International SAMPE Symposium, Anaheim, CA*, 35:734–743, April 1990.
- E. Carrera. A class of two dimensional theories for multilayered plates analysis. *Atti Accademia delle Scienze di Torino, Memorie Scienze fisiche*, 19-20:49–87, 1996a.
- E. Carrera. c^0 reissner-mindlin multilayered plate elements including zig-zag and interlaminar stress continuity. *International Journal of Numerical Methods in Engineering*, 39:1797–1820, 1996b.
- E. Carrera. c^0 requirements-models for the two dimensional analysis of multilayered structures. *Composite Structures*, 37:373–383, 1997.
- E. Carrera. Evaluation of layer-wise mixed theories for laminated plates analysis. *AIAA J.*, 36(5):830–839, 1998.
- E. Carrera. Multilayered shell theories that account for a layer-wise mixed description. part i. governing equations. *AIAA J.*, 37(9):1107–1116, 1999a.
- E. Carrera. Multilayered shell theories that account for a layer-wise mixed description. part ii. numerical evaluations. *AIAA J.*, 37(9):1117–1124, 1999b.
- E. Carrera. Layer-wise mixed models for accurate vibration analyses of multilayered plates. *Journal of Applied Mechanics*, 65:820–828, 1999c.
- E. Carrera. A priori vs a posteriori evaluation of transverse stresses in multilayered orthotropic plates. *Composite Structures*, 48:245–260, 2000.
- E. Carrera. Developments, ideas and evaluations based upon reissner’s mixed variational theorem in the modelling of multilayered plates and shells. *Applied Mechanics Review*, 54:301–329, 2001.
- E. Carrera. Theories and finite elements for multilayered, anisotropic, composite plates and shells. *Archives of Computational Methods in Engineering*, 9(2):87–140, 2002.

- E. Carrera. Theories and finite elements for multilayered plates and shells: A unified compact formulation with numerical assessment and benchmarking. *Archives of Computational Methods in Engineering*, 10(3):215–296, 2003a.
- E. Carrera. Historical review of zig-zag theories for multilayered plates and shells. *Appl.Mech.Rev*, 56(3):287–307, 2003b.
- E. Carrera and L. Demasi. Classical and advanced multilayered plate elements based upon pvd and rmvt. part 1: Derivation of finite element matrices. *International Journal for Numerical Methods in Engineering*, 55(2):191–231, 2002a.
- E. Carrera and L. Demasi. Classical and advanced multilayered plate elements based upon pvd and rmvt. part 2: Numerical implementations. *International Journal for Numerical Methods in Engineering*, 55(3):253–291, 2002b.
- F. K. Chang and G. S. Springer. The strengths of fiber reinforced composite bends. *Journal of Composite Materials*, 20(30):30–45, 1986.
- D. Chapelle and K. J. Bathe. *The Finite Element Analysis of Shells - Fundamentals*. Springer, 2003.
- D. J. Chen, D. K. Shah, and W. S. Chan. Interfacial stress estimation using least-square extrapolation and local stress smoothing in laminated composites. *Computers and Structures*, 58:765–774, 1996. doi:10.1016/0045-7949(95)00181-F.
- K. N. Cho, C. W. Bert, and A. G. Striz. Free vibrations of laminated rectangular plates analyzed by higher-order individual-layer theory. *J. Sound Vib*, 145:429–442, 1991.
- M. Cho and R. R. Permerter. Efficient higher order composite plate theory for general lamination configurations. *AIAA Journal*, 31(7):1299–1305, 1993.
- E. Cosserat and F. Cosserat. *Theories des corps deformable*. In *Traite de Phisique*, 2nd edition, 1999.
- D. Coutellier, J. C. Walrick, and P. Geoffroy. Presentation of a methodology for delamination detection within laminated structures. *Composite Science and Technology*, 66(6): 837–845, 2006.
- P. J. Crothers, K. Drechsler, D. Feltinc, I. Herszberga, and T. Kruckenbergd. Tailored fibre placement to minimise stress concentrations. *Composites Part A: Applied Science and Manufacturing*, 28:619–625, 1997.
- C. M. Dakshina Moorthy and J. N. Reddy. Recovery of interlaminar stresses and strain energy release rates in composite laminates. *Finite Elements in Analysis and Design*, 33(1):1–27, 1999.
- S. De Miranda and F. Ubertini. On the consistency of finite element models in thermoelastic analysis. *Computer Methods in Applied Mechanics and Engineering*, 190:2411–2427, 2001.

- S. De Miranda and F. Ubertini. Recovery of consistent stresses for compatible finite elements. *Computer Methods in Applied Mechanics and Engineering*, 191(15-16):1595–1609, 2002.
- L. Demasi. Treatment of stress variables in advanced multilayered plate elements based upon reissner’s mixed variational theorem. *Computers and Structures*, 84(19-20):1215–1221, 2006.
- L. Demasi. Mixed plate theories based on the generalized unified formulation. part i: Governing equations. *Composite Structures*, 87(1):1–11, 2008.
- M. T. DiNardo and P. A. Lagace. Buckling and postbuckling of laminated composite plates with ply dropoffs. *AIAA J.*, 27(10):1392–1398, 1989.
- G. Duvaut, G. Terrel, F. Lènè, and V. E. Verijenko. Optimization of fiber reinforced composites. *Composite Structures*, 48:83–89, 2000.
- M. L. Enders and P. C. Hopkins. Developments in the fiber placement process. In *36th International SAMPE Symposium, San Diego, CA*, 36:778–790, 1991.
- D. O. Evans. Fiber placement. technical report. *Cincinnati Machine*, 2001.
- C. Farhat. A lagrange multiplier based divide and conquer finite element algorithm. *J. Comput. Sys. Engrg.*, 2:149–156, 1991.
- C. Farhat and F. X. Roux. A method of finite element tearing and interconnecting and its parallel solution algorithm. *International Journal for Numerical Methods in Engineering*, 32(6):1205–1227, 1991. 10.1002/nme.1620320604.
- C. Farhat, C. Lacour, and D. Rixen. Incorporation of linear multipoint constraints in substructure based iterative solvers. part 1: a numerically scalable algorithm. *International Journal for Numerical Methods in Engineering*, 43(6):997–1016, 1998.
- C. Farhat, K. Pierson, and M. Lesoinne. The second generation feti methods and their application to the parallel solution of large-scale linear and geometrically non-linear structural analysis problems. *Computer Methods in Applied Mechanics and Engineering*, 184(2-4):333–374, 2000a.
- C. Farhat, K. Pierson, and M. Lesoinne. The second generation feti methods and their application to the parallel solution of large-scale linear and geometrically non-linear structural analysis problems. *Comp. Meth. Appl. Mech. Eng.*, 184:333–374, 2000b.
- C. A. Felippa. A survey of parametrized variational principles and applications to computational mechanics. *Computer Methods in Applied Mechanics and Engineering*, 113:109–139, 1994.
- C. A. Felippa. On the original publication of the general canonical functional of linear elasticity. *J. Appl. Mech.*, 67(1):217–219, 2000.
- Z. Gürdal and R. Olmedo. In-plane response of laminates with spatially varying fiber orientations: Variable stiffness concept. *AIAA Journal*, 31(4):8, 1993.

- Z. Gürdal, B. F. Tatting, and K. C. Wu. Tow-placement technology and fabrication issues for laminated composite structures. *46th AIAA/ASME/ASCE/AHS/ASC Structures, Structural Dynamics and Materials Conference*, 2005.
- Z. Gürdal, B. F. Tatting, and K. C. Wu. Variable stiffness composite panels; effects of stiffness variation on the in-plane buckling response. *Composites part B: engineering*, 39(5):911–922, 2008.
- P. N. Harrison and E. R. Johnson. A mixed variational formulation for interlaminar stresses in thickness-tapered composite laminates. *Int. J. Solids Structures*, 33(16):2377–2399, 1996.
- P. Hauret and M. Ortiz. Bv estimates for mortar methods in linear elasticity. *Computer Methods in applied Mechanics and Engineering*, 195(37):4783–4793, 2006.
- M. R. Hestnes. Method of conjugate gradients for solving linear systems. *J. Res. Nat. Bur. Standards*, 49:409–436, 1952.
- F. B. Hildebrand, E. Reissner, and G. B. Thomas. Notes on the foundations of the theory of small displacements of orthotropic shells. *NACA TN-1833*, Washington, D.C., 1938.
- E. Hinton and B. Irons. Least square smoothing of experimental data using finite elements. *Strain-J. Br. Soc. Strain Meas.*, 4:24–27, 1968.
- J. S. Hinton, E. Campbell. Local and global smoothing of discontinuous finite element functions using a least squares method. *International Journal for Numerical Methods in Engineering*, 8(3):461–480, 1974. 10.1002/nme.1620080303.
- F. Z. Hu, C. Soutis, and E. C. Edge. Interlaminar stresses in composite laminates with a circular hole. *Composite Structures*, 37:223–232, 1997.
- M. W. Hyer and R. F. Charette. Use of curvilinear fiber format in composite structure design. *AIAA Journal*, 29(6):1011–1015, 1991.
- M. W. Hyer and H. H. Lee. The use of curvilinear fiber format to improve buckling resistance of composite plates with central circular holes. *Composite Structures*, 18:239–261, 1991.
- E. V. Iarve. Spline variational three dimensional stress analysis of laminated composite plates with open holes. *International Journal of Solids and Structures*, 33(14):2095–2118, 1996.
- E. V. Iarve and N. J. Pagano. Singular full-field stresses in composite laminates with open holes. *International Journal of Solids and Structures*, 38(1):1–28, 2001.
- D. C. Jegley, B. F. Tatting, and Z. Gürdal. Optimization of elastically tailored tow-placed plates with holes. In *Proceedings of the 44th AIAA/ASME/ASCE/AHS/ASC Structures, Structural Dynamics and Materials (SDM) Conference*, Norfolk, VA, USA, Apr 2003. AIAA.

- D. C. Jegley, B. F. Tatting, and Z. Gürdal. Tow-steered panels with holes subjected to compression or shear loading. In *Proceedings of the 46th AIAA/ASME/AHS/ASC Structures, Structural Dynamics and Materials (SDM) Conference*, Austin, TX, USA, Apr 2005. AIAA.
- H. Jing and K. G. Tzeng. Refined shear deformation theory of laminated shells. *AIAA Journal*, 31:765–773, 1993.
- R. M. Jones. *Mechanics of Composite Materials*. Taylor and Francis, 2nd edition, 1999.
- T. Kant and K. Swaminathan. Estimation of transverse/interlaminar stresses in laminated composites - a selective review and survey of current developments. *Composite Structures*, 49(1):65–75, 2000.
- C. Kashtalyan, M. Soutis. Strain energy release rate for off-axis ply cracking in laminated composites. *Int. J. Fracture*, 112(2):3–8, 2001.
- C. Kashtalyan, M. Soutis. Analysis of local delaminations induced by angle ply matrix cracks. *Int. J. Solids and Structures*, 39(6):1515–1537, 2002.
- S. Klinkel and W. Wagner. A geometrical non-linear brick element based on the eas-method. *Int. J. Numer. Methods Engrg*, 40:4529–4545, 1997.
- W. T. Koiter. A consistent first approximation in the general theory of thin elastic shells. In *Proceedings of First Symposium on the Theory of Thin Elastic Shells*, North Holland, Amsterdam, 1959.
- H. Kraus. *Thin elastic shells*. John Wiley, 1967.
- J. Kruis. *Domain Decomposition Methods for Distributed Computing*. Saxe-Coburg Publications, 2007. 1202055.
- J. Kruis and K. Matous. Solving laminated plates by domain decomposition. *Advances in Engineering Software*, 33:445–452, 2002. doi:10.1016/S0965-9978(02)00075-3.
- P. A. Lagace and K. J. Bonello. Damage accumulation in graphite/epoxy laminates due to cyclic gradient stress fields. *Journal of Reinforced Plastics and Composites*, 12:1111–1135, 1993.
- T. A. Laursen. *Computational contact and impact mechanics: fundamentals of modeling interfacial phenomena in nonlinear finite element analyses*. Springer-New York, 2003.
- K. Lee and S. W. Lee. A postprocessing approach to determine transverse stresses in geometrically nonlinear composite and sandwich structures. *Journal of Composite Materials*, 37(24):2207–2224, 2003.
- T. Lee, H.C. Park, and S.W. Lee. A super-convergent stress recovery technique with equilibrium constraint. *International Journal for Numerical Methods in Engineering*, 40(6): 1139–1160, 1997.
- S. G. Lekhnitskii. Strength calculation of composite beams. *Vestnik Inzhen. i Tekhnikov*, (9), 1935.

- P. Lesaint. *Superconvergence of the gradient of finite element solutions*. RAIRO Anal. Numer. 1979, 1979.
- K. H. Lo, R. M. Christensen, and E. M. Wu. A higher-order theory of plate deformation. part 2: Laminated plates. *ASME J. Appl. Mech*, 44:669–676, 1977.
- C. S. Lopes. *Damage and Failure of non-conventional composite laminates*. PhD thesis, Delft University of Technology, The Netherlands, June 2009.
- C. S. Lopes, P. P. Camanho, Z. Gürdal, and B. F. Tatting. Progressive failure analysis of tow-placed, variable-stiffness composite panels. *International Journal of Solids and Structures*, 44(25-26):8493–8516, 2007. 10.1016/j.ijsolstr.2007.06.029.
- C. S. Lopes, Z. Gürdal, and P. P. Camanho. Variable-stiffness composite panels: Buckling and first-ply failure improvements over straight-fibre laminates. *Computers and Structures*, 86:897–907, 2008.
- R. H. MacNeal. A simple quadrilateral shell element. *Computers and Structures*, 8:175–183, 1978.
- P. Maimì, P. P. Camanho, J. A. Mayugo, and C. G. Dàvila. A continuum damage model for composite laminates - part i: Constitutive model. *Mechanics of Materials*, 39:897–908, 2007a.
- P. Maimì, P. P. Camanho, J. A. Mayugo, and C. G. Dàvila. A continuum damage model for composite laminates - part ii: Computational implementation and validation. *Mechanics of Materials*, 39:909–919, 2007b.
- R. H. McNeal. Perspective on finite elements for shell analysis. *Finite Elements in Analysis and Design*, 30:175–186, 1998.
- J.A. Mondo, M.J. Pasanen, R.J. Langone, and J.P. Martin. Advances in automated fiber placement of aircraft structures. 1997.
- A. Mota and J. F. Abel. On mixed finite element formulations and stress recovery techniques. *International Journal for Numerical Methods in Engineering*, 47(1-3):191–204, 2000.
- A. Mukherjee and B. Varughese. Design guidelines for ply drop-off in laminated composite structures. *Composites Part B*, 32:153–164, 2001.
- H. Murakami. Laminated composite plate theory with improved in-plane responses. *Journal of Applied Mechanics*, 53(3):661–666, 1986.
- C. Muser and N. J. Hoff. Stress concentrations in cylindrically orthotropic plates with radial variation of the compliances. *Progress in Science and Engineering of Composites*, pages 389–396, 1982.
- A. K. Noor. Global-local methodologies and their application to nonlinear analysis. *Finite Elements in Analysis and Design*, 2:333–346, 1986.

- A. K. Noor and W. S. Burton. Assessment of shear deformation theories for multilayered composite plates. *Appl.Mech.Rev*, 42(1):1–13, 1989.
- A. K. Noor and W. S. Burton. Assessment of computational models for multilayered composite shells. *Appl.Mech.Rev*, 43(4):67–98, 1990.
- A. K. Noor and M. Malik. An assessment of five modeling approaches for thermomechanical stress analysis of laminated composite panels. *Comput Mech*, 25(1):43–58, 2000.
- A. K. Noor, Y. H. Kim, and J. M. Peters. Transverse shear stresses and their sensitivity coefficients in multilayered composite panels. *AIAA J.*, 32(6):1259–1269, 1994.
- A. Nosier, R. K. Kapania, and J. N. Reddy. Free vibration analysis of laminated plates using a layer-wise theory. *AIAA journal*, 31:2335–2346, 1993.
- T. K. O'Brien. Characterization of delamination onset and growth in a composite laminate. *Damage in Composite Materials*, ASTM STP 775, K.L. Reifsneider, Ed., American Society for Testing and Materials:140–167, 1982.
- J. T. Oden and H. J. Brauchli. On the calculation of consistent stress distributions in finite element approximations. *International Journal for Numerical Methods in Engineering*, 3(3):317–325, 1971.
- R. Olmedo and Z. Gürdal. Composite laminates with spatially varying fibre orientations: Variable stiffness panel concept. In *Proceedings of the 33th AIAA/ASME/ASCE/AHS/ASC Structures, Structural Dynamics and Materials (SDM) Conference*. AIAA, 1992.
- R. Olmedo and Z. Gürdal. Buckling response of laminates with spatially varying fiber orientations. In *Proceedings of the 34th AIAA/ASME/ASCE/AHS/ASC Structures, Structural Dynamics and Materials (SDM) Conference*. AIAA, 1993.
- N. J. Pagano. Exact solutions for composite laminates in cylindrical bending. *Journal of Composite Materials*, 3:398–411, 1969.
- N. J. Pagano. Exact solutions for rectangular bidirectional composites and sandwich plates. *Journal of Composite Materials*, 4(1):20–34, 1970.
- N. J. Pagano. Stress fields in composite laminates. *International Journal of Solids and Structures*, 14:385–400, 1978.
- N. J. Pagano and G. A. Schoepner. Delamination of polymer matrix composites: Problems and assessments. *Comprehensive Composite Materials*, 2:433–528, 2000.
- H. Parish. A continuum-based shell theory for non-linear applications. *Int. J. Numer. Methods. Engrg.*, 38:1855–1883, 1995.
- J. W. Park and Y. H. Kim. Predictor-corrector procedure for displacements, stresses and their sensitivity coefficients in composite panels. *J Compos Mater*, 33(13):1222–1243, 1999.
- J. W. Park and Y. H. Kim. Local recovery of through-the-thickness stresses in laminated composite plates. *Composite Structures*, 59:291–296, 2003.

- M.J. Pasanen, J.P. Martin, R.J. Langone, and J.A. Mondo. Advanced composite fiber placement process to application. 1997.
- P. Pedersen. On thickness and orientational design with orthotropic materials. *Structural Optimization*, 3:69–78, 1991.
- G. Prathap and B. P. Naganarayana. Consistent force resultant distributions in displacement elements with varying sectional properties. *International Journal for Numerical Methods in Engineering*, 29(4):775–783, 1990.
- G. Prathap and B. P. Naganarayana. Consistent thermal stress evaluation in finite elements. *Computers and Structures*, 54(3):415–426, 1995.
- M. A. Puso. A 3d mortar method for solid mechanics. *International Journal for Numerical Methods in Engineering*, 59(3):315–336, 2004. 10.1002/nme.865.
- Inc. Python. *Python v2.6.4 documentation*, 2006.
- C. C. Rankin, F. A. Brogan, W. A. Loden, and H. D. Cabiness. *STAGS Users Manual*. Lockheed Martin Missiles and Space Co., Inc., Sunnyvale, California, USA, June 2000.
- K.M. Rao and H. R. Meyer-Piening. Analysis of thick laminated anisotropic composite plates by the finite element method. *Composite Structures*, 15:185–213, 1990.
- B. K. Rath and Y. C. Das. Vibration of layered shells. *J. Sound. Vib.*, 28:737–757, 1973.
- B. D. Reddy and J. C. Simo. Stability and convergence of a class of enhanced strain methods. *SIAM J. Numer. Anal.*, 32(6):1705–1728, 1995.
- J. N. Reddy. *Energy Principles and Variational Methods in Applied Mechanics*. Second Edition, John Wiley, New York, 2002.
- J. N. Reddy. *Mechanics of Laminated Composite Plates and Shells: theory and analysis*. CRC Press, 2nd edition, 2004.
- J. N. Reddy and D. H. Robbins. Theories and computational models for composite laminates. *Appl. Mech. Rev.*, 47(6):147–169, 1994.
- E. Reissner. On a certain mixed variational theorem and a proposed application. *International Journal for Numerical Methods in Engineering*, 20(7):1366–1368, 1984.
- E. Reissner. On a mixed variational theorem and on a shear deformable plate theory. *International Journal for Numerical Methods in Engineering*, 23:193–198, 1986.
- J. G. Ren. A new theory of laminated plates. *Composite Science and Technology*, 26:225–239, 1986a.
- J. G. Ren. Bending theory of laminated plates. *Composite Science and Technology*, 27:225–248, 1986b.
- H. R. Riggs, A. Tessler, and H. Chu. c^1 -continuous stress recovery in finite element analysis. *Computer Methods in Applied Mechanics and Engineering*, 143:299–316, 1997.

- D. Rixen. *Computational Methods: Parallel Processing*. Encyclopedia of Vibration, S. G. Braun, D. J. Ewins, S. S. Rao Editors, Academic Press Ltd., 2001.
- D. J. Rixen and F. Magoulès. Domain decomposition methods: Recent advances and new challenges in engineering. *Comput. Methods Appl. Mech. Engrg*, 196:1345–1346, 2007.
- R. E. Rowlands. Strength (failure) theories and their experimental correlation. *Failure Mechanics of composites*, 1985.
- K. J. Saeger, P. A. Lagace, and D. J. Shim. Interlaminar stresses due to in-plane gradient stress fields. *Journal of Composite Materials*, 36:211–227, 2002.
- D. J. Shim and P. A. Lagace. Damage and delamination characteristics i composite laminates with ply-dropoffs under static and cyclic in-plane loads. In *Proceedings of the Joint American Society for Composites / American Society for Testing and MaterialsComitee D30 - Nineteenth Technical Conference*. American Society for Composites, 2004.
- D. J. Shim and P. A. Lagace. Mechanisms and structural parameters affecting the interlaminar stress field in laminates with ply drop-offs. *Journal of Composite Materials*, 40: 345–369, 2006.
- J. C. Simo and F. Armero. Geometrically nonlinear enhanced mixed methods and the method of incompatible modes. *International Journal for Numerical Methods in Engineering*, 33:1413–1449, 1992.
- J. C. Simo and T. J. R. Hughes. On the variational foundations of assumed strain methods. *ASME J. Appl. Mech.*, 53:41–54, 1986.
- J. C. Simo and M. S. Rifai. A class of mixed assumed strain methods and the method of incompatible modes. *International Journal for Numerical Methods in Engineering*, 29 (8):1595–1638, 1990. 10.1002/nme.1620290802.
- R. Slavkovic, M. Zivkovic, and Kojic M. Enhanced 8-node three dimensional solid and 4-node shell elements with incompatible generalized displacements. *Commun. Appl. Numer. Methods*, 10:699–709, 1994.
- S. Srinivas. A refined analysis of composite laminates. *J. Sound Vib.*, 30:495–507, 1973.
- H. Stolarsky and T. Belytschko. Limitation principles for mixed finite elements based on the hu-washizu variational formulation. *Comp. Methods Appl. Mech. Eng*, 60:195–216, 1987.
- B. F. Tatting. *Analysis and Design of Variable Stiffness Composite Cylinders*. PhD thesis, Virginia Polytechnic Institute and State University, Oct 1998.
- B. F. Tatting and Z. Gürdal. Analysis and design of tow-steered variable stiffness composite laminates. In *American Helicopter Society Hampton Roads Chapter, Structure Specialists' Meeting*, Williamsburg, VA, USA, October 2001. American Helicopter Society.
- B. F. Tatting and Z. Gürdal. Design and manufacture of elastically tailored tow placed plates. Technical report, Aug 2002. NASA/CR-2002-211919.

- B. F. Tatting and Z. Gürdal. Automated finite element analysis of elastically-tailored plates. Technical report, Dec 2003. NASA/CR-2003-212679.
- R. I. Taylor, P. J. Beresford, and E.L. Wilson. A non-conforming element for stress analysis. *International Journal for Numerical Methods in Engineering*, 10:1211–1219, 1976.
- A. Tessler. A higher-order plate theory with ideal finite element suitability. *Computer Methods in Applied Mechanics and Engineering*, 85:183–205, 1991.
- A. Tessler, H. R. Riggs, C. E. Freese, and G. M. Cook. An improved variational method for finite element stress recovery and a posteriori error estimation. *Comput. Methods Appl. Mech. Engrg*, 155:15–30, 1998.
- A. Toledano and H. Murakami. A higher-order laminated plate theory with improved in-plane responses. *International Journal of Solids and Structures*, 23:111–131, 1987a.
- A. Toledano and H. Murakami. A composite plate theory for arbitrary laminated configurations. *Journal of Applied Mechanics*, 54(4):181–189, 1987b.
- S. W. Tsai and E.M. Wu. A general theory of strength for anisotropic materials. *Journal of Composite Materials*, 5(1):58–80, 1971.
- F. Ubertini. Patch recovery based on complementary energy. *International Journal for Numerical Methods in Engineering*, 59:1501–1538, 2004.
- T. K. Varadan and K. Bhaskar. Bending of laminated orthotropic cylindrical shells-an elasticity approach. *Composite Structures*, 17:141–156, 1991.
- L. Vu-Quoc and X. G. Tan. Optimal solid shells for non-linear analyses of multilayer composites. i. statics. *Computer Methods in Applied Mechanics and Engineering*, 192(9-10):975–1016, 2003a.
- L. Vu-Quoc and X. G. Tan. Optimal solid shells for non-linear analyses of multilayer composites. ii. dynamics. *Computer Methods in Applied Mechanics and Engineering*, 192(9-10):1017–1059, 2003b.
- C. Waldhart. *Analysis of tow-placed, variable stiffness laminates*. PhD thesis, Virginia Polytechnic Institute and State University, Blacksburg, VA, June 1996.
- C. Waldhart, Z. Gürdal, and C. Ribbens. Analysis of tow placed, parallel fiber, variable stiffness laminates. In *Proceedings of the 37th AIAA/ASME/ASCE/AHS/ASC Structures, Structural Dynamics and Materials (SDM) Conference*, Salt Lake City, UT, USA, 1996. AIAA.
- K. Washizu. *Variational Methods in Elasticity and Plasticity*. Oxford: Pergamon Press, 1982.
- J. M. Whitney. The effect of transverse shear deformation on the bending of laminated plates. *Journal of Composite Materials*, 3(3):534–547, 1969.

- N. E. Wiberg, F. Abdulwahab, and S. Ziukas. Enhanced superconvergent patch recovery incorporating equilibrium and boundary conditions. *International Journal for Numerical Methods in Engineering*, 37(20):3417–3440, 1994.
- P. Wriggers and J. Korelc. On enhanced strain methods for small and finite deformations of solids. *Computational Mechanics*, 18(6):413–428, 1996.
- K. C. Wu. *Thermal and Structural Performance of Tow-Placed, Variable Stiffness Panels*. PhD thesis, Delft University of Technology, 2006.
- K. C. Wu, Z. Gürdal, and J. H. Starnes. Structural response of compression-loaded, tow-placed, variable stiffness panels. In *Proceedings of the 43rd AIAA/ASME/AHS/ASC Structures, Structural Dynamics and Materials (SDM) Conference*, Denver, CO, USA, Apr 2002. AIAA.
- S. S. Yau and T. W. Chou. Strength of woven-fabric composites with drilled and molded holes. *ASTM Special Technical Publication*, pages 423–437, 1988.
- S. T. Yeo and B. C. Lee. Equivalence between enhanced assumed strain method and assumed stress hybrid method based on the hellinger-reissner principle. *Int. J. Numer. Methods in Engineering*, 39:3083–3099, 1996.
- Y. Y. Yu. A new theory of elastic sandwich plates. one dimensional case. *Journal of Applied Mechanics*, 37:1031–1036, 1959.
- O. C. Zienkiewicz and R. L. Taylor. *The Finite Element Method: The Basis*. Butterworth-Heinemann, 2000.
- O. C. Zienkiewicz and J. Z. Zhu. The superconvergent patch recovery and a posteriori error estimates. part 1: The recovery technique. *International Journal for Numerical Methods in Engineering*, 33(7):1331–1364, 1992a.
- O. C. Zienkiewicz and J. Z. Zhu. The superconvergent patch recovery and a posteriori error estimates. part 2: Error estimates and adaptivity. *International Journal for Numerical Methods in Engineering*, 33(7):1365–1382, 1992b.
- M. Zlamal. *Some superconvergence results in the finite element method*. In *Mathematical Aspects of Finite Element Methods*, Galligani I, Magenes E (eds), springer edition, 1977.

Curriculum vitae

Christian Fagiano was born on the 11th of August of 1980 in Turin, Italy. There he completed the basic education level, the secondary education level and the higher education in aerospace engineering at the Polytechnic of Turin where he graduated Cum Laude. His M.Sc thesis consisted in the development of higher order plate finite elements able to analyse multilayer composite laminates subjected to multifield problems, i.e. thermo-piezo-mechanical analyses. In particular, formulations based on the classical Principle of Virtual Displacements and the Reissner Mixed Variational Theorem were developed and compared with results available in the open literature. This subject was developed under the supervision of Prof.Dr. Erasmo Carrera.

Between September 2005 and December 2005 he worked at Alenia Aeronautica in Turin in the Armament's safety staff of the Eurofighter Typhoon 2000 aircraft. His duty was the analysis of the probabilistic ultimate failure of the armament's components in all the possible mission configurations.

Between December 2005 and June 2006 he worked as a researcher at the Polytechnic of Turin in collaboration with Prof.Dr. Erasmo Carrera. The subject of his research was the finite element modeling of composite structures subjected to multifield problems, i.e. piezo-magnetic-mechanical analyses. In particular, his studies were addressed to the development of higher order plate finite elements based on the Reissner's Mixed Variational Theorem.

In June 2006, he enrolled in a Ph.D. programme at TU Delft under the supervision of Prof. Dr. Zafer Gürdal and Dr. M.M. Abdalla. His thesis covers the computational modeling of non-conventional composites laminates, i.e. tow-placed laminates, in which fabrications features are also taken into account. He was assigned the task of coming up with algorithms suitable for the recovery of interlaminar stresses in such laminates. Particular attention was also paid to tailor commercial finite element packages and extend them to carry out simulations based on his algorithms.



